

CEN2010

Segovia (Spain)

June 15-18, 2010



Following the spirit initiated by the 1st Conferencia Española de Nanofotónica, held in Tarragona in 2008, we launch the 2nd edition that will be conducted in Segovia during 15-18 June 2010. The Conference aims to gather all the groups carrying out research in Nanophotonics in Spain (as well as somewhere else with interest in the research in Nanophotonics performed here). It intends to spread the research results achieved by all the different Spanish groups and to promote the establishment or reinforcement of contacts between them, as a mean to help the community to become more visible and dynamic.

The Conference technical program aspires to address a wide area of research related to nanophotonics, metamaterials and subwavelength optics. Topics will include all aspects of the research, ranging from fundamental science to nanofabrication or applications.

The Conference will be organized in thematic sessions composed of plenary invited talks and contributed scientific communications (oral and poster).

The meeting will be structured in the following thematic lines, but interactions among them will be promoted:

1. Photonic materials and photonic bandgap structures
2. Plasmonics and extraordinary transmission
3. Metamaterials
4. Near field optics (only Poster Session)
5. Nanophotonics applications



Moreover, during the Conference five “Special Topical Meetings” will be organised, where researchers and students will have the opportunity to meet and discuss around a specific topic that shows a high strategic interest or a big development capability for Nanophotonics. A Moderator will take charge of each Special Topical Meeting, making a brief introduction on the state of the art of the topic, and then conducting the subsequent debate. The Special Topics chosen and their Moderators are:

- **Nanophotonics for solar cells:** Lluís Marsal (URV, Tarragona)
- **Nanophotonics for sensors and biosensors:** Andreu Llobera and Cesar Fernandez (IMB-CNM, Barcelona)
- **Nanophotonics for bio-applications and bio-imaging:** Carlo Manzo (IBEC, Barcelona)
- **Nanophotonics for Terahertz optics and devices:** Mario Sorolla (UPNA, Pamplona)
- **Nanophotonics for integrated and quantum optics:** Benito Alen (IMM-CNM, Madrid)

Finally, thanks must be directed to the staff of all organising institutions whose hard work has helped the smooth organisation and planning of this conference.

THE ORGANISING COMMITTEE

Chairs

Pablo Aitor Postigo	IMM-CSIC
Maria Ujue Gonzalez	IMM-CSIC

Organising Committee

Javier Aizpurua	CSIC-DIPC-UPV/EHU
Antonio Correia*	Fundación Phantoms
Antonio Garcia Martín	IMM-CSIC
Maria Ujue Gonzalez	IMM-CSIC
Lluís Marsal	URV
Jordi Martorell	ICFO
Hernan Miguez	ICMSE-CSIC
Josep Pallares	URV
Pablo Aitor Postigo	IMM-CSIC
Romain Quidant	ICFO
Juan Jose Saenz	UAM

Scientific Committee

Ramon Alcubilla	UPC
Benito Alen	IMM-CSIC
Gaspar Armelles	IMM-CSIC
Gonçal Badenes	ICFO
Salvador Balle	UIB
Alvaro Blanco	ICMM-CSIC
Jose M. Calleja	UAM
Enrique Calleja	UPM
Francesc Diaz	URV
Concepcion Domingo	IEM-CSIC
Javier Garcia de Abajo	IO-CSIC
Francisco J. Garcia-Vidal	UAM
Rainer Hillenbrand	CIC nanoGUNE
Niek van Hulst	IFCO
Luis M. Liz-Marzan	UV-CSIC
Cefe Lopez	ICMM-CSIC
Javier Marti	CTN-UPV
Luís Martin Moreno	UZ-CSIC
Juan Martinez-Pastor	ICMUV
Francisco Meseguer	UPV-CSIC
Fernando Moreno	UC
Manuel Nieto-Vesperinas	ICMM-CSIC
Jose Sanchez-Dehesa	UPV
Jose A. Sanchez Gil	IEM-CSIC
Jan Siegel	IO-CSIC
Mario Sorolla	UPNA
Clivia Sotomayor	ICN-CIN2
Luis Viña	UAM

*Contact – antonio@phantomsnet.net

Technical Organising Committee

Carmen Chacon	Fundacion Phantoms
Maite Fernandez	Fundacion Phantoms
Jorge F. Torrado	IMM-CSIC
Melih Kaldirim	IMM-CSIC
Diana Martin	IMM-CSIC
Luis Javier Martinez	IMM-CSIC
Luis Enrique Muñoz	IMM-CSIC
Concepcion Narros	Fundacion Phantoms
Ivan Prieto	IMM-CSIC
Jose Luis Roldan	Fundacion Phantoms

CEN2010 Organisers



CEN2010 Sponsors



CEN2010 Exhibitors



CEN2010 Exhibitors



Iberlaser, s.a.

Electro-Óptica Científica e Industrial
Instrumentación y Láseres

Iberlaser was setup in 1993, and is based in Madrid-Spain. Our principal mission statement is provide research Spanish market with the novel instrumentation and highly qualified servicing .
Our lines of products include:

Bio-technology: Complete Microscopy solutions.

Laser Technology: CW and Pulsed lasers covering the range UV-VIS-IR

Low light Imaging: High performance digital cameras and imaging software packages

Solar Simulators and illumination sources

Spectroscopy: Spectrographs and detectors. Time resolved and steady state fluorimeters.

Surface chemistry: Interface Analysis, Dip coaters, Monolayers preparation and characterization. Microbalance QCM.

Contact us:

Web: www.iberlaser.es

Email: info@iberlaser.com

Tel: 91 658 67 60 Fax: 91 654 17 00

Avda. Pirineos, 7 - Oficina 2-8b

28700 San Sebastián de los Reyes (Madrid) **SPAIN**



Laser 2000 is the expert distributor devoted solely to optics and photonics. Target markets are Science and Research, Biotechnology and Healthcare, Energy and Photovoltaics, Image processing, Security, Defence and Space, Light and Colour Measurements, Industry,...

We help innovative and quality manufacturers making their products wide known; we help customers from our technical knowledge, support and advice, making them aware of those products. Key ones are:

- Lasers (DPSS, diode, fibre, deep UV to mid-IR, SLM,...)
- LEDs, broadband and fluorescence sources
- Detectors, power and energy measurement, beam analysis
- Spectrometers and spectroradiometers
- Imaging, light and colour measurement
- Optomechanics, positioning and motion control

We are present in the whole of Western Europe and active in Spain and Portugal since October 2006

Contact us:

Web: www.laser2000.es

Email: juanluis@laser2000.es

Tel: +34 650 529 806 Fax: +34 976 299 150

Laser 2000, Sales office Iberia

c/ Doctor Palomar 28, 1ªA

50002 - Zaragoza, **SPAIN**



MTB Spain, founded in October 1993, distributes and provides after sales service for leading manufacturers in the field of Spectroscopy, Lasers, Metrology and Surface Analysis Instrumentation.

MTB Spectroscopy and Lasers division is the exclusive distributor of the following companies:

1. Horiba Jobin Yvon, world wide leader in Raman Spectrometers, Micro-Raman and combined FT-IR – Raman Spectrometers, Fluorometers, Elipsometers, CCD's & ICCD's, Monochromators and Gratings.
2. JDSU, one of the major manufacturers of Diode Lasers
3. EKSPILA, European manufacturer of Solid State Lasers (Diode Pumped, OPO) and ns / ps Lasers for scientific applications.
4. Sacher Lasertechnik, leader in Littman/Metcalf and Littrow cavities Lasers, suitable for Raman, Fluorescence and Absorption Spectroscopy and atom cooling and trapping.

MTB Image, Test & Measurement division distributes FRT – Fries Research & Technology, leader in optical surface characterisation from the same sample location, using Multi Sensor Metrology. Between the most used sensors are Chromatic White Light, Confocal Microscope, White Light Interferometer, Thin Film Reflectometer and AFM - Atomic Force Microscope.

MTB not only provides equipments but also complete solutions for specific applications, combining different analysis techniques such as Raman, TCSPC Fluorescence, AFM, SNOM, TERS and Photoluminescence.

Contact us:

Web: www.mtb.es

Sandrine Grenet

División Láser y Espectroscopía

M. T. BRANDAO ESPAÑA, S.L.

Ronda de Poniente, 12, 1º, A

28760 TRES CANTOS (Madrid) **SPAIN**

Tel. +34 918 062 240

Fax +34 918 031 536

CEN2010

Segovia (Spain)

June 15-18, 2010

SCIENTIFIC PROGRAMME

SCIENTIFIC PROGRAMME

Tuesday June 15, 2010

09h:30-13:30	Nanomagma Short Training Course Confirmed Professors Remi Carminati (ESPCI, France) Alfonso Cebollada (IMM-CSIC, Spain) F.J. Garcia-Vidal (UAM, Spain) Antonio Garcia-Martin (IMM-CSIC, Spain)	
13h30-15h10	Registration CEN2010 (<i>Session: Nanophotonic Applications</i>) - Chairman: Lluís Marsal (Universitat Rovira i Virgili, Spain)	
15h15-15h30	Opening – Welcome	
15h30-16h10	Claude Weisbuch (Ecole Polytechnique, France)	I
p.	<i>"Improvements in Light Emitters by Controlling Spontaneous Emission: From LEDs to Biochips"</i>	
16h10-16h30	Elisabet Xifre Perez (Centro de Tecnologías Físicas, CSIC-ICMM/UPV, Spain)	O
p.	<i>"Add-drop filter based on silicon spherical microcavities"</i>	
16h30-16h50	Nicolas Large (CSIC-UPV/EHU and DIPC, Spain)	O
p.	<i>"Photoconductively loaded plasmonic nanoantennas as a building block for ultracompact optical switches"</i>	
16h50-17h10	Rafael Betancur (ICFO, Spain)	O
p.	<i>"Optical control of the exciton diffusion length in organic solar cells"</i>	
17h10-17h30	Roberto Fenollosa (Univ. Politécnica de Valencia - CSIC, Spain)	O
p.	<i>"Photoluminescence and Aging Effects in Photonic Microcavities Based on Porous Silicon Microspheres"</i>	
17h30-18h00	Coffee Break – Poster Session & Instrument Exhibition	
	(Session: Nanophotonic Applications) - Chairman: Antonio Garcia-Martin (IMM-CNM-CSIC, Spain)	
18h00-18h20	Juan Jose Saenz (UAM, Spain)	O
p.	<i>"Nanoparticle Dynamics in Non-Conservative Optical Vortex Fields"</i>	
18h20-18h40	Maria Mendez (Universitat Rovira i Virgili, Spain)	O
p.	<i>"Eu³⁺:La₂O₃ nanoparticles dispersed into P3HT as a down converter material for exploiting the solar spectrum"</i>	
18h40-19h00	Mauricio Moreno (University of Barcelona, Spain)	O
p.	<i>"Theoretical Study of Colorimetric Resonant Structures for Biosensing Applications"</i>	
19h00-19h20	Daniel Hill (KTH, Sweden)	O
p.	<i>"A highly integrated optical sensor for point of care label free identification of pathogenic bacteria strains and their antibiotic resistance"</i>	
21:00	Welcome reception	

SCIENTIFIC PROGRAMME

Wednesday June 16, 2010

(Session: Plasmonics) - Chairman: Jose A. Sanchez-Gil (Instituto de Estructura de la Materia - CSIC, Spain)		
09h00-09h40	Anatoly V. Zayats (The Queen's University of Belfast, UK)	I
p.	<i>"New trends in plasmonic nanophotonics"</i>	
09h40-10h00	Diana Martin Becerra (IMM-CNM-CSIC, Spain)	O
p.	<i>"Tailoring the modulation depth in Au/Co/Au magnetoplasmonic switches"</i>	
10h00-10h20	Esteban Moreno (UAM, Spain)	O
p.	<i>"Domino plasmons for subwavelength terahertz circuitry"</i>	
10h20-10h40	Olalla Perez-Gonzalez (UPV/EHU-CSIC, Spain)	O
p.	<i>"Optical spectroscopy of conductive molecular junctions in plasmonic cavities"</i>	
10h40-11h00	Vicent Reboud (ICN-CIN2, Spain)	O
p.	<i>"Enhanced photoluminescence in printed 2D polymer photonic structures via surface plasmon enhancement"</i>	
11h00-11h30	Coffee Break – Poster Session & Instrument Exhibition	
(Session: Plasmonics) - Chairman: Fernando Moreno (Universidad de Cantabria, Spain)		
11h30-11h50	Antonio Garcia Martin (IMM-CNM-CSIC, Spain)	O
p.	<i>"Plasmon-Induced Magneto-Optical Activity in Nanosized Gold Disks"</i>	
11h50-12h10	Rogelio Rodriguez-Oliveros (Instituto de Estructura de la Materia - CSIC, Spain)	O
p.	<i>"Plasmon Optical Nanoantennas: Characterization, Design, and Applications in Nanophotonics"</i>	
12h10-12h30	Francisco Javier Valdivia (ICMM - CSIC, Spain)	O
p.	<i>"Light transport by sets and chains of Mie resonances: whispering gallery modes and localized plasmons. Effects on extraordinary transmission"</i>	
12h30-12h50	Sol Carretero-Palacios (Universidad de Zaragoza, Spain)	O
p.	<i>"Localized Extraordinary Optical Transmission through sub-wavelength apertures"</i>	
12h50-13h10	Mario Sorolla (Universidad Publica de Navarra, Spain)	O
p.	<i>"Study of terahertz extraordinary transmission resonances depending on polarization"</i>	
13h10-13h30	Alejandro Manjavacas (Instituto de Optica - CSIC, Spain)	O
p.	<i>"Vacuum and thermal friction in rotating particles"</i>	
13h30-15h30	Lunch	
Poster Session & Instrument Exhibition		
15h30-17h30	Coffee Break – Poster Session & Instrument Exhibition	
17h30-18h00	Coffee Break – Poster Session & Instrument Exhibition	
(Session: Plasmonics) - Chairman: Maria Ujue Gonzalez (IMM-CNM-CSIC, Spain)		
18h00-18h40	Kurt Busch (Karlsruhe University, Germany)	I
p.	<i>"Advanced material models for nano-plasmonic systems"</i>	
18h40-19h00	Christin David (Instituto de Optica - CSIC, Spain)	O
p.	<i>"Spatial Nonlocality in the Optical Response of Metal Nanoparticles"</i>	
19h00-19h20	Rafael Abargues Lopez (Materials Science Institute of the University of Valencia, Spain)	O
p.	<i>"Ag-polymer nanocomposites for LSPR sensing"</i>	
19h20-19h40	Pablo Albella (CSIC-DIPC, Spain)	O
p.	<i>"Plasmonics with new materials: Gallium. A comparison between experiment and a numerical model based on the Discrete Dipole Approximation (DDA)"</i>	
19h40-20h00	Pablo Alonso-Gonzalez (CIC nanoGUNE, Spain)	O
p.	<i>"Phononic antennas"</i>	
21h30	Conference Dinner Restaurant "Jose Maria" Calle del Cronista Lecea, 11 (Segovia)	

SCIENTIFIC PROGRAMME

Thursday June 17, 2010

09h00-10h20	Meeting “Building bridges for a stronger (all inclusive) Photonics in Spain”	
<i>(Session: Metamaterials) - Chairman: Alvaro Blanco (ICMM-CSIC, Spain)</i>		
10h20-11h00	Stefan Linden (Universitat Bonn, Germany)	I
p.	<i>"Recent Progress on Photonic Metamaterials"</i>	
11h00-11h20	Marco Leonetti (ICMM-CSIC, Spain)	O
p.	<i>"Optical gain in DNA-DCM for lasing in photonic materials"</i>	
11h20-11h40	Poster Session - Coffee Break & Instrument Exhibition	
11h40-12h00	Juan Luis Garcia-Pomar (Fraunhofer Institute for Physical Measurement Techniques IPM, Germany)	O
p.	<i>"Nonlinearity caused by local field effects between a two level system and a metamaterial"</i>	
12h00-12h20	Jose Sanchez-Dehesa (Universidad Politecnica de Valencia, Spain)	O
p.	<i>"Anisotropic behavior of two-dimensional photonic crystals in the homogenization limit"</i>	
12h30-13h30	Special Topical Meetings	
	Nanophotonics for solar cells: Lluís Marsal (URV, Tarragona)	
	Nanophotonics for sensors and biosensors: Andreu Llobera and Cesar Fernandez (IMB-CNM, Barcelona)	
	Nanophotonics for bio-applications and bio-imaging: Carlo Monzo (IBEC, Barcelona)	
	Nanophotonics for Terahertz optics and devices: Mario Sorolla (UPNA, Pamplona)	
13h30-15h30	Lunch	
15h30-17h30	Poster Session & Instrument Exhibition	
17h30-18h00	Coffee Break – Poster Session & Instrument Exhibition	
<i>(Session: Nanophotonic Applications) - Chairman: Juan Jose Saenz (UAM, Spain)</i>		
18h00-18h20	Johannes Stiegler (CIC nanoGUNE Consolider, Spain)	O
p.	<i>"Nanoscale Free-Carrier Profiling of Individual Semiconductor Nanowires by Infrared Near-Field Plasmon Resonance Spectroscopy"</i>	
18h20-18h40	Guillermo Muñoz-Matutano (Instituto de Ciencias de los Materiales de la Universitat de Valencia, Spain)	O
p.	<i>"Micro-photoluminescence from InAs/GaAs quantum dot pairs and molecules grown by droplet epitaxy"</i>	
18h40-19h00	M^a Dolores Martin Fernandez (UAM, Spain)	O
p.	<i>"Exciton emission dynamics of single-photon emitters based on InP/(Ga, In) P quantum dots"</i>	
19h00-19h20	Alexey Nikitin (Universidad de Zaragoza, Spain)	O
p.	<i>"Norton waves in Plasmonics"</i>	
19h20-19h40	Manfred Niehus (Instituto de Telecomunicações - Polo Aveiro, Portugal)	O
p.	<i>"Dispersion engineered tapered fiber photonic nanowires"</i>	
19h40-20h00	Blas Garrido (University of Barcelona, Spain)	O
p.	<i>"Toward the realization of an efficient Si-based light source emitting at 1.55 μm"</i>	

SCIENTIFIC PROGRAMME

Friday June 18, 2010

(Session: Photonic Materials and Photonic Bandgap Structures) - Chairman: Pablo Sanchis (Universidad Politécnica de Valencia, Spain)		
09h00-09h40	Christian Seassal (Universite de Lyon & INL, France)	I
p.	<i>"Slow light in photonic crystals for photovoltaics"</i>	
09h40-10h00	Ibon Alonso Villanueva (Tekniker, Spain)	O
p.	<i>"Organic second-order distributed feedback lasers fabricated by nanoimprint lithography"</i>	
10h00-10h20	Gabriel S. Lozano Barbero (ICMSE-CSIC, Spain)	O
p.	<i>"Towards a full understanding of the growth dynamics, optical response and crystalline structure of self-assembled photonic colloidal crystal films"</i>	
10h20-10h40	Juan F^a Galisteo Lopez (ICMM-CSIC, Spain)	O
p.	<i>"Enhanced emission in self-assembled photonic crystals by hybrid photonic-plasmonic modes"</i>	
10h40-11h00	Pablo Aitor Postigo (IMM-CNM-CSIC, Spain)	O
p.	<i>"Fabrication of two dimensional photonic crystal micro and nanocavities: from ultra low threshold lasers to solid-state quantum light emitters"</i>	
11h00-11h30	Coffee Break – Poster Session & Instrument Exhibition	
(Session: Photonic Materials and Photonic Bandgap Structures) - Chairman: Juan Galisteo (ICMM-CSIC, Spain)		
11h30-11h50	Fernando Ramiro Manzano (Centro de Tecnologías Físicas, Unidad Asociada CSIC-ICMM/UPV, Spain)	O
p.	<i>"Influence of Corrugated Surfaces Templates in Colloidal Crystal Thin Films Growth"</i>	
11h50-12h10	Francesc Diaz (Universitat Rovira i Virgili, Spain)	O
p.	<i>"Exploring the possibilities of fabrication of photonic crystals on inorganic materials with non-linear optical and laser properties"</i>	
12h10-12h30	Daniel Navarro-Urrios (MIND-IN2UB - Universitat de Barcelona, Spain)	O
p.	<i>"Whispering gallery mode optical characterization on Si rich Si₃N₄ active microdisk resonators"</i>	
12h30-12h50	Javier Garcia Castello (Nanophotonics Technology Center - Universidad Politecnica de Valencia, Spain)	O
p.	<i>"Photonic crystal waveguide sensor for low concentration DNA detection"</i>	
12h50-13h10	Pablo Sanchis Kilders (Valencia Nanophotonics Technology Center, Universidad Politecnica de Valencia, Spain)	O
p.	<i>"Slow wave and resonator structures to enhance silicon photonic modulator performance"</i>	
13h10-13h30	Concluding Remarks	

CEN2010

Segovia (Spain)

June 15-18, 2010

ABSTRACTS

Invited Contributions (Index)

Kurt Busch (Karlsruhe University, Germany)	p.
<i>"Advanced material models for nano-plasmonic systems"</i>	
Stefan Linden (Universitat Bonn, Germany)	p.
<i>"Recent Progress on Photonic Metamaterials"</i>	
Christian Seassal (Universite de Lyon, INL - Institut des Nanotechnologies de Lyon, France)	p.
<i>"Slow light in photonic crystals for photovoltaics"</i>	
Claude Weisbuch (Ecole Polytechnique, France)	p.
<i>"The Physics of Photonic Crystals LEDs"</i>	
Anatoly V. Zayats (The Queen's University of Belfast, United Kingdom)	p.
<i>"New trends in plasmonic nanophotonics"</i>	

Oral Contributions (Index)

Rafael Abargues Lopez (Materials Science Institute of the University of Valencia, Spain)	p.
<i>"Ag-polymer nanocomposites for LSPR sensing"</i>	
Pablo Albella (CSIC - DIPC, Spain)	p.
<i>"Plasmonics with new materials: Gallium. A comparison between experiment and a numerical model based on the Discrete Dipole Approximation (DDA)"</i>	
Ibon Alonso Villanueva (Tekniker, Spain)	p.
<i>"Organic second-order distributed feedback lasers fabricated by nanoimprint lithography"</i>	
Pablo Alonso-Gonzalez (CIC Nanogune, Spain)	p.
<i>"Phononic antennas"</i>	
Rafael Betancur (ICFO, Spain)	p.
<i>"Optical control of the exciton diffusion length in organic solar cells"</i>	
Sol Carretero-Palacios (Universidad de Zaragoza, Spain)	p.
<i>"Localized Extraordinary Optical Transmission through sub-wavelength apertures"</i>	
Christin David (Instituto de Optica - CSIC, Spain)	p.
<i>"Spatial Nonlocality in the Optical Response of Metal Nanoparticles"</i>	
Francesc Diaz (Universitat Rovira i Virgili, Spain)	p.
<i>"Exploring the possibilities of fabrication of photonic crystals on inorganic materials with non-linear optical and laser properties"</i>	
Roberto Fenollosa (Univ. Politecnica de Valencia - CSIC, Spain)	p.
<i>"Photoluminescence and Aging Effects in Photonic Microcavities Based on Porous Silicon Microspheres"</i>	
Juan Francisco Galisteo Lopez (ICMM-CSIC, Spain)	p.
<i>"Enhanced emission in self-assembled photonic crystals by hybrid photonic-plasmonic modes"</i>	
Javier Garcia Castello (Nanophotonics Technology Center - Universidad Politecnica de Valencia, Spain)	p.
<i>"Photonic crystal waveguide sensor for low concentration DNA detection"</i>	
Antonio Garcia-Martin (IMM-CNM-CSIC, Spain)	p.
<i>"Plasmon-Induced Magneto-Optical Activity in Nanosized Gold Disks"</i>	
Juan Luis Garcia-Pomar (Fraunhofer Inst. for Physical Measurement Techniques IPM, Germany)	p.
<i>"Nonlinearity caused by local field effects between a two level system and a metamaterial"</i>	
Blas Garrido (University of Barcelona, Spain)	p.
<i>"Toward the realization of an efficient Si-based light source emitting at 1.55 μm"</i>	
Daniel Hill (KTH, Sweden)	p.
<i>"A highly integrated optical sensor for point of care label free identification of pathogenic bacteria strains and their antibiotic resistance"</i>	

Nicolas Large (Centro de Fisica de Materiales CSIC-UPV/EHU and DIPC, Spain)	p.
<i>"Photoconductively loaded plasmonic nanoantennas as a building block for ultracompact optical switches"</i>	
Marco Leonetti (ICMM-CSIC, Spain)	p.
<i>"Optical gain in DNA-DCM for lasing in photonic materials"</i>	
Gabriel S. Lozano Barbero (ICMSE-CSIC, Spain)	p.
<i>"Towards a full understanding of the growth dynamics, optical response and crystalline structure of self-assembled photonic colloidal crystal films"</i>	
Alejandro Manjavacas (Instituto de Optica - CSIC, Spain)	p.
<i>"Vacuum and thermal friction in rotating particles"</i>	
Diana Martin Becerra (IMM-CNM-CSIC, Spain)	p.
<i>"Tailoring the modulation depth in Au/Co/Au magnetoplasmonic switches"</i>	
Maria Dolores Martin Fernandez (Universidad Autonoma de Madrid, Spain)	p.
<i>"Exciton emission dynamics of single-photon emitters based on InP/(Ga, In) P quantum dots"</i>	
Maria Mendez (Universitat Rovira i Virgili, Spain)	p.
<i>"Eu³⁺:La₂O₃ nanoparticles dispersed into P3HT as a down converter material for exploiting the solar spectrum"</i>	
Mauricio Moreno (University of Barcelona, Spain)	p.
<i>"Theoretical Study of Colorimetric Resonant Structures for Biosensing Applications"</i>	
Esteban Moreno (Universidad Autonoma de Madrid, Spain)	p.
<i>"Domino plasmons for subwavelength terahertz circuitry"</i>	
Guillermo Muñoz-Matutano (Instituto de Ciencias de los Materiales de la Universitat de Valencia, Spain)	p.
<i>"Micro-photoluminescence from InAs/GaAs quantum dot pairs and molecules grown by droplet epitaxy"</i>	
Daniel Navarro-Urrios (MIND-IN2UB - Universitat de Barcelona, Spain)	p.
<i>"Whispering gallery mode optical characterization on Si rich Si₃N₄ active microdisk resonators"</i>	
Manfred Niehus (Instituto de Telecomunicações - Polo Aveiro, Portugal)	p.
<i>"Dispersion engineered tapered fiber photonic nanowires"</i>	
Alexey Nikitin (Universidad de Zaragoza, Spain)	p.
<i>"Norton waves in Plasmonics"</i>	
Olalla Perez-Gonzalez (UPV/EHU - DIPC, Spain)	p.
<i>"Optical spectroscopy of conductive molecular junctions in plasmonic cavities"</i>	
Pablo Aitor Postigo (IMM-CNM-CSIC, Spain)	p.
<i>"Fabrication of two dimensional photonic crystal micro and nanocavities: from ultra low threshold lasers to solid-state quantum light emitters"</i>	

Fernando Ramiro Manzano (Centro de Tecnologías Físicas, Unidad Asociada CSIC-ICMM/UPV, Spain)	p.
<i>"Influence of Corrugated Surfaces Templates in Colloidal Crystal Thin Films Growth"</i>	
Vincent Reboud (Catalan Institute of Nanotechnology and (ICN-CIN2), Spain)	p.
<i>"Enhanced photoluminescence in printed 2D polymer photonic structures via surface plasmon enhancement"</i>	
Rogelio Rodriguez-Oliveros (Instituto de Estructura de la Materia - CSIC, Spain)	p.
<i>"Plasmon Optical Nanoantennas: Characterization, Design, and Applications in Nanophotonics"</i>	
Juan Jose Saenz (Universidad Autónoma de Madrid, Spain)	p.
<i>"Nanoparticle Dynamics in Non-Conservative Optical Vortex Fields"</i>	
Jose Sanchez-Dehesa (Universidad Politécnica de Valencia, Spain)	p.
<i>"Anisotropic behavior of two-dimensional photonic crystals in the homogenization limit"</i>	
Pablo Sanchis Kilders (Valencia Nanophotonics Technology Center, Universidad Politécnica de Valencia, Spain)	p.
<i>"Slow wave and resonator structures to enhance silicon photonic modulator performance"</i>	
Mario Sorolla (Universidad Pública de Navarra, Spain)	p.
<i>"Study of terahertz extraordinary transmission resonances depending on polarization"</i>	
Johannes Stiegler (CIC nanoGUNE Consolider, Spain)	p.
<i>"Nanoscale Free-Carrier Profiling of Individual Semiconductor Nanowires by Infrared Near-Field Plasmon Resonance Spectroscopy"</i>	
Francisco Javier Valdivia (ICMM-CSIC, Spain)	p.
<i>"Light transport by sets and chains of Mie resonances: whispering gallery modes and localized plasmons. Effects on extraordinary transmission"</i>	
Elisabet Xifre Perez (Centro de Tecnologías Físicas, Unidad Asociada CSIC-ICMM/UPV, Spain)	p.
<i>"Add-drop filter based on silicon spherical microcavities"</i>	

Alphabetical Order

Rafael Abargues Lopez (Materials Science Institute of the University of Valencia, Spain)	ORAL	p.
<i>"Ag-polymer nanocomposites for LSPR sensing"</i>		
Pablo Albella (CSIC - DIPC, Spain)	ORAL	p.
<i>"Plasmonics with new materials: Gallium. A comparison between experiment and a numerical model based on the Discrete Dipole Approximation (DDA)"</i>		
Ibon Alonso Villanueva (Tekniker, Spain)	ORAL	p.
<i>"Organic second-order distributed feedback lasers fabricated by nanoimprint lithography"</i>		
Pablo Alonso-Gonzalez (CIC Nanogune, Spain)	ORAL	p.
<i>"Phononic antennas"</i>		
Rafael Betancur (ICFO, Spain)	ORAL	p.
<i>"Optical control of the exciton diffusion length in organic solar cells"</i>		
Kurt Busch (Karlsruhe University, Germany)	INVITED	p.
<i>"Advanced material models for nano-plasmonic systems"</i>		
Sol Carretero-Palacios (Universidad de Zaragoza, Spain)	ORAL	p.
<i>"Localized Extraordinary Optical Transmission through sub-wavelength apertures"</i>		
Christin David (Instituto de Optica - CSIC, Spain)	ORAL	p.
<i>"Spatial Nonlocality in the Optical Response of Metal Nanoparticles"</i>		
Francesc Diaz (Universitat Rovira i Virgili, Spain)	ORAL	p.
<i>"Exploring the possibilities of fabrication of photonic crystals on inorganic materials with non-linear optical and laser properties"</i>		
Roberto Fenolosa (Univ. Politecnica de Valencia - CSIC, Spain)	ORAL	p.
<i>"Photoluminescence and Aging Effects in Photonic Microcavities Based on Porous Silicon Microspheres"</i>		
Juan Francisco Galisteo Lopez (ICMM-CSIC, Spain)	ORAL	p.
<i>"Enhanced emission in self-assembled photonic crystals by hybrid photonic-plasmonic modes"</i>		
Javier Garcia Castello (Nanophotonics Technology Center - Universidad Politecnica de Valencia, Spain)	ORAL	p.
<i>"Photonic crystal waveguide sensor for low concentration DNA detection"</i>		
Antonio Garcia-Martin (IMM-CNM-CSIC, Spain)	ORAL	p.
<i>"Plasmon-Induced Magneto-Optical Activity in Nanosized Gold Disks"</i>		
Juan Luis Garcia-Pomar (Fraunhofer Inst. for Physical Measurement Techniques IPM, Germany)	ORAL	p.
<i>"Nonlinearity caused by local field effects between a two level system and a metamaterial"</i>		
Blas Garrido (University of Barcelona, Spain)	ORAL	p.
<i>"Toward the realization of an efficient Si-based light source emitting at 1.55 μm"</i>		

Daniel Hill (KTH, Sweden)	ORAL	p.
<i>"A highly integrated optical sensor for point of care label free identification of pathogenic bacteria strains and their antibiotic resistance"</i>		
Nicolas Large (Centro de Fisica de Materiales CSIC-UPV/EHU and DIPC, Spain)	ORAL	p.
<i>"Photoconductively loaded plasmonic nanoantennas as a building block for ultracompact optical switches"</i>		
Marco Leonetti (ICMM-CSIC, Spain)	ORAL	p.
<i>"Optical gain in DNA-DCM for lasing in photonic materials"</i>		
Stefan Linden (Universitat Bonn, Germany)	INVITED	p.
<i>"Recent Progress on Photonic Metamaterials"</i>		
Gabriel S. Lozano Barbero (ICMSE-CSIC, Spain)	ORAL	p.
<i>"Towards a full understanding of the growth dynamics, optical response and crystalline structure of self-assembled photonic colloidal crystal films"</i>		
Alejandro Manjavacas (Instituto de Optica - CSIC, Spain)	ORAL	p.
<i>"Vacuum and thermal friction in rotating particles"</i>		
Diana Martin Becerra (IMM-CNM-CSIC, Spain)	ORAL	p.
<i>"Tailoring the modulation depth in Au/Co/Au magnetoplasmonic switches"</i>		
Maria Dolores Martin Fernandez (Universidad Autonoma de Madrid, Spain)	ORAL	p.
<i>"Exciton emission dynamics of single-photon emitters based on InP/(Ga, In) P quantum dots"</i>		
Maria Mendez (Universitat Rovira i Virgili, Spain)	ORAL	p.
<i>"Eu³⁺:La₂O₃ nanoparticles dispersed into P3HT as a down converter material for exploiting the solar spectrum"</i>		
Mauricio Moreno (University of Barcelona, Spain)	ORAL	p.
<i>"Theoretical Study of Colorimetric Resonant Structures for Biosensing Applications"</i>		
Esteban Moreno (Universidad Autonoma de Madrid, Spain)	ORAL	p.
<i>"Domino plasmons for subwavelength terahertz circuitry"</i>		
Guillermo Muñoz-Matutano (Instituto de Ciencias de los Materiales de la Universitat de Valencia, Spain)	ORAL	p.
<i>"Micro-photoluminescence from InAs/GaAs quantum dot pairs and molecules grown by droplet epitaxy"</i>		
Daniel Navarro-Urrios (MIND-IN2UB - Universitat de Barcelona, Spain)	ORAL	p.
<i>"Whispering gallery mode optical characterization on Si rich Si₃N₄ active microdisk resonators"</i>		
Manfred Niehus (Instituto de Telecomunicações - Polo Aveiro, Portugal)	ORAL	p.
<i>"Dispersion engineered tapered fiber photonic nanowires"</i>		
Alexey Nikitin (Universidad de Zaragoza, Spain)	ORAL	p.
<i>"Norton waves in Plasmonics"</i>		
Olalla Perez-Gonzalez (UPV/EHU - DIPC, Spain)	ORAL	p.
<i>"Optical spectroscopy of conductive molecular junctions in plasmonic cavities"</i>		

Pablo Aitor Postigo (IMM-CNM-CSIC, Spain)	ORAL	p.
<i>"Fabrication of two dimensional photonic crystal micro and nanocavities: from ultra low threshold lasers to solid-state quantum light emitters"</i>		
Fernando Ramiro Manzano (Centro de Tecnologías Físicas, Unidad Asociada CSIC-ICMM/UPV, Spain)	ORAL	p.
<i>"Influence of Corrugated Surfaces Templates in Colloidal Crystal Thin Films Growth"</i>		
Vincent Reboud (Catalan Institute of Nanotechnology and (ICN-CIN2), Spain)	ORAL	p.
<i>"Enhanced photoluminescence in printed 2D polymer photonic structures via surface plasmon enhancement"</i>		
Rogelio Rodriguez-Oliveros (Instituto de Estructura de la Materia - CSIC, Spain)	ORAL	p.
<i>"Plasmon Optical Nanoantennas: Characterization, Design, and Applications in Nanophotonics"</i>		
Juan Jose Saenz (Universidad Autónoma de Madrid, Spain)	ORAL	p.
<i>"Nanoparticle Dynamics in Non-Conservative Optical Vortex Fields"</i>		
Jose Sanchez-Dehesa (Universidad Politécnica de Valencia, Spain)	ORAL	p.
<i>"Anisotropic behavior of two-dimensional photonic crystals in the homogenization limit"</i>		
Pablo Sanchis Kilders (Valencia Nanophotonics Technology Center, Universidad Politécnica de Valencia, Spain)	ORAL	p.
<i>"Slow wave and resonator structures to enhance silicon photonic modulator performance"</i>		
Christian Seassal (Université de Lyon, INL - Institut des Nanotechnologies de Lyon, France)	INVITED	p.
<i>"Slow light in photonic crystals for photovoltaics"</i>		
Mario Sorolla (Universidad Pública de Navarra, Spain)	ORAL	p.
<i>"Study of terahertz extraordinary transmission resonances depending on polarization"</i>		
Johannes Stiegler (CIC nanoGUNE Consolider, Spain)	ORAL	p.
<i>"Nanoscale Free-Carrier Profiling of Individual Semiconductor Nanowires by Infrared Near-Field Plasmon Resonance Spectroscopy"</i>		
Francisco Javier Valdivia (ICMM-CSIC, Spain)	ORAL	p.
<i>"Light transport by sets and chains of Mie resonances: whispering gallery modes and localized plasmons. Effects on extraordinary transmission"</i>		
Claude Weisbuch (Ecole Polytechnique, France)	INVITED	p.
<i>"The Physics of Photonic Crystals LEDs"</i>		
Elisabet Xifre Perez (Centro de Tecnologías Físicas, Unidad Asociada CSIC-ICMM/UPV, Spain)	ORAL	p.
<i>"Add-drop filter based on silicon spherical microcavities"</i>		
Anatoly V. Zayats (The Queen's University of Belfast, United Kingdom)	INVITED	p.
<i>"New trends in plasmonic nanophotonics"</i>		

Poster Session (47)				
Presenting Author	Country	Topic	Poster Title	Page
Alphabetical Order				
Aguilo	Magdalena	Spain	nanophotonics applications	<i>Synthesis and characterization of optical nanocrystals. A step forward towards new promising transparent nanoceramics</i>
Alcaraz de la Osa	Rodrigo	Spain	nanophotonics applications	<i>An analysis of magnetic materials through an extension of the discrete dipole approximation</i>
Bello	Frank	Spain	nanophotonics applications	<i>Control of the index of refraction in coherently driven media with magnetoelectric cross coupling</i>
Campo	Giulio	Italy	plasmonics and extraordinary transmission	<i>Magneto-optical studies in magneto-plasmonic nano-structured particles</i>
Canet-Ferrer	Josep	Spain	photonic materials and photonic bandgap structures	<i>Determinaton of purcell effect in I7-type photonic crystal microcavities wth embedded inas/inp quantum wires</i>
Chamarro	Pedro	Spain	nanophotonics applications	<i>Organic MEMS/NEMS based bulk heterojunction photovoltaic cells with 3D electrodes</i>
Cos Corcoles	Joaquin	Spain	photonic materials and photonic bandgap structures	<i>Optical characterization of anisotropic porous silicon structures</i>
Costa Kramer	Jose Luis	Spain	plasmonics and extraordinary transmission	<i>Surface plasmon resonance in plastic optical fiber sensors: gold film orientation and thickness dependencies</i>
Diaz	Francesc	Spain	nanophotonics applications	<i>Synthesis and characterization of Tm doped Lu2O3 nanocrystalline powder</i>
Dominguez	Sagrario	Spain	photonic materials and photonic bandgap structures	<i>1D photonic crystal for solar cell applications</i>
Esteban	Ruben	Spain	plasmonics and extraordinary transmission	<i>Interplay between linear antenna modes and gap cavity modes within a single flat-gap nanoantenna</i>
Fernandez Torrado	Jorge	Spain	plasmonics and extraordinary transmission	<i>Transverse magneto-optical effects in Fe antidot arrays</i>
Ferre-Borrull	Josep	Spain	photonic materials and photonic bandgap structures	<i>FDTD study of quasi-random photonic structures obtained by electrochemical etching</i>
Froufe	Luis	Spain	photonic materials and photonic bandgap structures	<i>Enhanced optical gain in photonic crystals</i>
Garcia-Camara	Braulio	Spain	metamaterials	<i>Size Evolution of the Fröhlich Resonance for Magnetic Nanoparticles</i>
Garcia-Lopez	Oscar	Spain	nanophotonics applications	<i>Dual Core Antiguide (DCA): A new platform for active - passive photonic integration.</i>
Gomez-Medina	Raquel	Spain	photonic materials and photonic bandgap structures	<i>Radiative corrections to the polarizability tensor of an electrically small anisotropic dielectric particle</i>
Gutierrez Rodrigo	Sergio	Spain	plasmonics and extraordinary transmission	<i>Transmission of light through arrays of holes in "optically" thin films</i>
Hernandez	Sergi	Spain	nanophotonics applications	<i>Size dependence of nonlinear optical response in Si-nanocrystals</i>

Hernandez	David	Spain	photonic materials and photonic bandgap structures	<i>Controlling the optical properties of macroporous silicon structures</i>	
Huidobro	Paloma A	Spain	plasmonics and extraordinary transmission	<i>Transformation Optics for Plasmonics</i>	
Inclan	Luis	Spain	Metamaterials	<i>Miniaturization Strategies for Soft/Hard and High Impedance Surfaces Design at Microwaves Frequencies</i>	
Jacak	Witold	Poland	plasmonics and extraordinary transmission	<i>Plasmon-induced enhancement of light absorption in metallic nano-modified semiconductor</i>	
Le Gac	Gaelle	Spain	near field optics	<i>Impact of a SNOM probe on photonic crystal optical modes</i>	
Lopez Garcia	Martin	Spain	photonic materials and photonic bandgap structures	<i>Easy implementation tuning of self-assembled photonic-plasmonic crystals</i>	
Lopez-Tejeira	Fernando	Spain	plasmonics and extraordinary transmission	<i>In search of optimal performance for surface-plasmon Bragg mirrors</i>	
Marques-Hueso	Jose	Spain	near field optics	<i>Subwavelength focusing at optical frequencies achieved by an inverse designed photonic silicon integrated device</i>	
Marsal	Lluis	Spain	nanophotonics applications	<i>Synthesis and characterization of polymer nanopillars for photonic and optoelectronic applications</i>	
Martin Cano	Diego	Spain	plasmonics and extraordinary transmission	<i>Energy transfer between quantum emitters mediated by plasmonic waveguides</i>	
Martinez Maestro	Laura	Spain	nanophotonics applications	<i>Thermal imaging of liquids using luminescent NaYF₄:Yb³⁺,Er³⁺ nanoparticles.</i>	
Martinez-Marco	Mariluz	Spain	nanophotonics applications	<i>Plasmonic sensor based on gold nanodisc structures for sensing of toxic organic molecules</i>	
Mas	Sara	Spain	nanophotonics applications	<i>Analysis of chromatic dispersion in symmetric and asymmetric silicon slot waveguides</i>	
Mousavi	Sayed Hadi	Iran	photonic materials and photonic bandgap structures	<i>Synthesis and Nonlinear Optical Properties of AlN Nano-structures</i>	
Navarro-Urrios	Daniel	Spain	photonic materials and photonic bandgap structures	<i>Si nanoclusters coupled to Er³⁺ ions in a SiO₂ matrix for optical amplification</i>	
Nesterov	Maxim	Spain	plasmonics and extraordinary transmission	<i>Geometrically induced plasmonics from the optical to the terahertz regime</i>	
Paniagua Domínguez	Ramon	Spain	metamaterials	<i>Enhanced backscattering of light from randomly rough gratings on negative magnetic metamaterials</i>	
Pedruza Villalmanzo	Esteban	Spain	plasmonics and extraordinary transmission	<i>TiO₂/Au plasmonic nanocomposite for anti-reflection coatings</i>	
Postigo	Pablo Aitor	Spain	photonic materials and photonic bandgap structures	<i>Ultra low threshold room temperature lasing on photonic crystal microcavities with quantum wires</i>	

Prieto	Ivan	Spain	photonic materials and photonic bandgap structures	<i>Different strategies towards the deterministic coupling of a Single QD to a Photonic Crystal Cavity Mode</i>	
Rivas Gongora	David	Spain	photonic materials and photonic bandgap structures	<i>Thermal effects of quantum dots InAs/GaAs with In_xGa_{1-x}As confinement barriers</i>	
Rodriguez-Oliveros	Rogelio	Spain	plasmonics and extraordinary transmission	<i>Surface integral formulation for light scattering from 3D objects: surface plasmon resonances in metallic nanoantennas</i>	
Sanchez-Sobrado	Olalla	Spain	photonic materials and photonic bandgap structures	<i>Tailored Photoemission of Nanophosphors Embedded in Environmentally Responsive All-Nanoparticle based Optical Resonators.</i>	
Suarez Lacalle	Irene	Spain	nanophotonics applications	<i>Photonic Hall-effect for a single nanoparticle</i>	
Tomas-Navarro	Begoña	Spain	photonic materials and photonic bandgap structures	<i>Zero bandwidth mode on a split ring resonator loaded waveguide at cutoff</i>	
Truong	Vo-Van	Canada	plasmonics and extraordinary transmission	<i>Spectral Behaviour of Thick Metal Films Perforated with Nanoholes</i>	
Vitrey	Alan	Spain	near field optics	<i>Optical Near-Field Characterization of Plasmonic and Magnetoplasmonic Nanostructures</i>	
Yopez	Miztli	Spain	photonic materials and photonic bandgap structures	<i>Wave intensity fluctuations in small disordered systems</i>	

Poster Session (47)			
Presenting Author		Country	Poster Title
TOPIC: Metamaterials			
Garcia-Camara	Braulio	Spain	<i>Size Evolution of the Fröhlich Resonance for Magnetic Nanoparticles</i>
Inclan	Luis	Spain	<i>Miniaturization Strategies for Soft/Hard and High Impedance Surfaces Design at Microwaves Frequencies</i>
Paniagua Domínguez	Ramon	Spain	<i>Enhanced backscattering of light from randomly rough gratings on negative magnetic metamaterials</i>

Presenting Author		Country	Poster Title
TOPIC: Nanophotonics Applications			
Aguilo	Magdalena	Spain	<i>Synthesis and characterization of optical nanocrystals. A step forward towards new promising transparent nanoceramics</i>
Alcaraz de la Osa	Rodrigo	Spain	<i>An analysis of magnetic materials through an extension of the discrete dipole approximation</i>
Bello	Frank	Spain	<i>Control of the index of refraction in coherently driven media with magnetoelectric cross coupling</i>
Chamarro	Pedro	Spain	<i>Organic MEMS/NEMS based bulk heterojunction photovoltaic cells with 3D electrodes</i>
Diaz	Francesc	Spain	<i>Synthesis and characterization of Tm doped Lu2O3 nanocrystalline powder</i>
Garcia-Lopez	Oscar	Spain	<i>Dual Core Antiguides (DCA): A new platform for active - passive photonic integration.</i>
Hernandez	Sergi	Spain	<i>Size dependence of nonlinear optical response in Si-nanocrystals</i>
Marsal	Lluis	Spain	<i>Synthesis and characterization of polymer nanopillars for photonic and optoelectronic applications</i>
Martinez Maestro	Laura	Spain	<i>Thermal imaging of liquids using luminescent NaYF4:Yb3+,Er3+ nanoparticles.</i>
Martinez-Marco	Mariluz	Spain	<i>Plasmonic sensor based on gold nanodisc structures for sensing of toxic organic molecules</i>
Mas	Sara	Spain	<i>Analysis of chromatic dispersion in symmetric and asymmetric silicon slot waveguides</i>
Suarez Lacalle	Irene	Spain	<i>Photonic Hall-effect for a single nanoparticle</i>

Presenting Author		Country	Poster Title
TOPIC: Near Field Optics			
Le Gac	Gaëlle	Spain	<i>Impact of a SNOM probe on photonic crystal optical modes</i>
Marques-Hueso	Jose	Spain	<i>Subwavelength focusing at optical frequencies achieved by an inverse designed photonic silicon integrated device</i>
Vitrey	Alan	Spain	<i>Optical Near-Field Characterization of Plasmonic and Magnetoplasmonic Nanostructures</i>

Presenting Author		Country	Poster Title
TOPIC: Photonic Materials and Photonic Bandgap Structures			
Canet-Ferrer	Josep	Spain	<i>XPS and STM study of Metalorganic nanostructures</i>
Cos Corcoles	Joaquin	Spain	<i>Luminescent nanocomposites for photonic sensing</i>
Dominguez	Sagrario	Spain	<i>1D photonic crystal for solar cell applications</i>

Ferre-Borrull	Josep	Spain	<i>Development of superparamagnetic nanocomposite: The effect of nanoparticles dispersion and matrix structure on magnetic properties</i>
Froufe	Luis	Spain	<i>Application of gold nanocolloidal system to obtain gallium nitride nanowires by Sublimation Sandwich Method</i>
Gomez-Medina	Raquel	Spain	<i>Radiative corrections to the polarizability tensor of an electrically small anisotropic dielectric particle</i>
Hernandez	David	Spain	<i>Controlling the optical properties of macroporous silicon structures</i>
Lopez Garcia	Martin	Spain	<i>Easy implementation tuning of self-assembled photonic-plasmonic crystals</i>
Mousavi	Sayed Hadi	Iran	<i>Influence of boron on the nanocrystalline silicon films grown by plasma enhanced CVD</i>
Navarro-Urrios	Daniel	Spain	<i>Striking effect of temperature on conductivity of polyurethane/CNT nanocomposites</i>
Postigo	Pablo Aitor	Spain	<i>Ultra low threshold room temperature lasing on photonic crystal microcavities with quantum wires</i>
Prieto	Ivan	Spain	<i>Different strategies towards the deterministic coupling of a Single QD to a Photonic Crystal Cavity Mode</i>
Rivas Gongora	David	Spain	<i>Nanoparticle Electrofluidization</i>
Sanchez-Sobrado	Olalla	Spain	<i>Zero valent iron nanoparticles for in-situ remediation</i>
Tomas-Navarro	Begoña	Spain	<i>Cationic Surfactants Based on Renewable Raw Materials: New Emulsifiers for Elaboration of Nanoparticles of Dispersed Oil</i>
Yepez	Miztli	Spain	<i>Wave intensity fluctuations in small disordered systems</i>

Presenting Author	Country	Poster Title	
TOPIC: Plasmonics and Extraordinary Transmission			
Campo	Giulio	Italy	<i>Magneto-optical studies in magneto-plasmonic nano-structured particles</i>
Costa Kramer	Jose Luis	Spain	<i>Surface plasmon resonance in plastic optical fiber sensors: gold film orientation and thickness dependencies</i>
Esteban	Ruben	Spain	<i>Interplay between linear antenna modes and gap cavity modes within a single flat-gap nanoantenna</i>
Fernandez Torrado	Jorge	Spain	<i>Transverse magneto-optical effects in Fe antidot arrays</i>
Gutierrez Rodrigo	Sergio	Spain	<i>Transmission of light through arrays of holes in "optically" thin films</i>
Huidobro	Paloma A	Spain	<i>Transformation Optics for Plasmonics</i>
Jacak	Witold	Poland	<i>Plasmon-induced enhancement of light absorption in metallic nano-modified semiconductor</i>
Lopez-Tejeira	Fernando	Spain	<i>In search of optimal performance for surface-plasmon Bragg mirrors</i>
Martin Cano	Diego	Spain	<i>Energy transfer between quantum emitters mediated by plasmonic waveguides</i>
Nesterov	Maxim	Spain	<i>Geometrically induced plasmonics from the optical to the terahertz regime</i>
Pedruza Villalmanzo	Esteban	Spain	<i>TiO₂/Au plasmonic nanocomposite for anti-reflection coatings</i>
Rodriguez-Oliveros	Rogelio	Spain	<i>Surface integral formulation for light scattering from 3D objects: surface plasmon resonances in metallic nanoantennas</i>
Truong	Vo-Van	Canada	<i>Spectral Behaviour of Thick Metal Films Perforated with Nanoholes</i>

CEN2010

Segovia (Spain)

June 15-18, 2010

INVITED SPEAKERS

PLENARY SESSION

Advanced material models for nano-plasmonic systems

Kurt Busch

Institut für Theoretische Festkörperphysik
Karlsruhe Institute of Technology
76128 Karlsruhe, Germany
kurt@fpf.uni-karlsruhe.de

Plasmonic systems offer a tremendous potential for the controlled delivery and extraction of electromagnetic energy to and from metallic nano-particles as well as molecules and quantum dots that are located in their immediate vicinity. In view of the increasing sophistication of fabrication and spectroscopic characterization, quantitative computational approaches thus face the corresponding challenge of incorporating into their frameworks the strong nonlinear optical response of the metallic nano-structures themselves as well as the strongly modified light-matter interaction that is mediated by them.

In this talk, we report on our progress in applying the Discontinuous-Galerkin Time-Domain DGTD (DGTD) method to the quantitative analysis of nano-plasmonic systems. This includes the efficient modeling of complex geometric features via curvilinear finite elements, the improvement of the time-stepping scheme via a judicious choice of the numerical flux, and the incorporation of optically anisotropic media. In addition, we describe advanced material models that are based on a coupled-system dynamics approach. For instance, modified light-matter interactions in plasmonic systems can be treated via the Maxwell-Bloch equations and the nonlinear optical response of metallic nano-particles can be dealt with by treating the corresponding free electrons hydrodynamically, i.e., as a plasma in confined geometry.

Recent Progress on Photonic Metamaterials

Stefan Linden

Physikalisches Institut, Universität Bonn, Nußallee 12, 53115 Bonn, Germany
linden@physik.uni-bonn.de

At optical frequencies, electromagnetic waves interact with natural materials via the electronic polarizability of the materials. By contrast, the corresponding magnetizability is negligible. As a result, we can only directly manipulate the electric component of light while we have no immediate handle on the magnetic component.

Photonic metamaterials open up a way to overcome this constraint. The basic idea is to create an artificial crystal with sub-wavelength periods. Analogous to an ordinary optical material, such a photonic metamaterial can be treated as an effective medium. However, proper design of the elementary building blocks ("artificial atoms") of the photonic metamaterial allows for a non-vanishing magnetic response at optical frequencies - despite the fact that photonic metamaterial consist of non-magnetic constituents. This artificial magnetism can even lead to a negative index of refraction.

In this presentation, I will review our results and present new experiments on the spectroscopy of individual "artificial atoms", electrical tuning of magnetic metamaterials, coupling effects in metamaterials, and chiral metamaterials.

Slow light in photonic crystals for photovoltaics

Christian Seassal^a, Guillaume Gomard^{a,b}, Ounsi El Dair^{a,b}, Xianqin Meng^{a,b},
Emmanuel Drouard^a, Anne Kaminski^b, Alain Fave^b, Mustapha Lemiti^b

Université de Lyon, Institut des Nanotechnologies de Lyon-INL, UMR CNRS 5270

^aEcole Centrale de Lyon, F-69134 Ecully, France

^bINSA Lyon, F-69621 Villeurbanne, France

Christian.Seassal@ec-lyon.fr

Thanks to the development of nanophotonics, new concepts have recently been proposed to control light trapping and absorption efficiency in photovoltaic (PV) solar cells. These approaches may be based on the surface plasmons, diffraction on a patterned surface, or light coupling into photonic crystal (PC) Bloch modes. Absorption control is all the more important in the case of PV cells based on very thin absorbing layers: for cost issues but also considering the limited carrier diffusion length in such materials, their thickness should be kept as low as possible, which is generally achieved at the expense of the conversion efficiency.

In this communication, we will report on the increase of the absorption efficiency in very thin layers of absorbing materials, periodically patterned as planar PCs. This enables to couple the incident light into the absorbing medium, and to control the photon "lifetime", in particular through the use of surface addressable slow light resonances.

We will illustrate the interest of this generic concept with an absorbing medium of hydrogenated amorphous silicon (a-Si:H). Patterning such layers may be achieved using low cost technologies like laser holography or nanoimprint. We will show both theoretically and experimentally that this way of photon trapping may be used to control the absorption over a very wide spectral range. The absorption efficiency may be increased by 50% in the whole 300-750nm range, just by drilling a 1D or 2D photonic lattice within the layer. Additionally, due to the intrinsic nature slow light modes, the absorption efficiency is relatively independent to the angle of incidence. We will also show how such an absorbing PC can be integrated in a typical thin film solar cell structure, including transparent and metallic electrode; these additional layers enable a further control of light trapping and of the photon lifetime in the absorbing layer.

The Physics of Photonic Crystals LEDs

C. Weisbuch

Laboratoire de Physique de la Matière Condensée, CNRS, Ecole Polytechnique, Palaiseau,
France and Materials department, UCSB, Santa Barbara, CA, USA

Photonic crystal (PhC) based LEDs display a rare blend of fundamental and applied concepts in semiconductor physics.

This is due to the fact that the properties of PhC-LEDs rely on a mix of intrinsic optical properties of the materials (most often nitrides these days) originating from their electronic structure and of electromagnetic properties of the PhC.

Focussing on the latter, PhC LED studies allow in-depth understanding of properties of PhCs such as determination of their key parameters (real and imaginary dispersion curves of the band structures for instance). This is to be contrasted with studies dealing with the better established confinement properties of PhCs which rely on non-propagating modes in the photonic forbidden bandgap and therefore mainly explore bandgap states, whereas PhC LEDs allow to explore propagating states of the photonic band structures.

In a series of recent papers in the nitride materials system, we have determined band structures of PhC lattices such as triangular¹ and Archimedean tilings². These studies are a clearcut example how physics in devices is a powerful tool to extract fundamental properties of matter (here light propagation in periodic structures).

Turning to studies of physics of devices led to explore various structures which could pave the way to ultimate efficiency LEDs. We showed³ in particular that the optimum PhC structures would depend on the materials' index of refraction, being the triangular lattice for nitrides, while lattices with more nearest neighbours, such as Archimedean tilings lattices, are required for GaAs materials due to their higher index of refraction. We also showed that surface PhC structures have some limitations to extract low order guided modes while embedded PhC structures appear to be optimum⁴.

Applications are here of major importance: PhC LEDs could be a favoured solution for ultra-high efficiency LEDs to be used in tomorrow's solid state lighting, with foreseen huge energy savings. The challenge is very actual as several states and countries are on the verge of forbidding sales of incandescent light bulbs in favour of higher efficiency solutions, and as today's preferred one is the high efficiency compact fluorescent lamp (CFL) due to its availability and low cost. The challenge to PhC LEDs is to reach efficiencies similar to CFLs or higher, with fabrication technologies allowing large volume production, low cost and high fabrication yield.

References

¹ A. David et al. Applied Physics Letters 87, 101107, 2005

² A. David et al., Applied Physics Letters 88 073510 2006

³ A. David, H. Benisty H and C. Weisbuch, IEEE Journal of Display Technology, 3, 133-48. 2007

⁴ E. Matioli et al., Applied Physics Letters 96 031108, 2010

New trends in plasmonic nanophotonics

Anatoly V. Zayats

Centre for Nanostructured Media, The Queen's University of Belfast,
Belfast BT7 1NN, United Kingdom

a.zayats@qub.ac.uk

<http://www.nano-optics.org.uk>

Recent advances in nanofabrication and subwavelength optical characterisation have led to the development of a new area of nanophotonics concerned with routing and conditioning of optical signals in scalable and integratable devices. In this context, plasmonics which is dealing with surface electromagnetic excitations in metallic structures, may provide a great deal of flexibility in photonic integration in all-optical circuits since with surface plasmons the problem of light manipulation can be reduced from three to two dimensions. Surface plasmon polaritons, the electromagnetic excitations coupled to collective motion of conduction electrons near a metal surface, are emerging as a new optical information carrier that enables signal manipulation and processing on the subwavelength scale. Plasmonic metamaterials play crucial role in the development of novel paradigms such as negative refractive index engineering, superlensing and optical cloaking.

A variety of passive plasmonic elements such as mirrors, lenses, waveguides, resonators, etc. have been demonstrated. The development of active plasmonic elements capable of controlling light on the nanoscale dimensions with external electronic or optical stimuli is on the agenda.

In this paper we will discuss various realisations of plasmonic components for integrated nanophotonic circuits with particular emphasis on the active functionalities such all-optical and electro-optical modulation and amplification of plasmonic signals, dispersion management dispersion management. These functionalities facilitate possible applications of plasmonics in telecommunication networks, integrated photonics and lab-on-a-chip systems.

CEN2010

Segovia (Spain)

June 15-18, 2010

ORAL CONTRIBUTIONS

PLENARY SESSION

Ag-polymer nanocomposites for LSPR sensing

Rafael Abargues*, J. Marques-Hueso, R. Gradess, J. Canet-Ferrer, J. L. Valdés, J. P. Martínez-Pastor

Instituto de Ciencia de los Materiales, Universidad de Valencia, P.O. Box 22085, 46071 Valencia, Spain.

*Rafael.Abargues@uv.es

In the past decade, plasmon-based optical sensors have been one of the most preferred sensing platforms for detection of biomolecules with high sensitivity and low cost. It is well-known that SPR/LSPR strongly depends on the refractive index of the surrounding medium (substrate, solvent, and adsorbates) of the surface/nanostructure [1]. In this work, we present a novel LSPR sensing platform based on Ag nanoparticles (NPs) embedded in a polymer thin film [2]. Ag NPs are in situ synthesized inside the host polymers by a one-step procedure during the bake step of the formation of a nanocomposite thin film (Fig. 1).

We have used polyvinyl alcohol (PVA) and Novolac as the host polymers for Ag NPs due to the ability of the secondary alcohol and phenolic groups to reduce Ag(I) to Ag(0), their excellent film forming properties and optical transparency. Moreover, they are hydrogels, this is, they can swell in aqueous medium and retain a significant amount of water within its structure without dissolving. As a result, water and analyte diffusion is allowed. Additionally, these materials can be also the basis to fabricate biochip sensors since they can be patterned by e-beam and UV lithography [3,4,5]. To validate the use of Ag nanocomposite thin film as a potential chemosensor/biosensor, we used 2-mercaptoethanol (HSCH₂CH₂OH) as analyte, because thiols interact very strongly with metal surface. The typical procedure for the analyte binding reaction simply consists on immersing the nanocomposite thin film in the analyte solution for several minutes to achieve the maximum chemisorption of the analyte molecules.

Fig. 2a exhibits the LSPR absorption curve of the Ag-PVA nanocomposite thin film before and after immersing into an analyte aqueous solution of 5×10^{-6} M for 180 min. As can be observed, the LSPR of an Ag-PVA film significantly changes in wavelength, intensity and FWHM. These curves can be nicely fitted by Lorentzian functions in order to obtain more precise values of all spectroscopic parameters: λ_{LSPR} , FWHM (Γ_{LSPR}) and peak intensity, before/after immersing the thin film into the analyte solution for a given concentration. The chemisorption of 2-mercaptoethanol on metal NPs embedded in the polymer thin film is irreversible due to the strong interaction of the Ag-S bond. As a result, the analyte cannot be desorbed to return the nanosensor to its initial state. This is not a limitation since this nanocomposite-based sensor is easy-to-prepare, easy-to-use and low-cost, which are the bases of a fully disposable sensing platform technology.

We demonstrate chemosensing capabilities of Ag-PVA nanocomposite with a LOD below 20 nM, by measuring either the LSPR wavelength shift ($\Delta\lambda_{\text{LSPR}}$) as a function of the analyte concentration (Fig. 2b). $\Delta\lambda_{\text{LSPR}}$ is taken as representative of the change in the dielectric environment of the NPs. The sensor response to the analyte can be tuned by varying the nanocomposite properties such as film thickness and nanoparticle concentration.

We observed a similar behaviour for Ag-Novolac nanocomposite. Fig. 3a shows the LSPR absorption of an Ag-Novolac film for different immersing times into a 2-mercaptoethanol aqueous solution of 0.01 M. The analyte binding at Ag NPs is strongly time-dependent. The main advantage of this nanocomposite is the possibility of miniaturization due to its lithographic properties. Fig. 9b shows an example of the fabrication of LSPR-based microsensors by means of UV-lithography. We observe in Fig.3b an optical microscope image of a 100 μm -side square structure of Ag-DNQ-Novolac nanocomposite before and after the analyte binding reaction. We notice a significant difference in the absorption of the nanocomposite after 48 hours of immersion into the analyte solution.

PVA and Novolac-based Ag nanocomposites can be used as qualitative or semi-quantitative sensor for thiol molecules (and possibly quantitative for other molecules). Moreover they provide a fast, non-expensive and large-scale fabrication method for plasmonic devices. Because the proposed nanocomposites are easy-to-prepare, easy-to-use and low-cost, a fully disposable sensing platform technology may be developed on it.

References

- [1] J.N. Anker, W.P. Hall, O. Lyandres, N.C. Shah, J. Zhao, and R.P. Van Duyne, *Nature Materials* **7**, (2008), 442.
- [2] Gradess R, Abargues R., Habbou A., Canet-Ferrer J., Pedrueza E., Russell A., Valdés J.L.,

Martínez-Pastor J.P. *J Mater Chem*, **19**, (2009), 9233-9240.

[3] Abargues, R.; Marques-Hueso, J.; Canet-Ferrer J.; Pedrueza E.; Valdes J.L.; Jimenez E.; Martínez-Pastor, J. P. *Nanotechnology*, **19**, (2009), 355308.

[4] Marqués-Hueso J, Abargues R, Canet-Ferrer J, Agouram S, Valdés JL, Martínez-Pastor JP, **26**, (2010), 2825-30.

[5] Marqués-Hueso J, Abargues R, Valdés JL, Martínez-Pastor JP, *ACS Nano* submitted (2010)

Figures



Fig 1. A) Schematic steps involved in the formation of Ag-PVA nanocomposite thin film; B) Image of the Ag-PVA film spincoated on soda-lime glass and C) TEM image..

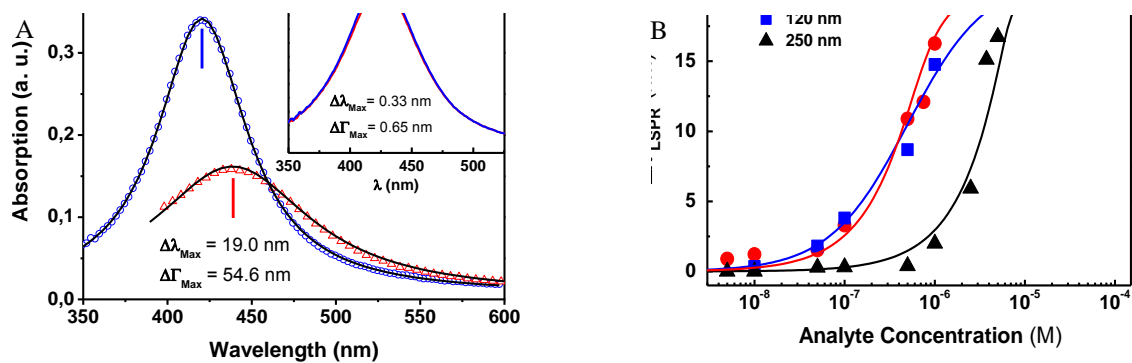


Fig 2: a) LSPR curve of a Ag-PVA thin film before and after immersing on an aqueous solution of mercaptoethanol during 180 min. The effect of pure water is shown as an inset of this figure. B) $\Delta\lambda_{LSPR}$ response of Ag-PVA nanosensors as a function of the mercaptoethanol concentration for different film thickness: 80, 130 and 250 nm.

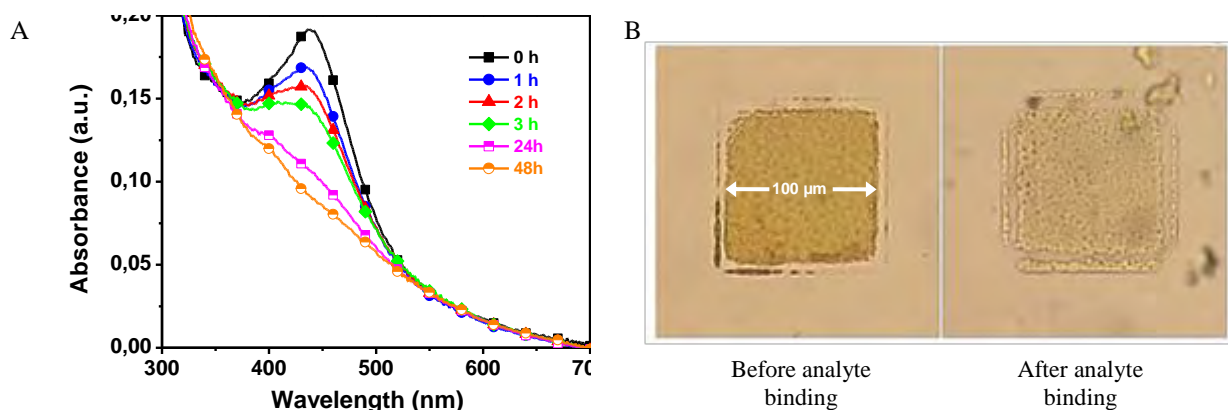


Fig 3. Absorbance of a Ag-Novolac film immersed in a 0.01 M Mercaptoethanol-water solution. b) 100 μm -side square microstructures of Ag-Novolac nanocomposite before (left) and after (right) immersion in the mercaptoethanol solution.

Plasmonics with new materials: Gallium. A comparison between experiment and a numerical model based on the Discrete Dipole Approximation (DDA)

P. Albella^{1,6}, Pae C Wu², Tong-Ho Kim², April S. Brown², Yang Yang³, M. Losurdo⁴, G. Bruno⁴, J.M. Saiz¹, F. González¹, G. Videen⁵, H. O. Everitt^{2,3} and F. Moreno¹

1) *Group of Optics. Department of Applied Physics. University of Cantabria. 39005 Santander (Spain)*

2) *Department of Electrical and Computer Engineering. Duke University. Durham. North Carolina 27708 (USA)*

3) *Department of Physics. Duke University. Durham. North Carolina 27708 (USA)*

4) *Institute of Inorganic Methodologies and of Plasmas-CNR, and INSTM. Via Orabona, 4-70126 Bari (Italy)*

5) *U.S. Army Research Laboratory, AMSRD-ARL-CI-ES, 2800 Powder Mill Road, Adelphi, Maryland 20783 (USA)*

6) *Donostia International Physics Center, DIPC Paseo Manuel Lardizabal 4, Donostia-San Sebastian, 20018. (Spain)*

morenof@unican.es

The optical properties of metal nanoparticles (NPs), especially those made of silver and gold, have attracted the interest of many researchers during the last fifteen years for their use in many nanotechnology applications. These include biosensing, optical communications, nanocircuitry, SERS, microscopy, emission and absorption enhancements of photonic devices and plasmonic waveguiding [1-8]. Unlike gold and silver nanoparticles, which exhibit localized surface plasmon resonances (LSPR's) primarily in the visible and IR wavelengths, other elements, like Gallium, present an interesting resonant behavior in the UV spectral region [9]. Recently, it has been shown that such material deposited on substrates can be an interesting alternative for the development of new plasmonic devices working at UV photon energies [10].

One of the tasks of this research is to analyze numerically the plasmon resonances shown by Gallium NPs deposited on Sapphire substrates, as measured by Wu et al. [10] (Fig. 1). We explore the behavior of these resonances as a function of different system parameters, such as particle size and geometry, polydispersity, particle geometrical distribution, etc. (Figs 2 a,b). The numerical simulations have been performed using the Discrete Dipole Approximation (DDA) method, [11]. This has proven extremely useful when dealing with NPs interacting with substrates [12, 13].

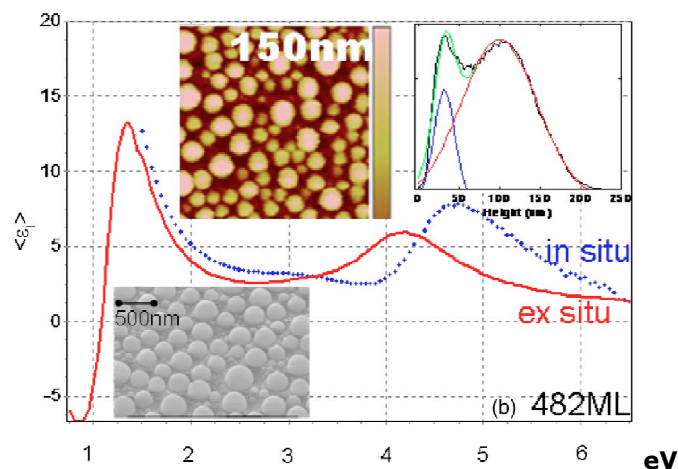


Fig 1. (a) Absorption spectrum of Ga nanoparticles deposited on sapphire substrates (see bottom inset of a SEM image). Upper right inset shows a sample histogram from AFM images (upper left inset) that reveals a bimodal distribution of particle sizes (see ref [10] for more details).

Our DDA simulations show the dependence of different aspects of morphology on the resulting spectra. The spectra can be interpreted as the result of a combination of different effects. Our results shown in Figure 2 suggest that the small particles (≈ 40 nm) contribute mainly to the high energy resonance (Fig. 2a), and the large particles (≈ 100 nm) contribute to the low energy peak (Fig. 2b). Interaction between NPs also plays a role, as the orientation of interacting NPs transverse or longitudinal to the incident scattering plane may shift the resonances or enhance certain regions of the spectra. Finally, transverse and longitudinal effects due to the incident polarization (circularly polarized in the experiment) were considered (a contribution to the explanation of these effects was already suggested in [10]).

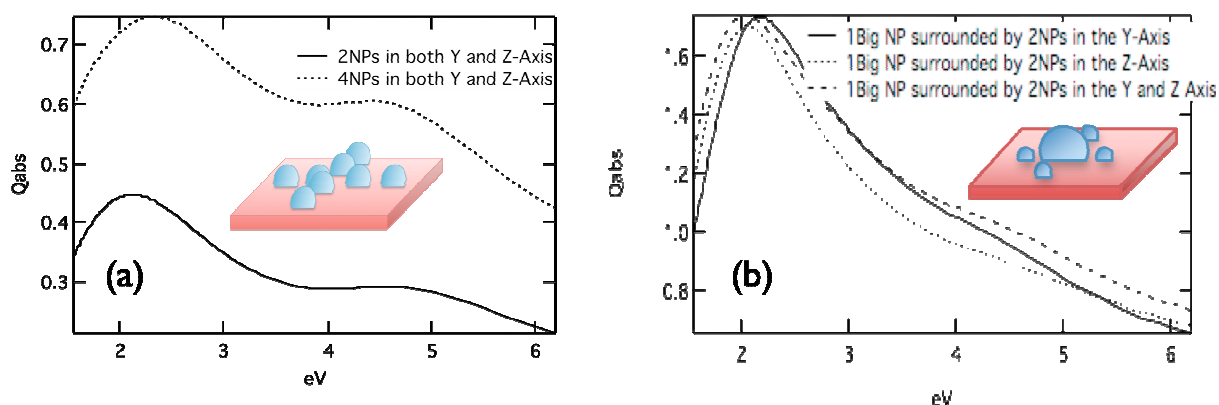


Fig. 2 Numerical DDA calculation of the absorption efficiency for the geometrical configuration shown in each respective inset (see text for details). a) Small-particle configuration. b) Large-small particle configuration.

References

- [1] J. J. Mock, M. Barbic, D. R. Smith, D. A. Schultz, and S. Schultz, *J. Chem. Phys.* **116** (2002), 6755
- [2] E. Hutter and J. H. Fendler, *Adv. Mater. (Weinheim, Ger.)* **16** (2004), 1685
- [3] A. Maier and H. Atwater, *J. Appl. Phys.* **98** (2005), 011101
- [4] A. V. Krasavin, K. F. MacDonald, A. S. Schwanecke, and N. I. Zheludev, *Appl. Phys. Lett.* **89** (2006), 031118
- [5] T. Kalkbrenner, U. Hakanson, A. Schädle, S. Burger, C. Henkel, V. Sandoghdar, *Phys. Rev. Lett.* **95** (2005), 200801
- [6] N. Engheta, *Science* **317** (2007), 1698
- [7] R.G. Freeman, K.C. Grabar, K.J. Allison, R.M. Bright, J.A. Davis, A.P. Guthrie, M.B. Hommer, M.A. Jackson, P.C. Smith, D.G. Walter, and M.J. Natan, *Science* **267** (1995), 1629
- [8] H.A. Atwater and A. Polman, *Nat. Materials* **9** (2010), 205
- [9] E.J. Zeman and G.C. Schatz, *J. Phys. Chem.* **91** (1987), 634
- [10] P.C. Wu, T. Kim, A.S. Brown, M. Losurdo, G. Bruno and H.O. Everitt, *Appl. Phys. Lett.* **90** (2007), 103119
- [11] B. T. Draine and P. J. Flatau, User Guide for the Discrete Dipole Approximation Code DDSCAT 6.1 (2004), <http://arxiv.org/abs/astro-ph/0409262v2>.
- [12] K.L. Kelly, E. Coronado, L.L. Zhao and G.C. Schatz, *J. Phys. Chem B* **107** (2003), 668
- [13] P. Albella, F. Moreno, J. M. Saiz, and F. González, *Opt. Express* **16** (2008), 12872

Acknowledgements

This research has been supported by MICINN (Ministerio de Ciencia e Innovación) through project FIS2007-60158, by USAITC-A (US Army International Technology Centre-Atlantic) through project R&D1390-PH-01 and by the U.S. Army Aviation and Missile RD&E Center. The authors thankfully acknowledge this support and also the computer resources provided by the *Red Española de Supercomputación* node *Altamira* at the Instituto de Física de Cantabria.

Organic second-order distributed feedback lasers fabricated by nanoimprint lithography

V. Trabadelo¹, A. Juarros¹, A. Retolaza¹, S. Merino¹, I. Alonso¹, V. Navarro-Fuster², M.G. Ramirez², P.G. Boj², I. Vragovic², J.M. Villalvilla², J.A. Quintana², M.A. Díaz-García²

¹Micro and Nanotechnology Department, Tekniker, Avda. Otaola 20, 20600 Eibar, Spain

²Instituto Universitario de Materiales de Alicante, Universidad de Alicante, 03080 Alicante, Spain
ialonsovillanueva@tekniker.es

Solid-state lasers based on semiconducting polymers have become an active field of research in the past few years [1]. Polystyrene (PS) films doped with perylenediimide (PDI) derivatives have shown a great potential in this regard due to its highly photostable optically-pumped amplified spontaneous emission (ASE) at low threshold [2]. On the other hand, the use of distributed feedback (DFB) structures as resonant cavities, significantly enhance the lasing properties of organic materials, providing single-mode emission and lower pumping thresholds [1]. In order to get such a structured medium, nanoimprint lithography (NIL) is one of the most promising techniques for grating fabrication, even for future industrial applications, because its high throughput, low cost and high fidelity pattern transfer.

In this work we first present the fabrication by thermal NIL and dry etching of second-order DFB gratings in SiO₂ (periodicity of 368 nm and equal line and space) on which PS films doped with 0.5 wt% of a PDI derivative were spin-coated afterwards [3]. Several grating depths (340, 220 and 105 nm) were obtained by varying the etching time. Furthermore, we also imprinted DFB gratings directly on the active material using the same master stamp. This way the dry-etching step can be avoided, so the fabrication process for this kind of devices becomes more cost-effective.

Both types of lasers showed highly photostable laser emission at around 572 nm, when pumped at 533 nm with a pulsed Nd:YAG laser. This wavelength is close to 570 nm, which constitutes the second low-loss transmission window in poly(methylmethacrylate). Hence, they could be particularly interesting in the field of data communications based on polymer optical fibres. On the other hand, as shown in the figure below, thresholds were drastically reduced with respect to the ASE threshold of a sample without grating. Moreover, the performance of the devices with gratings directly embossed on the doped PS film was superior, in terms of threshold, than that of devices with gratings fabricated on SiO₂.

Acknowledgements: This work is funded by the “Ministerio de Ciencia e Innovación” and the European Community (FEDER) through grant MAT2008-06648-C02. MGR is supported by a CSIC fellowship within the program JAE.

References:

- [1] I. D.W. Samuel, G.A. Turnbull, Chem. Rev., **107** (2007) 1272.
- [2] E. M. Calzado, J. M. Villalvilla, P.G. Boj, J. A. Quintana, R. Gómez, J. L. Segura, M. A. Díaz-García, Appl. Opt., **18** (2007) 3836.
- [3] V. Trabadelo, A. Juarros, A. Retolaza, S. Merino, M.G. Ramírez, V. Navarro-Fuster, J.M. Villalvilla, P.G. Boj, J.A. Quintana, M.A. Díaz-García, Microelectron. Eng., **87** (2010) 1428

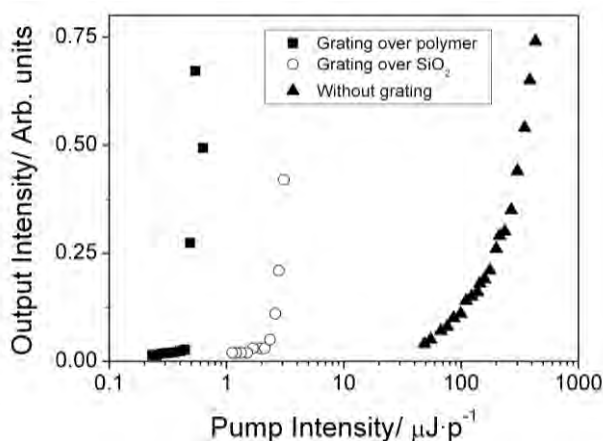


Figure. Output intensity versus pump intensity for DFB devices with gratings on the polymer and on SiO₂. For comparison purposes, data for a film deposited on SiO₂ without grating are included.

Phononic antennas

P. Alonso-González^{1*}, M. Schnell¹, I. Fernández-Martínez², J. Martínez² and R. Hillenbrand^{1,3}

¹ Nanooptics Laboratory, CIC nanoGUNE, 20018, Donostia-San Sebastian, Spain

² Microelectronics Institute of Madrid (IMM-CNM-CSIC), 28760, Tres Cantos, Madrid, Spain

³ IKERBASQUE, Basque Foundation for Science, 48011 Bilbao, Spain

palonso@nanogune.eu

Optical and infrared antennas based on metal nanostructures have been widely studied during the last years in the field of nanophotonics. Their capability to confine and enhance optical fields at deep sub-wavelength scales via the formation of surface plasmon polaritons [1] has led to the development of novel devices ranging from nanoscale photo-detectors [2] to highly sensitive nanobiosensors [3].

At mid-infrared frequencies also surface phonon polaritons exist. Despite their sharp polaritonic resonances [4] and application potential in nanophotonics [5,6], these infrared counterparts to surface plasmon polaritons have been barely explored for the design of antenna structures. As surface phonon polaritons rely on the infrared or terahertz excitation of lattice vibrations in polar crystals, they offer totally different material classes for antenna fabrication, such as semiconductors and insulators. Here we present, for the first time, the design, fabrication and characterization of SiC “phononic antennas”, which exhibit fundamental dipolar antenna resonances at around 10 μm wavelengths. Analogous to plasmonic antennas, strong field confinement and enhancement is achieved by localized surface phonon polariton excitation.

The figure shows the topography and near-field images of a 35 nm thick SiC antenna of 700 nm in diameter. The images were taken by scattering-type scanning near field optical microscopy (s-SNOM) [7], which allows recording both amplitude and phase of the z-component of the antenna near fields. The imaging wavelength was $\lambda_{\text{in}}=10.78 \mu\text{m}$. We observe strong near-field amplitude signals at the disk edges according to the polarization of the incident electric field. At the disk center a phase jump of about 180° occurs, which indicates that the enhanced fields at the disk edges oscillate in opposite direction. This provides direct experimental evidence of a strong dipolar near-field mode in a deep subwavelength-scale antenna structure as small as $\lambda/15$.

Altogether, our results show that antenna properties such as confinement and enhancement of optical fields can be achieved by non-metallic “phononic” structures, which opens a new route for the manipulation and control of mid-infrared fields at deep sub-wavelengths scales.

References

- [1] M. Schnell, A. Gracia-Etxarri, A. J. Huber, K. Crozier, J. Aizpurua and R. Hillenbrand, *Nature Photonics*, **3**, (2009) 287.
- [2] L. Tang, S. E. Kocabas, S. Latif, A. K. Okyay, D-S. Ly-Gagnon, K. C. Saraswat and D. A. B. Miller, *Nature Photonics*, **2**, (2008) 226.
- [3] H. Xu, E. J. Bjerneld, M. Käll and L. Börjesson, *Physical Review Letters*, **83**, (1999) 4357.
- [4] R. Hillenbrand, T. Taubner and F. Keilmann, *Nature*, **418**, (2002) 159.
- [5] A. J. Huber, B. Deutsch, L. Novotny and R. Hillenbrand, *Appl. Phys. Lett.*, **92**, (2008) 203104.
- [6] J. A. Schuller, T. Taubner and M. L. Brongersma, *Nature Photonics*, **3**, (2009) 658.
- [7] F. Keilmann and R. Hillenbrand, *Philos. Trans. R. Soc. London, Ser. A*, **362**, (2004) 787.

Figures

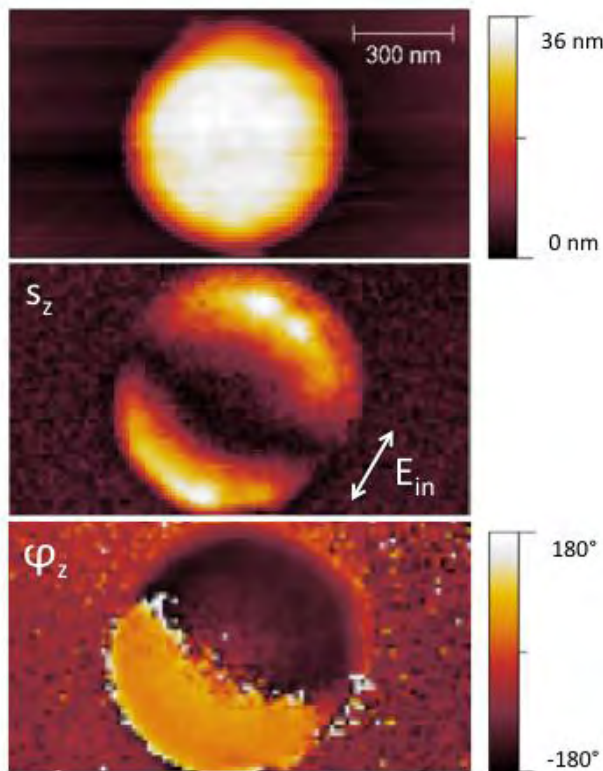


Figure. Topography and near-field images of a 35 nm-thick SiC disk on a SiC substrate at a wavelength of $\lambda=10.78 \mu\text{m}$. The images labeled as S_z and φ_z show the amplitude and phase of the near-field z-component, respectively

Optical control of the exciton diffusion length in organic solar cells

Rafael Betancur¹, Xavier Elias¹, Saverio Pasini¹, Luat T. Vuong¹, Roberto Macovez¹ and Jordi Martorell^{1,2}

¹ICFO-Institut de Ciències Fòtoniques, 08860 Castelldefels (Barcelona), Spain

²Departament de Física i Enginyeria Nuclear, Universitat Politècnica de Catalunya, 08222 Terrassa (Barcelona),
rafael.betancur@icfo.es

One of the bottlenecks to high efficiency in organic solar cells (OSC) is constituted by the short diffusion length of excitons. Typically this diffusion length is on the order of 10nm which is many times shorter than the absorption length of many of the materials employed in organic photovoltaics. One way around this problem came with the bulk hetero-junction OSCs. However, this device architecture limits the ability of the separated charges to reach the electrodes, and an optimization of the efficiency of the device would require a controlled 3-D nano-structuring to provide the proper channels to increase the mobility of these charges.

An alternative route was recently proposed and consists in using an optical cavity to increase the diffusion length [1]. It was shown that it is possible to increase the exciton lifetime by changing the electromagnetic environment of the exciton when placing a high quantum yield fluorescence photovoltaic materials within a non-symmetric optical cavity. As in the Purcell effect [2], the spontaneous emission of the radiative system in the excited state (exciton) is inhibited. Numerical calculations in Ref. [1] indicated that by using a device architectural design where the electrodes are a high reflecting mirror and a thin metal forming a non symmetric optical cavity, one would be able to enhance the efficiency of an OSC by 3 times. Additional numerical results also from Ref. [1] showed that this factor could be further increased to about 5 or 6 times if additional nano-structuring were introduced. If we consider that bi-layer OSC can have efficiencies of up to 3%, by implementing such photonic control one would be able to achieve OSC with 15% efficiency or higher.

To achieve such efficiencies, however, there are many hurdles that must be overcome. Although highly fluorescent polymers such as PPV or MEH-PPV have shown good photovoltaic properties when combined with the appropriate electron acceptor [3], the best organic electron acceptors, such as fullerenes, do not show much fluorescence at all. Laser dyes such as rhodamines which are highly fluorescent in solution and have shown good electron acceptor behavior [4], when packed in a solid film, their fluorescence is quenched down to a value below 1%. Another major issue is that the most common OSC device architecture uses an ITO layer as a transparent electrode. To form an open optical cavity one would require two metallic electrodes which could act as good conductors as well as mirrors to control the fluorescence.

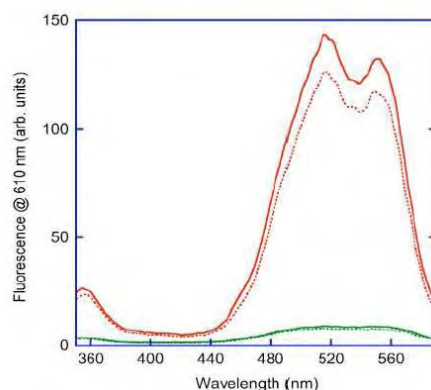


Fig. 1 Fluorescence measured at 610 nm when the pumping wavelength changes from 350 to 590 nm. The fluorescence of a thin solid sample of bare Rh6G is shown in green when deposited on an exciton blocking (solid line) or quenching (dashed line). The fluorescence of Rh6G linked to a PMMA backbone is shown in red when deposited on an exciton blocking (solid line) or quenching (dashed line). In the Rh6G-PMMA sample, PAA was added as a spacer between the Rh6G-PMMA chains.

Here we show, on the one hand, that by chemically binding highly fluorescent chromophores in a non-conjugated polymer chain, the fluorescent quantum yield in a solid film can be enhanced by more than 16 times. On the other hand, the route to provide an optical cavity control of the fluorescence is achieved by replacing the ITO electrode in a bi-layer cell with an ultrathin metal electrode. The organic bi-layer is sandwiched in between such electrode which is partially reflecting in the region where the organic active layer fluoresces, and another which is a good conductor and acts as a highly reflecting mirror.

The comparison between the fluorescence of spin-coated Rhodamine 6G (Rh6G) and the Rh6G chemically bound to the PMMA backbone is shown in Fig. 1. When comparing the red and green curves from Fig. 1, we observe that the fluorescence efficiency increases by more than 16 times. In the same figure we show the comparison of the fluorescence when the solid layer is deposited on an exciton blocking or quenching substrate. These preliminary results seem to indicate that the polymer backbone does not affect negatively the exciton diffusion length.

Table 1 Comparison of the working parameters of an OSC when the bottom electrode is an ITO substrate or a thin metal electrode which is partially reflecting at the fluorescent band of the photovoltaic material used.

Semi-transparent contact	Reflectivity (%)	Current (mA/cm ²)	V _{oc} (mV)	Fill factor (%)
ITO	9.8	-0.33±0.07	1026±18	34±2
5 nm metal	11,77±0,90	-0.086±0.011	946±45	25±2
10 nm metal	24,37±1,46	-0.074±0.017	934±53	25±2
15 nm metal	37,01±2,13	-0.025±0.006	782±77	17±3

We have also studied the performance of an OSC when the ITO transparent electrode is replaced by a thin metal electrode that could be used to form the fluorescence control optical cavity. Preliminary results which are summarized in Table 1 indicate that when a 10 nm thick metal electrode is used the reflectivity is close to 25% while the parameters that characterize the solar cell are similar to those of the cell fabricated with a 5 nm electrode which exhibits a reflectivity of only 12%. Open circuit voltage is considerably high for all the fabricated cells, however, there is a significant reduction of the short circuit current for the cells with the metal electrodes relative to the one that uses ITO. It is expected that an optimization of the metal composition of such electrode will significantly reduce such difference.

In summary, we have been able to establish the route to fabricate OSC where the exciton diffusion length can be controlled using an optical cavity. We have shown that it is possible to partially prevent the fluorescence quenching of molecular dyes in solid by fixing the position of the chromophore to a polymer backbone. Preliminary results indicate that it is possible to fabricate OSC using only metals as electrodes. The reflectivity provided by the semitransparent electrode of the solar cells we fabricated is sufficient to form the optical cavity necessary to control the exciton diffusion length in cells fabricated with high quantum yield fluorescent materials. The results presented open the route to fabricate highly efficient bi-layer organic cells.

References

- [1]. Luat T. Vuong, Gregory Kozyreff, Rafael Betancur, and Jordi Martorell, "Cavity-controlled radiative recombination of excitons in thin-film solar cells," *Appl. Phys. Lett.* 95, 233106 (2009).
- [2]. E. M. Purcell, "Spontaneous emission probabilities at radio frequencies," *Phys. Rev.* 69, 37 (1946).
- [3]. Maksudul M. Alam and Samson A. Jenekhe, "Efficient Solar Cells from Layered Nanostructures of Donor and Acceptor Conjugated Polymers," *Chem. Mater.* 16, 4647-4656 (2004).
- [4]. Kohshin Takahashi, Jyun-ichi Nakamura, Takahiro Yamaguchi, Teruhisa Komura, Shoji Ito, and Kazuhiko Murata, "Enhanced Photocurrent Quantum Yield by Electronic Interaction between Zinc Porphyrin and Rhodamine B Molecules in Al/Dye/Au Sandwich-Type Solar Cell," *J. Phys. Chem. B* 101, 991-997 (1997).

Localized Extraordinary Optical Transmission through sub-wavelength apertures

S. Carretero-Palacios¹, Sergio G. Rodrigo¹, L. Martín-Moreno¹, F.J. García-Vidal²

¹Instituto de Ciencia de Materiales de Aragón and Departamento de Física de la Materia Condensada, CSIC-Universidad de Zaragoza, E-50009 Zaragoza, Spain

²Departamento de Física Teórica de la Materia Condensada, Universidad Autónoma de Madrid, Madrid 28049, Spain
sol@unizar.es

Introduction

Sub-wavelength apertures periodically arranged may transmit electromagnetic waves beyond the cut-off wavelength with a much higher intensity than if they were isolated. Confined electromagnetic modes at each side of a metal film may provide an efficient tunneling channel for photons passing through such array of holes. This is the so-called Extraordinary Optical Transmission [1].

Results

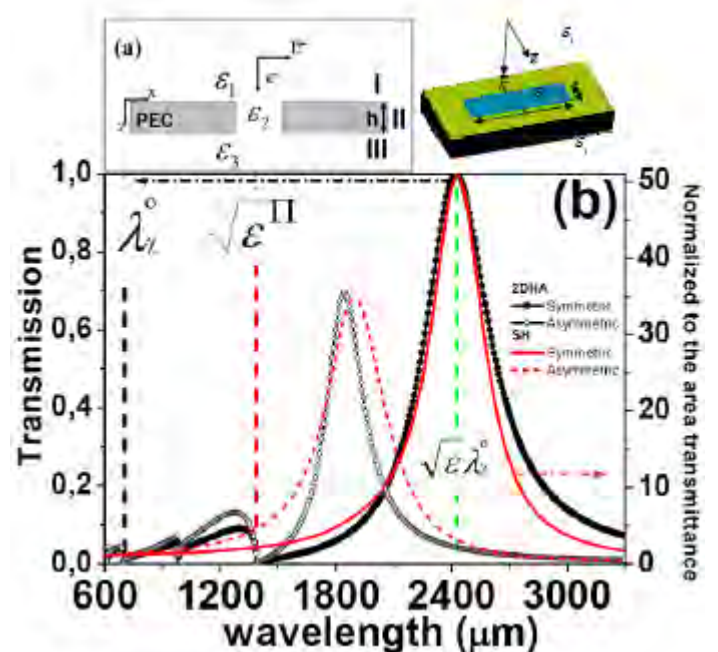
We analyze theoretically resonances appearing at wavelengths beyond the cut-off of the holes [2], [3]. We name this phenomenon Localized Extraordinary Optical Transmission (LEOT). Interestingly, no surface modes are involved; therefore, the physical mechanism is valid for both single holes (SH) and hole arrays (2DHA).

In particular, we will give analytical expressions for the LEOT peak position as a function of the film thickness (h), and the dielectric constants of the environment (the cover, the substrate, and inside the holes, ϵ_1 , ϵ_3 , ϵ_2 , respectively) for both symmetric ($\epsilon_1 = \epsilon_3$) and asymmetric ($\epsilon_1 \neq \epsilon_3$) configurations, for any hole shape of high aspect ratio (See Fig.1). Furthermore, the peak position is not the only spectral property affected by the dielectric environment, but also LEOT peak intensities are drastically modified. These results explain the unexpected fact reported by recent experiments in the THz regime about enhanced transmission [4] through isolated holes at wavelengths red-shifted from the cutoff wavelength.

FIG.1: (a) Schematic of the investigated structure. Panel (b): for $h = 1\mu\text{m}$, rectangular holes with: $a_x = 10\mu\text{m}$, $a_y = 350\mu\text{m}$, and $\epsilon_2 = 1.0$, the figure shows transmission curves through a 2DHA ($P=400\mu\text{m}$) placed in a symmetric environment (full symbols) and on a substrate (empty symbols). With solid line it is shown the normalized to the area transmission of a SH in the symmetric configuration. The dashed line depicts the same but for the asymmetric case. The dielectric constant of either the cover and/or the substrate is chosen to be 12.

References

- [1] T. W. Ebbesen et al. *Nature (London)* **391**, 667 (1998)
- [2] A. Degiron et al., *Opt. Commun* **239** (2004)
- [3] K. J. Klein Koerkamp et al., *Phys. Rev. Lett.* **92**, 1839901 (2004)
- [4] M. A. Seo et al., *Opt. Express*, **16**, 20484, (2008)



Spatial Nonlocality in the Optical Response of Metal Nanoparticles

Christin David and F. Javier García de Abajo

Instituto de Óptica – CSIC, Serrano 121, 28006 Madrid, Spain
christin.david@io.cfmac.csic.es

Experimental access to particle sizes and interparticle spacings of below 10 nm is now available for metallic dimers [1], tips [2], and shell structures [3], in which spatial dispersion (nonlocality) in the materials response is known to play an important role. However, most electromagnetic calculations of nanostructures rely on local, frequency-dependent dielectric functions [4], sometimes incorporating a phenomenological damping to account for finite-size effects [5].

Spatial nonlocality is known to play an important role at distances of a few nanometers [6] leading to significant plasmon broadening and blue shift [7], but few efforts have been made to theoretically investigate nonlocal effects in a rigorous way. The optical response of nanosized metallic structures is greatly influenced by quantum confinement of their conduction electrons, which adds up to the intrinsic nonlocality in the response of homogeneous bulk media.

In this talk, we present two different approaches to account for nonlocality in metal nanoparticles: (a) the non-retarded specular reflection model (SRM) [8-9] and (b) the retarded hydrodynamical model [10-11]. Comparison with available experiments results in excellent agreement with our parameter-free modeling of nonlocal effects, which produce dramatic changes with respect to the customary local theory. We show that nonlocal effects in both models produce sizable plasmon blue shift and broadening in single metal nanoparticles as well as in dimers (see Fig. 1).

Analysis of the plasmon resonance dependence on the interparticle spacing and nanoparticle size allows us to separate nonlocal and retardation effects, but there are common conditions for which both of them coexist, giving rise to competing mechanisms of field enhancement and mode displacement. This study is particularly relevant for broad, active areas involving applications of local field enhancement to biosensing and nonlinear optics.

References

- [1] M. Danckwerts, L. Novotny *Phys. Rev. Lett.* **98** (2007), 026104.
- [2] P. S. Kumar, I. Pastoriza-Santos, B. Rodríguez-González, F. J. García de Abajo, L. M. Liz-Marzán, *Nanotechnology* **19** (2008), 015606.
- [3] E. Prodan, C. Radloff, N. J. Halas, P. Nordlander, *Science* **302** (2003), 419–422.
- [4] V. Myroshnychenko, J. Rodríguez-Fernández, I. Pastoriza-Santos, A. M. Funston, C. Novo, P. Mulvaney, L. M. Liz-Marzán, F. J. García de Abajo, *Chem. Soc. Rev.* **37** (2008), 1792–1805.
- [5] U. Kreibig, C. v. Fragstein, *Z. Physik* **224**, (1969) 307–323.
- [6] U. Kreibig, M. Vollmer, *Optical Properties of Metal Clusters*, Springer-Verlag, Berlin, 1995.
- [7] J. Renger, R. Quidant, N. van Hulst, L. Novotny, *Phys. Rev. Lett.* **104** (2010), 046803.
- [8] R. H. Ritchie, A. L. Marusak, *Surf. Sci.* **4** (1966), 234–240.
- [9] F. J. García de Abajo, *J. Phys. Chem. C.* **112** (2008), 17983–17987.
- [10] F. Bloch, *Z. Phys.* **81** (1933), 363–376.
- [11] F. J. García de Abajo, *Rev. Mod. Phys.* **82** (2010) 209–275.

Figures

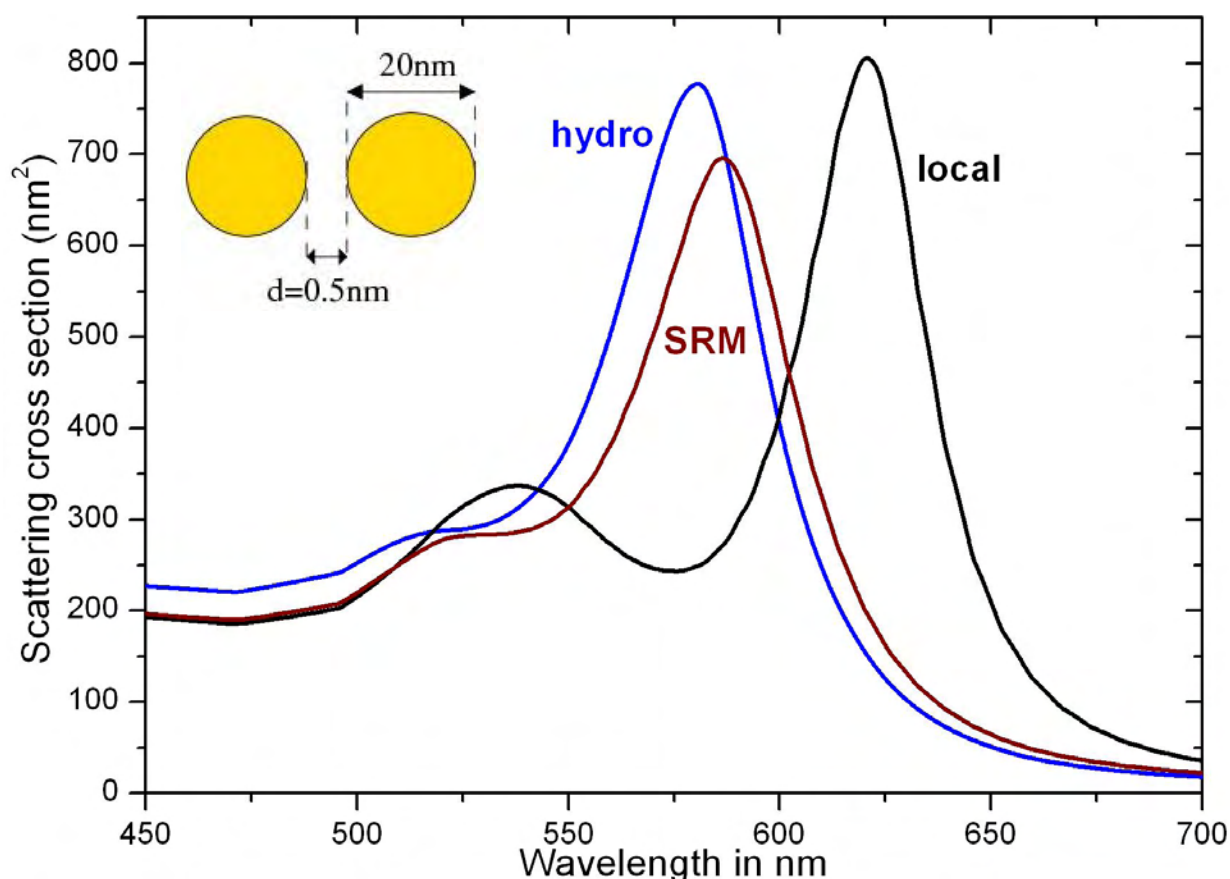


Figure 1. Extinction spectra for a gold dimer with 0.5 nm spacing between Au spherical particles of 20 nm in diameter. The external field is parallel to the interparticle axis. Local and nonlocal calculations are compared. Nonlocal calculations are presented both using the specular reflection model (SRM) and the hydrodynamic model (hydro).

Exploring the possibilities of fabrication of photonic crystals on inorganic materials with non-linear optical and laser properties

F. Díaz, J.J. Carvajal, G. Raj Kumar, W. Bolaños, X. Mateos, J. Massons, M. Aguiló

Física i Cristal·lografia de Materials i Nanomaterials (FiCMA-FiCNA), Universitat Rovira I Virgili, Campus Sescelades, c/ Marcel·lí Domingo s/n, E-43007 Tarragona, Spain
f.diaz@urv.cat

Photonic crystals (PCs) are a class of dielectric or semiconductor materials with artificially fabricated periodicity of the refractive indexes. Such class of materials has been subject of considerable research interest for more than a decade, since, with a proper design, they exhibit prohibited spectral bands for concrete wavelengths (photonic band gaps) and they can serve as instruments to manipulate light generation and light flow [1]. These photonic crystals exist in one dimension (1D), two dimension (2D), and three dimension (3D) forms, and can be easily produced in polymers [2]. However, to produce such 1D, 2D and 3D PCs on inorganic materials with optical properties is a more challenging objective, and several techniques have been tested for their fabrication [3]. In fact, one of the main challenges for the production of photonic structures with higher dimensionality is the fabrication of these structures with sufficient precision to prevent scattering losses blurring the crystal properties. For this reason, the fabrication techniques for such structures have to be analyzed carefully.

In this paper we analyze the results obtained using four different techniques of fabrication of such 1D, 2D and 3D PCs on crystals with non-linear optical properties belonging to the KTiOPO_4 (KTP) family, such as the same KTP and RbTiOPO_4 (RTP), and also on LiNbO_3 . Photonic crystals fabricated in nonlinear optical materials, or non-linear photonic crystals (NPC) have been an attractive topic for their modulation of the non-linear coefficient $\chi^{(2)}$ together with a periodic modulation of the linear susceptibility $\chi^{(1)}$. Such structures can be generated by fabricating a surface relief structure on the surface of a non-linear optical material. In this way the refractive index and the $\chi^{(2)}$ susceptibility are modulated periodically between the values of the nonlinear optical material and those of the surrounding medium. Such structures can enhance, phase match or even hold a non-vanishing second-order interaction even if the material is centrosymmetric. Also, this kind of structures may allow to demonstrate backward parametric oscillation, a non-linear effect predicted many years ago but that has not been demonstrated experimentally. Furthermore, new non-linear optical effects have also been expected to occur, such as the generation of asymmetric diffraction patterns of the second-harmonic generated light that we reported very recently.

We also explored the possibilities of fabricating those PCs in thin epitaxial layers of materials with laser applications as they are the monoclinic potassium double tungstates, $\text{KRE(WO}_4)_2$, grown on substrates of the same family. Those materials are well known for the large absorption and emission cross sections that active lanthanide ions exhibited when they are hosted in this family of materials, and also because concentration quenching effects for emissions of lanthanide ions in these crystals are low due to the large distance among lanthanide ions in these structures. In these crystals we are especially interested in analysing generation and propagation of light through PC structures.

The techniques used to fabricate such PCs include laser ablation, selective wet-chemical etching in periodically poled non-linear optical crystals, focused ions beam (FIB) and an alternative approach to fabricate PCs by combining two well known techniques: the fabrication of porous silicon membranes and the epitaxial growth of the materials of interest by liquid phase epitaxy (LPE) techniques [4].

Ultrafast laser ablation constitute a unique tool for micro-machining a diverse range of materials. This technique uses very short and intense laser pulses to remove thin layers from the surface of a bulk target by means of a physical mechanism different from those taking place in conventional laser ablation. The collateral thermal and mechanical effects around the ablated area are diminished to such an extent that precision and quality of the microstructures higher than those obtained with other techniques can be achieved. By using this technique we prepared 1D and 2D PCs on the surface of KTP and RTP crystals.

Ferroelectric domains of opposite spontaneous polarization present different etching speeds when dipped in some acid mixtures. This property has been used to reveal the domain pattern at the surface of periodically poled crystals. However, the selective etching process provides further capabilities for versatile surface engineering of domain-engineered crystals, allowing the production of deep, high

aspect ratio structures, with side-walls that can be extremely smooth. This allowed us to generate 1D PCs on LiNbO_3 periodically poled crystals.

FIB is a suitable micro-machining tool to modify or machine materials at the micro- and nanoscale, and 2D PC structures can be fabricated by drilling a periodic pattern of holes with the appropriate diameters and separated by the adequate distances. Using this technique we fabricated 2D PCs on thin layers of $\text{KY}_{0.60}\text{Gd}_{0.18}\text{Lu}_{0.21}\text{Er}_{0.01}(\text{WO}_4)_2$ grown on $\text{KY}(\text{WO}_4)_2$ substrates that contained straight and bending defects that allowed the propagation of light through straight and bending waveguides.

Finally, we developed a procedure for fabricating 2D and 3D photonic crystals in four steps: (i) preparation of high-quality ordered macro-porous silicon templates, (ii) growth of thin layers of the desired materials within the pores of the silicon templates, (iii) polishing of the top or bottom surface of the epitaxial layers, and (iv) selective etching of the silicon matrix. In this way we prepared 2D and 3D PCs of KTP and $\text{KYb}(\text{WO}_4)_2$.

All these structures have been characterized morphologically and optically. Some details of the micro- and nanostructured PCs fabricated on these materials can be seen in Figure 1.

References

- [1] E. Yablonovitch, Phys. Rev. Lett, **58** (1987) 2059.
- [2] X. Hu, P. Jiang, C. Ding, H. Yang, Q. Gong, Nature Photonics, **2** (2008) 185.
- [3] J.J. Carvajal et al., J. Lumin., **129** (2009) 1441.
- [4] A. Peña, S. Di Finizio, T. Trifonov, J.J. Carvajal et al., Adv. Mater., **18** (2006) 2220.

Figures

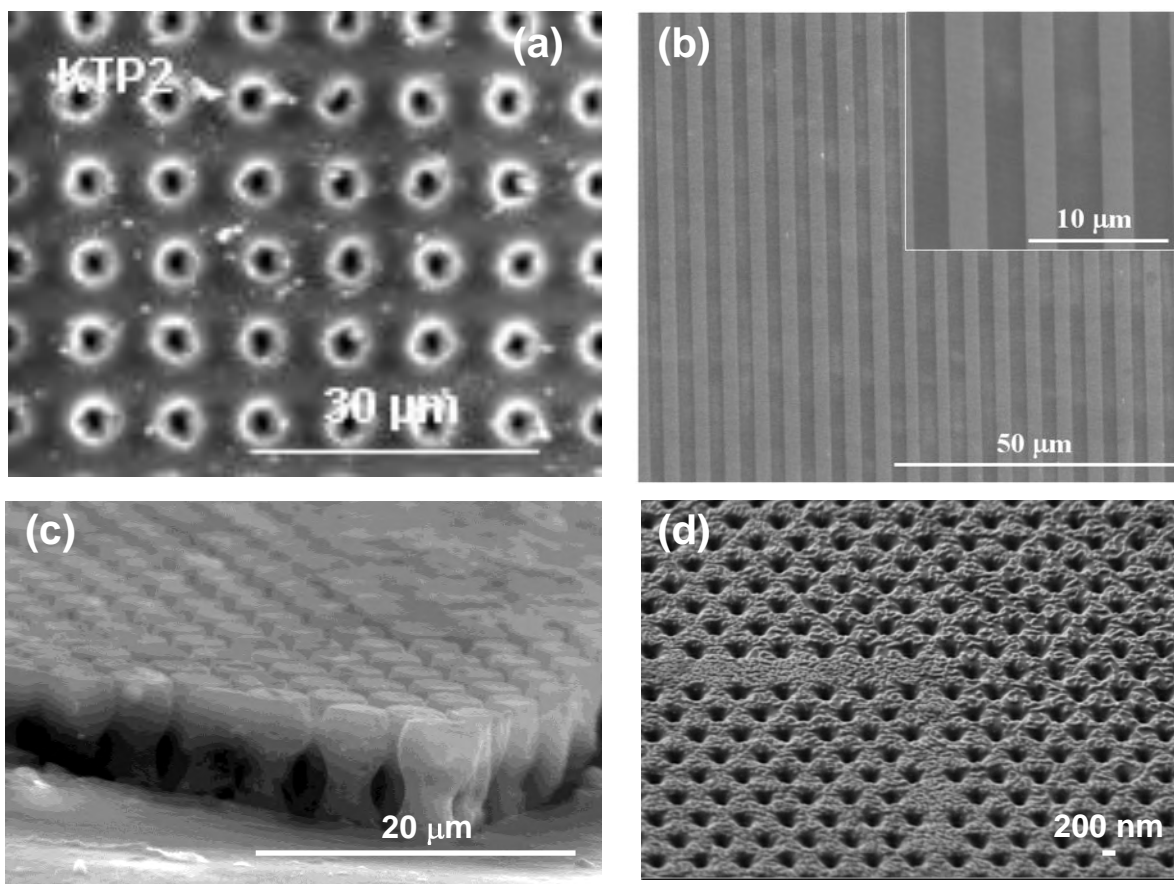


Figure 1. (a) 2D PC fabricated by ultrafast laser ablation on the surface of a KTP crystal. (b) 1D PC fabricated by selective wet-chemical etching on a periodically poled LiNbO_3 crystal. (c) 3D KTP PC fabricated by epitaxial growth within the pores of a silicon membrane. (d) 2D PC with a 90° bending waveguide fabricated by FIB on a $\text{KY}_{0.60}\text{Gd}_{0.18}\text{Lu}_{0.21}\text{Er}_{0.01}(\text{WO}_4)_2 / \text{KY}(\text{WO}_4)_2$ epitaxy.

Photoluminescence and Aging Effects in Photonic Microcavities Based on Porous Silicon Microspheres

R. Fenollosa, F. Ramiro-Manzano, M. Tymczenko, F. Meseguer

Unidad Asociada CSIC-UPV, Centro de Tecnologías Físicas, Universidad Politécnica de Valencia, Avda Tarongers s/n, 46022, Valencia, Spain, and Instituto de Ciencia de Materiales de Madrid (CSIC), Sor Juana Inés de la Cruz, 3, Cantoblanco, 28049, Madrid, Spain.
rfenollo@ter.upv.es

Photonic microcavities constitute a field of research that has attracted the attention of many researchers from all over the world.¹ The fact that light can be confined in a very reduced volume of the order of 1 micrometer or even less is very interesting not only from the point of view of basic science but also from the point of view of technological applications. For instance, very sensitive chemical sensors based on the light interaction with matter could be achieved by means of microcavities because the electromagnetic field can be greatly enhanced inside them.² So far, planar microcavities based on different materials like silicon, indium gallium arsenide phosphide, silicon nitride, etc. were successfully obtained.³ However, only a reduced number of materials like for instance silica, poly-styrene, silicon, etc. has been able to be shaped in a spherical geometry and having a surface smooth enough so as to allow them work as optical microresonators.^{4,5}

Here, we report on porous silicon particles.⁶ They were synthesized by chemical vapour deposition of disilane gas under controlled conditions of temperature, pressure, and decomposition time. Because the particles are highly spherical and their surface is very smooth (see Fig. 1), and also because of their high refractive index value, they can work as photonic microcavities with well defined resonating modes. These modes were identified in the near infrared range and they experience large (hundreds of nanometers) and fast (nanometers per minute) shifts upon the exposure of the microspheres to the open atmosphere (see Fig. 2). We have attributed this behaviour to a highly porous nature of the microspheres and to an oxidation process. This hypothesis has been confirmed by Transmission Electron Microscopy and by Mid-Infrared Spectroscopy.

The nano-porous nature of the microspheres produces the typical photoluminescence of electrochemically fabricated porous silicon (see Fig. 3). This is a very important characteristic because it may allow light amplification and therefore lasing in a single microsphere by taking advantage of the microcavity light confinement effect.

References

- [1] K. J. Vahala, *Nature*, **424** (2003) 839.
- [2] A. M. Armani, R. P. Kulkarni, S. E. Fraser, R. C. Flagan, K. J. Vahala, *Science*, **317** (2007) 783.
- [3] S. Noda, A. Chutinan, M. Imada, *Nature*, **407** (2000) 608.
- [4] M. L. Gorodetsky, A. A. Savchenkov and V. S. Ilchenko, *Opt. Lett.*, **21** (1996) 453.
- [5] R. Fenollosa, F. Meseguer and M. Tymczenko, *Adv. Mater.*, **20** (2008) 95.
- [6] R. Fenollosa, F. Ramiro-Manzano, M. Tymczenko, F. Meseguer, submitted to *Journal of Materials Chemistry*.

Figures

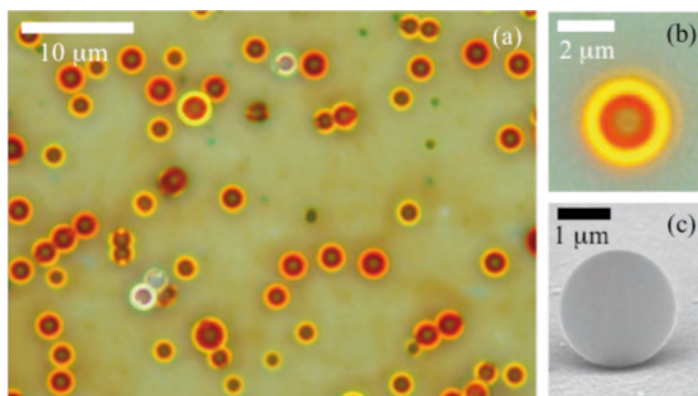


Fig. 1 Optical microscopy images at 1000X magnification showing: (a) Porous silicon microspheres obtained by decomposing disilane at 400 °C. (b) A zoomed image (at the same magnification) of a single microsphere. (c) Scanning Electron Microscopy image at 45000X magnification of a porous silicon microsphere of about 2 micrometers in diameter illustrating its spherical perfection and smooth surface.

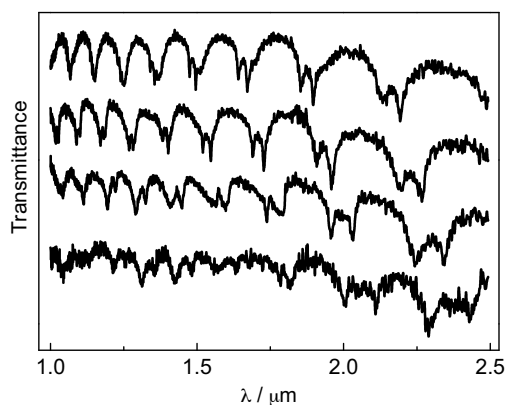


Fig. 2 Optical transmittance spectra of a porous silicon microsphere of about 3 micrometers in diameter. They were measured in vacuum (bottom spectrum) and after different exposure times: 1 hour, 20 hours and 120 hours (2nd, 3rd and 4th spectra from bottom to top respectively). The resonating modes correspond to the dips of the spectra. They blue-shift as the exposure time of the microsphere to the open air increases.

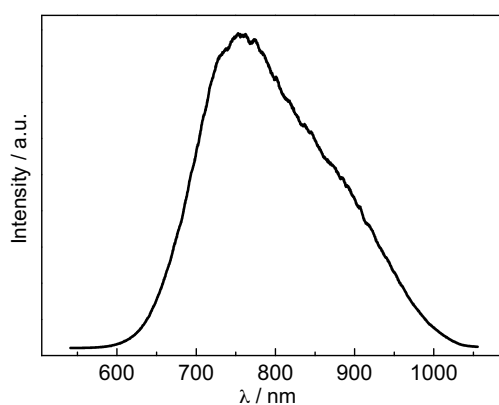


Fig. 3 Photoluminescence signal of a cluster of porous silicon microspheres. The excitation source was the 488 nm line of an Ar laser.

Enhanced emission in self assembled photonic crystals by hybrid photonic-plasmonic modes

M. López-García, **J.F. Galisteo-López**, A. Blanco, C. López

Instituto de Ciencias de Materiales de Madrid (CSIC), c/ Sor Juana Inés de la Cruz 3, 28049, Cantoblanco, (Madrid) Spain

galisteo@icmm.csic.es

A. García-Martín

Instituto de Microelectrónica de Madrid (CSIC), c/ Isaac Newton 8, 28760, Tres Cantos, (Madrid) Spain

Coupling between plasmonic and photonic systems has become one of the most efficient ways to obtain small scale waveguiding and emitting devices [ⁱ]. In this work, a novel structure for obtaining enhanced emission in a hybrid plasmonic-photonic structure is presented. The samples under study consist of large area close-packed ordered monolayers of dye doped polystyrene spheres grown on a thin (60nm) gold film. This system allows surface resonant plasmonic modes to couple efficiently to photonic ones leading to the formation of localized surface plasmon polariton (SPP) modes, propagating waveguide modes and hybrid ones [ⁱⁱ].

The dispersion relation of these modes is retrieved by means of angle and polarization resolved reflectance measurements for different crystallographic orientations. Comparison with calculated reflectance spectra as well as the spatial distribution of the electric field in the system allows us to identify different mode types. Field enhancement inside the spheres is seen to be much larger than that obtained for similar samples grown on dielectric substrates evidencing the role of the metallic layer in preventing leakage losses into the substrate [ⁱⁱⁱ].

Finally we have studied the effect of such field enhancement on the emission of the dye by studying angle and polarization resolved photoluminescence (PL). We have observed that enhanced emission is obtained for those modes where the field is mainly concentrated in the region containing the emitter (i.e. polymeric spheres). A comparison with a reference system monolayer of dye doped spheres deposited on silicon, further points to the efficiency of our samples to obtain enhanced emission. The spectral tunability of the mode dispersion with sphere size makes this system a versatile one for many applications involving efficient emitting devices.

References:

-
- ⁱ R.F. Oulton, V.J. Sorger, T. Zentgraf, R-M. Ma, C. Gladden, L. Dai, G. Bartal and X. Zhang, *Nature*, **461**, 629 (2009).
 - ⁱⁱ R.M. Cole, Y. Sugawara, J.J. Baumber, S. Mahajan, M. Abdelsalam and P.N. Barlett, *Phys. Rev. Lett*, **97**, 137401 (2006).
 - ⁱⁱⁱ Y. Kurokawa, H. Miyazaki, Y. Jimbo, *Phys. Rev. B*, **69**, 155117 (2004).

Figures :

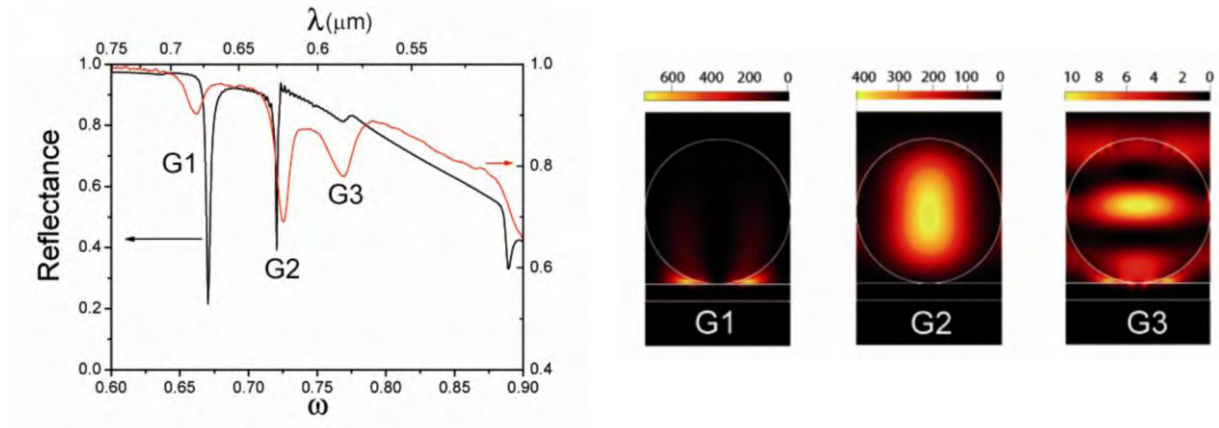


Figure 1: Left : Calculated (black curve) and measured (red curve) normal incidence reflection spectra of a ML of 520nm PS spheres grown on a gold substrate. Right: Total field intensity distribution of selected modes (as indicated in spectra).

Photonic crystal waveguide sensor for low concentration DNA detection

V. Toccafondo¹, J. García-Rupérez¹, M. J. Bañuls², A. Griol¹, **J. G. Castelló¹**, S. Peransi-Llopis² and A. Maquieira²

1: Valencia Nanophotonics Technology Center, Universidad Politécnica de Valencia, Camino de Vera s/n, 46022 Valencia, Spain.

2: Instituto de Reconocimiento Molecular, Dpto de Química, Universidad Politécnica de Valencia, Camino de Vera s/n, 46022 Valencia, Spain.
vertocca@ntc.upv.es

Integrated photonic sensors are currently attracting an increasing interest because of their high potential for a fast label-free analysis of very low concentrations of analytes, such as proteins, bacteria or DNA for instance [1]. Particular interest is focused on planar devices in silicon, such as ring resonators [2,3], photonic crystal based structures [4,5], or Mach-Zehnder Interferometers [6], as they are very sensitive to refractive index variation, have a small size, and can be fabricated on very large scale using CMOS fabrication techniques. In this work, we report experimental results showing the detection of double-strand DNA using a photonic crystal waveguide (PCW) based sensor, obtaining a lower detection limit of 22.2nM.

The PCWs used for the detection were fabricated in a silicon-on-insulator (SOI) wafer with 250nm-thick silicon layer on a 3µm-thick buried oxide layer. They were designed to have a guided TE mode with its band edge located around $\lambda=1550\text{nm}$, for what a lattice constant of 390nm and a hole radius of 111nm was selected. Light is coupled/collected to/from the PCW using 500nm-wide singlemode waveguides. 20µm-long PCWs were fabricated using e-beam lithography and Inductively Coupled Plasma (ICP) etching. A scanning electron microscopy (SEM) picture of the PCW is shown in Fig. 1.(a).

Surface activation is performed by exposing the chip to pure 3-isocyanatepropyl triethoxysilane vapour for 30 min. Then, a drop of streptavidin 0.1mg/ml in 0.1x phosphate buffer saline (PBS) is deposited on the sensing area and incubated in a humid chamber overnight at room temperature. Finally, a solution of ovalbumin protein (OVA) 1% in PBS 0.1x is spread all over the chip and incubate for 30 minutes to block the remaining active sites.

For the experimental characterization, the TE transmission spectrum near the band edge of the PCW was continuously acquired using a tunable laser with a resolution of 1pm, as shown in Fig. 1.(b). In this region, transmission peaks created by the excitation of multiple-k modes in the slow-wave regime near the band edge and the cavity created in the PCW with the access waveguides appear, which are used to perform the sensing, as shown in the inset of Fig. 1.(b). The sensing experiment begins flowing the PBS 0.1x at 10µl/min (a flow cell is placed on the top of the chip and this flow rate is maintained for all the experiment) to obtain the baseline for the buffer solution. Then, we switched to a double-strand DNA solution with the end of one strand marked with biotin which has a high binding affinity with the streptavidin and will bind to the protein attached in the PCW surface, thus inducing a shift in the peak position. The end of the other strand is marked with digoxigenin (DIG) which has no affinity with streptavidin and is used later to confirm the binding of the DNA to the PCW surface by flowing anti-DIG antibody. Figs. 2.(a) and 2.(b) show the flowing sequence and the peak shift obtained for each substance.

For the lowest DNA concentration (0.2µM) we measured a peak shift of $\Delta\lambda_{\text{DNA}}=5.8\text{pm}$ (1544.764nm-1544.7582nm). The noise level was estimated to be 0.645pm (standard deviation of peak position during continuous PBS1 flow), thus giving a lower detection limit of 22.2nM for direct DNA detection, what is in line (or even better) with state-of-the-art values reported for other planar photonic structures such as ring resonators [3]. Moreover the shift we observed when flowing anti-DIG (higher than 0.6nm) clearly confirms the binding of the DIG-marked DNA on the chip.

This work was carried out within the FP7-ICT-223932-INTOPSENS project, funded by the European Commission, and by Spanish MICINN under contracts TEC2008-06333 and CTQ2007-64735/BQU.

References

- [1] X. Fan, I.M. White, S.I. Shopova, H. Zhu, J.D. Suter, Y. Sun, *Anal. Chim. Acta*, **620** (2008), 8-26.
- [2] K. De Vos, I. Bartolozzi, E. Schacht, P. Bienstman, R. Baets, *Opt. Express*, **15** (2007), 7610-7615.

- [3] A. Ramachandran, S. Wang, J. Clarke, S.J. Ja, D. Goad, L. Wald, E.M. Flood, E. Knobbe, J.V. Hryniewicz, S.T. Chu, D. Gill, W. Chen, O. King, B.E. Little, *Biosens. Bioelectron.*, 23 (2008), 939-944.
- [4] N. Skivesen, A. Têtu, M. Kristensen, J. Kjems, L.H. Frandsen, P.I. Borel, *Opt. Express*, 15 (2007), 3169-3176.
- [5] D. Dorfner, T. Zabel, T. Hürlimann, N. Hauke, L. Frandsen, U. Rant, G. Abstreiter, J. Finley, *Biosens. Bioelectron.*, 24 (2009), 3688-3692.
- [6] A. Densmore, M. Vachon, D.-X. Xu, S. Janz, R. Ma, Y.-H. Li, G. Lopinski, A. Delâge, J. Lapointe, C.C. Luebbert, Q.Y. Liu, P. Cheben, J.H. Schmid, *Opt. Lett.*, 34 (2009), 3598-3600.

Figures

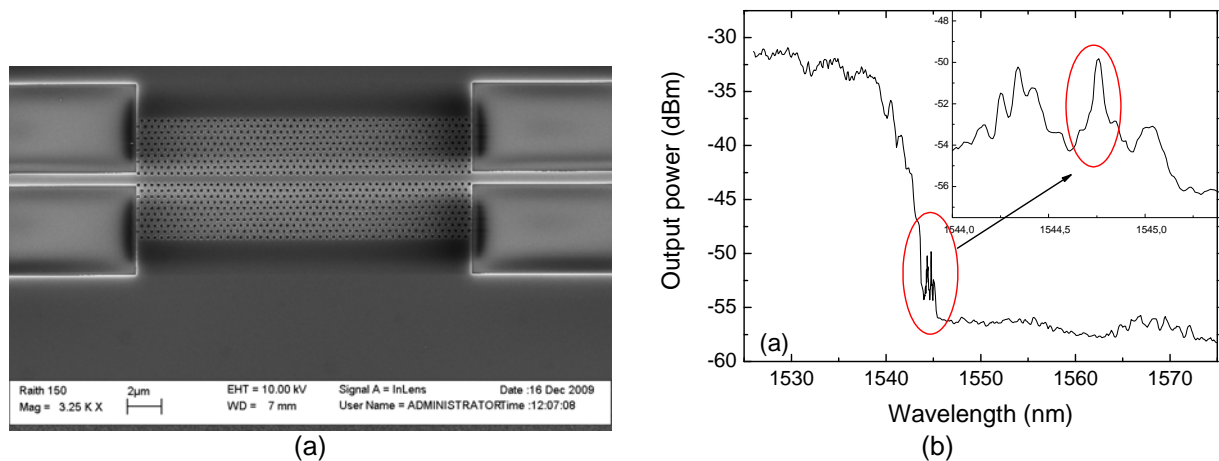


Fig. 1. (a) SEM image of the photonic crystal waveguide used for the sensing, (b) Spectrum of the photonic crystal waveguide in the region of the band edge.

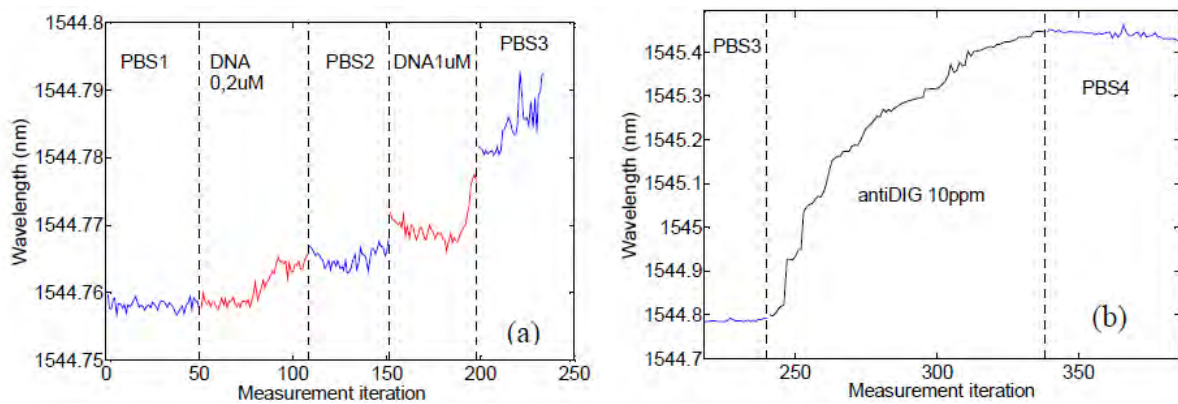


Fig. 2. Wavelength shift vs measurement iteration (each iteration lasts approximately 1 minute), for double-strand DNA (left) and anti-DIG (right) flowing. Flowing sequence is: PBS 0.1x, DNA 0.2 μ M, PBS 0.1x, DNA 1 μ M, PBS 0.1x, anti-DIG 10ppm, and PBS 0.1x (all were flown for more than 30 minutes to ensure molecular binding).

Plasmon-Induced Magneto-Optical Activity in Nanosized Gold Disks

A. García-Martín¹, B. Sepúlveda², J.B. González-Díaz¹, L. Lechuga², and G. Armelles¹

¹Instituto de Microelectrónica de Madrid, Consejo Superior de Investigaciones Científicas, C/Isaac Newton 8 (PTM) 28760 Tres Cantos, Spain

²Centro de Investigación en Nanociencia y Nanotecnología (CIN2) ICN-CSIC, Facultat de Ciències, Campus UAB, 08193 Bellaterra, Spain
antonio@imm.cnm.csic.es

The excitation of surface plasmons has proven a very useful means to raise other physical phenomena like in surface Raman scattering (SERS), fluorescence emission, high harmonic generation or the magnetooptical Kerr effect (MOKE). Focusing on the MOKE, it has been shown that the influence of surface plasmons can lead to a noticeable enhancement of the magneto-optical (MO) activity for ferromagnetic nanoparticles[1], or more for combinations of noble metal-ferromagnetic nanofilms and nanodisks[2,3].

When considering MO activity together with plasmonic excitations, the nanostructures developed required the incorporation of a ferromagnetic material to benefit from their high MO response at very low magnetic fields. So far, no attempt on nanostructures consisting exclusively in noble metals has been made since the magnetic field required to obtain a measurable response is expected to exceed those experimentally available (more than 100T). However, the excitation of a surface plasmon in a metal could lead to a drastic reduction of the magnetic field necessary to be able to observe MO activity in noble metal structures. This is the scope of this work, where we present for the first time the MO response of a series of pure gold nanostructures[4].

We apply a magnetic of 0.8T to analyze the Kerr rotation and ellipticity of disordered gold nanodisks and nanoholes obtained from continuous gold films grown over a glass substrate using colloidal lithography. We show that the MO response is controlled by the surface plasmon excitation, its spectral position depending on the aspect ratio of the particles/holes. Figure 1 shows that a peak and an S-like structure for the Kerr rotation and ellipticity respectively appear at the same energy region where the surface plasmon is excited. As the diameter of the nanodisks/holes increases, these features shift to lower energies (higher wavelengths), in accordance with the modification of the spectral position of the plasmon excitation due to the variation of the aspect ratio. We will show that this effect is due to the increase of the magnetic Lorentz force induced by the large collective movement of the conduction electrons in the nanostructures when the LSPR is excited. To understand the physical mechanism of the effect, we will rely on a simple approach based on the polarizability of a metal nanoparticle in the presence of a static magnetic field. The emergence of MO effects in pure plasmonic nanostructures may then find important applications in plasmonic modulators or in the improvement of the biosensing performance of metal nanostructures [5].

References:

- [1] J.B. Gonzalez-Diaz et al., *Adv. Mat.* **19**, (2007) 2643
- [2] J.B. Gonzalez-Diaz et al., *Phys. Rev. B.* **76**, (2007) 153402
- [3] J.B. Gonzalez-Diaz et al., *Small* **4**, (2008) 202
- [4] B. Sepulveda, et al., *Phys. Rev. Lett.* **104**, (2006) 147401
- [5] B. Sepulveda, et al., *Opt. Lett.* **31**, (2006) 1085

Figures:

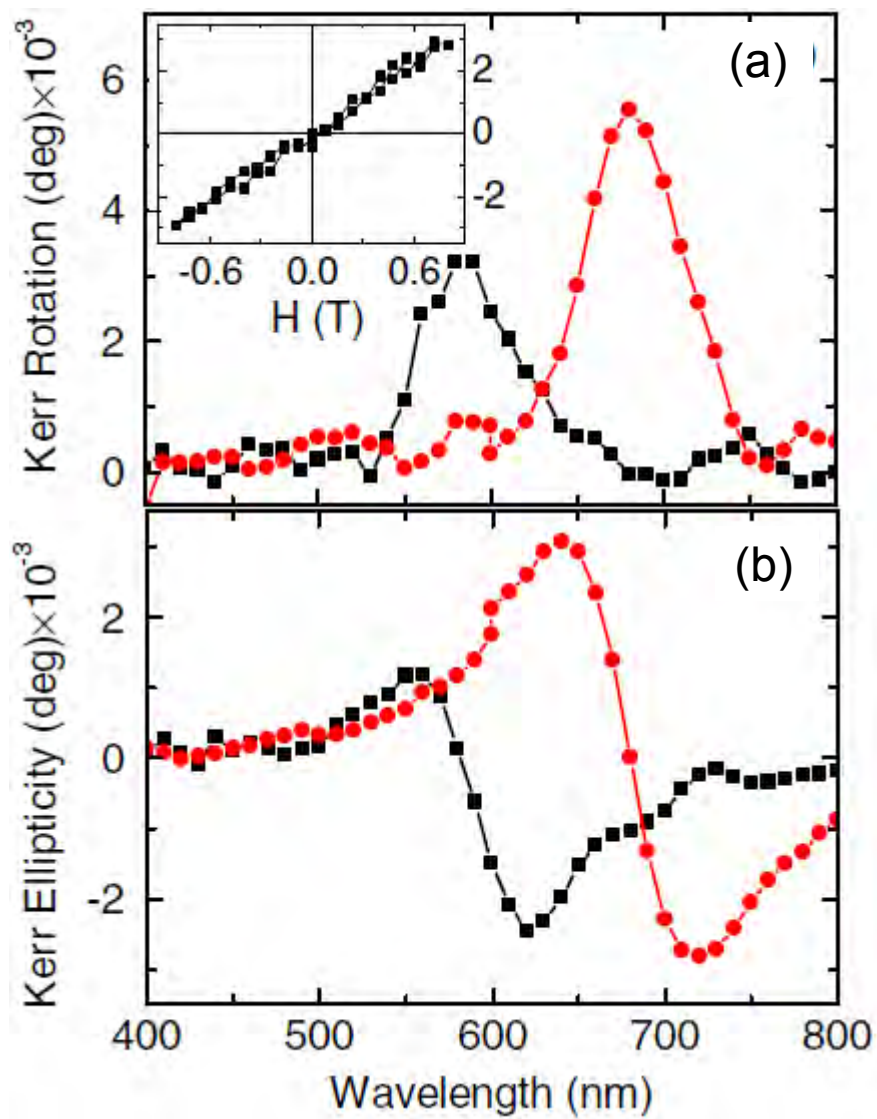


Fig. 1: MO Kerr rotation (a) and ellipticity (b) of gold nanodisks (D=70nm, h= 32nm) (squares) and (D=20nm, h= 20nm) (circles). The inset in (a) represents the Kerr rotation variation as a function of the magnetic field for the Au nanodisks with D=70nm, h= 32nm.

Nonlinearity caused by local field effects between a two level gain medium and a metamaterial

J.L. Garcia-Pomar, R. Beigang and M. Rahm

Department of Physics and Research Center OPTIMAS, University of Kaiserslautern,
Kaiserslautern 67663, Germany
Fraunhofer Institute for Physical Measurement Techniques IPM, Freiburg 79110, Germany
garciapomar@physik.uni-kl.de

The embedding of active media with gain to metamaterials is a main goal to overcome the problems related to the high intrinsic loss of metals at higher frequencies. A recent work [1] has shown that tailoring gain into metamaterials does not result in a simple compensation of the loss in the medium, but rather in an overall modification of the total system in a way that the gain properties of the hybrid system are affected. In this context, we study the nonlinear effects of hybrid metamaterial/gain material systems which can be essential for future applications of metamaterials. Furthermore, such systems can serve as a source of interesting new phenomena as for instance absorption cancellation near resonant transitions in analogy with the characteristics of the electromagnetically induced transparency (EIT).

In our model, we considered a two level atomic system (2LS) coupled to a metamaterial that was composed of a single layer of SRRs. The SRRs were described in the dipole approximation whereas the 2LS was treated according to a semi-classical model. The coupling between both systems is caused by the electromagnetic interaction of the local fields that penetrate the SRRs and the atomic two-level medium. The theory of such a model has been thoroughly studied in Ref. [1].

To determine the magnitude of the linear and nonlinear response of the hybrid system we described the local fields of the SRRs and the 2LS as the sum of the external field E_{ext} and the local electric fields E_{loc} at the location of the SRR and the 2LS, respectively. Thereby, it was assumed that the local electric field at the location of the 2LS was generated by the polarization fields of the SRR whereas the local electric field at the location of the SRRs was produced by the polarization fields of the 2LS. In order to take the coupling efficiency between both systems into account, we introduced a phenomenological coupling constant \mathcal{Q} . By this means, we could describe the local fields $E_L^{(1)}$ of the 2LS and $E_L^{(2)}$ of the SRR system as

$$\begin{aligned} E_L^{(1)} &= E_{ext} + \mathcal{Q} P_{SRR} \\ E_L^{(2)} &= E_{ext} + \mathcal{Q} P_{12} \end{aligned} \quad (1)$$

where P_{SRR} and P_{12} are the macroscopic polarization of the SRR and the 2LS respectively, given by:

$$\begin{aligned} P_{SRR} &= N_{SRR} \mu_{SRR} \rho_{SRR} \\ P_{12} &= N_{12} \mu_{12} \rho_{12} \end{aligned} \quad (2)$$

where $N_{SRR, (12)}$ is the density of SRR, (atoms), $\mu_{SRR, (12)}$ is the dipole transition moment of the SRR (two-level system from the ground to excited state), and ρ is the slowly varying amplitude of the coherence.

From the Liouville equation for the reduced density matrix of the SRR we obtained for the equation of the SRR in the rotating wave approximation

$$\dot{\rho}_{SRR} = -i(\Delta_{SRR} - i\gamma_{SRR})\rho_{SRR} + i\frac{\mu_{SRR}}{\hbar} E_L^{(2)}, \quad (3)$$

where $\Delta_{SRR} = \omega - \omega_{SRR}$ is the detuning of the external field frequency ω from the resonance frequency ω_{SRR} of the SRR; and γ_{SRR} is the damping constant of the SRR.

In analogy, the dynamics of two level system with ground state $|1\rangle$ and excited state $|2\rangle$ that interacts with an optical field closely tuned to the atomic resonance, can be described by the Maxwell-Bloch equations [2]

$$\begin{aligned} \dot{\rho}_{12} &= -i(\Delta_{12} - i\gamma_{12})\rho_{12} - i\frac{\mu_{12}}{\hbar} E_L^{(1)} w \\ \dot{w} &= -\Gamma_{12}(w + 1) + i\left(\rho_{12}^* \frac{\mu_{12}}{\hbar} E_L^{(1)} - \rho_{12} \frac{\mu_{12}}{\hbar} E_L^{*(1)}\right), \end{aligned} \quad (4)$$

where ρ_{12} is the amplitude of the coherence, $\Delta_{12}=\omega-\omega_{12}$ is the detuning, γ_{12} and Γ_{12} are the transversal and longitudinal damping of the 2LS, respectively. w is the population inversion; we assume that the equilibrium value, corresponding to the ground state, is -1 . By inserting Eqs. (1) and (2) into Eqs. (3) and (4) we obtained a complete system from which we could calculate the effective electric susceptibility χ of the system as a function of the macroscopic polarization fields as:

$$\chi = V_{12} \frac{P_{12}(\rho_{12}, w)}{\epsilon_0 E_{ext}} + V_{SRR} \frac{P_{SRR}(\rho_{SRR}, w)}{\epsilon_0 E_{ext}}, \quad (5)$$

where $V_{12,(SRR)}$ is the volume fraction of the gain material(2LS(SRR)) in the system.

For illustrating the physical effects of the nonlinearity in the system it is convenient to represent the effective susceptibility as a power series expansion of the external electric field

$$\chi = \chi^{(1)} + \chi^{(3)} |E_{ext}|^2 + \chi^{(5)} |E_{ext}|^4 + \dots \quad (6)$$

to convert Eq. (5) in the form of Eq. (6) we performed a Taylor expansion of the population inversion w in terms of $x=|E_{ext}|^2/|E_s|^2$ where E_s is the analogous of the saturation field strength [3] of this system. Introducing this expansion in Eq. (5) we obtain the expression given by Eq.(6).

We will show that w changes from -1 to other values when high external fields are applied. This change involves two nonlinear effects: the amplitude change of the susceptibility response and the modification of the resonance frequency.

In Fig. 1 we show the parameter range where the different orders of the Taylor expansion of the susceptibility are valid when there is not inversion or pumping and for same resonance frequencies.

In our presentation, we will show how nonlinear effects induce saturation effects and cascaded processes in a hybrid SRR/2LS system due to local field interactions and will discuss how the nonlinearities influence the dynamic characteristics of the composed system

In conclusion, we calculated the nonlinear electric susceptibilities for a metamaterial that was coupled to a two level gain material. Starting from the corresponding Maxwell Bloch equations we could evaluate the contributions of the linear, third and fifth-order electric susceptibility of the hybrid system to the overall nonlinear response by means of a Taylor expansion in the population inversion of the two-level gain medium. Our results for the nonlinearities in the susceptibility show the range of validity of the different approximations and the underlying physic responsible for these nonlinear effects. Finally, we show effects in the dynamic of the system when it is pumped.

References

- [1] M. Wegener, J. L. Garcia-Pomar, C. M. Soukoulis, N. Meinzer, M. Ruther and S. Linden, , *Optics Express* **16**, (2008), 19785-19798.
- [2] R. W. Boyd, *Nonlinear Optics*, 2nd ed. _Academic Press, New York, (2003)
- [3] K. Dogaldeva, R. W. Boyd and J.E. Sipe, *Phys. Rev. A*, **76**, (2007) 063806.

Figures

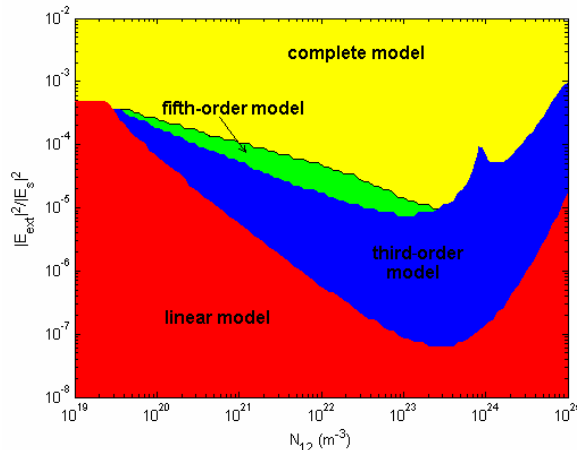


Fig. 1: (Color online) The ranges of validity of the different orders of the susceptibility in function of the dipole density N_{12} of the two level system and the parameter $x=|E_{ext}|^2/|E_s|^2$.

Toward the realization of an efficient Si-based light source emitting at 1.55 μm

O. Jambois¹, J.M Ramirez¹, Y. Berencen¹, D. Navarro-Urrios¹, S. Hernández¹, A. Anopchenko², A. Marconi², N. Prtljaga², N. Daldosso², L. Pavesi², J.-P. Colonna³, J.-M. Fedeli³ and **B. Garrido**¹

¹ Departament d'Electrònica, Universitat de Barcelona, Carrer Martí i Franquès 1,
Barcelona 08028, Spain

² Nanoscience Laboratory, Department of Physics, University of Trento, Via Sommarive 14, Povo
(Trento) 38121, Italy

³ CEA, LETI, Minatec 17 rue des Martyrs, 38054 Grenoble cedex 9, France

ojambois@el.ub.es

For several years, silicon-based photonic devices have been widely considered in order to develop integrated circuits allowing to overcome the microelectronic bottlenecks. The challenge for silicon photonics is to manufacture low-cost information processing components by using standard and mature CMOS technology. Numerous photonic devices have already been developed in the last years for light propagation, modulation or detection on silicon substrates. The ultimate goal for the photonic and electronic convergence would be to monolithically integrate powerful Si-based light sources into the CMOS photonic integrated circuits.

Some encouraging works have reported the possibility to obtain efficient Si-based light emitting diodes [1,2,3]. Even stimulated emission by optical pumping of an Er doped Si-based material has been reported [4], but some effort have still to be pursued in order to increase the emitted power, and achieve the realization of an injection Si-based laser.

In this work, we report a systematic study of the electroluminescence (EL) properties and mechanisms of Si-rich silicon oxides doped with Er ions, by correlating the study of transport mechanisms and electroluminescence spectra. Three different techniques have been used to fabricate the active layer: LPCVD, PECVD, and ion implantation. Different Si excess were introduced, and various annealing treatment were performed in order to form Si nanoclusters (Si-nc) from the SRSO layers. Those nanoclusters are known to have an enhanced radiative emission in the visible respect to bulk when they are crystalline due to quantum confinement (figure 1a), or act as efficient sensitizers for the luminescence of Er ions at 1.5 μm when they are amorphous (figure 1b). A total of about 20 different wafers have been processed.

The devices were excited in DC excitation. We find that the three techniques of deposition give different power efficiency that we attribute to the different matrix defect concentration induced by each technique. Two kinds of transport mechanisms could be observed in function of the annealing treatment. In one case, the transport is made by hopping from Si-nc to Si-nc and low EL power is obtained. In the other case, the injection of hot electrons is observed, as suggested by the I-V characteristics (see figure 2), leading to a higher EL power of some 0.1-1 μW at 1.5 μm , that we attribute to direct impact excitation of the Er ions by the injected electrons. In order to achieve optical gain for the realization of a Si-based laser, the number of inverted Er ions has been estimated. In the best case, it has been possible to invert about 10% of the Er population. Some improvement is finally proposed to increase the optical power by the use of AC excitation.

References

- [1] O. Jambois Y. Berencen, K. Hijazi, M. Wojdak, A. J. Kenyon, F. Gourbilleau, R. Rizk, and B. Garrido, Journ. Appl. Phys. **106**, 063526 (2009).
- [2] O. Jambois, F. Gourbilleau, A. J. Kenyon, J. Montserrat, R. Rizk, B. Garrido, Optics Express **18**, 2230 (2010).
- [3] A. Marconi, A. Anopchenko, M. Wang, G. Pucker, P. Bellutti, L. Pavesi, Appl. Phys. Lett. **94**, 221110 (2009).
- [4] N. Daldosso, D. Navarro-Urrios, M. Melchiorri, and L. Pavesi, F. Gourbilleau, M. Carrada, R. Rizk, C. García, P. Pellegrino, B. Garrido, and L. Cognolato, Appl.Phys. Lett. **86**, 261103 (2005).

Figures

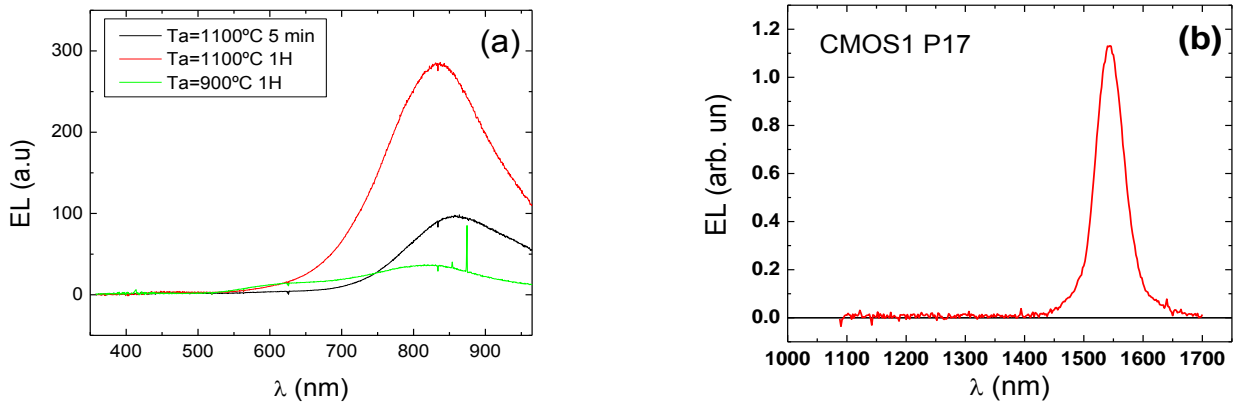


Figure 1 : Electroluminescence spectra of a) Si nanocrystals b) Er ions sensitized by Si nanoclusters.

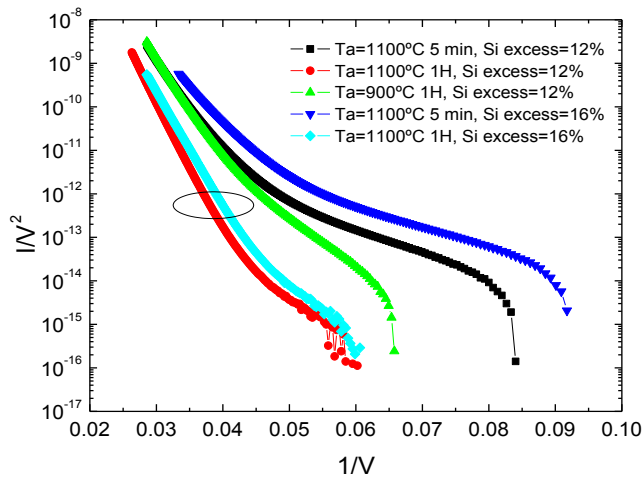


Figure 2 : Fowler-Nordheim representation of the I-V characteristics, suggesting direct impact excitation of the Er ions.

A highly integrated optical sensor for point of care label free identification of pathogenic bacteria strains and their antibiotic resistance

D. Hill^{a*}, V. Toccafondo^b, J. Garcia-Rupérez^b, A. Griol^b, J. Garcia-Castelló^b, A. C. Krüger^c, M. Kristensen^c, T. Claes^d, J. Gironès-Molera^d, K. De Vos^d, E. Schacht^d, R. Baets^d and P. Bienstman^d

^a Microsystem Technology Laboratory, School of Electrical Engineering, KTH – Royal Institute of Technology, Stockholm, Sweden

^b Centro de Tecnología Nanofotónica, Universidad Politécnica de Valencia, Camino de Vera s/n, 46022 Valencia, Spain

^c Århus University - Interdisciplinary Nanoscience Center, Århus, Denmark

^d Ghent University, Ghent, Belgium

*danhill@kth.se

We overview our recent developments in nanophotonic biosensor arrays for the detection of whole bacteria and PCR products. The work is part of the EU InTopSens project, with the aim to demonstrate the feasibility of a rapid diagnostic test for sepsis. This requires detecting the presence and identification of bacteria species from whole blood and their antibiotic resistance profile, which can be accomplished through the detection of the presence of specific DNA strands. Our principal approach is by the simultaneous measurement of bacterial nucleic acid strands on a 64 sensor spot array, to identify the presence of *e-coli*, *streptococcus aureus* or *coagulase negative staphylococci*, as well as the β Lactams and fluoroquinolones resistance markers.

Recent publications [1, 2] have demonstrated slot waveguide ring resonator sensors with a detection limit as low as 5×10^{-6} RIU and a sensitivity as high as 240 nm/RIU over a 7K temperature operating window, without need of external temperature control or individual sensor calibration. A detection limit of 1×10^{-7} RIU for TM polarized light has been recently shown [3] for Mach-Zehnder based DNA sensing.

For simplicity of experimental design, photonic sensor development within the project has to date been carried out on immunoassays rather than bacteria and/or nucleic acids. The next steps will be in meeting the challenge of extreme temperature ramping for the sample DNA melting (at 95 °C) and subsequent hybridization (at 60 °C). Initial developments in the first sensor 'base technology' for SOI silicon photonic wires began by replacing strip ring resonators [4] with slot-waveguides rings in order to improve sensitivity and the limit of detection for DNA hybridization sensing. Experiments with biotin/avidin showed [5] the resonators to have 298 nm/RIU sensitivity and 4.2×10^{-5} RIU detection limit for changes in the refractive index of the top cladding, a 3.5x increase in sensitivity over the base technology but a poorer detection limit due to bending and surface roughness losses. In an alternative approach to a structure with an improved detection limit Mach-Zehnder Interferometers with folded waveguides have been realized. Developments in the second sensor 'base technology' of SOI silicon photonic crystals have led to a sensitivity of 82.5 nm/RIU for the TE cutoff wavelength which corresponds to a detection limit of 2.2×10^{-4} RIU, an factor of 2.5 improvement compared to that previously seen [6].

The authors acknowledge support of the European Commission through the FP7-ICT-InTopSens project (223932).

References

- [1] C. F. Carlborg et al., A packaged optical slot-waveguide ring resonator sensor array for multiplex label-free assays in labs-on-chips, Lab Chip, 2010, DOI: 10.1039/b914183a
- [2] K. B. Gylfason et al., On-chip temperature compensation in an integrated slot-waveguide ring resonator refractive index sensor array, Optics Express, submitted.
- [3] L. M. Lechuga et al., Biosensing microsystem platforms based on the integration of Si Mach-Zehnder interferometer, microfluidics and grating couplers, Proc. SPIE, Vol. 7220, 72200L (2009)
- [4] K. De Vos et al, Silicon-on-Insulator microring resonator for sensitive and label-free biosensing, Optics Express, no. 12 (2007), 15, 7610-7615
- [5] T. Claes et al, Label-free biosensing with a slot waveguide based ring resonator in silicon-on-insulator, IEEE Photonics Journal, no. 3 (2009), 1, 197-204
- [6] N. Skivesen, et al, Photonic-crystal waveguide biosensor, Optics Express, no. 6 (2007), 15, 3169-3176.

Photoconductively loaded plasmonic nanoantennas as a building block for ultracompact optical switches

Nicolas Large^{1,2}, Martina Abb³, Javier Aizpurua¹ and Otto L. Muskens³

¹Centro de Física de Materiales CSIC-UPV/EHU and Donostia International Physics Center DIPC, Paseo Manuel de Lardizabal 4, Donostia-San Sebastian 20018, Spain

²CEMES-CNRS / Université de Toulouse, France

³School of Physics and Astronomy, University of Southampton, Highfield, Southampton SO17, 1BJ, United Kingdom

O.Muskens@soton.ac.uk; aizpurua@ehu.es

Plasmonics has emerged recently as an extremely promising technological research area. Active control over subwavelength optical fields is important in several application fields (sensing, optical communication and quantum information technology). In the terahertz (THz) range, the conductivity of semiconductor has been used to control the transport of THz waves through the coupling to the surface plasmon modes of nanostructures [1]. Recent works have shown control over progressive loading of a nanoantenna, which could be understood in the framework of circuit theory [2].

Here we explore a plasmonic nanoantenna switch as a novel building block for ultracompact nonlinear photonic devices. We propose that the large light-matter interaction strength and fast dynamics of a single nanoantenna can be used to control both far- and near-fields. Tunability of the nanoantenna by impedance loading of its nanogap using a dielectric medium has been studied both experimentally and theoretically [3,4]. Our nanoantenna switch is based on a similar but conceptually very distinct approach using photoconductive loading of the nanoantenna gap. Figure 1 represents the principle of the photoconductively loaded nanoantenna built by two gold nanorods separated by a gap filled with amorphous silicon. The photoconductive gap loading results in a transition from a capacitively coupled (“OFF”) to conductively coupled (“ON”) state.

To investigate theoretically this concept we use the Boundary Elements Method (BEM) in a full electromagnetic calculation including retardation [5,6]. This method consists in solving Maxwell's equations by means of a distribution of surface charge densities and currents at the surfaces of the objects that interact selfconsistently with the incoming field. Figure 2 shows the extinction spectra of the nanoantenna for two free carrier densities (N_{eh}) resulting in the two switching “OFF” and “ON” states. The transition from the unswitched to the switched state results in a large red shift of the antenna resonance, an increase of the radiation efficiency (insets) and a strong modification of the near-field distribution (not shown here). The theoretical concept is generally applicable to a wide range of experimental designs and will be of importance for applications involving nonlinear optics and SERS, quantum emitters and coherent control.

References

- [1] H.-T. Chen et al, *Nature Phot.* 3, 148 (2009).
- [2] M. Schnell, A. Garcia-Etxarri, A. J. Huber, K. Crozier, J. Aizpurua, R. Hillenbrand, *Nature Phot.* 3, 287 (2009).
- [3] A. Alù and N. Engheta, *Nature Phot.* 2, 307 (2008).
- [4] J. Berthelot et al, *Nano Lett.* 9, 3914 (2009). [5] F. J. García de Abajo and A. Howie, *Phys. Rev. Lett.* 80, 5180 (1998). [6] J. Aizpurua et al, *Phys. Rev. B* 71, 235420 (2005).

Figures

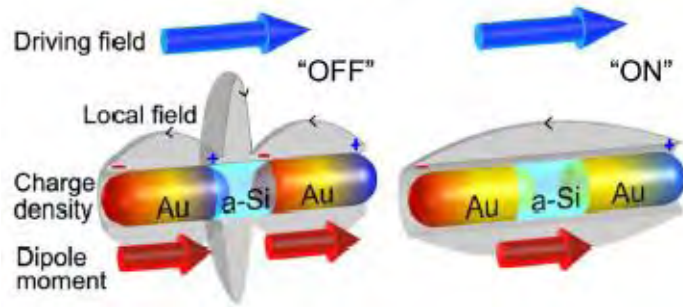


Figure 1- Principle of operation of the antenna switch, showing transition from capacitively coupled gap ("OFF") to conductively coupled gap ("ON").

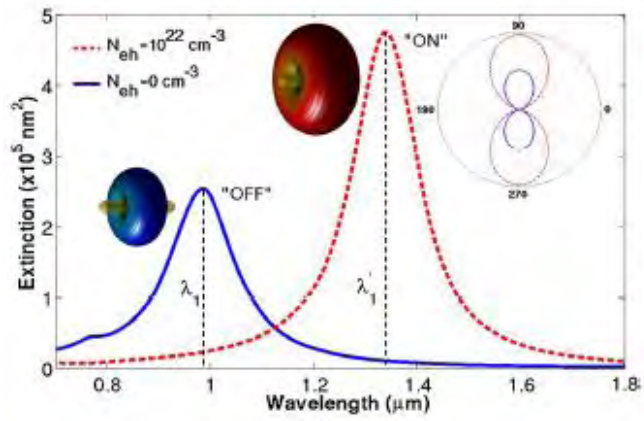


Figure 2- Calculated extinction spectra of nanoantenna switch, with radiation patterns (insets).

Optical gain in DNA-DCM for lasing in photonic materials*

Marco Leonetti, Riccardo Sapienza, Marta Ibisate, Claudio Conti and Cefe López
Photonic Cryatal group ICMM, Sor Juana Inés de la Cruz, 3, Cantoblanco, 28049 Madrid, Spain.

marcoleonetti1@gmail.com

We present a detailed study of the gain length in an active medium obtained by doping of DNA strands with 4-(dicyanomethylene)-2-methyl-6-(4-dimethylaminostyryl)-4H-pyran dye molecules. The superior thermal stability of the composite and its low quenching permit one to obtain an optical gain coefficient larger than 300 cm^{-1} . We also demonstrate that such an active material is feasible for the infiltration into photonic nanostructures, allowing one to obtain fluorescent photonic crystals and promising lasing properties.

Nanoengineered devices and metamaterials are offering nowadays novel ways of controlling light propagation and amplification ranging from random systems [1] to photonic crystals [2]. Nanostructured lasers are typically realized on a subwavelength structured dielectric matrix, either periodically or randomly, in which an active medium is inserted to provide optical gain. Their optimization has often been focused on the increase in the matrix quality and refractive index contrast, while recently more efficient active media like fluorescent polymers [3,4] or dye doped semiconductors [5] have proven to enhance light amplification.

Within these novel materials, DNA strands intercalated with dye molecules have been proposed as efficient and stable gain media [6]. The superior thermal stability of the composite (up to 250°C) and its low quenching owing to a controlled proximity of the dye molecules attached to the DNA provide an enhancement of the emitted integrated luminescence with respect to the conventional polymer-dye composite [7]. This makes DNA-based dyes as optimal candidates to infiltrate nanostructures and to realize novel active photonic devices. Direct-gain measurements are the best way to compare the optical amplifications and efficiencies of active media [8,9]. At variance with simple luminescence experiments, gain studies are not affected by the sample thickness uncertainty or by variations in the outcoupling owing to the edge roughness.

We report on the characterization of the optical amplification of DNA films intercalated with a 4-(dicyanomethylene)-2-methyl-6-(4-dimethylaminostyryl)-4H-pyran (DCM) laser dye (DNA-DCM) by measuring the optical gain coefficient g , which reaches values as large as 300 cm^{-1} . We demonstrate how this material can be used to introduce an efficient gain into self-assembled photonic nanostructures.

Figure 1(a) shows the optical gain coefficient g as a function of the DNA-DCM weight percentage. The optimal amplification efficiency is obtained for a dye density between 2 and 3 wt. %, while at higher concentrations quenching phenomena decrease the effective optical amplification.

Figure 1(b) shows the optical gain coefficient as a function of the pump power for an optimal DNADCM ratio of 3 wt. %. For energies higher than $4 \text{ nJ}/\mu\text{m}^2$, the gain coefficient saturates, while above $9 \text{ nJ}/\mu\text{m}^2$ the gain reduction is due to optical damage.

We have also performed a lasing experiment on samples, with and without DNA, obtaining random lasing (RL) [10-12].

In Fig. 2(a) the normalized emission intensity is plotted versus the wavelength for different pump pulse energies. The spectral FWHM narrows from 85 to 15 nm by increasing the pump energy. Figure 2(b) shows the peak intensity (open squares) and FWHM (open triangles) as a function of the pump energy. This demonstrate the clear efficiency advantage of this material as the lasing threshold occurs at energy densities 10 times lower respect same sistem doped with standard dye.

In conclusion we measured optical gain coefficients with values as high as 300 cm^{-1} , with low quenching, and large thermal stability. Careful characterization of the gain length in the active material allows one to predict the lasing threshold and to efficiently design novel light-emitting nanostructures.

References

- [1] D. S. Wiersma, *Nat. Phys.*, **4**, (2008) 359.
- [2] Yu. A. Vlasov, K. Luterova, I. Pelant, B. Honerlage, and V. N. Astratov, *Appl. Phys. Lett.*, **71**, (1997) 1616.
- [3] D. Zhang, Y. Wang, and D. Ma, *Appl. Phys. Lett.*, **91**, (2007) 091115.
- [4] N. Balan, M. Hari, V. Parameswaran, and N. Nampoore, *Appl. Opt.*, **48**, (2009) 3521.
- [5] F. J. Duarte, *Appl. Phys. B*, **90**, (2008) 101.
- [6] A. J. Steckl, *Nat. Photonics*, **1**, (2007) 3.
- [7] Z. Yu, W. Li, J. A. Hagen, Y. Zhou, D. Klotzkin, J. G. Grote, and A. J. Steckl, *Appl. Opt.*, **46**, (2007) 1507.
- [8] A. Costela, O. García, L. Cerdán, I. García-Moreno, and R. Sastre, *Opt. Express*, **16**, (2008) 7023.
- [9] L. Dal Negro, P. Bettotti, M. Cazzanelli, D. Pacifici, and L. Pavesi, *Opt. Commun.* **229**, (2004) 337.
- [10] D. S. Wiersma and A. Lagendijk, *Phys. Rev. E*, **54**, (1996) 4256.
- [11] C. Conti, M. Leonetti, A. Fratolocci, L. Angelani, and G. Ruocco, *Phys. Rev. Lett.*, **101**, (2008) 143901.

Figure 1

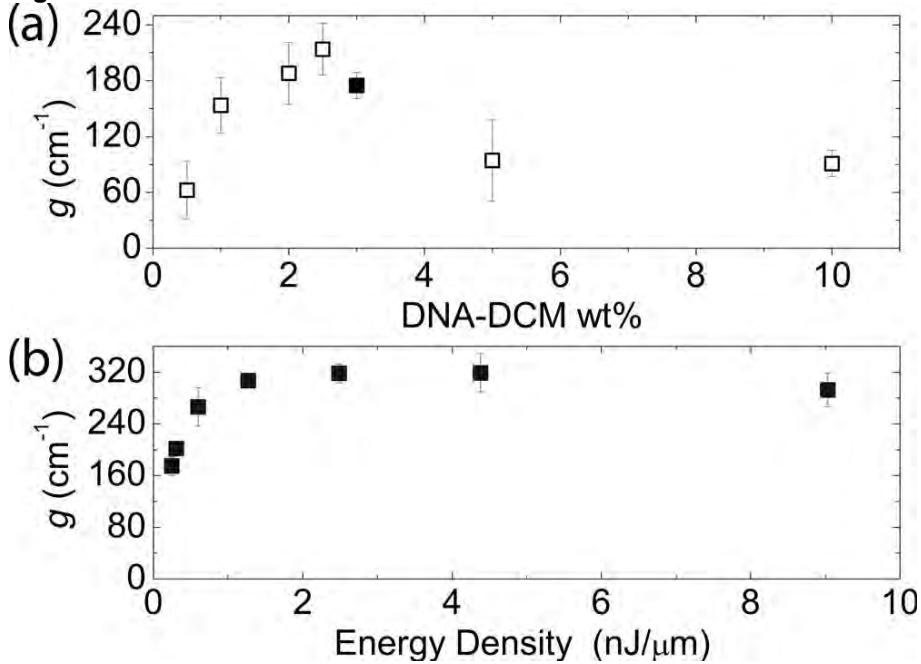
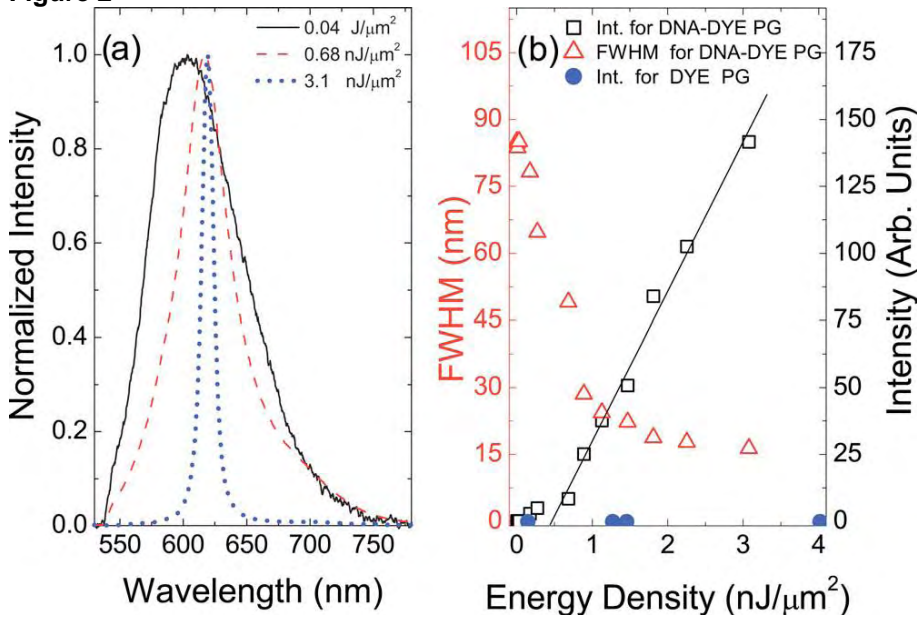


Figure 2



Towards a full understanding of the growth dynamics, optical response and crystalline structure of self-assembled photonic colloidal crystal films

Gabriel Lozano, Luis A. Dorado, Ricardo A. Depine, Hernán Míguez

Recent advances in the comprehension of the growth dynamics of colloidal crystal films opens the door to rational design of experiments aiming at fabricating lattices in which the density of intrinsic defects is minimized.[1,2] Since such imperfections have a dramatic effect on scattered light of wavelength smaller than the lattice constant, the evaluation of the experimental optical response at those energy ranges, based on the comparison to rigorous calculations, is identified as the most sensitive guide to accurately evaluate the progress towards the actual realization of defect-free colloidal crystals.[3] The importance of the existence of a certain distortion becomes particularly relevant at the above mentioned energy range. We have thoroughly analyzed the effect of fine structural features on the optical response to conclude that, rather than the generally assumed FCC lattice of spheres, opal films are better approximated by a rhombohedral assembly of distorted colloids. Interparticle distance of actual colloidal crystals coincides with the expected diameter for spheres belonging to the same close-packed (111) plane but differs significantly in directions oblique to the [111] one.[4]

[1] G. Lozano, H. Míguez, *Langmuir* **23**, 9933 (2007).

[2] G. Lozano, H. Míguez, *Appl. Phys. Lett.* **92**, 091904 (2008)

[3] G. Lozano, L. A. Dorado, D. Shinca, R. A. Depine, H. Míguez, *J. Mater. Chem.* **19**, 185 (2009)

[4] G. Lozano, L. A. Dorado, D. Shinca, R. A. Depine, H. Míguez, *Langmuir* **25**, 12860 (2009).

Vacuum and thermal friction in rotating particles

Alejandro Manjavacas and F. Javier García de Abajo
Instituto de Óptica – CSIC, Serrano 121, 28006 Madrid, Spain
Email: ama@io.cfm.csic.es

In this paper, we explore the thermal and vacuum electromagnetic friction [1] acting upon small rotating particles (see Fig.1a). Working in the framework of the linear response theory, our results are based in the application of the Fluctuation-Dissipation Theorem [2,3].

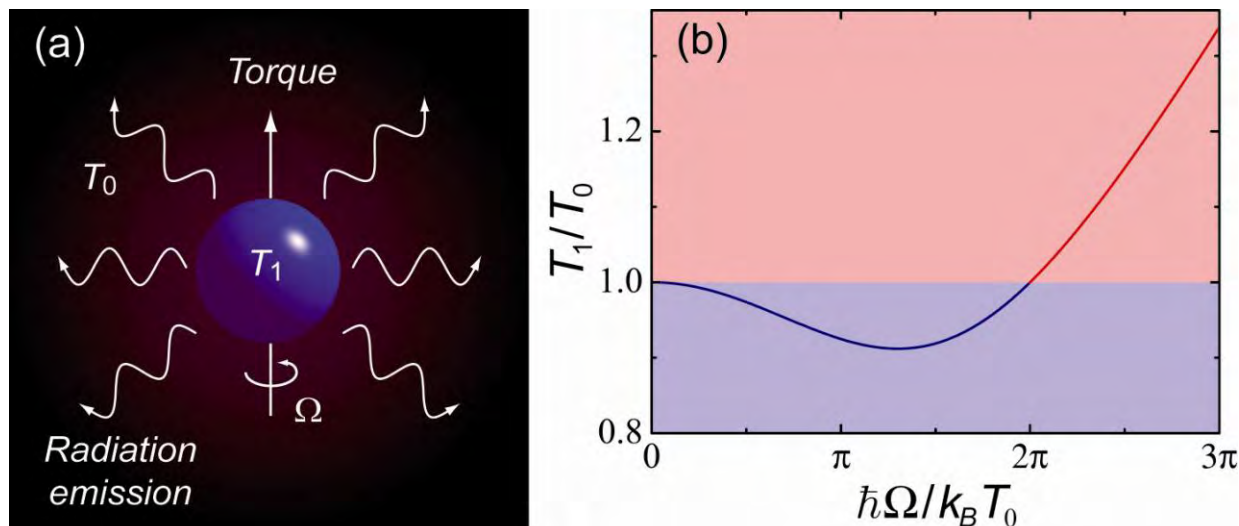


Figure 1. (a) System under study, consisting of an isotropic particle at temperature T_1 placed in vacuum at temperature T_0 . The particle is rotating around the z-axis with an angular frequency Ω , and suffers an electromagnetic interaction with the surrounding radiation field. Due to this interaction the particle experiences a torque and radiates a net power. (b) Ratio between the particle and the environment temperatures as a function of the rotational frequency Ω . While for high rotational frequencies the friction leads to the heating of the particle, in the opposite limit the particle is cooled.

Assuming the dipolar approximation, we can characterize the EM properties of the nanoparticle through its polarizability. Within this formalism we are able to present analytical expressions for the net power radiated by the particle, as well as for torque exerted on it by the vacuum fields. Following from these results we compute the evolution of the internal energy of the particle, which allows us to describe the variations in its temperature during the friction process.

At zero temperature, vacuum friction transforms mechanical energy into light emission and particle heating. However, particle cooling relative to the background occurs at finite temperature and low rotation velocity (see Fig. 1b). Radiation emission is boosted and its spectrum significantly departed from the black-body emission profile as the velocity increases.

Finally, we illustrate our work with numerical examples, in which we study the dynamics of rotating particles placed in different environments (e.g., molecular clouds in outer space). In particular, we present results for the time needed for a particle to slow down its rotation to half the initial speed due to interaction with a thermal EM bath. Our study can be relevant in the design of nano-devices comprising rotating parts, as well as in the control of spinning nanoparticles.

Acknowledgments

This work has been supported by the Spanish MICINN (MAT2007-66050 and Consolider NanoLight.es). A.M. acknowledges an FPU scholarship from the Spanish MEC.

References

- [1] J. B. Pendry, J. Phys. Condens. Matter. **9**, (1997) 10301.
- [2] H. B. Callen and T. A. Welton, Phys. Rev. **83**, (1951) 34.
- [3] R. Kubo, Rep. Prog. Phys. **29**, (1966) 255.

Tailoring the modulation depth in Au/Co/Au magnetoplasmonic switches

D. Martín-Becerra^{‡,1}, J. B. González-Díaz¹, V. V. Temnov², A. Cebollada¹, G. Armelles¹, T. Thomay³, A. Leitenstorfer³, R. Bratschitsch³, A. García-Martín¹, M. U. González¹

¹IMM-Instituto de Microelectrónica de Madrid (CNM-CSIC), Isaac Newton 8, PTM, E-28760 Tres Cantos, Madrid, Spain.

²Department of Chemistry, Massachusetts Institute of Technology, Cambridge (MA), USA

³Department of Physics and Center for Applied Photonics, University of Konstanz, Germany

[‡]diana.martin@imm.cnm.csic.es

The ability of surface plasmon polaritons (SPP) to confine optical fields beyond the diffraction limit makes them very attractive for the development of miniaturized optical devices. Several passive plasmonic systems have been successfully demonstrated in the last decade, but the achievement of nanophotonic devices with advanced functionalities requires the implementation of active configurations. This requires the capability to manipulate the surface plasmon polaritons with an external agent. Among the different control agents considered so far, the magnetic field holds a robust promise since it is able to directly modify the dispersion relation of SPP [1]. This modulation lies on the non-diagonal elements of the dielectric tensor, ϵ_{ij} . For noble metals, the ones typically used in plasmonics, these elements are unfortunately very small at reasonable field values. On the other hand, ferromagnetic metals have sizeable ϵ_{ij} values at small magnetic fields (proportional to their magnetization), but they are optically too absorbent. Thereby, a smart system to develop magnetic field sensitive plasmonic devices could be multilayers of noble and ferromagnetic metals [2, 3].

Based on these hybrid multilayers, a magnetoplasmonic switch has been recently demonstrated [4]. The switch has been implemented through a micro-interferometer consisting on a slit paired with a tilted groove (see figure 1). Illumination with a *p*-polarized laser beam at normal incidence results in the excitation of SPPs at the groove, which propagates towards the slit, where they are reconverted into free-space radiation (I_{SP}) and interfere with light directly transmitted through the slit (I_r). The interference term is given by $\sqrt{I_{SP}}\sqrt{I_r} \cos(k_{SP}d + \lambda_0)$, with k_{SP} the SPP wavevector and d the groove-slit distance. In our tilted groove configuration, d varies for each slit position, creating a pattern of maxima and minima in the light transmitted through the slit (optical interferogram, see image in fig. 1). When we apply an external periodic magnetic field high enough to saturate the sample (about 20 mT) in the direction parallel to the slit axis, k_{SP} is modified therefore shifting the interference pattern. Thus, at each slit position we detect a variation of the intensity synchronous with the applied magnetic field (magnetoplasmonic interferogram, see graph in fig. 1). The analysis of both interferograms allows us to extract the SPP wavevector modulation, Δk . The full intensity modulation depth of the system is given by the product $\Delta k \times d$.

The modulation obtained in this basic configuration of the magnetoplasmonic switch, Au/Co/Au multilayers in air, is $\Delta k \sim 0.5 \times 10^{-3} \mu\text{m}^{-1}$ for a wavelength of $\lambda_0 = 800 \text{ nm}$, reasonable although slightly low for practical applications. Optimization of the geometrical parameters to achieve the maximum possible modulation of the surface plasmon wavevector will provide a higher flexibility in the design of the magneto-plasmonic optical switches. A straightforward approach consists on the coverage of the metallic switch with a dielectric media with high ϵ_d , since the modulation Δk is proportional to $(\epsilon_d)^2$ [4]. We have then covered our magnetoplasmonic switches with a thin layer of PMMA ($\epsilon_d = 2.22$). Figure 2 shows the measured Δk for systems with 60 nm PMMA at $\lambda_0 = 633 \text{ nm}$ as compared to identical reference samples without PMMA. A fourfold enhancement of the modulation, in excellent agreement with the theoretical predictions, has been obtained. Nevertheless, the propagation distance of the plasmon decreases with the addition of overlayers, which will prevent the use of interferometers with large d and the intensity modulation depth will then be limited. Thus, a compromise between the modulation enhancement and the propagation distance of the SPP has to be achieved. The relevant figure of merit in this case is the product $\Delta k \times L_{SP}$. In fact, our theoretical results show that, adding the polymer cover, we can actually almost double that product. A detailed analysis of the behaviour of the magnetoplasmonic switches when covered with dielectric overlayers, both in terms of modulation enhancement and propagation distance, will be presented.

References:

- [1] R. F. Wallis, J. J. Brion, E. Burstein, and A. Hartstein, Phys. Rev. B **9** (1974) 3424.
- [2] J. B. González-Díaz, A. García-Martín, G. Armelles, J. M. García-Martín, C. Clavero, A. Cebollada, R. A. Lukaszew, J. R. Skuza, D. P. Kumah and R. Clarke, Phys. Rev. B **76** (2007) 153402.
- [3] E. Ferreiro-Vila, J. B. González-Díaz, R. Fermento, M. U. González, A. García-Martín, J. M. García-Martín, A. Cebollada, G. Armelles, D. Meneses-Rodríguez and E. Muñoz-Sandoval, Phys. Rev. B **80** (2009) 125132.
- [4] V. V. Temnov, G. Armelles, U. Woggon, D. Guzatov, A. Cebollada, A. Garcia-Martin, J. Garcia-Martin, T. Thomay, A. Leitenstorfer, and R. Bratschitsch, Nat. Photonics **4** (2010) 107.

Figures:

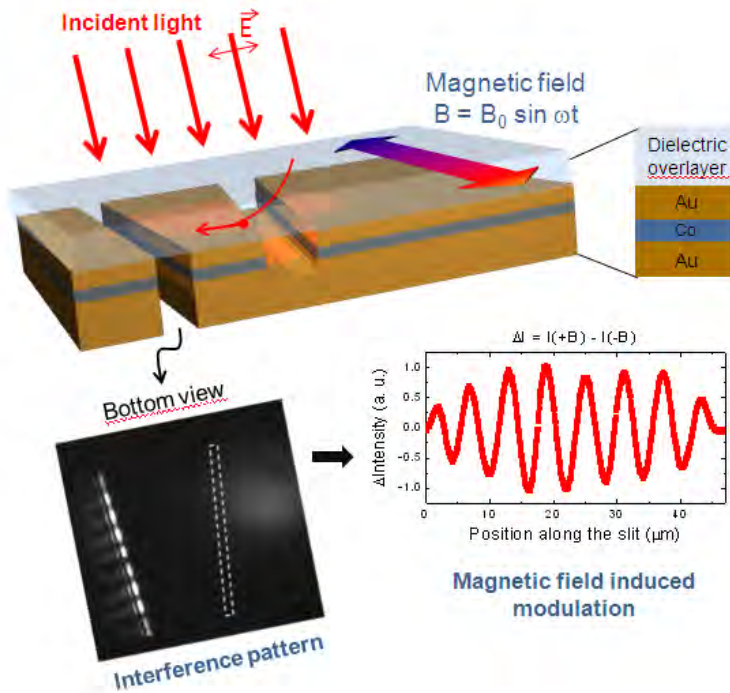
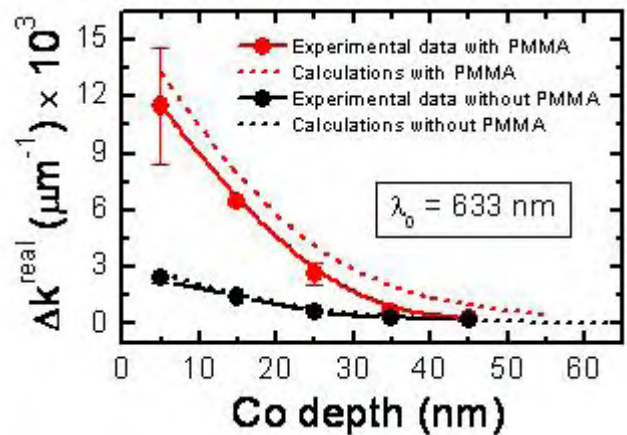


Figure 1: Sketch of the magneto-plasmonic micro-interferometer.

Figure 2: Comparison of the SPP wavevector modulation as a function of the Co layer position for Au/Co/Au micro-interferometers without dielectric overlayer and with 60 nm PMMA overlayer. The values correspond to $\lambda_0 = 633$ nm.



Exciton emission dynamics of single-photon emitters based on InP/(Ga, In) P quantum dots

M. D. Martín, A. K. Nowak, E. Gallardo, H. P. van der Meulen, L. Viña, and J. M. Calleja

Departamento de Física de Materiales, Universidad Autónoma de Madrid, E-28049 Madrid, Spain

J. M. Ripalda, L. González, and Y. González

Instituto de Microelectrónica de Madrid, CNM-CSIC, E-28760 Tres Cantos, Spain

dolores.martin@uam.es

The exciton recombination dynamics of individual InP/(Ga, In) P quantum dot (QD) single – photon emitters has been studied by time – resolved photoluminescence (TRPL) and photon correlation spectroscopy (PCS) as a function of temperature and dot size. An increase of temperature produces marked effects on the exciton photoluminescence (PL) decay time (τ_X) and on the anti-bunching time (τ_R). Both times are found to depend on the QD size. In small QDs both τ_X and τ_R increase with temperature, whereas in larger QDs τ_X remains constant and τ_R decreases for increasing temperature. A competition of the thermally activated Dark-to-Bright (DB) exciton transition and the thermal excitation of the carriers to - and from the QD give a good qualitative understanding of the observed results.

Self-assembled InP/(Ga,In) P QDs grown by molecular beam epitaxy are selected from the high energy tail of the ensemble PL emission in order to study single QDs with reduced influence of the neighboring ones. Both TRPL and PCS are performed under quasi-resonant excitation, either below the wetting layer absorption or in resonance with excited QD states. This minimizes the influence of carrier diffusion on the measured times. Temperature has been varied in the 10 – 40 K range. The TRPL is measured using a streak camera coupled to an imaging spectrometer (overall time resolution of 40 ps). For PCS we have used a Hanbury-Brown and Twiss interferometer coupled to one of the exits of a spectrometer. Three peaks are observed in the micro-PL spectra of each QD and are assigned to the exciton (X), bi-exciton (XX) and charged exciton (CX) recombination, respectively. The QD excited states have been identified by micro-PL excitation (PLE) measurements. We observe several peaks in the PLE spectra, which are indicative of QD excited states and of phonon-assisted absorption. QDs of different sizes have been selected considering their bi-exciton binding energy and their fine structure splitting.

For a given QD, the TRPL and PCS results indicate that in the X recombination both τ_X and τ_R are approximately twice as long as for XX, evidencing the XX decay into the X state. Upon increasing temperature, both τ_X and τ_R increase in small QDs (QD1, figure 1 (c) and (e)), as a result of the thermal excitation of holes out of the exciton, which reduces the emission probability of both X and XX. This occurs at low activation energies for small QDs ($E_h = 7$ meV), as measured from the $I_X/(I_X+I_{XX})$ intensity ratio (figure 1 (a)). In larger QDs (QD2 in figure 1) this activation energy is much higher ($E_h = 30$ meV, figure 1(b)) and therefore it is the DB exciton transition that dominates, leading to in a reduction of τ_R (figure 1 (f)). The τ_X value is found to be independent of temperature (figure 1 (d)) for QD2 as a result of the compensation between two competing effects: i) the DB transition, which reduces τ_X , and ii) the thermal scattering of carriers inside the QD, which delays their arrival to the ground state and therefore increases τ_X . Finally, preliminary experiments have revealed a marked reduction of τ_R upon resonant excitation at the QD p-states. Our results are relevant for the development of single photon emitters based on InP and working at high temperatures.

References

[1] A. K. Nowak, E. Gallardo, D. Sarkar, H. P. van der Meulen, J. M. Calleja, J. M. Ripalda, L. González, and Y. González, *Physical Review B* **80** (2009), 161305 (R).

Figures

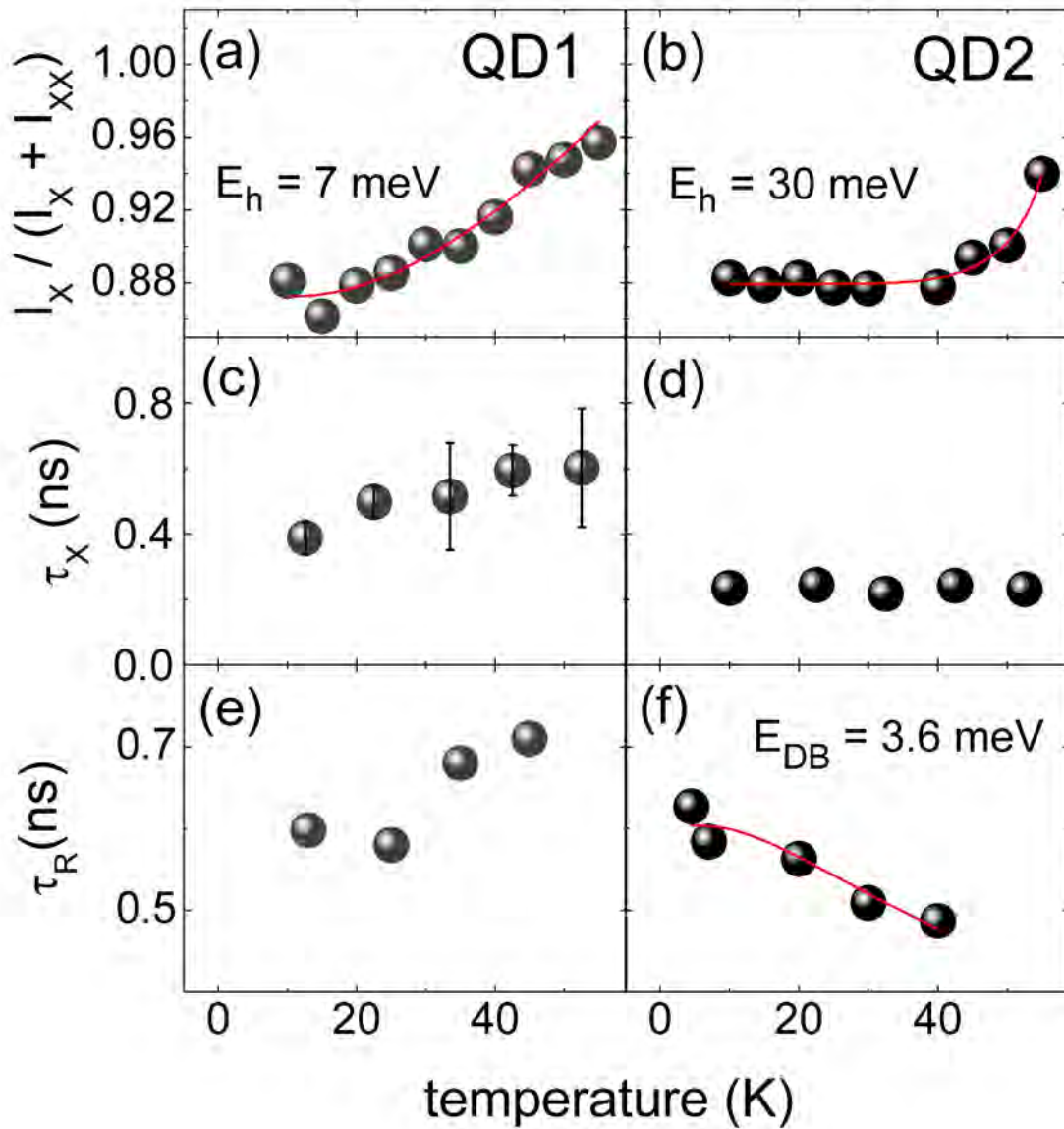


Figure 1. Temperature dependence of the QDs properties: (a), (b) PL intensity ratio of X and XX; (c), (d) X decay time τ_X ; (e), (f) X-X auto-correlation anti-bunching time τ_R .

Eu³⁺:La₂O₃ nanoparticles dispersed into P3HT as a down converter material for exploiting the solar spectrum

M. Méndez^{a,b,c}, L.F. Marsal^a, Y. Cesteros^b, J.J. Carvajal^c, E. Martínez-Ferrero^d, A. Giguere^e, D. Drouin^e, P. Formentín^a, J. Pallarès^a, P. Salagre^b, M. Aguiló^c, F. Díaz^c

^aDept. d'Enginyeria Electrònica, Univ. Rovira i Virgili (URV), E-43007 Tarragona (Spain)

^bDept. Química Física i Inorgànica, Univ. Rovira i Virgili (URV), Campus Sescelades, Marcel·lí Domingo, s/n, E-43007 Tarragona (Spain)

^cFísica i Cristal·lografia de Materials i Nanomaterials (FICMA-FICNA), Univ. Rovira i Virgili (URV), Campus Sescelades, Marcel·lí Domingo, s/n, E-43007 Tarragona (Spain)

^dInstitute of Chemical Research of Catalonia (ICIQ), Avd. Països Catalans, 16, E-43007 Tarragona (Spain)

^eDept. Electrical and Computer Engineering, Université de Sherbrooke, Sherbrooke, PQ, J1K 2R1
lluis.marsal@urv.cat

While down-converter (DC) phosphors have been investigated for decades in the lighting industry, the possibility of down-converting sunlight to enhance performance of solar cells was just been treated recently by Trupke et al. [1].

The concept of wavelength conversion in photovoltaics is to manipulate the incident solar spectrum using appropriate materials in order to convert photons from mismatched portions of the incident solar spectrum into photons within the wavelength range efficiently used by the photovoltaic cell. Many decades of research have gone into optimising silicon devices; however it seems that further advances can be made better by modifying the input spectrum, rather than improving the electronic properties of the device [2]. By placing a luminescent down converter material in contact with the photovoltaic cell, part of the energy in the near-UV region can be reconverted to energy in the visible and near-IR that can be efficiently absorbed by the photovoltaic cell.

We propose to use europium doped lanthanum oxide (Eu³⁺:La₂O₃) nanoparticles as a down converter material to enhance the efficiency of the P3HT organic solar cells. La₂O₃ nanocrystals doped with 5 mol % of Eu³⁺ were prepared using the modified Pechini method [3]. According to Park et al. [4] due to the concentration quenching effect, the maximum Eu³⁺ concentration for which quenching was not yet observed was determined to be about 5 mol %.

These nanoparticles absorb light in a broad band between 240 and 320 nm, while they emit only in discrete bands located between 580 and 710 nm, presenting a maximum of emission at around 625 nm (see dotted line in Fig.1 and 2).

The motivation for using materials containing rare-earths as DC materials is that this family of elements show luminescent properties over a wide range of wavelengths, extending from the near-infrared (NIR), through the visible (vis) to the ultraviolet (UV).

To study the properties as DCs of these nanoparticles, it was necessary to disperse them into a semiconductor polymeric thin film. This P3HT polymeric matrix possesses good mechanical toughness, chemical stability, and excellent processability. Besides giving improved properties, this semiconductor polymeric matrix gives the perfect conditions to convert the light emitted from the nanoparticles on energy in the solar cell. We prepared a mixture of P3HT in tetrahydrofuran (TFH) solvent and nanoparticles with a concentration of 15 wt% to respect the polymer. The mixture was stirred during 10 min. A spin coater device was used to make a thin film of this nanocomposite on a piece of quartz under nitrogen atmosphere by adding 1 ml of the mixed solution and then spinned at 500 rpm for 2 min. Figure 3a) shows the film obtained from P3HT and the nanoparticles where it is possible to see the transparent violet colour from the P3HT polymer and it high homogeneity.

The main reason of using this kind of semiconductor polymer, besides its good properties, was due to its absorption region band, as show Fig.3b). Semiconductor P3HT polymer covered partially the range of emission of Eu³⁺:La₂O₃ nanoparticles, including the most intense emission peak at 626 nm. However, the UV region was not affected for this polymer absorption indicating that the polymer did not absorb efficiently the range of wavelengths covered by the CTS band of the nanoparticles (see not dotted line in Figure 1 and 2). The light emitted from nanoparticles after down-conversion process has to be adsorbed by the polymer extending in this way the spectral range of a hypothetical solar cell based on these materials.

Acknowledgements

This project has been supported by the Spanish Government under projects MAT2008-06729-C02-02/NAN, TEC2009-09551, HOPE CSD2007-00007 (Consolider-Ingenio 2010), and AECID-A/024560/09, by the Catalan Authority under project 2009SGR1238, 2009SGR549, and 2009SGR235; and by the Research Center on Engineering of Materials and Systems (EMaS) of the URV. J.J.C. is supported by the Research and Innovation Ministry of Spain and European Social Fund under the

Ramón y Cajal program, RYC2006-858. EMF acknowledges the MICINN for a Juan de la Cierva fellowship.

References

- [1] T. Trupke, M.A. Green, P. Würfel, J. Appl. Phys., **92** (3) (2002) 1668.
- [2] B.S. Richards, Sol. Energ. Mater. Sol. Cell., **90** (2006) 1189.
- [3] M. Méndez, J.J. Carvajal, Y. Cesteros, M. Aguiló, F. Díaz, A. Guiguere, D. Drouin, E. Martínez-Ferrero, P. Salagre, P. Formentín, J. Pallarès, L.F. Marsal, Opt. Mater., (2010).
- [4] J.K. Park, S.M. Park, C.H. Kim, H.D. Park, S.Y. Choi, J. Mater. Sci. Lett, 20 (2001) 2231.

Figures

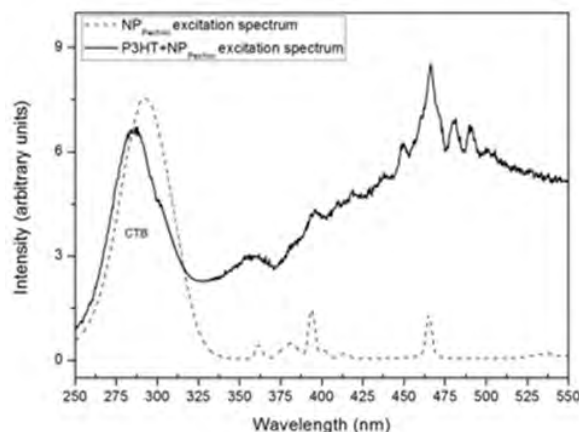


Figure 1. Excitation spectrum of the $\text{Eu}^{3+}:\text{La}_2\text{O}_3$ nanocrystals (dotted line) with a maximum peak at ~ 285 nm and excitation spectrum of the nanoparticles dispersed into P3HT polymeric matrix (not dotted line) with maximum at ~ 280 nm.

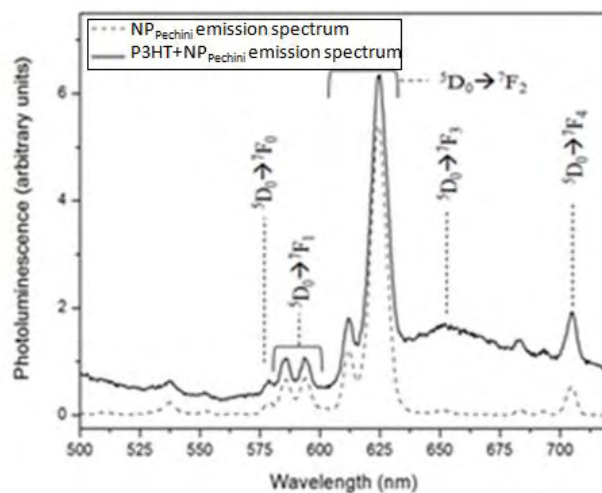


Figure 2. Emission spectrum of the nanoparticles (dotted line) and emission spectra of the nanoparticles dispersed into P3HT polymeric matrix (not dotted line).

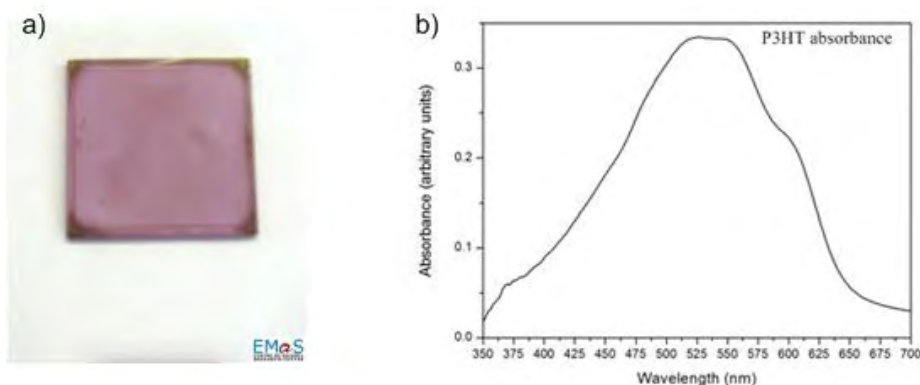


Figure 3a) Photograph of the P3HT polymer with nanoparticles on a piece of quartz; b) absorption spectrum of the P3HT with a wide band from 350 to 650 nm approximately.

Theoretical Study of Colorimetric Resonant Structures for Biosensing Applications

S. Hamid Keshmiri, Pilar Rodríguez-Franco, Nasser Darwish, Mario Montes[#], **Mauricio Moreno**
Department of Electronics. [#]Department of Optics and Applied Physics.
University of Barcelona, Department of Electronics, Barcelona, Spain
mauricio.moreno@ub.edu

In general, biosensors consist of a highly specific recognition element and a transducer that converts the molecular recognition event into a quantifiable signal. In the case of optically-based transduction methods, that do not require labelling of analytes with fluorescent compounds, they are of interest due to the relative assay simplicity and ability to study the interaction of small molecules and proteins that are not readily labelled. Direct optical methods include surface plasmon resonance (SPR) [1], evanescent wave devices [2], grating couplers [3] and others.

Optical Grating Couplers (OGC) are based in the highly dependence of the coupling angle in front of the local external refractive index. There are two main different modes of operation for monitoring refractive index changes in this type of optical biosensors: angular and spectral interrogation.

In angular interrogation there are different configurations: i) a monochromatic light is focused to create a range of illumination angles and directed into the waveguide grating. The reflected light is monitored with a CCD camera or other imaging detector. ii) It is also possible to measure the coupling angle rotating the sample and measuring the output light at the end of the waveguide; it is known as OWLS (Optical Waveguide Light-mode Spectroscopy) technique. iii) In our group we have developed an optical set-up for measuring the out-coupling angle in a two-grating configuration, without moving parts [4].

In spectral interrogation mode, a broadband spectrum light (white light) is sent on the grating surface and the reflected light is collected and monitored with a spectrometer. By observing the spectral location of the resonant peak wavelength value (PWV), one can monitor refractive index changes at or near the surface of the waveguide grating or, linking receptor molecules to the grating surface, complementary binding molecules can be detected without the use of any kind of fluorescent probe or particle label [5,6]. Laboratory equipment based in this technique is Corning Epic-system [7].

In this work we present optical design of diffraction gratings structures and spectral interrogation for biological applications. For our purpose we have used OptiFDTD 8.0 software. Figure 1 is a cross-section of the simulated structure: a glass substrate ($n=1.46$) with 200nm silicon nitride layer ($n=2.0$) working as a waveguide; a diffraction grating is etched on the surface with a period of $\Lambda=500\text{nm}$, 50% duty cycle. We use normal incidence and light polarized perpendicular to the grating period. The red layer represents any biolayer attached to the top surface in an external medium; we have used $n=1.5$ as the refraction index.

Figure 2 shows i) the reflectance spectrum, showing the resonant behaviour of this type of structure and ii) the shift of Peak Wavelength (PWV) due to the growth of a thin layer in the range of nanometres on the grating. Also we see how the PWV doesn't shift for thick protein layers; this means that above 500nm of thickness, the biolayer behaves as the external medium, saturating the shift effect.

The location of the PWV depends strongly on the geometry of the structure and on material properties: refractive index, depth, duty cycle, and period. In figure 3 we show the linear dependence of PWV versus the refractive indices of liquid solutions, using water ($n=1.333$), PBS ($n=1.339$), acetone ($n=1.36$), isopropyl alcohol ($n=1.38$), and sodium chloride solution ($n=1.4$) as standards.

For this structure we obtain a great theoretical sensitivity of $S=\Delta\lambda/\Delta n = 130 \text{ nm}$, higher than $S = 87.5 \text{ nm}$ in [5]. Taking account that we can resolve variations $\Delta\lambda=0.01\text{nm}$ for a standard spectrometer like the popular SD2000 (OCEAN OPTICS), we expect an approximately detection limit of $7\cdot 10^{-5}$ RIU (Refractive Index Units), which is enough for applications of surface molecular recognition.

References

- [1] "Surface plasmon resonance sensors: review"; Jiri Homola, Sinclair S. Yee, Günter Gauglitz; Sensors and Actuators B: Volume 54, 1999, Pages 3–15
- [2] "Micro- and nanoimmunosensors: technology and applications"; Laura M. Lechuga; Anal Bioanal Chem: Volume 384, 2006, Pages 44–46
- [3] "Optical grating coupler biosensors"; J.Vörös, J.J. Ramsden, G. Csúcs, I. Szendrő, S.M. De Paul, M. Textor, N.D. Spencer; Biomaterials: Volume 23, 2002, Pages 3699–3710
- [4] "Multi-analytic grating coupler biosensor for differential binding analysis"; N. Darwish, D. Caballero, M. Moreno, A. Errachid, J. Samitier; Sensors and Actuators B: Chemical, Volume 144, Issue 2, 17 February 2010, Pages 413-417
- [5] "Colorimetric resonant reflection as a direct biochemical assay technique"; B. Cunningham et al., Sensors and Actuators B: Volume 81, 2002, Pages 316-328
- [6] "Large-area submicron replica molding of porous low-k dielectric films and application to photonic crystal biosensor fabrication"; Microelectronic Engineering; Volume 84, Issue 4, April 2007, Pages 603-608
- [7] <http://www.corning.com/lifesciences/>

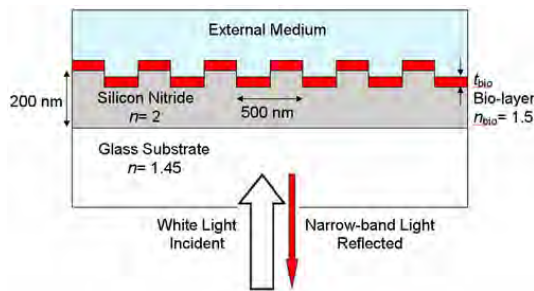


Figure 1. Cross section of the simulated structure: grating etched on a silicon nitride layer on a glass substrate. Grating period = 500nm

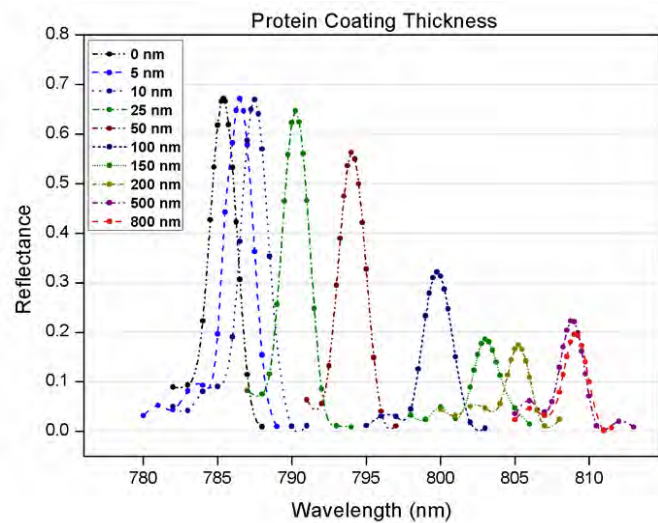


Figure 2. Peak Wavelength value shift in front to the thickness of the biolayer.

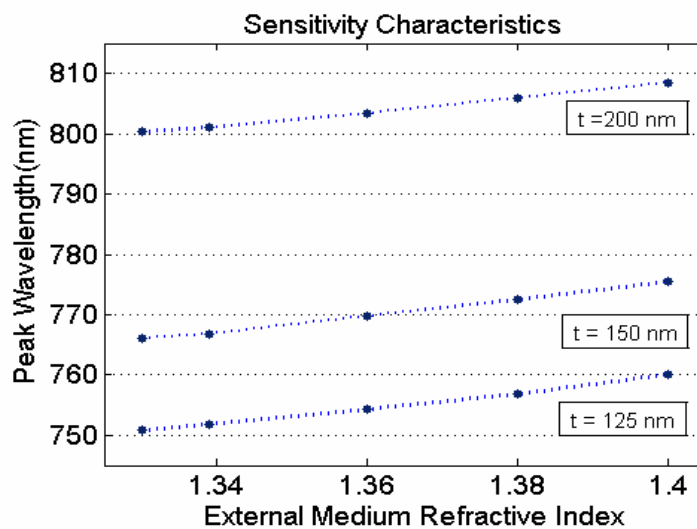


Figure 3. Peak Wavelength value shift for three values of thickness (t) of silicon nitride layer, in front of external refractive index.

Domino plasmons for subwavelength terahertz circuitry

Esteban Moreno¹, D. Martín-Cano¹, M. L. Nesterov^{1,2},
A. I. Fernández-Domínguez¹, L. Martín-Moreno³, F. J. García-Vidal¹

¹Departamento de Física Teórica de la Materia Condensada,
Universidad Autónoma de Madrid, E-28049 Madrid, Spain

²A. Ya. Usikov Institute for Radiophysics and Electronics,
NAS of Ukraine, 12 Academician Proskura Street, 61085 Kharkov, Ukraine

³Instituto de Ciencia de Materiales de Aragón (ICMA) and
Departamento de Física de la Materia Condensada,
CSIC-Universidad de Zaragoza, E-50009 Zaragoza, Spain

esteban.moreno@uam.es

Electromagnetic radiation in the terahertz (THz) regime is a central resource for many scientific fields such as spectroscopy, sensing, imaging, and communications. Within this context, the building of compact THz circuits would stand out as an important accomplishment. This requires the design of THz waveguides carrying tightly confined electromagnetic modes, preferably with the following properties. First, structures should be easily manufactured, planar, and monolithic. Second, subwavelength transverse size is also needed. Finally, absorption and bend losses should be small, and the waveguides sufficiently versatile for the design of key functional devices. Particularly important are in/out-couplers since they work as the interface to external waves. In this context, compact tapers able to laterally compress the modes down to the subwavelength level seem essential.

With the aim of addressing the above mentioned issues, in this paper a new approach for the spatial and temporal modulation of electromagnetic fields at terahertz frequencies is presented. The waveguiding elements are based on plasmonic and metamaterial notions and consist of an easy-to-manufacture periodic chain of metallic parallelepipeds protruding out of a metallic surface (Fig. 1, left). The electromagnetic modes supported by such structures are termed *domino plasmons*.

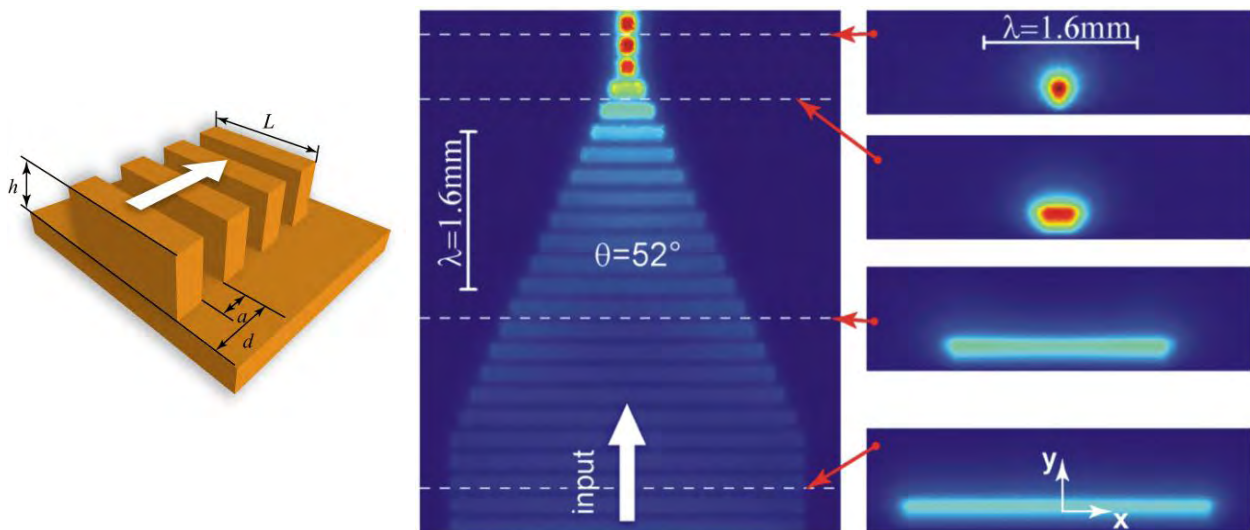


Fig. 1 Left: A domino plasmon structure consists of a periodic array of metallic box-shaped elements protruding out of a metallic substrate. Right: Top view and cross sections of a tapered domino structure, displaying the subwavelength field confinement and enhancement with negligible loss and reflection

The properties of domino plasmons are controlled by the structure geometry, the most important parameters being the periodicity, d , and the height, h , of the parallelepipeds. In the talk it will be shown that, when the operation frequency lies in the far infrared or the THz regime, the dispersion relation of domino plasmons is rather insensitive to the waveguide width, L . This surprising behavior can be

understood as a consequence of the existence of a metallic substrate and the fact that the gaps between consecutive parallelepipeds are open not only at the top but also at both lateral sides. In contrast with other conventional structures, the insensitivity to the waveguide lateral size of domino plasmons is achieved preserving at the same time a tight confinement even when the waveguide transverse dimension, L , is well in the subwavelength regime. This property enables the simple implementation of key devices, such as tapers (Fig. 1, right). Such elements allow the subwavelength confinement and enhancement of THz electromagnetic fields.

The ohmic absorption losses and the radiative losses in bent waveguides are characterized, finding reasonably low values. These properties, when considered together with the previously mentioned insensitivity to lateral width, suggest that domino plasmons could find application to build subwavelength THz devices and circuits. This is confirmed by the implementation of essential circuit elements such as power dividers, directional couplers, waveguide bends, and ring resonators. These elements are characterized by means of rigorous Finite Elements simulations, demonstrating the flexibility of the proposed concept and the prospects for terahertz applications requiring high integration density.

References

- [1] D. Martin-Cano, M. L. Nesterov, A. I. Fernandez-Dominguez, F. J. Garcia-Vidal, L. Martin-Moreno, and Esteban Moreno, *Opt. Express*, **18** (2010) 754.

Micro-photoluminescence from InAs/GaAs quantum dot pairs and molecules grown by droplet epitaxy

G. Muñoz-Matutano^a, J. Canet-Ferrer^a, B. Alén^b, P. Alonso-González^b, I. Fernández-Martínez^b, D. Fuster^a, M. Royo^c, J.I. Climente^c, J. Planelles^c, J. Martínez-Pastor^a, Y. González^b, F. Briones^b and L. González^b

^a Instituto de Ciencias de los Materiales, Universitat de València, POBox 22085, 46071 Valencia, Spain.

^b Instituto de Microelectrónica de Madrid (IMM-CNM- CSIC), Isaac Newton 8, E-28760, Tres Cantos Madrid, Spain.

^c Grupo de química cuántica. Universitat Jaume I de Castelló. guillermo.munoz@uv.es

guillermo.munoz@uv.es

We have investigated electric field dependence emission properties of single InGaAs/GaAs quantum dot pairs and molecules. These nanostructures were grown by droplet epitaxy [1]. This growth technique results in the formation of nanoholes where in-plane laterally aligned pairs of quantum dots (QDs) can be nucleated using the appropriate growth conditions. Compared with purely self-assembled methods, the droplet epitaxy technique allows to control separately the emission energy and nucleation density and produces good optical properties at the single QD level [2]. We have fabricated lateral electric field Schottky devices that allow to tune the energy levels of both QD and produce molecular coupling. We have found three different micro-photoluminescence (micro-PL) pictures, attached to single QD, QD pair (not coupled) and QD molecule (coupled) systems. Single QD picture is related to the 2% of possibilities to obtain only one QD at each nanohole. QD pair micro-PL evolution was found when distance between both QDs is too large to produce strong molecular coupling. Finally, it was found asymmetrical micro-PL features (figure 1) which are in good correspondence with theoretical framework based on full CI (Configuration Interaction) calculations and effective mass approximations. Although clear anticrossing optical signatures were not identified, this signature of lateral molecular coupling is not easily found in literature [3, 4], the asymmetric Coulomb blockade QD charging and Stark effect gives valuable information to confirm the molecular coupled system [5].

References:

- [1] P. Alonso-González, J. Martín-Sánchez, Y. González, B. Alén, D. Fuster, and L. González. *Crystal Growth and Design* 9 (2009) 2525 (2009).
- [2] P. Alonso-González, B. Alén, D. Fuster, Y. González, L. González, J. Martínez-Pastor. *Appl Phys Lett* 91 (2007) 163104 .
- [3] E. A. Stinaff , M. Scheibner, A. S. Bracker, I. V. Ponomarev, V. L. Korenev, M. E. Ware, M. F. Doty, T. L. Reinecke, D. Gammon. *Science* 311 (2006) 636 .
- [4] H. J. Krenner, K. Mueller, C. Lienau, T. Elsaesser, A. D. Wieck. *Phys Rev Lett* 94 (2005) 057402 .
- [5] J. Peng, C Hermannstädter, M Witzany, M Heldmaier, L Wang, S Kiravittaya, A Rastelli, O G. Schmidt, P Michler, G Bester, arXiv: 0910.5138v1 (2009).

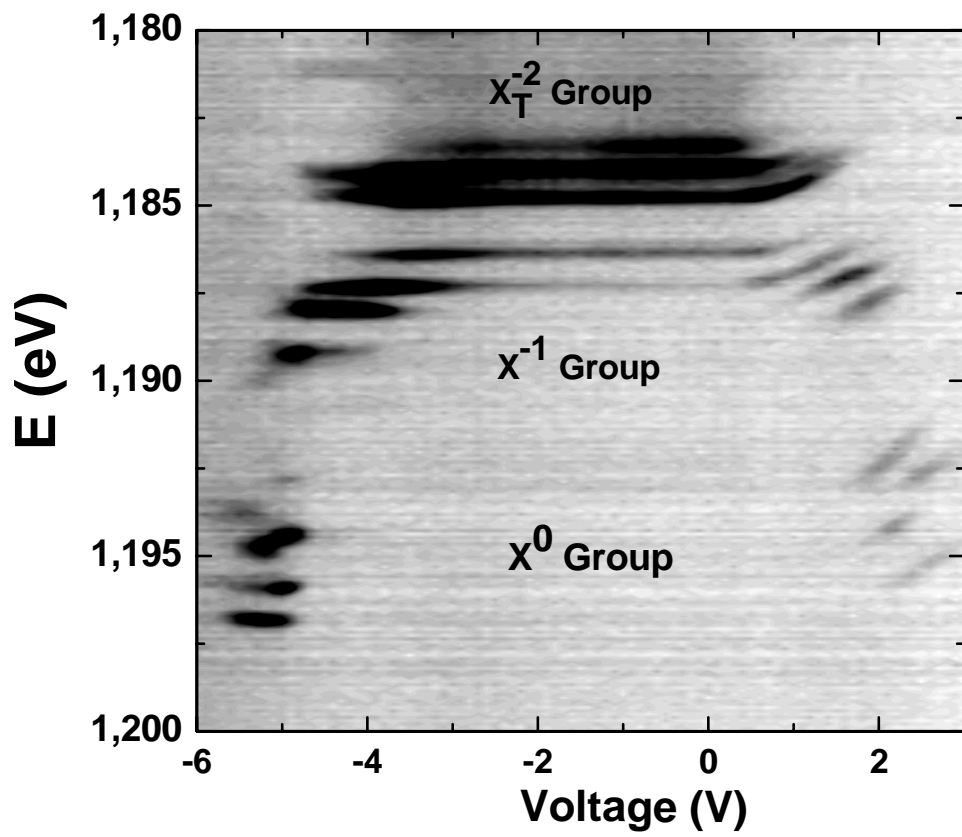


Figure 1. Voltage dependence sweep of the micro-PL from a coupled QD pair system.

Whispering gallery mode optical characterization on Si rich Si₃N₄ active microdisk resonators

D. Navarro-Urrios¹, F. Ferrarese-Lupi¹, J. Montserrat², C. Dominguez², and B. Garrido¹

¹ MIND-IN2UB, Dept. Electrònica, Universitat de Barcelona, C/ Martí i Franquès 1, 08028 Barcelona, Spain

² IMB-CNM, CSIC, Bellaterra, E-08193 Barcelona, Spain
dnavarro@el.ub.es

One of the major obstacles for large-scale silicon-based electronic-photonic integration is the absence of a compact and efficient silicon-based light source, due to the intrinsic inability of silicon to emit light efficiently. Various strategies for improving light emission in silicon have been demonstrated during the last decade [1], one of the most promising ones being the use of nanostructured silicon (Si-nc) in the form of clusters embedded in dielectric matrices. An intensive knowledge has been already obtained for Si rich SiO₂ materials, in which a SiO₂ medium surrounds the Si-nc. However, there are two drawbacks concerning this kind of material that should be taken into account for fabricating active photonic devices: i) the relatively low refractive index (1.5-1.6) with respect to SiO₂, which impacts on the compactness of the photonic devices; ii) this material is not ideal for the fabrication of stable and efficient electrically driven devices due to a huge barrier mismatch between Si and SiO₂. As a consequence, Si rich Si₃N₄ matrices have attracted attention since they present both a higher refractive index and a smaller band gap with respect to Si rich SiO₂. In addition, efficient light emission under optical and electrical pumping has been also reported recently [2,3].

On the other hand, monolithic circular resonators such as micro-disks, rings and toroids are triggering an intensive and rapidly evolving research due to the low fabrication complexity, which relaxes the ultrahigh resolution process needed to create photonic crystal cavities with similar properties. In circular optical microcavities electromagnetic fields at certain optical frequencies can be localized in ultra-small modal volumes by means of total internal reflection effect, leading to the so-called whispering gallery modes (WGM).

An interesting approach is to combine the light propagation and emission properties of Si rich Si₃N₄ matrices and the optical properties of microcavities. In this work we have done a simulation and experimental study of the WGM emission properties of single microdisk resonators with an optically active disk material made of luminescent Si-nc embedded in Si₃N₄ matrix deposited over a SiO₂ cladding.

By using a three-dimensional FDTD package we have done a study of the modal structure of the microresonators, i.e. the position and quality factors of the resonance peaks and electric field spatial distribution of the different modes inside the cavity, which were modified by varying the structural parameters of the optical elements.

In addition, we have produced a set of different samples where the Si₃N₄ stoichiometric material has been deposited by using the LPCVD deposition technique which has been subsequently suffered a double ion implantation of Si followed by an annealing procedure in N₂ atmosphere at 1100°C. The photonic structures have been afterwards defined by means of standard photolithographic techniques. On figure 1 we show an AFM image of one of the microdisk structures designed, where we have achieved an average surface roughness of less than 1nm.

Room temperature micro-PL measurements have been performed in order to characterize the on-plane emission spectrum of single microdisks. The microdisks close to a cleaved sample edge were excited vertically, while the WGM emission was monitored in the plane of disks. On the main panel of figure 2 we show the actual measurement of a 3µm radius microdisk, where several resonances are observed modulating the PL emission of the active material. On panel b), a zoomed part around 715nm of the spectrum is showed in order to show clearly the width of the observed resonances. As it can be seen from the lorentzian fit of a resonance present at 719nm, sub-nanometer WGM resonances are observed, corresponding to quality factors higher than 1200. These values are among the highest previously reported values in Si-nc-based systems [4,5] and are actually limited by the resolution of our experimental setup.

In addition, an increasing of the pumping flux is not generating a spectral widening of the resonances and high pumping powers does not seem to affect the quality of both the material and the cavities. This is in contrast to what observed in other reports of Si-nc based microcavities, where significant enlargements are observed associated to carrier absorption losses [4,5].

References

- [1] Silicon Photonics, edited by L. Pavesi and D. J. Lockwood □ Springer, Berlin, (2004)
- [2] N. M. Park, C. J. Choi, T. Y. Seong, and S. J. Park, Phys. Rev. Lett. **86**, □(2001) 1355
- [3] K.S. Cho, N.M. Park, T.Y. Kim, K.H. Kim, G.Y. Sung and J.H. Shin, Appl. Phys. Lett. **86** (2005) 071909
- [4] M. Ghulinyan, D. Navarro-Urrios, A. Pitanti, A. Lui, G. Pucker, and L. Pavesi, Opt. Express **16**, (2008), 13218
- [5] R. D. Kekatpure and M. L. Brongersma, Phys. Rev. A **78**, 023829 (2008)

Figures

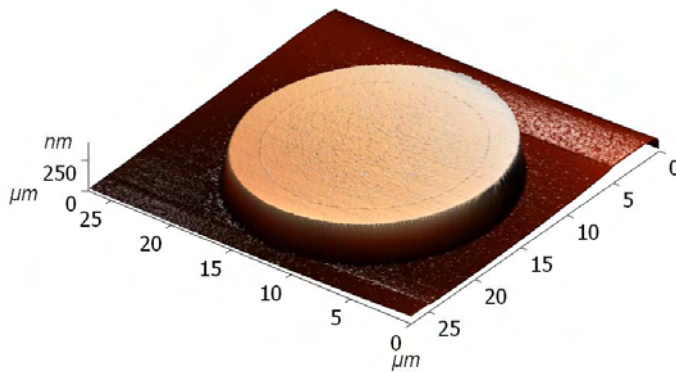


Figure 1. AFM image of a 10 μ m radius Si rich Si₃N₄ microdisk.

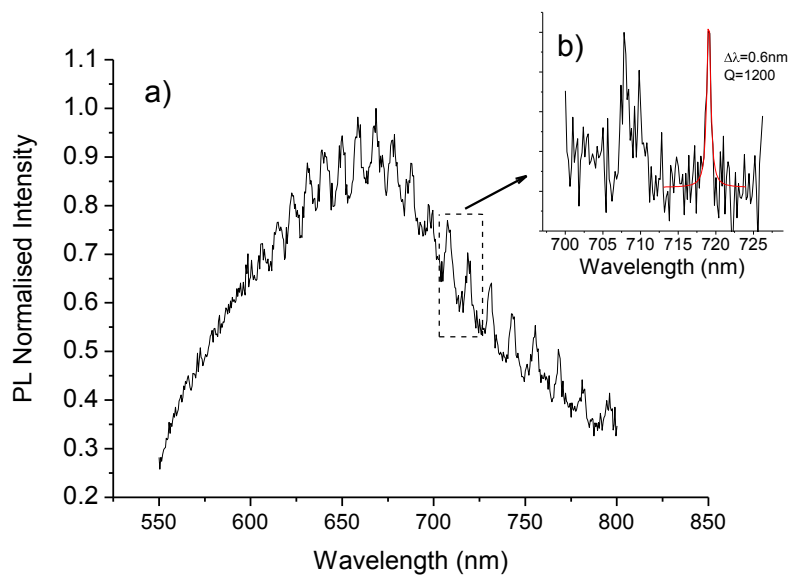


Figure 2. Panel a) Low resolution micro-PL spectrum of a 3 μ m radius microdisk. Panel b) High resolution spectrum of a particular part of the spectrum. The red curve shows a lorentzian fit of one of the resonances.

Dispersion engineered tapered fiber photonic nanowires

Manfred Niehus^{a,b}, Sérgio Ferreira^b, Gil G. Martins Fernandes^{a,c}, Armando Nolasco Pinto^{a,d}

^aInstituto de Telecomunicações, Campus Universitário de Santiago, 3810-193 Aveiro, Portugal

^bISEL|DEETC, R. Conselheiro Emídio Navarro 1, 1959-007 Lisboa, Portugal

^cDep.Física, Universidade de Aveiro, 3810-193 Aveiro, Portugal

^dDep. Electrónica, Telecomunicações e Informática, Universidade de Aveiro, 3810-193 Aveiro, Portugal

mniehus@av.it.pt

We present results on dispersion engineered tapered optical fiber based nanowires. Their characteristics are modelled and calculated, and compared with experimental results from group delay measurements. The detailed analysis is done with focus to applications. Important effects that are included in the analysis, and discussed therein, are the impact of refractive index profile change during the nanowire fabrication process at elevated temperatures, and the optical connection to the nanowire region through biconically tapered transition regions.

It is well known that the occurrence and characteristics of most non-linear optical effects strongly depend on the dispersion characteristics of devices [1]. The fabrication of tapered optical fibers through the flame brushing method is known to allow for a high precision fabrication of nanowires, and their optimization with regard to the desired device properties [2]. The coupling between modes is a characteristic property of tapered fibers, and can be employed in devices [2].

The analysis of most of the propagation characteristics of tapered optical fibers departs from a detailed analysis of the dispersion equations of cylindrical three layer waveguides, i.e. optical fibers with a finite clad and reduced clad diameters. The local mode dispersion relations are found by solving numerically the characteristic equation that is obtained when demanding as boundary conditions the continuity of transverse fields components and their derivatives, both at the radial core/clad and clad/air boundaries. As the properties of interest, i.e. the points of low (zero) group velocity dispersion, and its variation (flatness) correspond to the third resp. fourth order derivatives of the dispersion relation, it is important to numerically calculate a sufficiently elevated number of points.

Polynomial approximations are a convenient tool to approximate the numerical points with analytical functions, which accelerates the design process. However, care must be taken when dealing with higher order derivatives: the correlation between low order and high order precision has to be taken into account. We studied how the numerical precision and number of points, as well as the kind of polynomial methods, and tolerance, affects the precision when determining the zero dispersion point and its flatness. The results are simplified and convenient engineering design guidelines for this kind of structures.

We compare the predictions with experiments, and find good coincidence when taking into account the actual mode structure of the tapered fiber.

References

- [1] M. A. Foster, A.C. Turner, M. Lipson, and A.L. Gaeta, *Nonlinear optics in photonic nanowires*, Opt. Expr. 16, 1300 (2008).
- [2] M. Niehus, G.G.M.Fernandes, A.N.Pinto, *Design of a tunable single photon interferometer based on modal engineered tapered optical fibers*, to be published in SPIE Proc. Photonics Europe 2010.

Figures (next page)

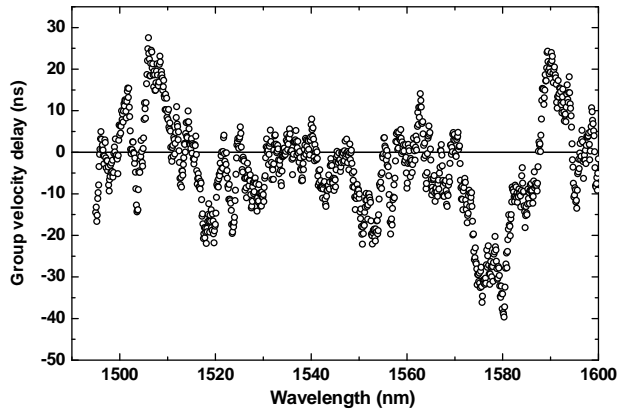


Figure 1
Experimental Results of Group Delay Experiments in Tapered Optical Fibers

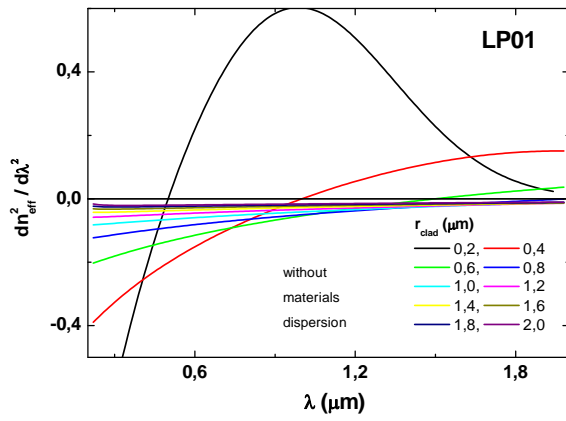


Figure 2
Theoretical Simulation of second order derivative of effective refractive index of fundamental mode in Tapered Optical Fibers, for several clad radii.

Norton waves in Plasmonics

A.Yu. Nikitin¹, Sergio G. Rodrigo¹, F. J. García-Vidal² and L. Martín-Moreno¹

¹Instituto de Ciencia de Materiales de Aragón and Departamento de Física de la Materia Condensada, CSIC-Universidad de Zaragoza, E-50009, Zaragoza, Spain

²Departamento de Física Teórica de la Materia Condensada, Universidad Autónoma de Madrid, E-28049 Madrid, Spain

alexeynik@rambler.ru

We present analytical results for the electromagnetic fields at the surface radiated by an aperture (both 2D, like a slit and 3D, like a hole) in a metal film. The expressions are valid for any metal, from the optical to the THz regime, and for distances to the aperture larger than a few tens of nanometers. The field pattern presents a rich behavior, which depends strongly on both distance to the aperture and angle with respect to the incident field. In the optical regime, surface plasmon polaritons (SPPs) have been thought to dominate the fields at the surface, beyond a transition region comprising 3–4 wavelengths from the source. In this work [1, 2], we demonstrate that at sufficiently long distances SPPs are not the main contribution to the field. Instead, for all metals, a different type of wave prevails, which we term Norton waves (NWs) for their resemblance to those found in the radio-wave regime at the surface of the Earth. Our results show that NWs are stronger at the surface than SPPs at distances larger than 6–9 SPP absorption lengths, the precise value depending on wavelength and metal. Moreover, NWs decay more slowly than SPPs in the direction normal to the surface.

References

[1] A. Y. Nikitin, S. G. Rodrigo, F. J. García-Vidal, and L. Martín-Moreno, “In the diffraction shadow: Norton waves versus surface plasmon polaritons in the optical region”, *New Journal of Physics* **11** (2009), 123020

[2] A. Y. Nikitin, F. J. García-Vidal, and L. Martín-Moreno, “The in-plane electromagnetic fields radiated by a small aperture in an optically thick metal film”, to be submitted

Optical spectroscopy of conductive molecular junctions in plasmonic cavities

O. Pérez-González^{1,2}, N. Zabala^{1,2}, A. Borisov³, N.J. Halas⁴, P. Nordlander⁵ and J. Aizpurua²

¹ Departamento de Electricidad y Electrónica, Univ. of the Basque Country (UPV/EHU), Bilbao, Spain.

² Donostia International Physics Center (DIPC) and Centro Mixto de Física de Materiales (CSIC-UPV/EHU), Donostia-San Sebastián, Spain.

³ Lab. des Collisions Atomiques et Moleculaires, CNRS-Université Paris-Sud, Orsay CEDEX, France.

⁴ Chemistry Department, Laboratory for Nanophotonics, Rice University, Houston, USA.

⁵ Physics Department, Laboratory for Nanophotonics, Rice University, Houston, USA.

olalla_perez@ehu.es

In the last decade fundamental advances have been achieved in the fields of molecular electronics [1] and plasmonics [2]. In particular, the optical properties of adjacent nanoshell pairs have been explained using exact numerical calculations and hybridization models [3]. Recent simultaneous measurements of electronic conduction and Raman spectroscopy in molecular junctions have suggested the possibility of sensing individual molecules [4], connecting both fields.

We study theoretically this connection between molecular electronics and plasmonics in a system composed of a molecular junction bridging a plasmonic cavity. More explicitly, we relate transport and optical properties through a model system consisting of a conductive bridge linking two gold nanoshells. The nanoshells are formed by a silica core surrounded by a gold shell and the molecular junction is modelled as a cylinder of radius a linking both nanoshells. The conductivity of the junction, σ , is related to its conductance, G , through the geometrical parameters of the system. Therefore, for a given size of the linker, we modify the conductivity of the junction varying the number n of quanta of conductance, nG_0 ($G_0 \equiv 2e^2/h \cong 77.5\text{mS}$). Maxwell's equations are solved via a boundary element method (BEM) [5] to obtain the electromagnetic fields and the optical extinction spectra.

We find two regimes in the optical response (see Figure 1). For the short wavelength regime, we first notice a broadening of the plasmon resonance as conductance is increased, followed by a slight blue-shift until a saturation point is reached. Then, the resonance becomes narrower again as conductance continues to be increased but its wavelength remains unaltered. We call this plasmon resonant mode the Bonding Dimer Plasmon (BDP). For the long wavelength regime, there is no appreciable change when conductance takes small values. However, for very large values of conductance, a new highly red-shifted resonance emerges. We call this resonance the Charge Transfer Plasmon (CTP) and its main feature is its tunability.

We use a simple resistor model to explain both the initial decrease of the optical extinction intensity of the BDP and its progressive recovery for further increase of the conductance. We also notice a slight blue-shift which corresponds to a screened Coulomb interaction at the junction between the gold shells. Moreover, we identify a threshold value of the conductance when the optical properties of the junction start being affected by the transport properties. This threshold conductance relates the time of flight of the electrons involved in the transport process with the time of the optical cycle of the plasmonic resonances of the cavity.

We believe that the study of this kind of spectral changes in plasmonic cavities might serve as a probe of molecular conductance and transport processes in the visible part of the spectrum, a range which is not accessible through electrical measurements.

References

[1] T. Dadoş Y. Gordin, R. Krahne, I. Khivrich, D. Mahalu, V. Frydman, J. Sperling, A. Yacoby, and I. Bar-Joseph, *Nature* **436**, (2005) 677.

[2] J. Aizpurua, G.W. Bryant, L.J. Ritcher and F.J. García de Abajo, *Phys. Rev. B* **71**, (2005) 235420.

[3] J.B. Lassiter, J. Aizpurua, L.I. Hernández, D.W. Brandl, I. Romero, S. Lal, J.H. Hafner, P. Nordlander and N.J. Halas, *Nano Lett.* **8**, (2008) 1212.

[4] D.R. Ward, N.J. Halas, J.W. Ciszek, J.M. Tour, Y. Wu, P. Nordlander and D. Natelson, *Nano Lett.* **8**, (2008) 919.

[5] F.J. García de Abajo and A. Howie, *Phys. Rev. Lett.* **80**, (1998) 5180.

Figures

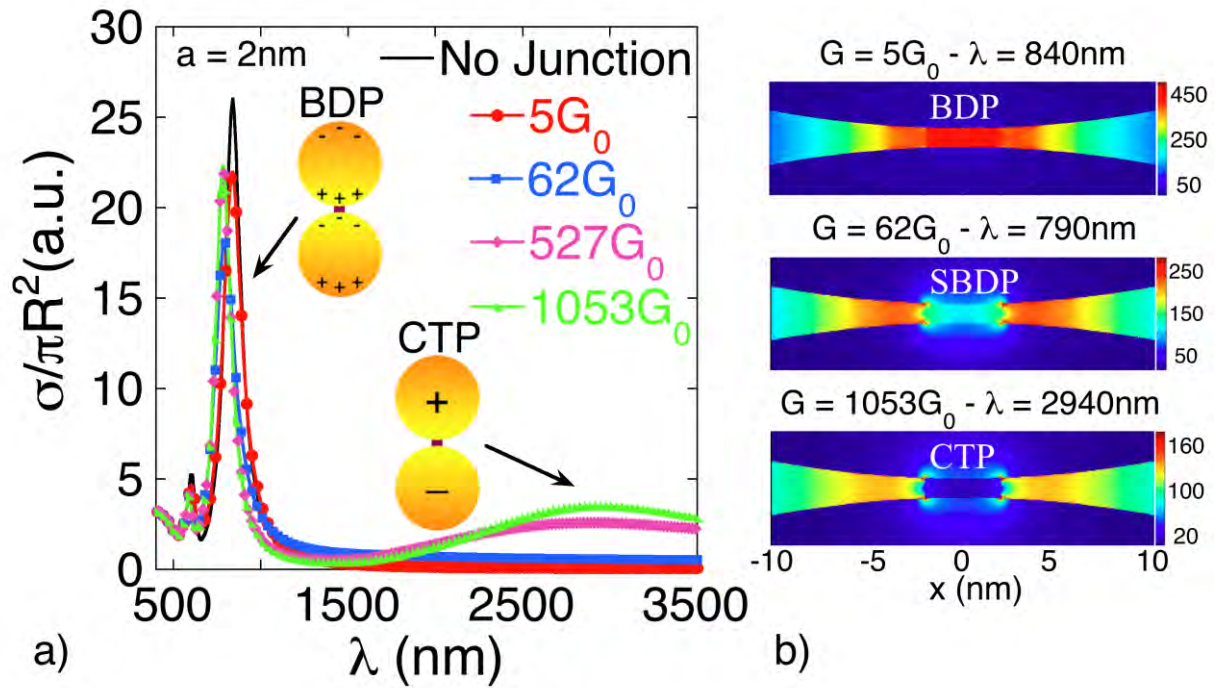


Figure 1: (Left) - Optical extinction spectra of a nanoshell dimer bridged by a conductive molecular junction of radius $a = 2\text{nm}$ as conductivity is increased via the increment of conductance. We can observe the variations in the behaviour of the plasmon resonance (BDP) and the emergence of the new resonance (CTP) in the IR part of the spectrum. (Right) - Near-fields patterns corresponding to the short wavelength regime (top and middle) and to the long wavelength regime (bottom), where the progressive expelling of the electric field out of the junction can be observed.

Fabrication of two dimensional photonic crystal micro and nanocavities: from ultra low threshold lasers to solid-state quantum light emitters

I. Prieto, L.J. Martínez, B. Alén, M. Kaldirim, L. E. Muñoz, D. Fuster, L. González, Y. Gonzalez, M. L. Dotor and **P.A. Postigo**

*Instituto de Microelectrónica de Madrid (CNM, CSIC), Isaac Newton 8,
E-28760, Tres Cantos Madrid, Spain*

aitor@imm.cnm.csic.es

Phone: +34 91 8060700 Fax: : +34 91 8060700

Two-dimensional photonic crystal lasers have been fabricated on III-V semiconductor slabs. Different structures based in the coupling of light between nanocavities have been fabricated like the hybrid lattice [1] or laser emitters with high quality factor L7 microcavities [2] and very low threshold values. The capability of confining light in very small dimensions allows for enhanced effects on cavity-QED. Photonic crystal cavities have been fabricated on self-assembled quantum nanostructures active material (like quantum rings and quantum dots) for the first time with special attention to the control of the polarization, quality factor and emission wavelength [3]. These structures open new ways for emission of single photons, emission of entangled photon pairs and optical quantum gates.

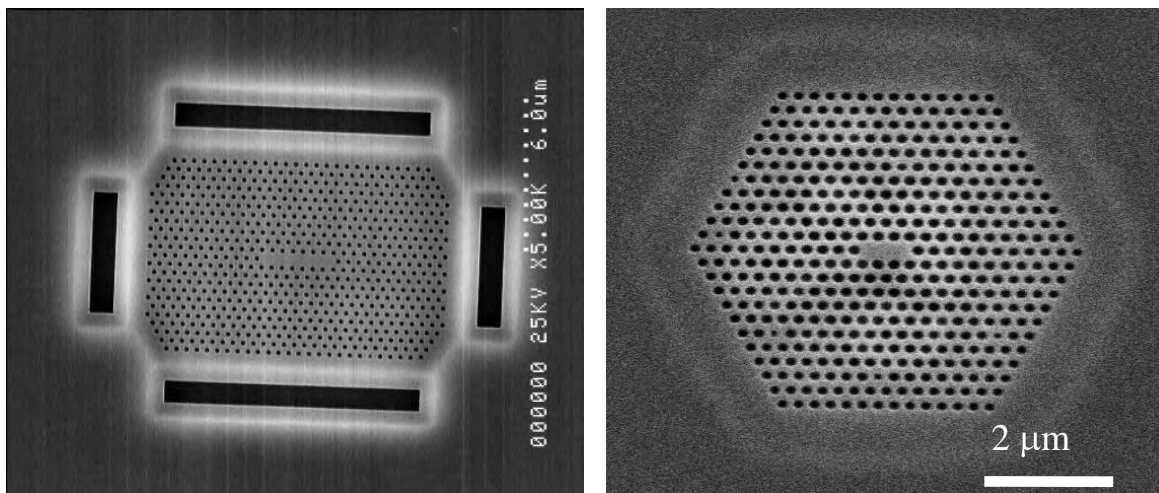


Fig.1. Left: L7-type microcavity fabricated on an InP substrate with quantum wires in the active region.

Right: L3-type cavity fabricated on a GaAs substrate with quantum rings.

References

- [1] L. J. Martínez, B. Alén, I. Prieto, J.F. Galisteo-López, M. Galli, L.C. Andreani, Ch. Seassal, P. Viktorovitch and P. A. Postigo "Two-dimensional surface emitting photonic crystal laser with hybrid triangular-graphite structure" *Optics Express*, 17(17), 15043-15051, (2009)
- [2] L. J. Martínez, B. Alén, I. Prieto, D. Fuster, L. González, Y. González, M.L. Dotor and P. A. Postigo, "Room temperature continuous wave operation in a photonic crystal microcavity laser with a single layer of InAs/InP self-assembled quantum wires". *Optics Express*, 17(17), 14993-15000, (2009)
- [3] Gallardo, E; Martínez, L J; Nowak, A K; Sarkar, D; Sanvitto, D; van der Meulen, H P; Calleja, J M; Prieto, I; Granados, D; Taboada, A G; García, J M; Postigo, P A "Single-photon emission by semiconductor quantum rings in a photonic crystal", *JOSA B*, Vol. 27 Issue 6, pp.A21-A24 (2010)

Influence of Corrugated Surfaces Templates in Colloidal Crystal Thin Films Growth

F. Ramiro-Manzano^{†‡}, E. Bonet[†], I. Rodríguez[†] and F. Meseguer^{†‡*}.

[†] Centro de Tecnologías Físicas, Unidad Asociada ICMM/CSIC-UPV.
Universidad Politécnica de Valencia, Av. Los Naranjos s/n, 46022 Valencia, Spain.

[‡] Instituto de Ciencia de Materiales de Madrid CSIC, 28049 Madrid, Spain.
ferraman@fis.upv.es

The influence of patterned surface on the growth of thin film colloidal crystals has been studied experimentally. Confined colloidal crystals show a manifold variety of closed packed structures, strongly dependent on the confinement length.[1-4] Also, the influence of substrates with topographically patterned surfaces has been demonstrated on the formation of three dimensional (3D) closed and non-closed packed colloidal crystals.[5-8] Templated growing surfaces have also been used to achieve zero dimensional (0D) and one dimensional (1D) colloidal nanostructures.[9]

We have built a wedge cell with a new confinement condition, using a flat and a corrugated plate. We make use of inexpensive grating substrates obtained from commercially available Digital Versatile Disks (DVDs) to process large size patterned surfaces. The new variables in the wedge confinement, introduced by the corrugated surface, groove size, pitch of the substrates, as well as the cell thickness value, dictate the particle decoration deposited on both the patterned and non-patterned confining plates.

We have analyzed the influence of patterned surfaces on the formation of one- and two-dimensional colloidal crystals. When the sphere diameter is of the order of the groove width of patterned substrates, a rich variety of particle decorations appear. However if particle size is much larger than template patterns, large domains of particle ordering are formed (Figure 1). Patterned substrates can also be useful for templating colloidal arrangements on flat substrates (Figure 2). Figure 3 shows the results obtained on the corrugated surface of the cell, in quasi-2D colloidal orderings, as our proposal theoretical models.

References

- [1] Pieranski, P.; Strzelecki, L.; Pansu, B. *Phys. Rev. Lett.* 1983, 50, 900.
- [2] Schmidt, M.; Löwen, H. *Phys. Rev. Lett.* 1996, 76, 4552.
- [3] Ramiro-Manzano, F.; Meseguer, F.; Bonet, E.; Rodríguez, I. *Phys. Rev. Lett.* 2006, 97, 028304.
- [4] Ramiro-Manzano, F.; Bonet, E.; Rodríguez, I.; Meseguer, F. *Phys. Rev. E* 2007, 76, 4.
- [5] vanBlaaderen, A.; Ruel, R.; Wiltzius, P. *Nature* 1997, 385, 321.
- [6] Hoogenboom, J. P.; Retif C.; de Bres E.; de Boer, M. V.; van Langen-Suurling, A. K.; Romijn, J.; van Blaaderen, A. *Nano Lett.* 2004, 4, 205. Yang, S. M.; Miguez, H.; Ozin, G.A. *Adv. Func. Mater.* 2002, 12, 425
- [7] Park, S. H.; Qin, D.; Xia, Y. *Adv. Mater.* 1998, 10, 1028.
- [8] Dzionkina, N. V.; Vancso G. J. *Soft Matter* 2005, 1, 265
- [9] Yin, Y. D.; Lu, Y.; Gates, B.; Xia, Y. N.; *J. Am. Chem. Soc.* 2001, 123, 8718.

Figures

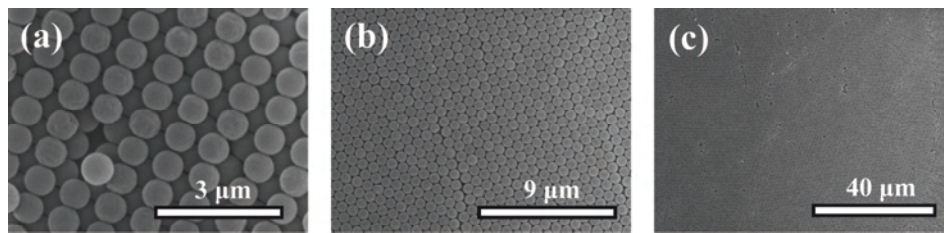


Figure 1. SEM images of particles whose size is larger than the groove width (particle size=770 nm) attached to the corrugated plate, being (a) buckling phase (b,c) triangular phase, being (b) a zoom image of (c).

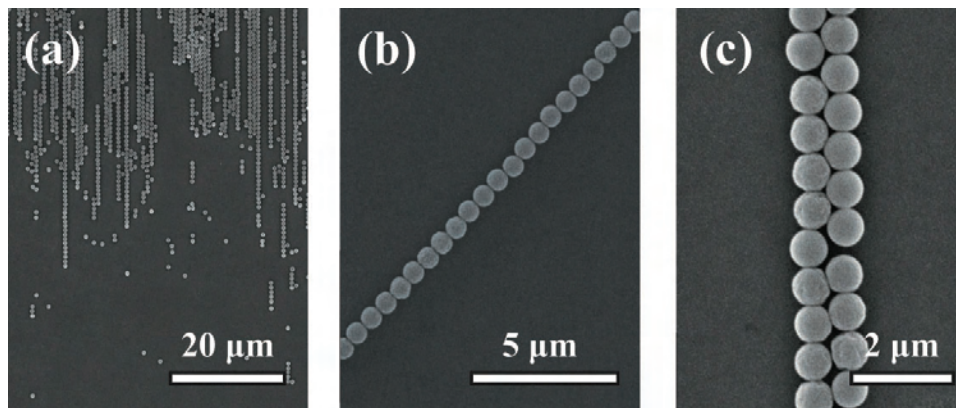


Figure 2. SEM images: (a) a parallel collection of particles rows, (b) a row of spheres arranged linearly, and (c) a strip composed by two rows. In all cases the particle size is 770 nm, and placed over the flat substrate.

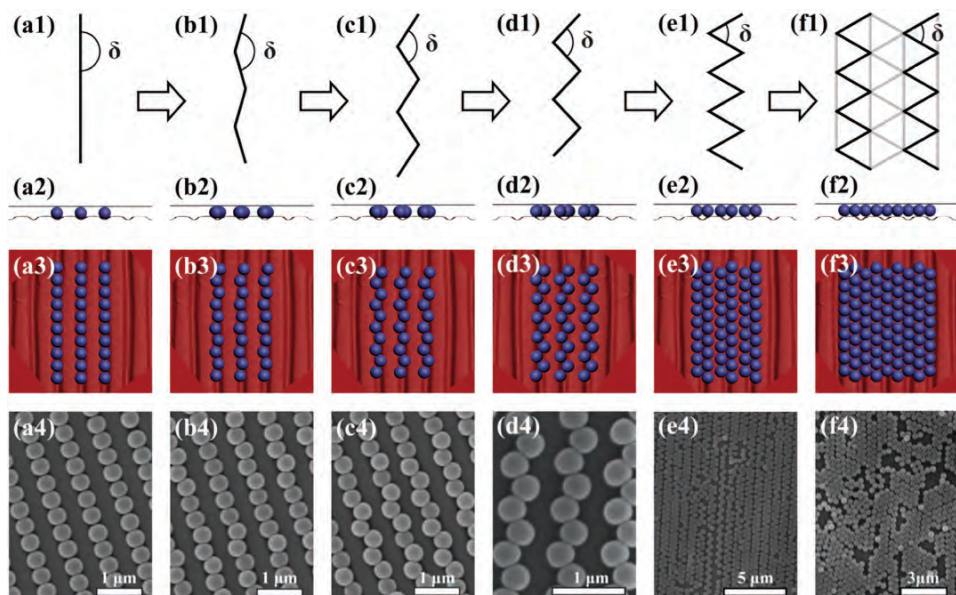


Figure 3. SEM images (bottom row) of different particle orderings, the cell thickness increasing from the left to the right side of the panel. Side (second row) and top (third row) views of the ordering model showing the sphere distribution in the grooves. The first row shows how the zig-zag angle of particle strips changes from 180 degrees (a) to 60 degrees (e). (f) A triangular arrangement of close packed spheres. The particle size is 380 nm.

Enhanced photoluminescence in printed 2D polymer photonic structures via surface plasmon enhancement

V. Reboud^{1*}, G. Leveque², T. Kehoe¹, D. Dudek¹, N. Kehagias¹, M. Striccoli³, T. Placido³, A. Panniello⁴, M. L. Curri³, J. A. Alducin⁵, D. Mecerreyes⁵ and C. M. Sotomayor Torres^{1,6}

¹Catalan Institute of Nanotechnology, Campus de Bellaterra, Edifici CM7, ES 08193 – Barcelona, Spain

* vincent.reboud@cin2.es

²Tyndall National Institute, University College Cork, Lee Maltings, Cork, Ireland

³CNR IPCF Sezione Bari c/o Dipartimento di Chimica, Università di Bari, Italy

⁴Dipartimento di Chimica, Università di Bari, via Orabona 4, I-70126 Bari, Italy

⁵New Materials Dep., CIC Nanogune and CIDETEC-Centre for Electrochemical Technologies Parque Tecnológico de San Sebastia Paseo Miramon 196, 20009 Donostia-San Sebastian (Spain)

⁶Catalan Institute for Research and Advanced Studies ICREA, 08010 Barcelona, Spain

We report on a method to enhance the light-emission efficiency of printable thin films of polymer doped with semiconducting nanocrystals (NCs) and with dye chromophores via metallic nanoparticles and via nanoimprinted photonic crystals. The two nanocomposite materials, embossed by using nanoimprint lithography (NIL) process, showed very good imprint properties and impressive enhancements in the spontaneous emission intensity of the incorporated emitters.

To prepare the printable polymers, small amounts of Au nanorods (NRs) with a double surface plasmon resonance were added to a mixture of PMMA-based copolymer and emitters [(CdSe)ZnS nanocrystals or rhodamine 6G (R6G)]. Figure 1a presents a schematic of the exciton-plasmon coupling in the nanocomposite polymer. A strong coupling is expected by matching the surface plasmon resonance frequency with the emission frequency of emitters (Figure 1b for R6G). The photoluminescence (PL) intensity reported in Figure 2a was recorded for different nanoparticles concentrations in the mixture. The measurements indicate an increase by a factor 14 in the emission intensity of the dye. This enhancement is attributed to an increased absorption and emission of R6G in presence of the metallic nanorods. A reduction of the lifetime confirmed the modification of the spontaneous emission rate of the emitters. Two dimensional silicon (2D) photonic crystal stamps with different lattice constants were successfully imprinted in the nanocomposite polymer by a standard NIL process. PL spectra of a nanoimprinted unpatterned sample without Au NRs, of a nanoimprinted unpatterned sample with the optimal concentration of Au NRs and of a 700 nm honeycomb lattice photonic crystal with the optimal Au NRs concentration are shown in Figure 2b. It is observed that the PL intensity for the PhC is 36 (green curve) as large as that of the unpatterned substrate without the Au NRs (black curve).

Similar results were obtained with the nanocomposite polymer containing the NCs. The additional challenge consisted to achieve a homogeneous dispersion of nanoparticles in the polymer matrix and to keep a good processability of the modified polymer for NIL process without altering their structural and chemical-physical properties of the nanoparticles. As shown by Figure 3a, the transfer pattern was excellent with roughness surface comparable to the Si stamp. A challenging TEM cross-section of the polymer film showed (Figure 3b) a homogenous dispersion of (CdSe)ZnS nanocrystals after patterning was achieved with success. By controlling the concentration of NCs and Au nanorods in the PMMA-based copolymer, an optimum is achieved showing an enhancement in the PL intensity by a factor 5.5 thanks to the Au nanoparticles incorporation.

In conclusion, 36-fold enhancement of PL intensity compared to an imprinted unpatterned and unprocessed sample is achieved at room temperature by using a printed photonic crystal in a dye-doped printable polymer and by coupling the dye emission to surface plasmons of metallic nanoparticles. An enhancement by a factor 14 has been achieved with semiconducting nanocrystals. Our results indicate that nanoimprint lithography is well suited to fabricate these challenging photonic structures in nanocomposite materials and that the combination of surface plasmons and nanoimprinted photonic structures in an active layer may lead to a new class of cost effective and high efficient OLEDs.

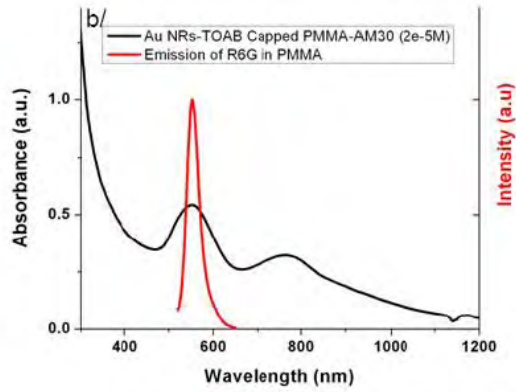
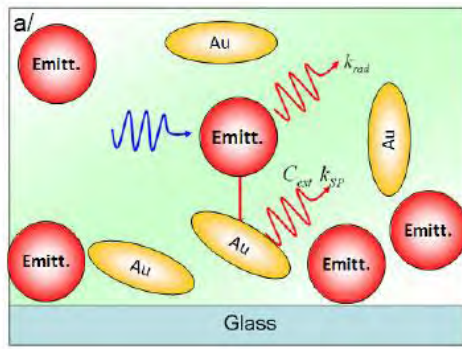


Figure 1: a/ Schematic of the coupling between the metallic nanoparticles and the emitters [(CdSe)ZnS or R6G], b/ Absorbance spectra of gold nanorods in PMMA-DMAEMA (black curve), PL intensity of R6G in the PMMA-based copolymer.

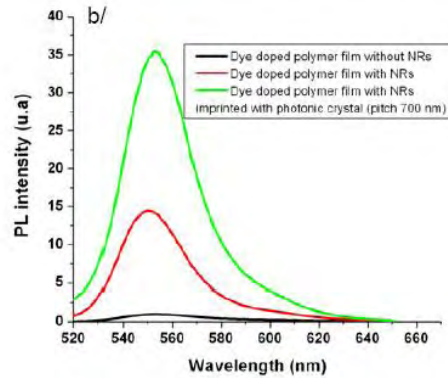
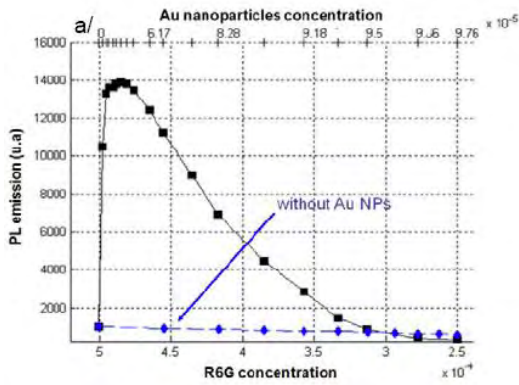


Figure 2: a/ Photoluminescence intensity of the functionalised polymer versus different R6G and gold nanorods concentrations. (blue curve: without Au NRs; black curve: with Au NRs), b/ PL spectra of the dye doped polymer film with and without Au nanorods (red, black), PL spectra of dye doped polymer film with Au nanorods imprinted with 2D photonic crystal (pitch 700 nm).

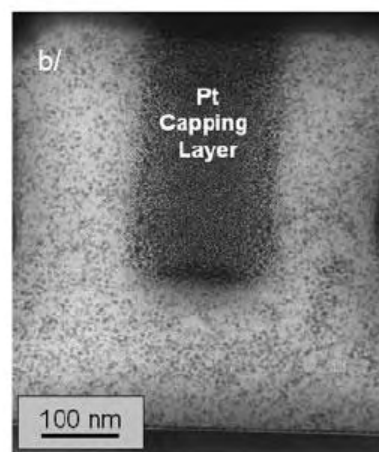
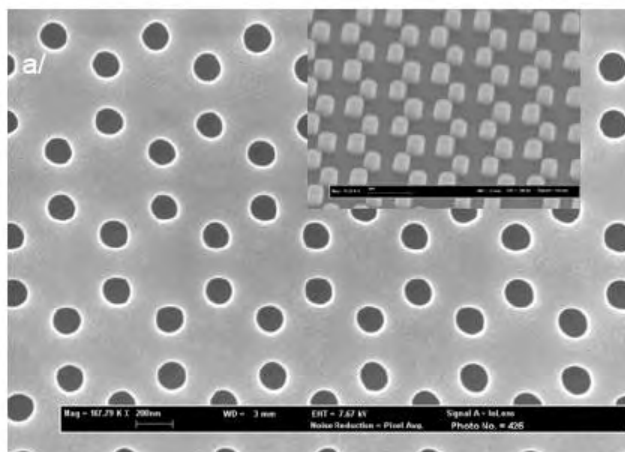


Figure 3: a/ SEM micrographs of nanoimprinted photonic crystals in PMMA-based copolymer doped with (CdSe)ZnS nanocrystals (Inset) SEM micrographs of tilted view of a silicon stamp containing two-dimensional array of pillars, b/ TEM cross-section of the nanoimprinted photonic crystals.

We gratefully acknowledge Mads Brøchner Christiansen and Anders Kristensen for the dye-doped polymer. The support of the EC-funded project NaPaNIL. The content of this work is the sole responsibility of the authors.

Plasmon Optical Nanoantennas: Characterization, Design, and Applications in Nanophotonics

R. Rodríguez-Oliveros⁽¹⁾, R. Paniagua⁽¹⁾, José A. Sánchez-Gil⁽¹⁾, V. Giannini⁽²⁾, D. Macías⁽³⁾,
and J. Gómez Rivas⁽⁴⁾

- (1) Instituto de Estructura de la Materia, Consejo Superior de Investigaciones Científicas, Serrano 121, Madrid 28006 (Spain)
(2) Experimental Solid State Group, Physics Department, Imperial College, London (UK)
(3) Laboratoire de Nanotechnologie et d'Instrumentation Optique (ICD-LNIO), Université de Technologie de Troyes (France)
(5) FOM Institute-AMOLF, c/o Philips Research Laboratories, Eindhoven (The Netherlands)
j.sanchez@iem.cfmac.csic.es

Complex metal nanostructures exhibit plasmon resonances that play a crucial role in various electromagnetic processes stemming from spontaneous emission occurring nearby [1-4]. In this regard, it is crucial first to characterize the localized plasmon resonances for a variety of metal nanoparticles. On the basis of a 2D surface integral equations in parametric coordinates [5], we have indeed calculated the scattering cross sections for nanowires of various shapes (circle, triangles, rectangles, and stars), either isolated or interacting, including near-field intensity maps (with corresponding enhancement factors) and surface charge distributions [4-6]. Good agreement with experimental results for the dimer nanoantennas used in enhanced fluorescence is in turn achieved [6]. In the case of metal nanoparticles resembling a star/flower, which have also been obtained experimentally, large enhancement factors are shown to occur (see Fig.1), making them specially suitable as SERS (surface-enhanced raman scattering) substrates [4].

In addition, we have developed theoretically and numerically a rigorous method to investigate the electromagnetic wave scattering from 3D objects with arbitrary surfaces and dielectric function [7]. The formulation is based on the surface integral equations for the electric and magnetic fields given by the Stratton-Chu formulas. The integral equations are generalized for a 3D object with its surface in parametric coordinates (recently derived for 2D objects in Ref. [5]). This formalism straightforwardly allows one to deal with an arbitrary number of scatterers and shapes, with the advantage that it scales with the scatterer surface (rather than its volume).

With regard to nanoantenna-enhanced photonics, single molecule fluorescence close to metallic nanoantennas has been thoroughly explored by calculating radiative and nonradiative decay rates (and quantum yields), addressing crucial issues as the modification and enhancement (or quenching) of spontaneous emission in (bio)molecular and optoelectronic systems, due to the strong impact on the local (near-field) electromagnetic density of states of surface-plasmon resonances in dimer nanoantennas [1,3]. The strong coupling of the optical emitter to the nanoantenna is also studied in the resulting near- and far-field patterns, which exhibit significant qualitative and quantitative variations [3]. Experimentally, resonant enhancement of the radiative and nonradiative decay rates of a fluorescent dye is observed for dimers with optically coupled arms with narrow (~20 nm) gaps [1], in agreement with our electrodynamic model calculations [1,3]. On the other hand, metallic nanowire trimers have been theoretically investigated, with associated multiple plasmon resonances that can be exploited to doubly enhanced inelastic and/or nonlinear optical processes [2]; this has straightforward implications for low efficiency emitters in, e.g., (bio)molecular sensing or optoelectronic devices.

The optimal design of nanoantennas with specific properties is, on the other hand, an aspect of the inverse problem that had not received too much attention until recently, despite being crucial from the point of view of applications. In order to find the optimal nanoparticle geometry that maximizes/minimizes a given optical property, we have made use of bio-inspired stochastic technique based on genetic algorithms, which exploits the surface integral equation formulation [5] to solve the direct scattering problem. The performance of this stochastic method is proved by showing how the optimization procedure converges to a nanostar geometry that exhibits a resonance at or near a given wavelength [8]. This method will be exploited to design metal nanoantennas optimizing quantum-dot photoluminescence.

We acknowledge partial support from: Spanish MICINN grants NANOPLAS (FIS2009-11264) and EMET (CSD2008-00066); Comunidad de Madrid grant (MICROSERES, S2009/TIC-1476); CSIC-CNRS exchange programs; and from the Dutch FOM research.

References

- [1] O. L. Muskens, V. Giannini, J. A. Sánchez-Gil, and J. Gómez Rivas, *Nano Lett.* **7** (2007) 2871.
- [2] V. Giannini and J. A. Sánchez-Gil, *Opt. Lett.* **33** (2008) 899.
- [3] V. Giannini, J. A. Sánchez-Gil, O. L. Muskens, and J. Gómez Rivas, *J. Opt. Soc. Am. B* (2009).
- [4] V. Giannini, R. Rodríguez-Oliveros, and J. A. Sánchez-Gil, *Plasmonics* **5** (2010) 99.
- [5] V. Giannini and J. A. Sánchez-Gil, *J. Opt. Soc. Am. A* **24** (2007) 2822.
- [6] O. L. Muskens, J. Gómez Rivas, V. Giannini and J. A. Sánchez-Gil, *Opt. Express* **15**, 17736 (2007).
- [7] R. Rodríguez-Oliveros and J. A. Sánchez-Gil, preprint.
- [8] A. Tassadit, D. Macías, J. A. Sánchez-Gil, P.-M. Adam, R. Rodríguez-Oliveros, submitted to *Superlattices & Microstructures*.

Figures

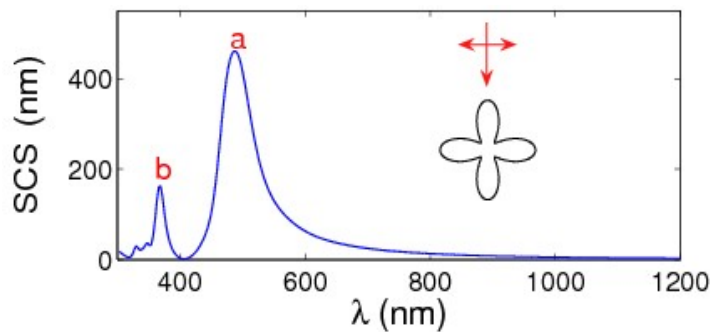


Figure 1: Scattering Cross Section for a Ag four-petal nanoflower with average radius of 30 nm and oscillation amplitude of 20 nm (blue curve). (a,b) Electric-near-field intensity distribution in log scale at both plasmon resonances [7].

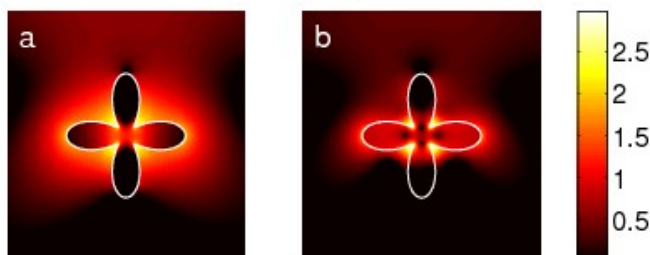
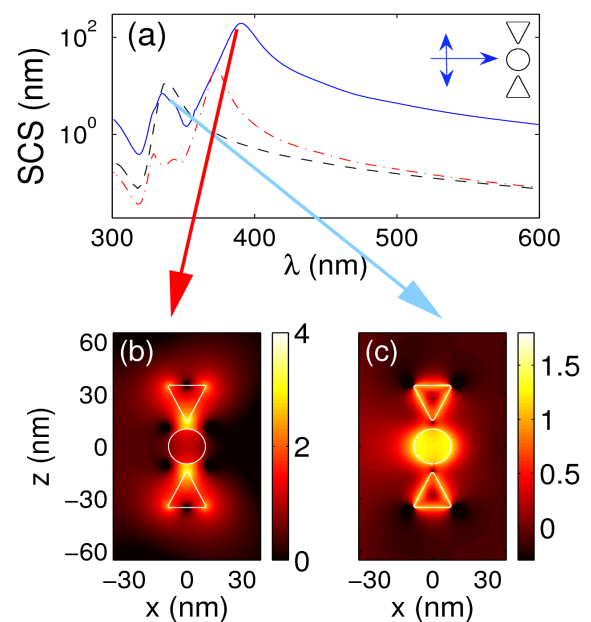


Figure 2: (a) Scattering cross section for a Ag trimer (solid curve) consisting of a cylinder with 20 nm of diameter between two triangles; each triangle has 20 nm of base and 20 nm of height. The distance between each triangle and the cylinder is 5 nm, the electromagnetic field impinging from the left (see inset), p polarization. SCS of a Ag triangular particle (dashed-dotted curve) and of a cylinder (dashed curve). (b), (c) Near electric field intensity in a log₁₀ scale (p polarization) at the plasmonic resonances, normalized to that of the incident field. (b) $\lambda=390$ nm, (c) $\lambda=334$ nm [2].



Particle Dynamics in Non-Conservative Optical Vortex Fields

S. Albaladejo¹, I. Zapata², M. I. Marques¹, M. Laroche³, J.M. Parrondo⁴,
F. Scheffold⁵, F. Sols² and **J.J. Saenz**¹

¹ Moving Light and Electrons (Mole) Group, Univ. Autónoma de Madrid, Spain.

² Dpto. Física de Materiales, Universidad Complutense de Madrid, Spain.

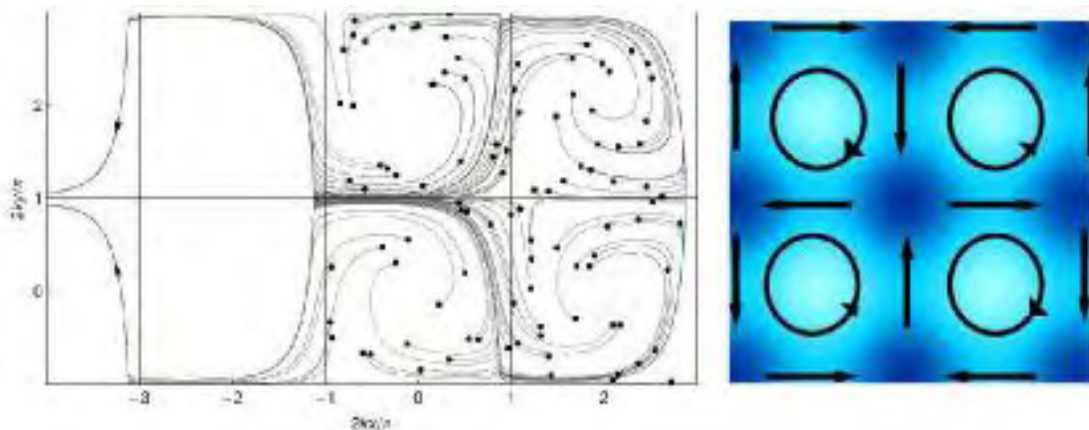
³ Institut d'Optique, CNRS, Université Paris-Sud, France.

⁴ Dpto. Física Atómica y Molecular, Universidad Complutense de Madrid, Spain

⁵ Department of Physics, University of Fribourg, Switzerland

Light forces on small (Rayleigh) particles are usually described as the sum of two terms: the dipolar or gradient force and the scattering or radiation pressure force. The scattering force is traditionally considered proportional to the Poynting vector, which gives the direction and magnitude of the momentum flow. However, as we will show, when the light field has a non-uniform spatial distribution of spin angular momentum, an additional scattering force arises as a reaction of the particle against the rotation of the spin. This non-conservative force term is proportional to the curl of the spin angular momentum of the light field¹. We will illustrate the relevance of the spin force in the particular simple case of a 2D field geometry arising in the intersection region of two standing waves².

We will also discuss the peculiar particle dynamics in the non-conservative force field of an optical vortex lattice³. Radiation pressure in the whirllight field (arising in the intersection region of two crossed standing waves²) plays an active role spinning the particles out of the whirls leading to a giant acceleration of free diffusion. Interestingly, we show that a simple combination of null-average conservative and nonconservative steady forces can rectify the flow of damped particles. We propose a "deterministic ratchet" stemming from purely stationary forces⁴ that represents a novel concept in dynamics with considerable potential for fundamental and practical implications.



References

- [1] S. Albaladejo, M. Laroche, M. Marques, J.J. Saenz, Phys.Rev.Lett. 102 , 113602 (2009)
- [2] A. Hemmerich, T.W. Hansch, Phys. Rev. Lett. 68, 1492 (1992).
- [3] S. Albaladejo, M.I. Marques, F. Scheffold, J.J. Saenz, Nano Letters, September 1 (2009).
- [4] I. Zapata, S. Albaladejo, J.M. Parrondo, J.J. Saenz, F. Sols, Phys. Rev. Lett. (2009)

Anisotropic behavior of two-dimensional photonic crystals in the homogenization limit

José Sánchez-Dehesa, Jorge Carbonell and Francisco Cervera

Grupo de Fenómenos Ondulatorios, Departamento de Ingeniería Electrónica,
Universidad Politécnica de Valencia, Valencia, Spain
jsdehesa@upvnet.upv.es

This work reports an experimental demonstration of the anisotropy predicted for photonic crystals based on two-dimensional rectangular arrays of dielectric rods (Alumina or FR4) in air. These structures have been studied in the long-wavelength limit (homogenization) by means of a microwave measurement set up. The effective dielectric permittivity ϵ_{eff} has been analysed along the two perpendicular directions in the lattice for the two cases of interest; E-mode excitation and H-mode excitation. It is found that ϵ_{eff} is isotropic for the E-mode case while it is anisotropic for the H-mode case. Data confirm homogenization theories based on plane wave expansions and simulations based on a finite-element method.

Photonic crystals made of arrays of dielectric rods in air have been theoretically studied in the long-wavelength limit (homogenization) because of their possible application as new materials for optical components. Thus, explicit formulas for the effective dielectric constants have been given [1, 2]. More recently, the homogenization of losses have been also studied for rods having the imaginary part of the dielectric constant much lower than the real part. In other words, the imaginary part of the effective dielectric constant has been predicted and it has the same behavior than the real part [3]; it is isotropic for the E-modes and anisotropic for the H-modes.

Experimental demonstration of the previously introduced concepts of isotropy or anisotropy of the effective parameter has been performed by means of a microwave measurement setup. 2D lattices made of alumina ($\epsilon_r = 9.4 - i9.4 \cdot 0.006$) or FR4 ($\epsilon_r = 4.4 - i4.4 \cdot 0.02$) rods of diameters $\phi = 4.2$ mm and 3.2 mm, respectively, have been fabricated. The lattice period employed is $p = 5$ mm for the Alumina samples and $p = 4$ mm for the FR4 samples. According to the lattice periodicity in the propagation direction is $2p = 10$ mm (8 mm) for the 0° incidence and $p = 5$ mm (4 mm) for the 90° incidence. A 2:1 ratio is therefore preserved between both lateral sides of the lattice, giving in practice a filling factor of $ff = 0.264$ and 0.254 for the Alumina and FR4 samples, respectively. With this geometry and taking into account the operation frequencies (2 – 7 GHz in the experiment), for the Alumina case, the normalized lattice parameter ranges from $p/\lambda_{2\text{GHz}} = 3.3\%$ to $p/\lambda_{7\text{GHz}} = 11.6\%$. Thus, the measured arrangement reasonably operates within homogenization conditions. In all cases, total length of the measured sample in the propagation direction is equal (approximately 10 cm), thus giving comparable results in terms of 'bulk' homogenized parameters. Additionally, two broadband horn antennas, covering the whole measured frequency range and with a wide front side lobe, are used to transmit and receive a quasi-plane wave with a vertically polarized **E**-field. In order to guarantee a minimum detectable power for the received signal above the noise floor of the network analyzer, the antennas are closely placed at variable distances between 55 and 125 cm. This range of separations permits to be sufficiently close to the far-field region (for the measured frequency range) when the characterized device is placed equally separated between both antennas.

The real part of the effective dielectric function has been obtained by extracting the refraction index from a measurement of the phase delay $\Delta\phi$ in samples with two different lengths l_1 and l_2 ,

$$n(\omega) = -\frac{\Delta\phi c_0}{\omega(l_2 - l_1)}$$

where c_0 is light speed. Results for the samples made with FR4 are shown in figures 1 and 2 and are in quantitative agreement with theoretical predictions.

The imaginary part of the effective dielectric function has been analyzed by transmission measurements. Results are depicted in Figs. 3 and 4, where it is shown how the transmittance spectra obtained under E-mode excitation are isotropic in the low frequency region while those obtained under H-mode excitation are anisotropic. Numerical simulations based on a finite-element method (COMSOL multiphysics) are also depicted for comparison purposes.

Acknowledgements

Work supported by MICIIN of Spain and by the USA Office of Naval Research.

References

- [1] P. Halevi, A. A. Krokhin and J. Arriaga, Phys. Rev. Lett., **82** (1999) 719.
 [2] A. A. Krokhin, P. Halevi, and J. Arriaga, Phys. Rev. B., **65** (2002) 115208.
 [3] A. A. Krokhin, L. Gumen, and J. Arriaga (private communication).

Figures 1 and 2:

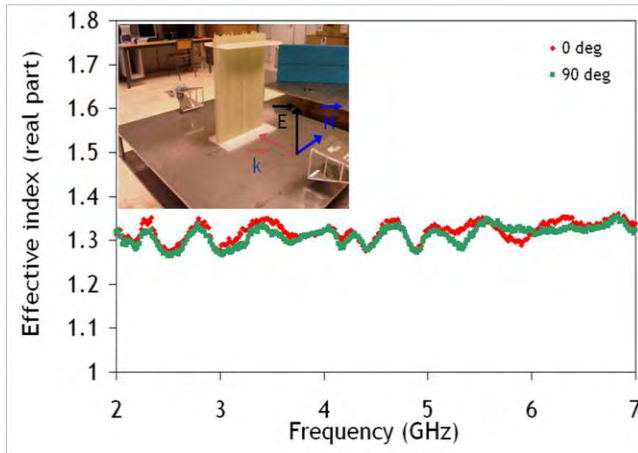


Figure 1.- Effective refractive index extracted from phase delay measurements performed on FR4 samples with lengths $l_1=100\text{mm}$ and $l_2=52\text{mm}$. These results correspond to E-mode excitation with two incidence angles (0° and 90°). Inset shows the employed experimental setup with the characterized sample illuminated with an E-polarization.

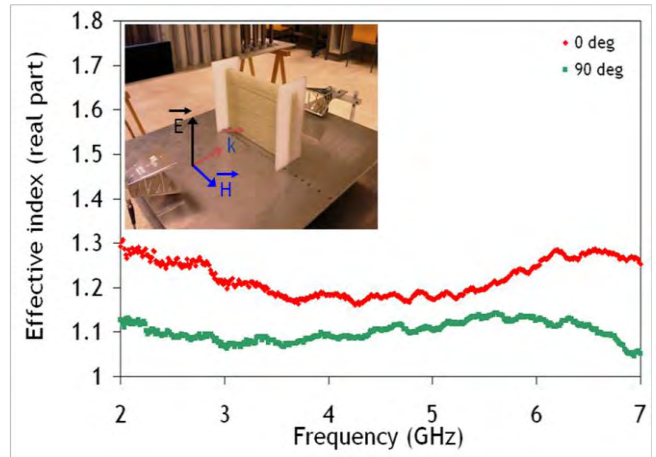


Figure 2.- Effective refractive index extracted from phase delay measurements performed on the FR4 samples. Results correspond to data obtained under H-mode excitation. Inset shows the employed experimental setup.

Figures 3 and 4:

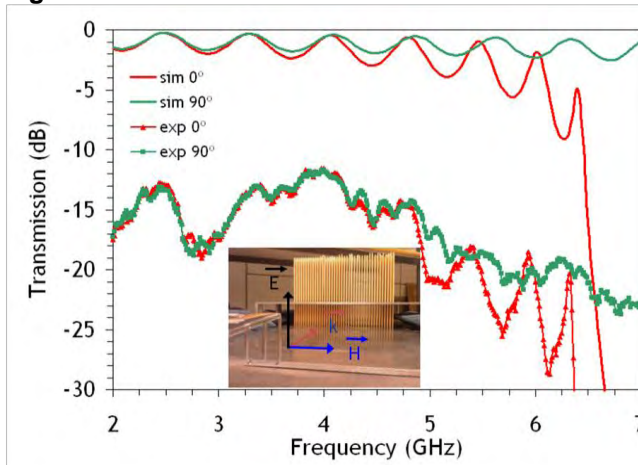


Figure 3.- Measured (symbols) and simulated (lines) transmission for Alumina structures under E-mode excitation wave with two incidence angles (0° and 90°). Inset shows the employed experimental setup with the characterized sample illuminated with an E-polarization.

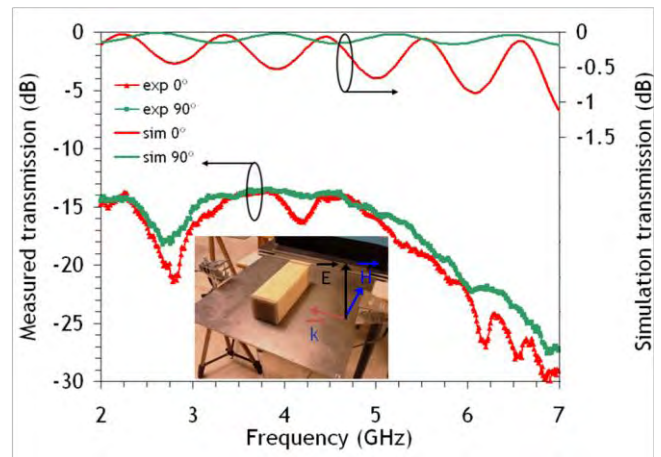


Figure 4 Measured (symbols) and simulated (lines) transmission for Alumina structures under H-mode excitation wave with two incidence angles (0° and 90°). Inset shows the employed experimental setup with the characterized sample illuminated with an H-polarization.

Slow wave and resonator structures to enhance silicon photonic modulator performance

Antoine Brimont, Javier Martí, **Pablo Sanchis**

Valencia Nanophotonics Technology Center, Universidad Politécnica de Valencia
Camino de Vera, s/n, 46022 Valencia, Spain
pabsanki@ntc.upv.es

High speed modulators will play a crucial role for the development of all optical networks. Future all optical networks will require operating speeds higher than 40 Gb/s specially in the metro network scenario which is expected to become the capacity bottleneck of the next coming years. Modulators are also key building blocks in important processing applications such as routing, tunable filters, optical gating, logic gates or switching. Silicon photonics is a promising platform to develop high performance modulators due to the potential of building cost-effective devices at industrial scale by making use of the already existing silicon processing technology and manufacturing infrastructures. Furthermore, electronic and optical functionalities can be monolithically integrated on the same chip.

Several ways have been investigated to develop silicon based modulators [1]. Among them the plasma dispersion effect has been demonstrated as the most effective way to modulate the refraction index in silicon. In this case, the free carrier concentration is altered by an external electrical field resulting in a change of the refractive index. So far, the highest speed operation was demonstrated by Intel in 2007 in a depleted vertical PN diode. However, a reduced modulation depth of only 1dB was achieved and the device size was in the millimeter range. Therefore, the ceaseless effort towards modulator performance enhancement in terms of speed, size and power consumption is still underway.

Slow-wave and resonator structures has been proposed as promising structures to enhance modulators performance. In both cases, the interaction between the free carriers and the optical structure is strengthened. This can lead to a significant reduction of the interaction length and hence allows for device shrinking down to a few hundred microns. Improvement in device size and power consumption can reach in practice up to one order of magnitude depending on the structure. In this paper, a qualitative study of modulator performance improvement due to slow wave and resonator structures is presented. Furthermore, experimental results are also shown demonstrating simulation and theoretical results.

Figure 1 shows a SEM image of (a) a corrugated waveguide and (b) a ring resonator structure. Corrugated waveguides are first analyzed and designed. This slow-wave structure consists of a rib waveguide with one-dimensional periodical transversal corrugation elements. The main characteristic of such structures is their capability to decrease the group velocity of the propagating wave. Passive design is first carried out. Up to ten times smaller interaction length with respect to conventional rib waveguides can be obtained for group velocities around $0.01c$ and a refractive index variation of 10^{-3} . Experimental results are then carried out to validate passive design showing group index values up to $n_G=72$ at wavelengths around $1.55\mu\text{m}$. Electrical simulations are also carried out and DC and transient results analyzed. Figure 2 shows the transient change in effective index for different group velocities and for voltage varying from 0 to -3V (rise time) and -3V to 0V (fall time). A modulation bandwidth up to 24GHz is derived from the obtained results.

Different configurations of ring resonator structures have also been investigated to enhance modulator performance in terms of extinction ratio and required voltage. Modulation based on the intensity and phase response of a ring resonator is analyzed and their performances compared. In both intensity and phase modulation approaches, extinctions ratios higher than 20dB can be achieved considering effective index changes lower than 10^{-4} and device sizes smaller than $100\mu\text{m}$. However, it can be concluded that better robustness against fabrication deviations can be easily achieved with phase modulators with respect to intensity modulators. Experimental results of a compact silicon ring resonator operating in depletion mode in a lateral PN junction are also shown. Figure 3 shows pictures of the experimental set-up and the amplitude variation of ring resonator based silicon modulator operated under forward bias. An extinction ratio up to 6dB for only 3V is demonstrated for forward bias operation. Furthermore, the device exhibits an electrical small signal bandwidth of 19GHz.

References

- [1] D. Marris-Morini, L. Vivien, G. Rasigade, E. Cassan, J. M. Fedeli, X. Le Roux, P. Crozat, S. Maine, A. Lupu, M. Halbwx, S. Laval, "Recent progress in high speed silicon-based optical modulators", Proceedings of the IEEE, vol. 97, no. 7, pp. 1199-1215, 2009.
- [2] A. Brimont, P. Sanchis and J. Martí, "Strong electro-optical modulation enhancement in a slow wave corrugated waveguide", Opt. Express, vol. 17, pp. 9204-9211, 2009.
- [3] F.Y. Gardes, A. Brimont, P. Sanchis, G. Rasigade, D. Marris-Morini, L. O'Faolain, F. Dong, J.M. Fedeli, P. Dumon, L. Vivien, T.F. Krauss, G.T. Reed, J. Martí, "High-speed modulation of a compact silicon ring resonator based on a reverse-biased pn diode", Opt. Express, vol. 17, no. 24, pp. 21986-21991, 2009.

Figures

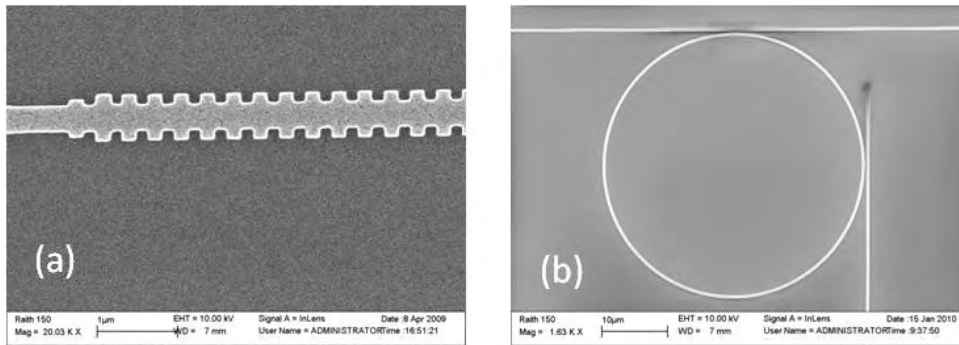


Figure 1.- SEM image of (a) a corrugated waveguide and (b) a ring resonator.

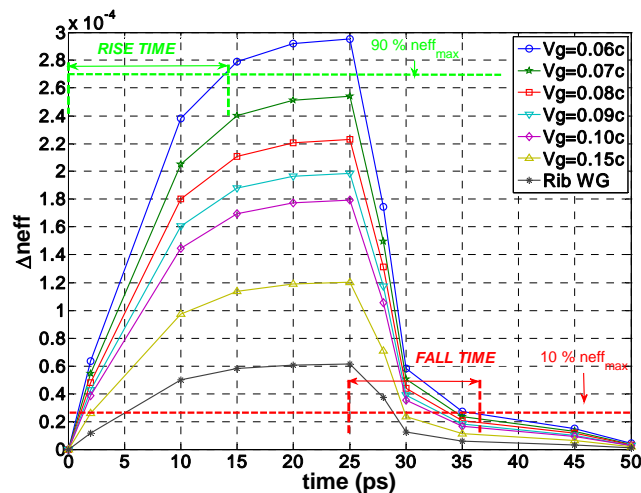


Figure 2.- Temporal variation of the effective index in a corrugated waveguide taking into account different group velocities. Result for a rib waveguide is also shown for the sake of comparison.

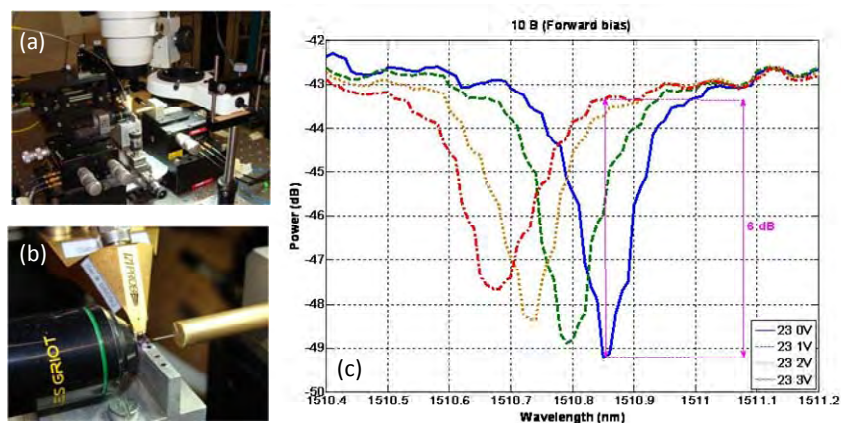


Figure 3.- (a)-(b) Pictures of the experimental set-up and RF probe and (c) amplitude variation in a ring resonator based silicon modulator operated under forward bias.

Study of terahertz extraordinary transmission resonances depending on polarization.

M. Navarro-Cía¹, M. Beruete¹, S. A. Kuznetsov², F. Falcone¹, I. Campillo³, **M. Sorolla**¹

¹Millimeter and Terahertz Waves Laboratory, Universidad Pública de Navarra, Campus Arrosadía s/n, Pamplona, Spain

²Novosibirsk State University, Research-and-Education Centre "Nanosystems and Modern Materials", Pirogova Str. 2, P.O. 630090 Novosibirsk, Russia

³CIC nanoGUNE Consolider, Tolosa Hiribidea 76, P.O. 20018 Donostia, Spain.

mario@unavarra.es

The topics of metamaterials [1,2] and extraordinary transmission [3] have attracted a lot of attention in the last years due to the intriguing properties associated to them. On the one hand, metamaterials have been a source of continuous development of new ideas and devices, as many well-established theories in electromagnetism were revisited with a different perspective. As a matter of fact, fascinating concepts such as negative refraction, perfect lensing and even invisibility were proposed after metamaterials. On the other hand, extraordinary transmission is mainly linked with plasmonics [4] which is a hot topic in today electromagnetism. It consists in high transmittance peaks arising in the cut-off region of subwavelength hole arrays. As mentioned, in its optical version, it is explained through surface plasmon polaritons [5]. However, its existence in other frequency ranges such as millimetre-waves where metals do not support plasmons showed that leaky waves [6], i.e. a kind of complex waves that can exist in periodic structures, are responsible for the high transmittance. A very important result we achieved in the past, is the possibility to have left-handed propagation by stacking hole arrays [7]. Thus, metamaterials and extraordinary transmission structures are closely linked with a very simple arrangement. Moreover, this result can be easily downscaled to other frequencies such as terahertz, infrared or visible, since extraordinary transmission has been found also in those regimes. From the knowledge obtained with the systematic experiments performed in millimetre-waves, we were able to miniaturize the structures of extraordinary transmission and get high transmission even with reduced spot illumination (illumination in the Fresnel zone of the incident gaussian beam) [8]. This result opened the door to extraordinary transmission structures working in the terahertz range [9]. The main modifications done to design miniaturized samples is (i) using a rectangular cell and (ii) loading the wafers with dielectric. In our terahertz experiments, the dielectric was polypropylene whose performance is highly satisfactory. This aspect is very important since it is cheap and easily available due to mass industrial production for the needs of the goods packaging sphere. Apart from those technical details, we found an unexpected resonance below cut-off for the "wrong" polarization, and we termed it as anomalous extraordinary transmission. In this presentation, we will focus on our developments in the terahertz range and will give some physical insight about the origin of anomalous extraordinary transmission.

References:

- [1] V. G. Veselago, Soviet Physics Uspekhi, 10(1968) 509.
- [2] R. Marqués, F. Martín, and M. Sorolla, Metamaterials with Negative Parameters: Theory, Design, and Microwave Applications, John Wiley and Sons, New York, 2008.
- [3] T. W. Ebbesen, H. J. Lezec, H. F. Ghaemi, T. Thio, P. A. Wolff, Nature, 391(1998), 667. [4] E. Ozbay, Science, 311(2006), 189.
- [5] J. B. Pendry, L. Martín-Moreno, and F. J. García-Vidal, Science, 305(2004), 847.
- [6] A. Hessel and A. A. Oliner, Applied Optics, 4(1965), 1275.
- [7] M. Beruete, M. Sorolla, and I. Campillo, Optics Express, 14(2006), 5445.
- [8] M. Beruete, M. Sorolla, M. Navarro-Cía, F. Falcone, I. Campillo and V. Lomakin, Optics Express, 15(2007), 1107.
- [9] S. A. Kuznetsov, M. Navarro-Cía, V. V. Kubarev, A. V. Gelfand, M. Beruete, I. Campillo, and M. Sorolla, Optics Express, 17(2009), 18184.

Figures:

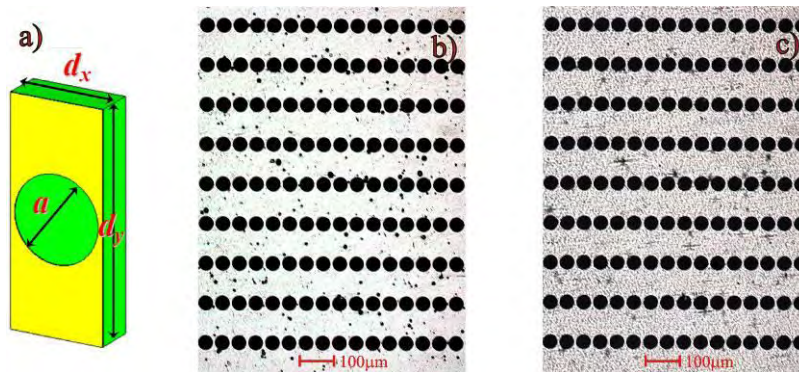


Fig. 1. Unit cell schematic (a) and photographs of the terahertz extraordinary transmission prototypes (b) and (c).

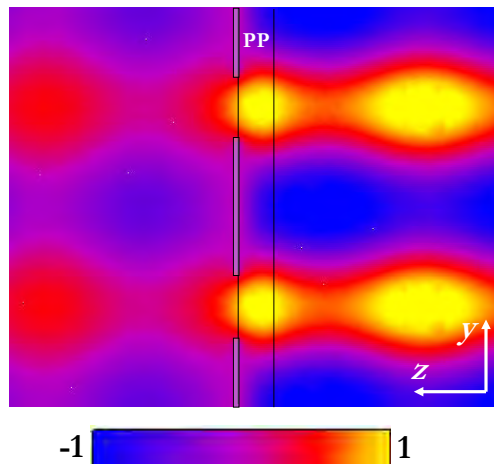


Fig. 2. Cross-sectional view of the electric field at the anomalous extraordinary transmission resonance.

Nanoscale Free-Carrier Profiling of Individual Semiconductor Nanowires by Infrared Near-Field Plasmon Resonance Spectroscopy

J.M. Stiegler¹, A.J. Huber², S.L. Diedenhofen³, J. Gómez Rivas³, R.E. Algra^{4,5,6}, E.P.A.M. Bakkers⁶, R. Hillenbrand^{1,7}

¹CIC nanoGUNE Consolider, 20018 Donostia - San Sebastian, Spain

²Neaspec GmbH, 82152 Martinsried, Germany

³FOM Institute AMOLF, c/o Philips Research Laboratories, 5656 AE Eindhoven, The Netherlands

⁴Materials Innovation Institute, 2628 CD Delft, The Netherlands

⁵Institute for Molecules and Materials, Solid State Chemistry Department, Radboud University Nijmegen, 6525 ED Nijmegen, The Netherlands

⁶Philips Research Laboratories, 5656 AE Eindhoven, The Netherlands

⁷IKERBASQUE, Basque Foundation for Science, 48011 Bilbao, Spain

j.stiegler@nanogune.eu

Semiconductor nanowires have gained tremendous interest in the recent years as potential building blocks for future nano-opto/electronic devices. [1-4] A successful implementation of semiconductor nanowires into devices essentially relies on the control and the experimental verification of the local free-carrier concentration. However, quantitative free-carrier profiling of individual nanowires is still a challenging task. Here we report a quantitative method, which is based on local infrared (IR) plasmon resonance spectroscopy employing scattering-type scanning near-field optical microscopy (s-SNOM).

s-SNOM is typically based on atomic force microscopy (AFM) where the tip is illuminated with a focused laser beam and the tip-scattered light is detected simultaneously to topography (see Fig. 1a). Using metallic tips, the strong optical near-field interaction between tip and sample modifies the scattered light allowing for probing the local dielectric properties with nanoscale resolution. Unavoidable background contributions are suppressed by vertical tip oscillation at frequency Ω and subsequent higher-harmonic demodulation of the detector signal at $n\cdot\Omega$ with $n\geq 2$ [8]. Combining this higher harmonic demodulation with interferometric detection, background-free near-field optical amplitude s_n and phase φ_n contrast imaging is possible. s-SNOM offers an excellent optical resolution in the 10nm range independent of the wavelength [5] and allows for IR mapping the chemical composition [6], structural properties such as strain [7], and free-carriers in semiconductor devices [8].

We use s-SNOM operating at IR frequencies between 890 and 1100 cm^{-1} to measure the free-carrier concentration in single modulation-doped InP nanowires. Fig. 1b shows a typical amplitude image of two nanowires, revealing three segments. The highly doped central segment appears much brighter than the two adjacent undoped segments. This contrast can be explained by a plasmon-resonant near-field interaction between the AFM tip and the free carriers in the doped nanowire segment. The near-field resonance occurs close to the plasma frequency of the free carriers and shifts to higher frequencies with an increasing free-carrier concentration n . We can thus determine the free-carrier concentration by fitting the experimental spectra with model calculations describing the tip-sample near-field interaction (Fig. 1c).

Imaging nanowires as thin as 20 nm, we find nanoscale variations of the free-carrier concentration, which can be attributed to local growth defects. [9] The spatial resolution we achieve in these experiments is about 20 nm ($\lambda/500$), i.e. nearly three orders of magnitude below the diffraction limit.

With s-SNOM we provide a contactless, non-destructive optical nanoscopy tool, which allows quantitative local measurements of the free-carrier concentration in semiconductor nanowires with nanoscale spatial resolution. Improved modeling and spectral extension of s-SNOM to the THz frequency range [10] could make the method a powerful tool for free-carrier profiling not only of nanowires, but also of other semiconductor nanodevices and photonic nanostructures.

References

- [1] M. H. Huang, S. Mao, H. Feick, H. Yan, Y. Wu, H. Kind, E. Weber, R. Russo, P. Yang, *Science* **292** (2001) 1897.
- [2] X. Duan, Y. Huang, R. Agarwal, and C. M. Lieber, *Nature* **421** (2003) 241
- [3] C. Colombo, M. Hei, Gratzel, A. Fontcuberta i Moral, *Appl. Phys. Lett.* **94** (2009) 173108.
- [4] M. D. Kelzenberg, D. B. Turner-Evans, B. M. Kayes, M. A. Filler, M. C. Putnam, N. S. Lewis, H. A. Atwater, *Nano Lett.* **8** (2008), 710.
- [5] F. Keilmann, R. Hillenbrand, *Phil. Trans. R. Soc. Lond. A* **362** (2004) 787.
- [6] B. Knoll, F. Keilmann, *Nature* **399** (1999) 134.
- [7] A. Huber, A. Ziegler, T. Kock, R. Hillenbrand, *Nat. Nanotechnol.* **4** (2007) 153
- [8] A. Huber, D. Kazantsev, F. Keilmann, J. Wittborn, R. Hillenbrand, *Adv. Mater.* **19** (2007) 2209
- [9] J. Stiegler, A. Huber, S. Diedenhofen, J. Gomez Rivas, R. Algra, E. Bakkers, R. Hillenbrand, *Nano Lett.* Advanced online publication (19. Mar. 2010) DOI10.1021/nl100145d.
- [10] A. Huber, F. Keilmann, J. Wittborn, J. Aizpurua, and R. Hillenbrand, *Nano Lett.* **8** (2008) 3766.

Figures

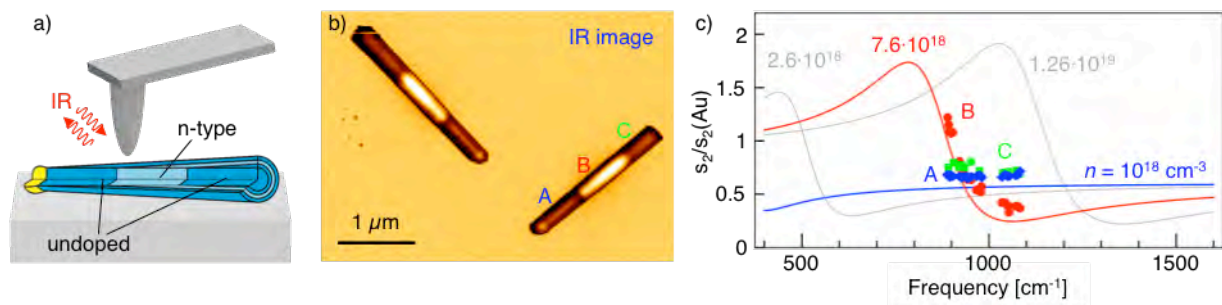


Figure 1: Infrared near-field mapping of modulation doped InP nanowires. (a) Schematic illustration of free-carrier profiling of modulation-doped semiconductor nanowires by infrared (IR) s-SNOM. (b) Amplitude s_2 image of two representative InP nanowires recorded at an IR laser frequency of 893 cm^{-1} . (c) Experimental (symbols) and calculated (solid lines) local IR near-field amplitude spectra along a single InP nanowire.

Light transport by sets and chains of Mie resonances: whispering gallery modes and localized plasmons. Effects on extraordinary transmission

F.J. Valdivia-Valero and M. Nieto-Vesperinas

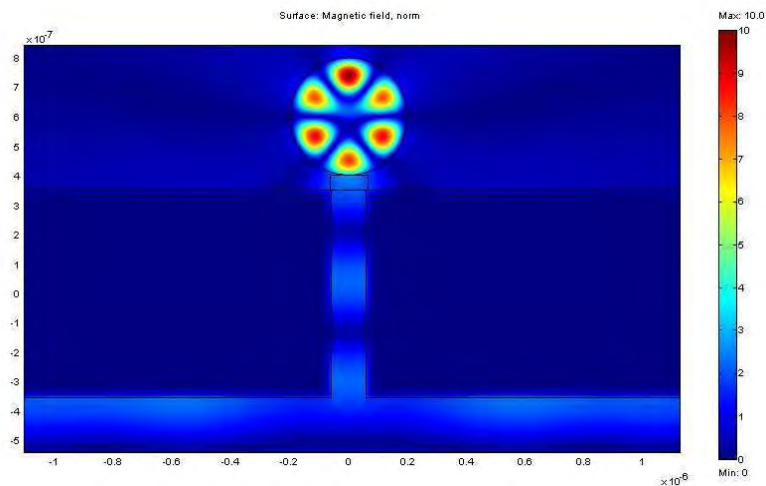
Instituto de Ciencia de Materiales de Madrid, C.S.I.C., Campus de Cantoblanco
28049 Madrid, Spain

mnieto@icmm.csic.es; fvaldivia@icmm.csic.es

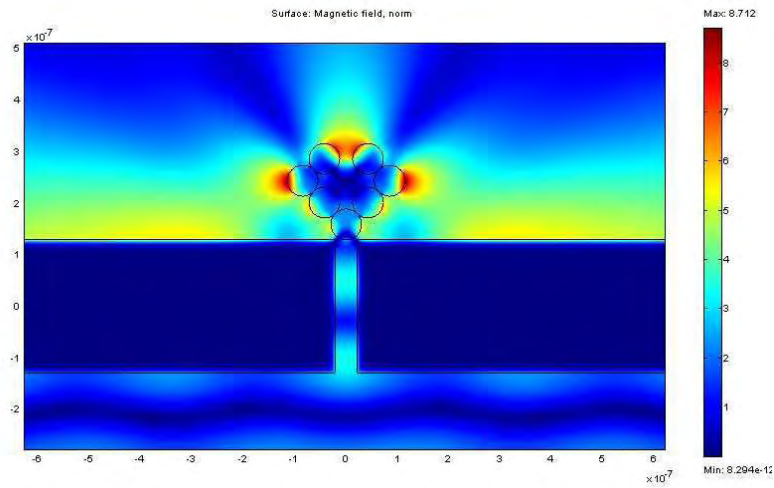
We study the excitation of Mie morphology dependent resonances (MDR), (i.e. whispering gallery modes in dielectric nanocylinders and of localized surface plasmons in metallic ones), by light transmitted through a subwavelength slit in a metallic slab. Calculations are done both by the finite elements method and using FDTD simulations. We discuss the effect of that excitation on extraordinary transmission by the slit, and compare it with cases in which there are only evanescent or weakly propagating waves at the exit of the aperture. In this way, we show the dominant role of the MDR over the aperture enhanced transmission as regards the resulting transmitted intensity and its concentration inside the cylinders. When sets of these particles are placed in front of the slit, like linear or bifurcated chains, with or without bends, one can control the concentration of MDR in the stationary state by designing the parameters, so that these surface waves are coupled by both waveguiding of the nanocylinder eigenmodes and by scattered propagating waves. Also, the choice of the wavelength and polarization of the illumination, allows to select the excitation of either bonding or antibonding states of the field transmitted through the aperture into the particles. Metallic cylinders can exhibit nanoantenna characteristics.

Besides, these MDR are further enhanced when a beam emerges from the slit, due to a periodic corrugation in the slab.

F.J. Valdivia-Valero and M. Nieto-Vesperinas, *Opt. Express* **18**, 6740 (2010).



Magnetic field modulus (A/m) of a slit in supertransmission. Wavelength: 750nm , p-polarization) in presence of a dielectric cylinder (refractive index $n = 3.670 + i0.005$, radius $r = 200\text{nm}$) placed at 50nm of the exit plane of the aperture. The WGH_{31} mode has been excited.



Magnetic field modulus (A/m) in a bifurcation with not vertical elbow (angle between chains at bifurcation: 90° , elbow angle: 90° . Distance between cylinders: $0nm$) of seven metallic cylinders (refractive index $n = 0.234 + i1.275$, radius $r = 60nm$) in front of a metallic slit (refractive index $n = 0.135 + i10.275$, slab width: $2562.96nm$, slab thickness: $258.13nm$, slit width: $43.02nm$) under p-polarization, wavelength: $346nm$). The LSP_{11} mode is excited.

Add-drop filter based on silicon spherical microcavities

E. Xifré-Pérez^{1,2}, J.D. Doménech³, R. Fenollosa^{1,2}, P. Muñoz³, J. Capmany³, F. Meseguer^{1,2}

¹Centro de Tecnologías Físicas, Unidad Asociada CSIC-UPV, Universidad Politécnica de Valencia, Camino de Vera s/n, 46022, Valencia, Spain,

²Instituto de Ciencia de Materiales de Madrid (CSIC), Sor Juana Inés de la Cruz 3, 28049, Cantoblanco, Madrid, Spain.

³iTEAM Research Institute, Universidad Politécnica de Valencia, Camino de Vera s/n, Valencia, Spain
exifre@fis.upv.es

Optical microcavities are very relevant structures for optical processing of light, because they can trap and confine electromagnetic energy during long times in very reduced volumes, enhancing this way light-matter interaction [1]. Among the different technological platforms on which microcavities can be produced, silicon is of uttermost importance because it can combine electronics and photonics at the same time in a single device [2]. Recently, some of us reported on the synthesis of silicon microspheres also called silicon colloids [3]. They are highly spherical particles with diameter from 0.5 to 5 μm and with a very smooth surface. This allows them working as photonic microcavities, with well defined Mie modes [3]. Here, we report on the coupling of silicon microspheres to Silicon-On-Insulator (SOI) waveguides at telecom wavelengths (C-band). For this purpose, devices consisting of SOI waveguides with microspheres deposited onto them are developed and their transmitted signal is measured. These measurements are compared with theoretical calculations of Mie modes of the microspheres. Previous reports about similar devices include 2D photonic crystal nanocavities coupled to photonic crystal waveguides [4], ring shaped cavities coupled to SOI waveguides [5], and half millimeter diameter silicon spheres coupled to optical fiber half couplers [6].

Silicon microspheres are obtained by chemical vapor deposition techniques, using di-silane as a precursor gas [3]. The as-grown samples consist of a substrate with many isolated and clustered spheres being the spheres poly-disperse with sizes from 0.5 to 5 μm . The size of the sphere determines which resonant modes possess a frequency within the transmission wavelength range of the silicon waveguide and can therefore be coupled to it. For this reason, we performed a selection of spheres (within the limited resolution of the optical microscope at 1000x magnification) having a diameter from 2.0 to 2.5 μm approximately. For the precise determination of the diameter of the microsphere, optical transmittance measurements were performed on each of the selected microspheres for the wavelength range from 1 to 4 μm . We used a Fourier Transform Infrared Spectrometer Bruker IF 66/S for that purpose. This allows identifying the resonant modes and precisely determining the sphere diameter by fitting the measured signal to Mie theory [3]. Only those microspheres having resonant modes within the transmission range of the waveguides were considered as candidates to build up the devices.

The accurate placement of the microspheres on top of the silicon waveguides was performed using a micromanipulation technique we have developed. Different needle-shaped tools were fabricated for the pick and place operation and for the fine positioning of the spheres on the waveguides. Figure 1 shows an optical microscopy image (top view) of a silicon microsphere on top of a waveguide. The diameter of the sphere shown in Fig. 1 is 2.49 μm , determined using the process described above.

The silicon waveguides used for this device were produced on a standard SOITEC wafer by deep UV lithography in an ePIXfab platform. They have a cross section of 500x220 nm^2 and their length is about 3 mm, finishing at their both ends by a grating coupler so that light can be easily in/out coupled to/from the waveguides [7]. Both, waveguides and couplers were designed for transmitting only TE polarized light around 1550 nm.

Light from an ASE source was coupled to the waveguide and the transmitted signal was measured by a spectrum analyzer. The direction and the polarization of light for the waveguide-microsphere device can be observed in the inset of Fig. 1. Figure 2 shows the light transmitted through the waveguide with the microsphere placed on it (solid line, left axis), as well as the calculation by Mie theory of the light transmitted through that microsphere when being isolated, i.e. without being placed on any substrate (dashed line, right axis). The deeps in transmission for the isolated sphere case correspond to whispering gallery modes, indicated in the figure by letters 'a' and 'b' for TM and TE modes respectively and followed by two sub-indexes that account for the mode order [3]. We have associated the deeps in

the transmitted signal through the waveguide to the coupling of light to the resonances of the microsphere. This way, the pronounced deep placed around 1535 nm would be originated from $b_{10,1}$ mode, the less marked deep around 1543 nm from $a_{9,1}$ mode and the much wider deep placed around 1580 nm from $a_{6,2}$ mode. However, some discrepancies between theory and experiment are observed. Mode $b_{7,2}$ does not give rise to a coupling effect and the coupled modes ($b_{10,1}$, $a_{9,1}$ and $a_{6,2}$) split into two deeps. Several reasons may explain these discrepancies. Firstly, while in the calculation the sphere is considered to be isolated, in the experiment it is placed on the silicon waveguide, therefore mode degeneracy would be broken due to the waveguide coupling. Secondly the control on the position of the microsphere is limited in the direction perpendicular to the waveguide, thus different coupling effects can be produced depending on this position. Thirdly, the microsphere may have some defects that could not be detected by optical microscopy and some type of absorption could be present. This would decrease the quality factor of the resonances. Nevertheless, it should be stressed the strong and peaked attenuation of the signal, of about 25 dB, achieved around 1535 nm.

We have demonstrated the coupling between a silicon waveguide and a silicon microsphere. The light transmitted through the waveguide has been attenuated up to 25 dB for a wavelength corresponding to one of the microsphere resonating modes. A splitting effect of the modes has also been observed.

References

- [1] K.J. Vahala, Nature, **424** (2003) 839.
- [2] L. Pavesi, in Silicon Photonics, Eds. D.J. Lockwood, Springer, Berlin, Germany 2004.
- [3] R. Fenollosa, F. Messegueur, and M. Tymczenko, Adv. Mater., **20** (2008) 95.
- [4] S. Noda, A. Chutinan, and M. Imada, Nature, **407** (2000) 608.
- [5] V.R. Almeida, C.A. Barrios, R.R. Panepucci, and M. Lipson, Nature, **431** (2004) 1081.
- [6] Y.O. Yilmaz, A. Demir, A. Kurt, and A. Serpengüzel, IEEE Phot. Tech. Lett., **17** (2005) 1662.
- [7] D. Taillaert, F.V. Laere, M. Ayre, W. Bogaerts, D.V. Thourhout, P. Bienstman, and R. Baets, JJAP Part-1, **45** (2006) 6071.

Figures

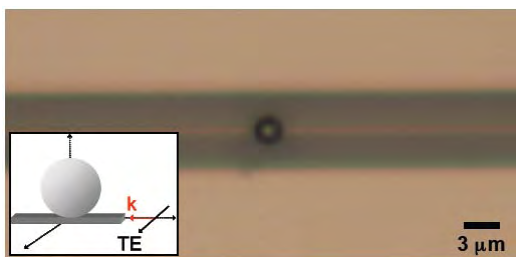


Figure 1. Optical microscopy image at 1000x magnification of a silicon microsphere placed on top of a silicon waveguide. Inset, schematic of the sphere and the waveguide showing the polarization of the transmitted light.

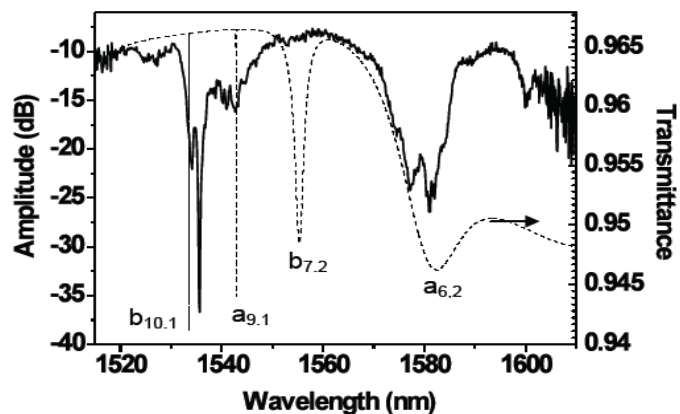


Figure 2. Measured light transmittance through a silicon waveguide with a silicon microsphere positioned on it (solid line, left axis). And simulation of the transmittance of the same silicon microsphere being isolated (dashed line, right axis).

CEN2010

Segovia (Spain)

June 15-18, 2010

POSTER CONTRIBUTIONS

Please, find your final **poster number** by looking up your name in the **Author Index** displayed in the Poster Exhibition Area.

Synthesis and characterization of optical nanocrystals. A step forward towards new promising transparent nanoceramics

M. Galceran*, M. C. Pujol, J. J. Carvajal, X. Mateos, **M. Aguiló** and F. Díaz

¹*Física i Cristal·lografia de Materials i Nanomaterials (FiCMA-FiCMA). Universitat Rovira i Virgili. Campus Sescelades, c/ Marcel·lí Domingo, s/n, E-43007 Tarragona, Spain
montserrat.galceran@urv.cat

Nanocrystalline materials are polycrystalline materials with a particle size in the nanometer range that have different physical, optical, electronic, chemical and structural properties, because they have a larger fraction of surface atoms than larger-scale materials [1]. These nanocrystals could be the first step for preparing nanoceramic laser material because of the enhancement of the sintering activity due to the nanometric size dimension [2]. Nanoceramics are very attractive as solid state lasers due to their several advantages respect to the bulk single crystal, such as low cost, easy fabrication and good mechanical and optical properties. Furthermore, ceramics significantly improve the thermal shock parameter and resistance to laser damage allowing high power laser operation [3].

Since 1998, highly transparent ceramic lasers have been fabricated by vacuum sintering, using nanocrystalline materials such as Nd:Y₃Al₅O₁₂ (Nd:YAG)[4], Nd:Lu₂O₃ [5], Yb:Sc₂O₃ [6], and Yb:Lu₂O₃ [7]. Recently, the high-pressure low-temperature technique (HPLT) has emerged to obtain transparent ceramic lasers such as YAG [8] and RE:YAG [9,10]. The most outstanding advantage of the HPLT method, with respect to other techniques, is the low sintering temperature required to prepare the ceramic material. In addition, it is a new, non-conventional method for avoiding grain growth during sintering.

KRE(WO₄)₂ (RE = Eu³⁺, Gd³⁺, Er³⁺ and Yb³⁺), RE₂O₃ (RE = Sc³⁺, Ho³⁺, Er³⁺, Yb³⁺ and Lu³⁺) nanocrystals for solid state laser applications were synthesized by the modified Pechini method [11,12,13] (figure 1). The Pechini method is an alternative sol-gel technology used to synthesize nanocrystals [14]. The sol-gel process offers several advantages, such as low cost, versatility, simplicity, low processing temperature and a high degree of homogeneity. The experimental variables were optimized as a function of the desired material to synthesize. The synthesis of nanocrystals is the starting point to obtain ceramic materials using the high pressure low temperature method (figure 2).



Fig. 1: Nanocrystals synthesized using the modified Pechini method.

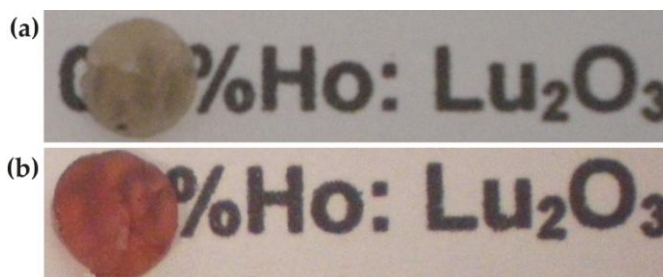


Fig. 2: (a) 0.5% at. Ho:Lu₂O₃ and (b) 10% at. Ho:Lu₂O₃ nanoceramics.

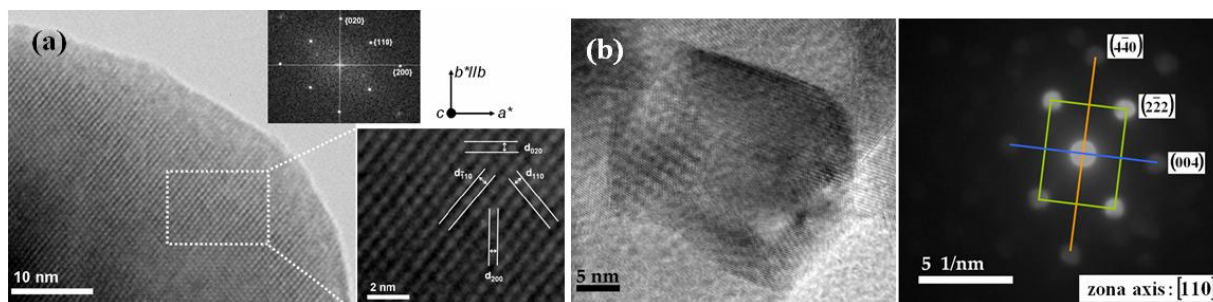


Fig. 3: HRTEM image and electron diffraction analyses of (a) KREW nanocrystals and (b) RE₂O₃ nanocrystals

The structural characterization of nanocrystals was investigated by a number of techniques, the most common being X-ray diffraction and electron diffraction. Figure 3 shows an example of high resolution

transmission electronic microscopy of the oxide nanocrystals, where it's possible to observe the lattice plane fringes indicating the high degree of crystallinity. The Fast Fourier Transform pattern and the electron diffraction pattern were used to index the lattice planes in accordance to their crystalline phase. On the other hand, the morphology, the average particle size and the particle size distributions were carried out using electronic microscopy (figure 4). Moreover, the optical absorption and luminescence measurements were performed at room and low temperature in order to determine the energy levels of the electronic states.

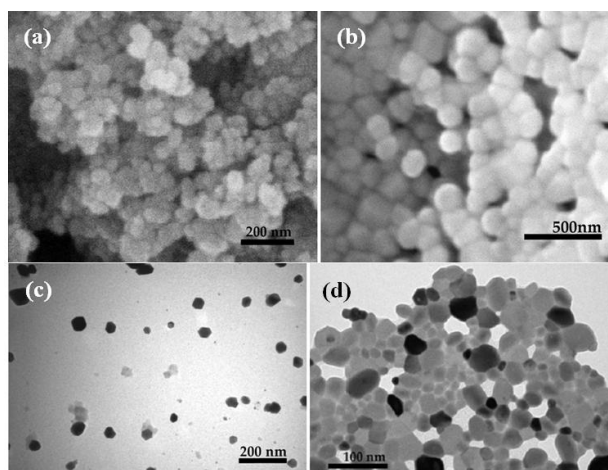


Fig. 4: SEM image of (a) KREW nanocrystals and (b) RE_2O_3 nanocrystals and TEM images of (c) KREW nanocrystals and (d) RE_2O_3 nanocrystals

References

- [1] G. Cao, "Nanostructures and Nanomaterials - Synthesis, Properties and Applications", Imperial College Press (2004).
- [2] C. Liu, X. Wang, Y. Jiang, Y. Wang and S. Hao, *Rare Metals*, **25** (2006), 471
- [3] A. Ikesue, Y. L. Aung, *Nature Photonics* **2** (2008) 721
- [4] J. Lu, K. Ueda, H. Yagi, T. Yanagitani, Y. Akiyama and A. A. Kaminskii, *Journal of Alloys and Compounds* **341** (2002) 220
- [5] J. Lu, K. Takaichi, T. Uematsu, A. Shirakawa, M. Musha, K. Ueda, H. Yagi, T. Yanagitani and A. A. Kaminskii, *Applied Physics Letters* **81** (2002) 4324
- [6] J. Lu, J. F. Bisson, K. Takaichi, T. Uematsu, A. Shirakawa, M. Musha, K. Ueda, H. Yagi, T. Yanagitani and A. A. Kaminskii, *Applied Physics Letters* **83** (2003) 1101.
- [7] K. Takaichi, H. Yagi, A. Shirakawa, K. Ueda, S. Hosokawa, T. Yanagitani and A. A. Kaminskii, *Physica. Status Solidi A* **202** (2005) R1
- [8] D. Hreniak and W. Streck, *Journal of Alloys and Compounds* **341** (2002) 183-186
- [9] R. Fedyk, D. Hreniak, W. Lojkowski, W. Streck, H. Matysiak, E. Grzanka, S. Gierlotka and P. Mazur, *Optical Materials* **29**, 1252-1257 (2007).
- [10] W. Streck, A. Bednarkiewicz, D. Hreniak, P. Mazur and W. Lojkowski, *Journal of Luminescence* **122-123** (2007) 70
- [11] M. Galceran, M. C. Pujol, M. Aguiló and F. Díaz, *Journal of Sol-Gel Science and Technology* **42** (2007) 79
- [12] M. Galceran, M. C. Pujol, M. Aguiló and F. Díaz, *Materials Science and Engineering B* **146** (2008) 7
- [13] M. Galceran, M. C. Pujol, M. Aguiló and F. Díaz *Journal Physical Chemistry C* **113** (2009) 15497.
- [14] M. P. Pechini, US Patent 3330697 (1967)

An analysis of magnetic materials through an extension of the discrete dipole approximation

R. Alcaraz de la Osa¹⁾, J. M. Saiz¹⁾, F. González¹⁾, P. Albella^{1), 2)}, and F. Moreno¹⁾

1) Universidad de Cantabria, Grupo de Óptica, Dpto. Física Aplicada
Facultad de Ciencias, Avda. Los Castros s/n, Santander, Spain

2) Centro de Física de Materiales CSIC-UPC/EHU and Donostia International Physics Center DIPC,
Paseo Manuel de Lardizabal 4, 20018, Donostia-San Sebastian Spain
alcarazr@unican.es

Recent advances in nanotechnology and nanoscience involving materials with magnetic properties (magneto-optical materials) [1,2,3,4] as well as those with unconventional optical properties (metamaterials) [5,6] have been performed, awakening a growing interest in this matter. The possibility of modeling the properties of such materials, and even design them in a customized way, is highly appreciated and currently constitutes a hot point. Furthermore, comparison and further agreement between experimental results and some theoretical framework is a constant requirement by researchers in those fields. In particular, the presence of a relative magnetic permeability μ_r different from 1 (even negative or tensorial) requires the revision and upgrading of the commonly available electromagnetic numerical methods [7,8].

In this sense, our Group has been working, during the last years, in the generalization of some widely used numerical methods, such as the extinction theorem [9]. Other approaches include Mie theory applied to materials with arbitrary optical constants ε and μ [10,11] and the discrete dipole approximation (DDA by its acronym in English) [12,13,14,15]. In this work we focus on the second: an extension of the DDA to the case of bianisotropic materials (both ε and μ tensorial magnitudes) [16]. The use of commercial software, like COMSOL, FDTD or DDSCAT (based on DDA), is helping as well to understand the required new point of view.

In this research we present an overview of the formalism of this extension together with some early results showing the potential of this new tool, and also verifying its reliability. At present, extinction, absorption and scattering cross-sections can be readily obtained, including scattering patterns at any given plane, and dipole moment distributions (3D) for \mathbf{p} and \mathbf{m} (electric and magnetic). Polarimetric calculations can also be accomplished for any given incident wave polarization. Also, inhomogeneities can be taken into account, providing a good position to study systems involving more than one material, like nanoshells [17].

To check the reliability of the code, we have performed some calculations on systems at reach for conventional methods. Two examples are displayed in the next figures. Figure 1 shows the well-known zero-backscattering feature of a small particle ($R \approx 0.01\lambda$) satisfying Kerker's condition ($\varepsilon = \mu$) [18]. Figure 2 shows the extinction efficiency of both a gold sphere of radius $R = 20$ nm, and a sphere with a dielectric ($\varepsilon = 2$) core (inclusion) of radius $R = 12$ nm and a metallic (gold) shell, for an external radius $R = 20$ nm. Comparison between our code [16] and the well-proved DDSCAT code from B. T. Draine [14,15] is also presented.

Acknowledgements

This research has been supported by MICINN (Ministerio de Ciencia e Innovación) under project #FIS2007-60158. The authors thankfully acknowledge the computer resources provided by the RES (Red Española de Supercomputación) node (Altamira) at Universidad de Cantabria. R. Alcaraz de la Osa also thanks the Ministry of Education of Spain for his FPU grant.

References

- [1] S. Albaladejo, R. Gómez-Medina, L.S. Froufe-Pérez et. al., *Optics Express*, **4** (2010), 3556-3567.
- [2] G. Ctistis, E. Papaioannou, P. Patoka et. al., *Nano Lett.*, **1** (2009), 1-6.
- [3] D. A. Smith, and K. L. Stokes, *Optics Express*, **12** (2006), 5746-5754.
- [4] N. B. Piller, and O. J. F. Martin, *Optics Letters*, **8** (1998), 579-581.
- [5] V.M. Agranovich, and Yu.N. Gartstein, *Metamaterials*, **1** (2009), 1-9.
- [6] A. Alu, and N. Engheta, *Optics Express*, **7** (2009), 5723-5730.
- [7] Y. You, G. W. Kattawar et. al., *Optics Express*, **3** (2008), 2068-2079.
- [8] P. C. Chaumet, and A. Rahmani, *JQSRT*, **1-2** (2009), 22-29.
- [9] P. Albella, F. Moreno, J. M. Saiz, and F. González, *Optics Express*, **11** (2007), 6857-6867.
- [10] B. García-Cámara, F. Moreno et. al., *JOSA A*, **2** (2008), 327-334.
- [11] B. García-Cámara, F. González et. al., *JOSA A*, **11** (2008), 2875-2878.
- [12] P. Albella, F. Moreno, J. M. Saiz, and F. González, *Optics Express*, **17** (2008), 12872-12879.
- [13] P. Albella, J. M. Saiz, J. M. Sanz et. al., *Optics Express*, **12** (2009), 1906-1908.
- [14] B. T. Draine, and P. J. Flatau, *JOSA A*, **4** (1994), 1491-1499.
- [15] B. T. Draine, and P. J. Flatau, <http://arXiv.org/abs/1002.1505v1> (2010).
- [16] R. Alcaraz de la Osa et. al., *Optics Express* (to be published).
- [17] J. Britt Lassiter, Mark W. Knight et. al., *Nano Lett.*, **12** (2009), 4326-4332.
- [18] M. Kerker, D.-S. Wang, and C. L. Giles, *JOSA*, **6** (1983), 765-767.

Figures

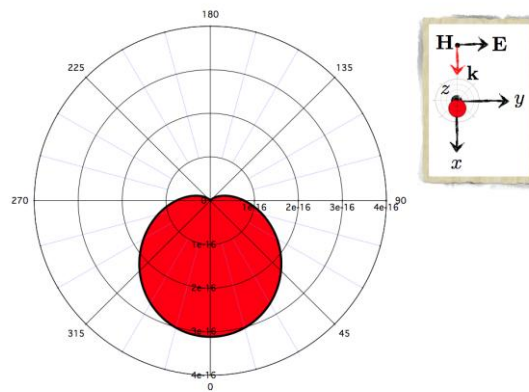


Figure 1: Scattering pattern of a sphere of radius $R \approx 0.01\lambda$ satisfying Kerker's condition ($\epsilon = \mu = 2$). The scattering plane coincides with the incident plane, with the incident wave being P-polarized.

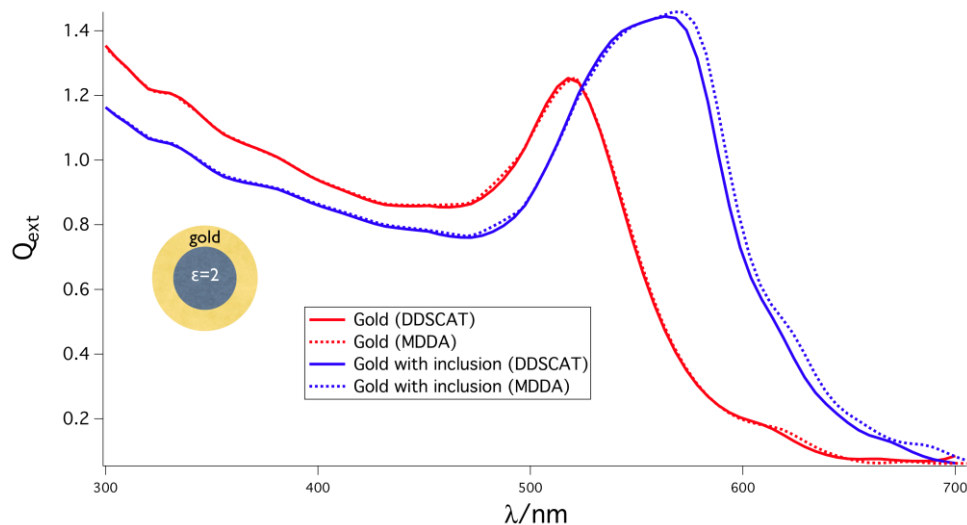


Figure 2: extinction efficiency of both a gold sphere of radius $R=20$ nm, and a sphere with a dielectric ($\epsilon=2$) core (inclusion) of radius $R=12$ nm and a metallic (gold) shell, for an external radius $R=20$ nm. Comparison between our code and the well-established DDSCAT code is also provided.

Control of the index of refraction in coherently driven media with magnetoelectric cross coupling

Frank Bello,¹ Jordi Mompart¹ and Veronica Ahufinger^{1,2}

¹ Departament de Física, Universitat Autònoma de Barcelona, E-08193 Bellaterra, Spain

² Institució Catalana de Recerca i Estudis Avançats (ICREA), Lluís Companys 23, E-08010 Barcelona, Spain

FrankDaniel.Bello@uab.cat

Optical metamaterials, or more specifically left-handed materials incorporating a negative phase velocity with power flow in the opposing direction, have been theoretically proven to exhibit phenomena such as sub-wavelength resolution, reverse Doppler effect, and Cherenkov radiation to name a few [1,2]. Although experiments have verified the existence of negative index materials [3,4] by inducing a strong magnetic and electric response from the medium, losses remain a major limitation in the optical regime [5,6]. For this purpose, it has been shown that some gases such as neon could be used to induce a negative index of refraction with low absorption rates affecting optical wavelengths of light in coherently driven media [7,8]. In addition, recent publications have pointed out that if one considers magnetoelectric cross coupling, a negative index of refraction can be achieved without requiring negative permeability, which has been the largest impediment thus far in the field, since typical transition magnetic dipole moments are smaller than electric ones by a factor of the order of the fine structure constant [9,10]. Using a semi-classical approach to model the interaction of light with atomic media, we simulate pump-probe experiments and investigate the effects of the material's response, i.e. its polarization and magnetization, that could lead to media which are tunable between the active and passive regimes as well as bistable in its permittivity and permeability. Potentially active and/or bistable media could be used to conceive a new class of "ambidextrous" materials which can be easily manipulated between left and right handedness.

References

- [1] V. G. Veselago, *Sov. Phys. Uspekhi*, **10** (1968) 509-514.
- [2] J. Pendry, *Phys. Rev. Lett.*, **85** (2000) 3966.
- [3] R. A. Shelby et al., *Science*, **292** (2001) 77.
- [4] D. R. Smith et al., *Phys. Rev. Lett.*, **84** (2000) 4184.
- [5] V. M. Shalaev, *Nature Photonics*, **1** (2007) 41-48.
- [6] W. Cai and V. M. Shalaev, *Optical Metamaterials: Fundamentals and Applications*, (Springer 2009) Ch. 2.
- [7] Q. Thommen and P. Mandel, *Phys. Rev. Lett.*, **96** (2006) 053601.
- [8] P. P. Orth et al., (2008) arXiv:0711.0303v1.
- [9] J. Kästel et al., *Phys. Rev. A*, **79** (2009) 063818.
- [10] J. Kästel et al., *Phys. Rev. Lett.*, **99** (2007) 073602.

Magneto-optical studies in magneto-plasmonic nano-structured particles

G. Campo, F. Pineider, C. de Julià Fernández, E. Fantechi, C. Sangregorio, A. Caneschi,
D. Gatteschi

Department of Chemistry, University of Florence, INSTM, 50019, Sesto Fiorentino, Italy
giulio.campo@fi.infn.it

This work is devoted to the study of the magneto-optical properties of magneto-plasmonic particle based nanostructures. Magneto-plasmonic systems conjugate two materials, a magnetic one (e.g. transition metal) and an element exhibiting localized surface plasmonic resonance (typically noble metals: Au, Ag). By combining these features, it has been recently demonstrated the possibility of developing active magneto-plasmonics systems in which it is possible the modulation of plasmon resonance with an external magnetic field. [5] Moreover, plasmon-mediated enhancement of the magneto-optical response is possible. [6,7,8] In particular, the conjugation of magnetic and plasmonic properties in nanoparticulated structures offers a wide variety of applications in biomedicine: in theranostics, in which the gold shell acts as a protecting agent for the magnetic core, [1] as a highly functionalisable surface, [2] as an optical heater [3] or as an active optical beacon. [4]

The novel magneto-optical properties of the magneto-plasmonic systems are investigated measuring the magnetic circular dichroism (MCD), whereby the different absorption of right- and left-circular polarized light is used to probe the magnetization state of an absorbing sample. Our experimental configuration allows us to carry out room-temperature spectroscopic measurements in the Vis-nIR range (400-1000 nm). In addition, we carried out magnetization cycles at different wavelength, in order to resolve the magnetic contributions due to different electronic transitions or contributions.

We analysed hybrid systems containing gold and ferrites in different geometries, that exhibit different levels of conjugation, thus a variable extent of interaction of magnetic and plasmonic functions, ranging from no interaction (separate gold and ferrite particles), to weak (particle heterodimers) and strong interaction (gold-core@ferrite-shell particles).

The first results indicate that the single MCD responses of the ferrite and noble metal do not sum linearly (i.e. mix of separate particles), suggesting a plasmon amplified MO response and an energy shift of the plasmonic resonance in the MO spectrum. In addition, the MCD study of our hybrid systems allowed us to separate the single MO components of plasmonic and magnetic compounds and to evaluate their degree of hybridization with one another.

- [1] L. Wang *et al.*, J. Mater. Chem., 2005, 15, 1821.
- [2] X. Zhao *et al.*, Anal. Chem. 2008, 80, 9091.
- [3] L. Wang *et al.*, Angew. Chem. Int. Ed. 2008, 47, 2439.
- [4] Q. Wei *et al.*, J. Am. Chem. Soc., 2009, 131, 9728.
- [5] V. Temnov *et al.*, Nature Photon., 2010, 4, 107.
- [6] P. Jain *et al.*, Nano Lett., 2009, 9, 1644.
- [7] Y. Li *et al.*, Nano Lett., 2005, 5, 1689.
- [8] G. Shemer *et al.*, J. Phys. Chem. B, 2002, 106, 9195.

Determinaton of purcell effect in L7-type photonic crystal microcavities wth embedded InAs/InP quantum wires.

J. Canet-Ferrer^a, G. Muñoz-Matutano^a, L. J. Martínez^b, B. Alén^b, J.P. Martínez-Pastor^a, I. Prieto^b, P.A. Postigo^b, D. Fuster^b, Y. González^b, L. González^b

^aInstituto de Ciencias de los Materiales, Universitat de València, PO. Box 22085, 46071 Valencia, Spain.

^bInstituto de Microelectrónica de Madrid (IMM-CNM- CSIC), Isaac Newton 8, E-28760, Tres Cantos Madrid, Spain

jose.canet-ferrer@uv.es

During the last decade it has been shown the spontaneous emission of an isolated quantum emitter can be coupled to single cavity mode [1]. More recently, the strong coupling between single quantum dots and two-dimensional photonic crystal micro-cavities has been demonstrated [2, 3]. In this work we have studied elongated L7-type cavities in 2D photonic crystals fabricated on InP substrates and containing InAs/InP QWRs grown by molecular beam epitaxy [4, 5], a promising system for telecommunication wavelengths. This system has been characterized by means of confocal micro-photoluminescence (micro-PL) and time resolved micro-photoluminescence (micro-TRPL) at 77K. The typical micro-PL spectrum of the quantum wires outside the cavities extends over 150 nm as shown in Fig. 1 (bottom), and typical decay times measured under low excitation regime varies between 2.1 and 2.6 ns (red squares on the top of Fig. 1). Recently it has been demonstrated room temperature continuous wave laser operation in the fundamental mode of L7 cavities [6]. For this reason, our samples are excited by means of a 980 nm wavelength laser diode (resonant to the InP barrier) avoiding the contribution of the stimulated emission. This way the cavity resonances can be studied below the lasing threshold. As a result, a noticeable enhancement of the spontaneous emission is observed mainly for the first three modes. This fact is consistent with the quality factors reached by the cavity resonances (21600, 7040 and 1640 for modes emitting on 1480, 1460 and 1410 nm respectively) and its small modal volume $\sim (\lambda/n)^3$. On the other hand, the micro-PL decay time values measured at these modes (blue spheres on the top of figure 1) are smaller than decay times measured at the quantum wires outside the cavity, which suggests a certain Purcell effect even though under low coupling regime (a Purcell Factor close to 1.5). Such result are going to be discussed and compared with previous reports together with the possibility to reach the strong coupling regime using self-assembled QWRs as active media [7, 8].

References

- [1] G.S. Solomon et al. PRL **86** (2001) 3903.
- [2] H. Mabuchi and A. Dcherty. Science **298** (2002) 1372.
- [3] K. Hennessy *et al.*, Nature **445** (2007) 896.
- [4] L. González *et al.*, Appl. Phys. Lett. **76** (2000) 1104.
- [5] L.J. Martínez et al. J. Vac. Sci. Technol. B **27** (2009) 1801.
- [6] L.J. Martínez et al. Optics Express **17** (2009) 14993.
- [7] H. Ryu and M. Notomi. Optics Letters **28** (2003) 2390.
- [8] K.A. Atlasov et al. Optics Expres **17** (2009) 12981.

Figures

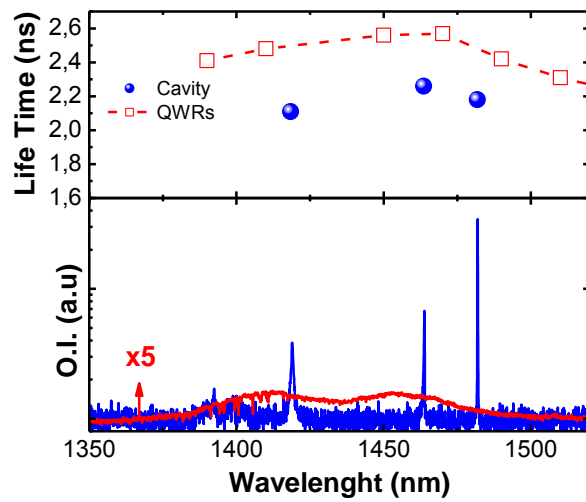


Figure 1. (Top) Micro-TRPL spectrum of InAs/InP quantum wires (red squares and dashed line) accompanied of the measured decay times at the cavity resonances (blue spheres). On the bottom, the emission of the different modes (blue line) is compared with QWR emission band (in red).

Organic MEMS/NEMS based bulk heterojunction photovoltaic cells with 3D electrodes

P. Chamorro-Posada¹, J. Martín-Gil¹, L. M. Navas-Gracia¹, S. K. Kassegne², P. Martín-Ramos², M. Majzoub², G. Ozturk²

¹Applied Optoelectronics Group for Agricultural Engineering, Universidad de Valladolid, Spain.

²MEMS Lab, College of Engineering, San Diego State University, CA, USA

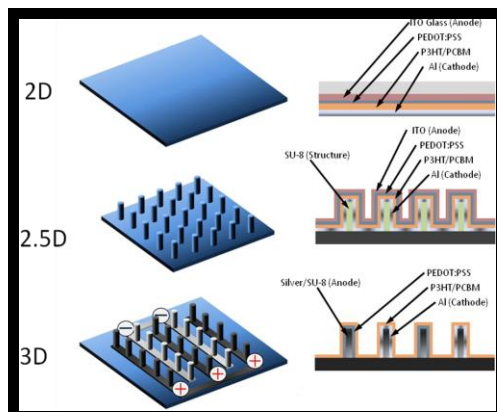
jesusmartingil@gmail.com

The field of organic electronics is entering its commercial phase. Organic solar cells are emerging as a major area of interest, prompted both by favorable government policy in alternative energy and by the increasing commercial opportunities as cell performance improves. Bulk heterojunction photovoltaic devices, based on polymer/fullerene-blend films, are advancing rapidly toward commercial viability since they can achieve a compromise between power conversion efficiency and compatibility with the type of manufacturing processes that enable low-cost production. Improvements in device efficiency are being achieved by focusing on new materials that have well-designed electronic energy levels capable of generating larger cell voltages, absorbing more light, improving charge separation, avoiding losses from the recombination of generated charges, and having optimal transport properties. Electrode materials are also an important subject of investigation, with the replacement of indium tin oxide (ITO) by lower cost printable inks being a particular focus. Nonetheless, an alternative strategy so as to achieve device efficiencies in excess of 4% is to improve the photocurrent by enhancing light absorption by increasing the exposed surface.

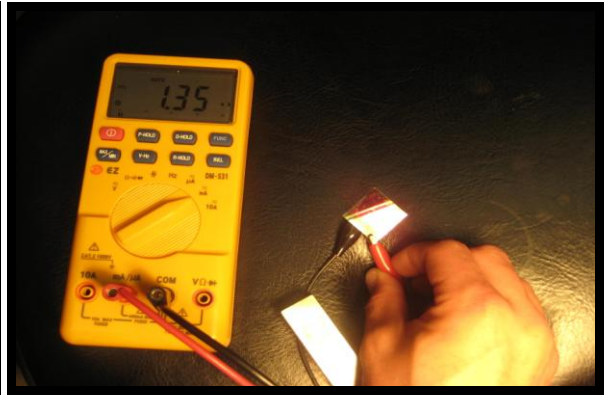
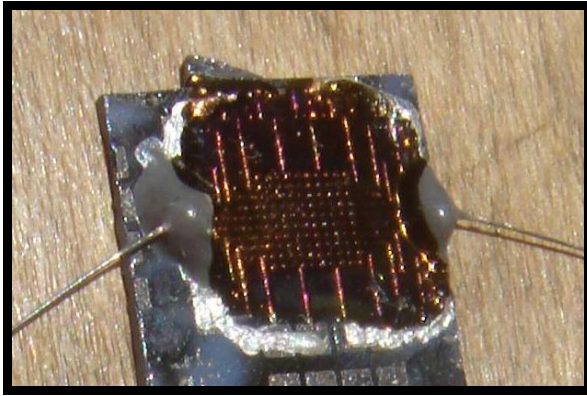
The Applied Optoelectronics Group for Agricultural Engineering, in collaboration with the MEMS Lab at San Diego State University (San Diego, CA), has developed a novel 3D architecture of organic PV cells that is, in most aspects, a significant departure from existing technologies. It consists of organic photoactive material and 3D carbon-based charge collectors with decreased diffusion length and increased light absorption area enabled by large electrode surface area. As shown in the figures, the core concept employs a 3-dimensional photovoltaic cell of several microns depth consisting of a large array of high-aspect ratio carbon electrodes of few microns diameter surrounded by a matrix of heterojunction photoactive material. The carbon electrodes introduced here replace conventional thin film metal electrodes such as aluminum and ITO which require expensive vacuum deposition (transparency is not a must, due to the electron flow direction, which is traditionally perpendicular to the surface). These 3D carbon electrodes are patterned through a lithography process followed by pyrolysis of SU-8 negative photoresist. The patterning consists of two layers: the bottom layer is for the wire traces that connect a series of anodes and cathodes separately whereas the second layer consists of the high-aspect ratio electrodes. Electrodes are not layered, but staggered. The photoactive material is spin-coated on the microarray of electrodes: heterojunction photoactive polymer such as a blend of P3HT (poly(3-hexylthiophene)) and PCBM (phenyl-C61-butyric acid methyl ester). All processes, except aluminum deposition, are performed under natural environment conditions.

A short circuit current density of 2.03 mA/cm² is demonstrated on a cloudy day under AM1.21G light.

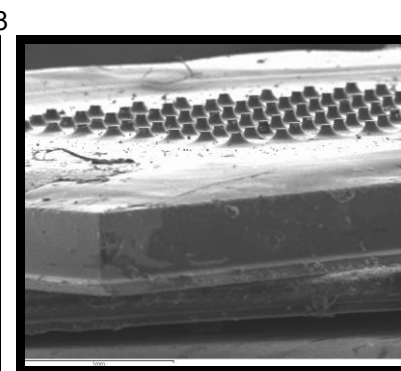
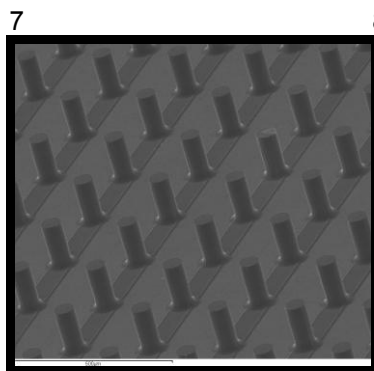
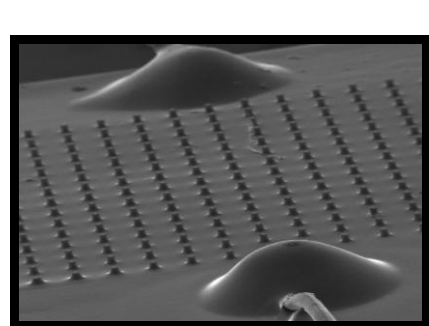
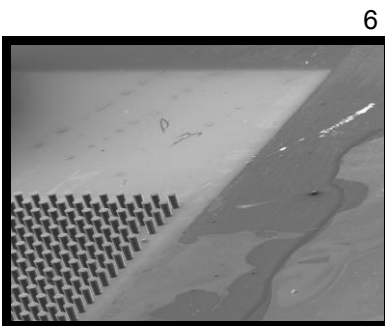
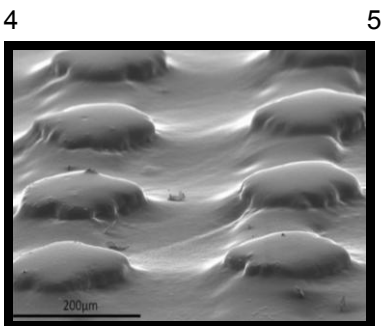
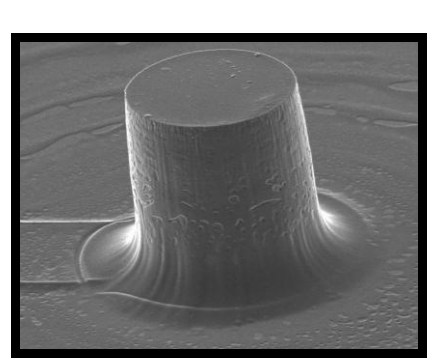
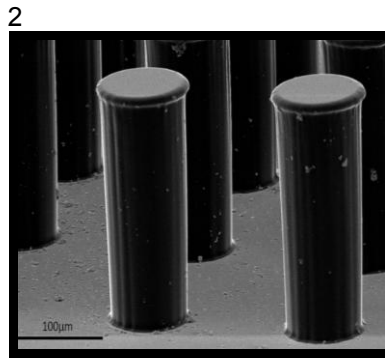
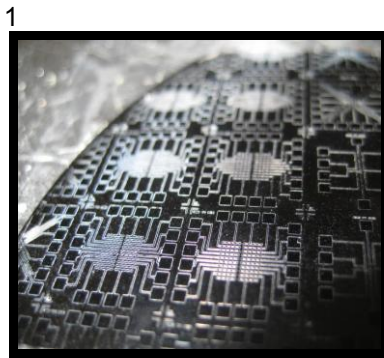
Figures



2D, 2.5D, and 3D concept representations



Fabricated devices



Manufacture steps (from left to right): (1) Electrical connection patterned wafer after the first lithography step; (2) SEM image of high aspect ratio SU-8 posts; (3) SEM image of a sample anode after PEDOT:PSS was applied; (4) SEM image of P3HT/PCBM coated SU-8 composite; (5) SEM image of aluminum electrode contact area; (6) Generation II chip with bonding pads; (7) SEM Images showing the micro array of electrodes in a single staggered chip; (8) SEM images of 10 x 10 Generation I chip at an 80° tilt angle (cross-section).

Optical characterization of anisotropic porous silicon structures

Joaquín Cos¹, Elisabeth Xifré-Pérez^{1,2}, Josep Ferré-Borrull¹, Josep Pallarès¹ and Lluís F. Marsal¹

(1) Departament d'Enginyeria Electrònica, Elèctrica i Automàtica
Universitat Rovira i Virgili Avda. Països Catalans 26, 43007 Tarragona, Spain

(2) Centro de Tecnologías Físicas, Unidad Asociada ICMM-CSIC/UPV
Universidad Politécnica de Valencia, Avda. de los Naranjos s/n, 46022 Valencia, Spain

lluis.marsal@urv.cat

1. Introduction

Porous silicon has attracted a great deal of attention because it makes it possible to produce a new generation of both active and passive optoelectronic devices [1]. This material can be obtained by HF electrochemical etching of silicon, which generates a range of refractive indices by changing the current density during anodization process. The thickness is determined by the time for which the current is applied [2]. It has excellent mechanical and thermal properties and is obviously compatible with silicon-based microelectronics. The anisotropy of Porous silicon has been reported in the literature [3] therefore in order to perform a good characterization of this kind of structures, an anisotropic numerical method must to be employed.

In this work we characterize by the transfer matrix method (TMM) [4] the dimensions and dispersion properties of two anisotropic porous silicon structures. From a previous analysis of the dimensions by mean of scanning electron microscopy (SEM) we fit these dimensions comparing the reflectance obtained by a Fourier transform infrared spectroscopy (FTIR) and the reflectance simulated by the TMM.

2. Results and discussion

The two structures analyzed in this work are composed by the stacking of two kinds of monolayers. The ordinary and extraordinary refraction index of these monolayers has been obtained by spectroscopic ellipsometry. The reflectance data has been obtained at an incident angle of 12° for the wavelength range of 1-4 μm at 5 nm intervals. The dispersive refractive index of the silicon substrate is obtained from [5].

The first structure is composed of two different layers, A and B. Table 1 summarizes the dimensions and refractive indexes obtained with SEM and ellipsometry and adjusted by TMM. Fig. 1 shows the three spectra, the experimental spectrum (square marker), the spectrum simulated by TMM considering the previous dimensions (dotted line) and the spectrum obtained by fitting the dimensions and dispersion (solid line). As it can be seen, a good adjustment can be obtained and only one of the features of the spectra is not matching with the experimental and simulated spectrum. The mismatch between the dimensions estimated by SEM and those estimated by fitting are 2,42% for the A layer and 6,20% for the B layer.

The second structure is composed of four layers, where the stacking is BABA. Table 2 summarizes the dimensions and refractive indexes obtained with SEM and ellipsometry and fitted by TMM. Fig. 2 shows the three spectra, the experimental spectrum (square marker), the spectrum simulated by TMM considering the previous dimensions (dotted line) and the spectrum obtained by fitting the dimensions and dispersion (solid line). As can be seen, again a good agreement between experimental and simulated spectrum is obtained. The differences between the dimensions obtained by SEM and our simulation are 3,42% for the first layer, 1,05% for the second layer, 4,95% for the third layer, and 8,84% for the fourth layer.

References

- [1] A. G. Cullis, L. T. Canham, and P. D. J. Calcott, *J. Appl. Phys.* **82**, 909 (1997).
- [2] L. Pavesi and P. Dubos, *Semicond. Sci. Tech.* **5**, 570 (1997)
- [3] V. Yu. Timoshenko, L. A. Osminkina, A. I. Efimova, L. A. Golovan, P. K. Kashkarov, D. Kovalev, N. Kuenzner, E. Gross, J. Diener, and F. Koch, *Phys. Rev. B*, **67**, 113405 (2003).
- [4] P. Yeh, *J. Opt. Soc. Am.* **69**, 742-756 (1979).
- [5] H. H. Li, *J. Phys. Chem. Ref. Data* **9**, 561 (1980).

4. Acknowledgements

This work was supported by Spanish Ministry of Ciencia e Innovacion (MICINN) under grant number TEC2009-09551, HOPE CSD2007-00007 (Consolider-Ingenio 2010) and AECID-A/024560/09.

Figures and tables

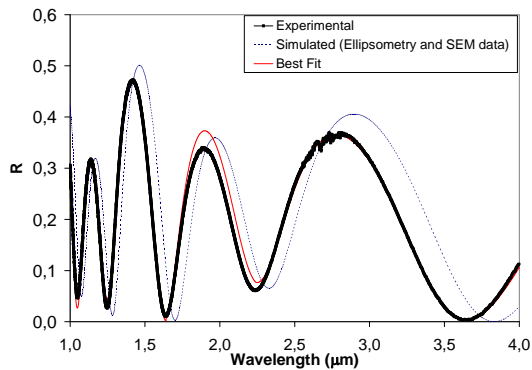


Figure 1. Experimental (square marker), simulated considering previous data (dotted line) and TMM fitting (solid line) reflectance for structure 1.

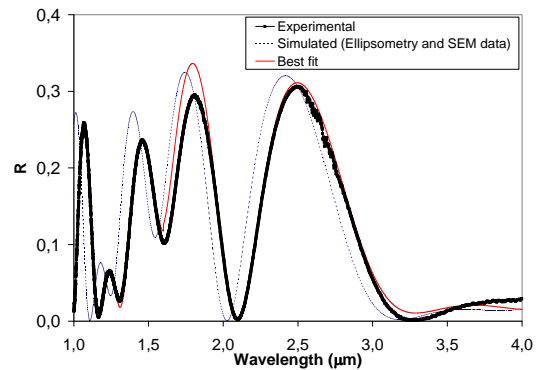


Figure 2. Experimental (square marker), simulated considering previous data (dotted line) and TMM fitting (solid line) reflectance for structure 2.

	Wavelength (μm)	A			B		
		n_o	n_e	d (μm)	n_o	n_e	d (μm)
Previous	1-4	1,41	1,55	0,62	1,83	2,02	1,29
TMM fitting	1-1,64	1,41	1,55	0,635	1,83	2,02	1,21
	1,64-2,24	1,41	1,55		1,8	2	
	2,24-4	1,4	1,53		1,79	1,98	

Table 1. Refraction index and length of the structure 1.

	Wavelength (μm)	B			A			B			A		
		n_o	n_e	d (μm)									
Previous	1-4	1,83	2,02	1,29	1,41	1,55	0,62	1,83	2,02	1,29	1,41	1,55	0,62
TMM fitting	1-1,3	1,84	2,02	0,725	1,41	1,55	0,385	1,84	2,02	0,785	1,41	1,55	0,48
	1,3-1,6	1,83	2,02		1,41	1,55		1,83	2,02				
	1,6-4	1,79	1,98		1,4	1,53		1,79	1,98				

Table 2. Refraction index and length of the structure 2.

Surface plasmon resonance in plastic optical fiber sensors: gold film orientation and thickness dependencies

Ana C. López-Pérez^{a,b}, Víctor M. Muñoz-Berti^{a,b}, Mauro Lomer^b, José Miguel López-Higuera^b, Benito Alén^a, Antonio García-Martín^a, **José Luis Costa-Krämer^{a,*}**

^a IMM-Instituto de Microelectrónica de Madrid,
Isaac Newton 8, 2870 Tres Cantos, Madrid, Spain;
^b Grupo de Ingeniería Fotónica, Universidad de Cantabria,
Avda. los Castros s/n, Santander, Spain.
kramer@imm.cnm.csic.es

Surface plasmon excitation using a variation of Kretschmann method based on light guiding through an optical fiber has been extensively studied in the literature. However, scarce studies exist concerning plastic optical based sensors, most probably due to their particularly bad propagation conditions. An inexpensive low cost sensor using this type of fiber is herein demonstrated. Through careful design, modeling and fabrication conditions a film/fiber configuration is obtained with a unique resonance. While both “frontal” and “oblique” (Fig.1) gold film depositions in curved fibers produce several plasmonic resonances, a parallel-planar film-fiber configuration produces a single spectral resonance (Fig.2) with a well defined gold thin film layer thickness dependence. Both sensor fabrication and measurement schemes will be presented, and the specific problems faced because of the multimodal character of the fiber described. A roadmap to design a low cost sensor based in the structures studied, and a theoretical formalism that describes the main experimental findings, based on the transmission matrix, will be presented

References

- [1] R. C. Jorgenson and S. S. Yee. A fiber-optic chemical sensor based on surface plasmon resonance. *Sensors and Actuators B*, 8:213, 1993.
- [2] M. Kanso, S. Cuenot, and G. Louarn. Sensitivity of optical fiber sensor based on surface plasmon resonance: modelling and experiments. *Plasmonics*, 3:49, 2008.
- [3] E. Kretschmann. The determination of the optical constants of metals by excitation of surface plasmons. *Zeitschrift fur Physik A*, 241:313, 1971.
- [4] S. N. Kasarova, N. G. Sultanova, C. D. Ivanov, and I. D. Nikolov. Analysis of the dispersion of optical plastic materials. *Optical Materials*, 29:1481, 2007.
- [5] A. K. Sharma, R. Jha, and B. D. Gupta. Fiber-optic sensors based on surface plasmon resonance: A comprehensive review. *IEEE Sens. J.*, 7:1118, 2007.
- [6] R. K. Verma and B. D. Gupta. Theoretical modelling of a bi-dimensional u-shaped surface plasmon resonance based fibre optic sensor for sensitivity enhancement. *Journal of Physics D: Applied Physics*, 41:095106, 2008.
- [7] F. Villuendas and J. Pelayo. Optical fibre device for chemical sensing based on surface plasmon excitation. *Sensors and Actuators A*, 21:142, 1990

Figures

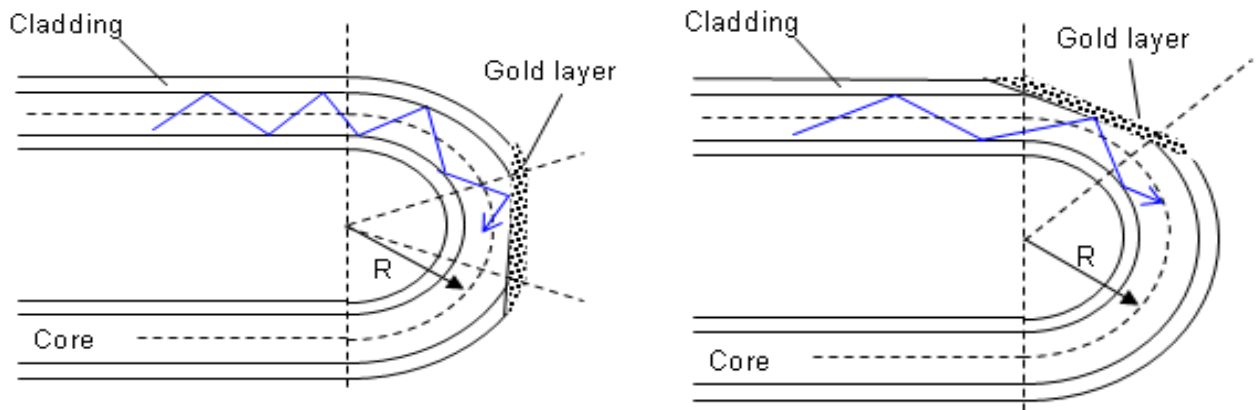


Fig.1 “Frontal” and “oblique” thin film configurations for the surface plasmon resonance in curved plastic optical fiber sensors.

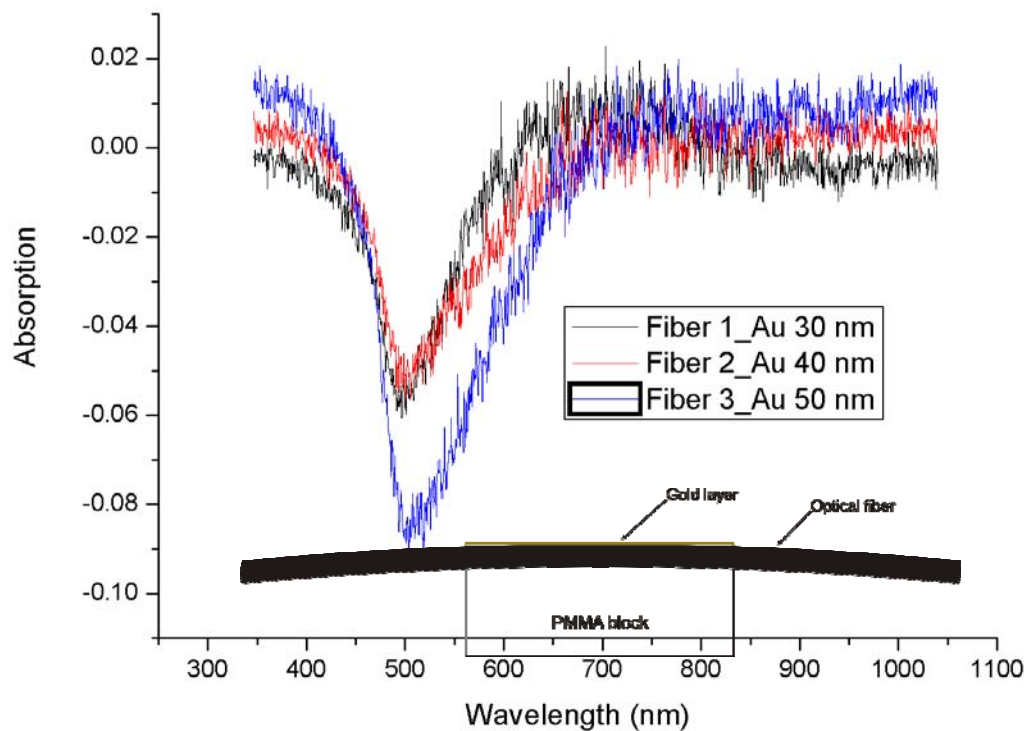


Fig.2 Gold thickness dependence of the plasmonic absorption in the parallel-planar film-fiber configuration. The gold thicknesses were 30, 40 and 50 nm for fiber 1, 2 & 3 respectively. The inset shows the fiber - gold film design scheme.

Synthesis and characterization of Tm doped Lu₂O₃ nanocrystalline powder

E. W. Barrera^{1,*}, M. C. Pujol¹, C. Cascales², C. Zaldo², K. H. Park³, S. B. Choi⁴, F. Rotermund⁴,
J. J. Carvajal¹, X. Mateos¹, M. Aguiló¹, and F. Díaz¹

1. Física i Cristal·lografia de Materials i Nanomaterials (FiCMA-FiCNA), Universitat Rovira i Virgili (URV), Campus Sescelades, c/ Marcel·lí Domingo, s/n, E-43007 Tarragona, Spain
- 2 Instituto de Ciencia de Materiales de Madrid, CSIC, Calle Sor Juana Inés de la Cruz, Cantoblanco, E-28049 Madrid, Spain
3. Korea Advanced Nano Fab Center (KANC), 443-270 Suwon, Republic of Korea
4. Division of Energy Systems Research, Ajou University, San 5 Wonchun, 443-749 Suwon, Republic of Korea,
elixirwilliam.barrera@urv.cat

Rare earth (RE) doped materials are drawing much attention for many display and lighting devices such as plasma displays panels, electroluminescence and light-emitting diodes [1,2] since they can offer higher luminous efficiencies and lower manufacturing costs. On the other hand, the synthesis and preparation of RE doped nanocrystals of some laser materials is the first step in order to obtain their transparent laser ceramic. The use of ceramics as an alternative to single crystals is justified in some compounds, in which the crystal growth is difficult and has a high cost. Furthermore, the ceramics show better thermo-mechanical properties, such as the thermal shock parameter and resistance to the laser damage [1]. Highly transparent cubic ceramic materials Y₃Al₅O₁₂ (YAG) and RE sesquioxides RE₂O₃ have received great attention due to the improvement reached in nanocrystalline technology [2,3,4]. The RE₂O₃ oxides are interesting as laser materials for high power applications due to their high thermal conductivity, low phonon energy values and strong crystal field for the active ion [5].

We focused our attention in Lu₂O₃ doped with thulium (Tm³⁺). The tunable laser emission of Tm³⁺ around two microns has many interesting applications such as remote sensing and medicine, for instance, based on the atmospheric transparency window and the absorption of water at this wavelength range, respectively. It is well-known that the Lu₂O₃ matrix is highly chemical and thermal stable and has a broad optical transparency from the visible to the NIR regions [6]. The synthesis of nanocrystals with high crystalline quality and narrow size distribution is an important first step towards obtaining transparent laser ceramic materials. These two factors allow a more dense packing of the particles and minimizing light scattering.

Tm³⁺ doped Lu₂O₃ nanocrystals Lu_{2-x}Tm_xO₃ with x = 0.01 – 0.3 (i.e., 0.5 - 15 mol at. % Tm³⁺) were synthesized by a modified Sol-gel Pechini method. The maximum temperature at which these crystals have been synthesized has been 1073 K. In all cases, the obtained nanoparticles crystallize in the cubic system, with the space group of symmetry Ia $\bar{3}$. The mean particle size in all the cases was below 100 nm. We studied the evolution of the grain size with temperature and linear thermal expansion coefficient has been determined, 7.5 x 10⁻⁶ K⁻¹, and a grain growth activation energy value 76 kJ/mol for x = 0.15. No grain growth was observed until sintering at 1073 K. It has been observed in literature that there is a dependence of the grain size growth in relation with the doping-RE³⁺ concentration [7]. However, no dependence of the size was observed as a function of Tm³⁺ content.

The photoluminescence spectra show the large crystal field splitting characteristic of sesquioxides. We have observed that the ³H₄ and ³F₄ luminescence decays after short pulse excitation at 800 nm with low enough Tm³⁺ concentration exhibit non exponential kinetics, which can be analytically reproduced by the sum of two exponential regimes. The shortest one would correspond to the emission of Tm³⁺ ions at the surface of the nanoparticles and the longest one to Tm³⁺ ions in the body of the nanoparticles, which in principal should approach to the value obtained in Tm-doped Lu₂O₃ bulk single crystals. The fast and slow decay components decrease with increasing Tm³⁺ concentration.

Cathodoluminescent properties of the thulium doped nanocrystals have been investigated. The blue emission of the thulium doped nanocrystals had a CIE chromaticity coordinates of x=0.200, y=0.156 with a dominant wavelength of 468 nm. A color purity of 54% has been obtained in comparison with CIE Standard Illuminant C. The excitation voltage for cathodoluminescence measurement was 15 kV and the probe current 20 nA. Besides the major blue emission peak at 457 nm, a few minor peaks at 362, 724 and 812 nm were identified. (there are peaks at other positions, which are attributed to other lanthanide elements contamination.) These peaks are characteristic of transitions between electronic energy levels of Tm³⁺ ions. The major peak centered at 457 nm corresponds to the transition from

$^1G_4 \rightarrow ^3H_6$, while the transitions from $^1D_2 \rightarrow ^3H_6$, $^1G_4 \rightarrow ^3F_4$, and $^1G_4 \rightarrow ^3H_5$ of the Tm^{3+} ion are related to the emission peaks at 364, 680 and 813 nm, respectively.

References

- [1] A. Ikesue, Y. Lin Aung, Nature Photonic, 2, (2008) 721-727.
- [2] S. Shionoya, W.M. Yen, Phospor Handbook, CRC press, New York, (1997).
- [3] T. Yanagitani, H. Yagi, M. Ichikawa. Japanese Patent No. 10-101333 (1998).
- [4] T. Yanagitani, H. Yagi, Y. Yamasaki. Japanese Patent No. 10-101411 (1998).
- [5] J. A. Capobianco, F. Vetrone, J. C. Boyer, and M. Bettinelli, Opt. Mater., 19, (2002) 259–68.
- [6] L. Q. An, J. Zhang, M. Liu, S. W. Wang, J. Lumin. 122, (2007) 125-127.
- [7] A. Ikesue, I. Furusato, K. J. Kamata, J. Am. Ceram. Soc. 78, (1995) 225-228

Figures

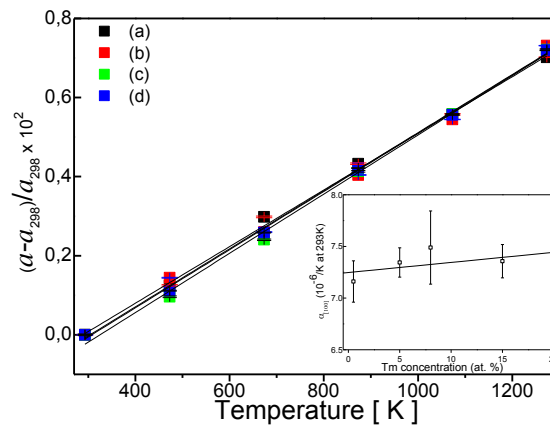


Fig. 1 Relative thermal evolution of the cell parameter a for $Tm:Lu_2O_3$ nanocrystals: (a) 0.5 at. %. (b) 5 at. %. (c) 8 at. %. (d) 15 at. %.

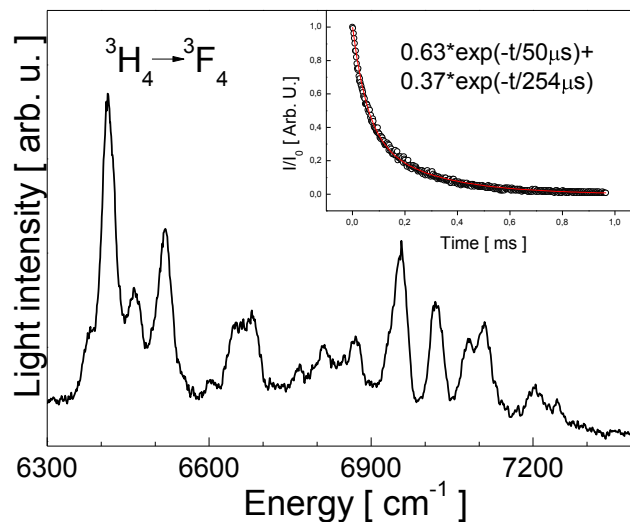


Fig. 2. 300 K $^3H_4 \rightarrow ^3F_4$ photoluminescence of 5 at. % Tm nanoparticles excited at $\lambda_{EXC} = 800$ nm. Inset: Photoluminescence intensity decay of this transition at 300 K recorded at $\lambda_{EMI} = 1558$ nm fitted with two exponential decays of the (I/I_0) vs t dependency.

1D Photonic Crystal for Solar Cell Applications

¹S. Domínguez, ¹J. Bravo, ¹O. García, ²M. Ezquer, ²M. J. Rodríguez and ²A. R. Lagunas

¹FideNa, C\ Tajonar S/N, Pamplona, 31006, Navarra

²CENER, Ciudad de la Innovación, nº7, Sarriguren, 31621, Navarra

Sagrario.dominguez@fidenas.es

Many efforts have been done to improve light trapping in solar cells by reducing the reflectance on the top surface [1-3]. Even though new technologies are coming up [4-6], silicon solar cells are the most widespread type of solar cell in the current market so improving their efficiency is still interesting. In this work, a very easy method to pattern 1D photonic crystals (PC) on silicon solar cells to improve the light trapping is presented.

Several PCs have been simulated using OptiFDTD software with the objective of choosing the best structure to reduce the reflectance at the silicon surface. To minimize the number of simulations, a Design of Experiments (DOE) technique has been used to study the relationship between the reflectance of the surface and the PC's dimensions (p , a , h). With DOE, three sorts of structures have been studied obtaining the optimum dimensions for each kind of PC. A diagram of the different PC studied is shown in Fig.1. Simulations have concluded that rectangular PCs have lower reflectance than the others types.

Several rectangular PCs have been fabricated with Laser Interference Lithography (LIL) and Reactive Ion Etching (RIE). LIL is a method to easily pattern large areas (in the range of 10cm diameter) with nano-gratings or nano-grids [7] on a photoresist. The tool used for this work is known as "Lloyd's Mirror" and uses the interference of a coherent laser beam. Images of fabricated PCs obtained with Scanning Electron Microscope (SEM) are shown in Fig.2a) and b). The reflectance of this fabricated PC has been measured with a spectrophotometer and compared with simulation results. One example is shown in Fig.3, where the good agreement between both data can be seen.

In summary, 1D PCs can be easily patterned in large areas to reduce the reflectance on silicon solar cells. The pattern could be done on others substrates, so this improvement could be applicable to others types of solar cells. Also, different structures could be done in the future with this method to reduce even more the reflectance.

References

- [1] C. Eisele, C. E. Nebel and M. Stutzmann, *Journal of Applied Physics* (2001) Vol. 89, No.12
- [2] H.Stiebig, N.Senoussaoui, T. Brammer and J. Müller, *Solar Energy Materials & Solar Cells* 90 (2006), 3031-3040
- [3]P. Bermel, C.Luo, L.Zeng, L.C.Kimerling and J.D.Joannopoulos, *Optics Express* (2007) Vol.15, No.25
- [4] D. Wei, *Dye Sensitized Solar Cells, Review* (2010)
- [5] I. Prieto, B. Galiana, P.A Postigo, C.Algora, L.J.Martínez, and I. Rey-Stolle, *Applied Physics Letters* 94, 191102-1 (2009)
- [6] S.B Mallick, M. Agrawal and P.Peumans, *Optics Express* (2010) Vol. 18, No.6
- [7] H Smith, *Physica E* 11 (2001) .104-109.

Figures

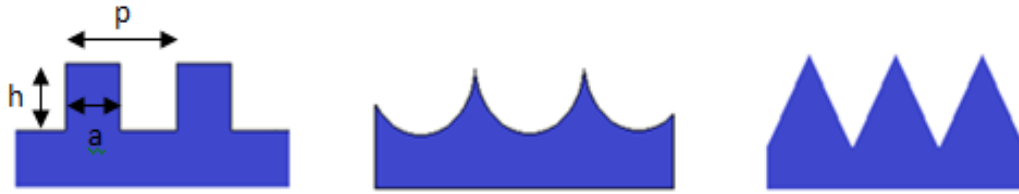


Fig.1 1D Types of PC studied.

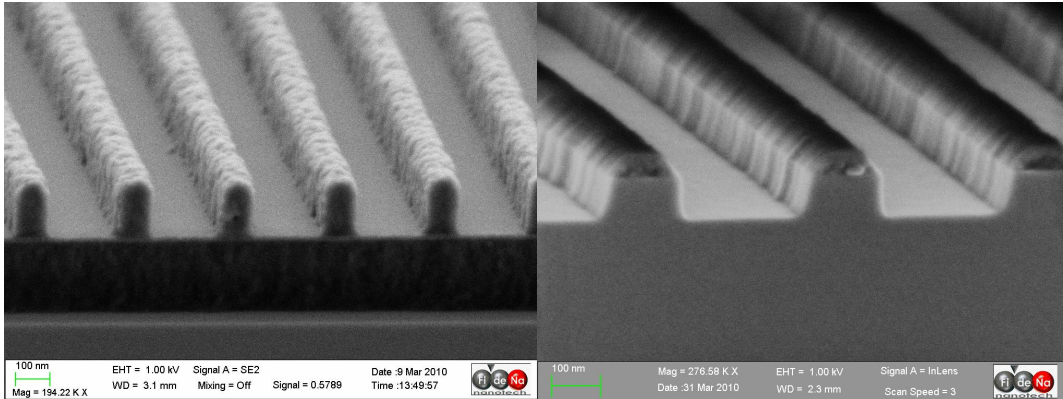


Fig.2 a) Pattern transferred to the photoresist on top of an anti-reflecting layer and the Si. b) Transference of the pattern to the Si of the substrate by RIE.

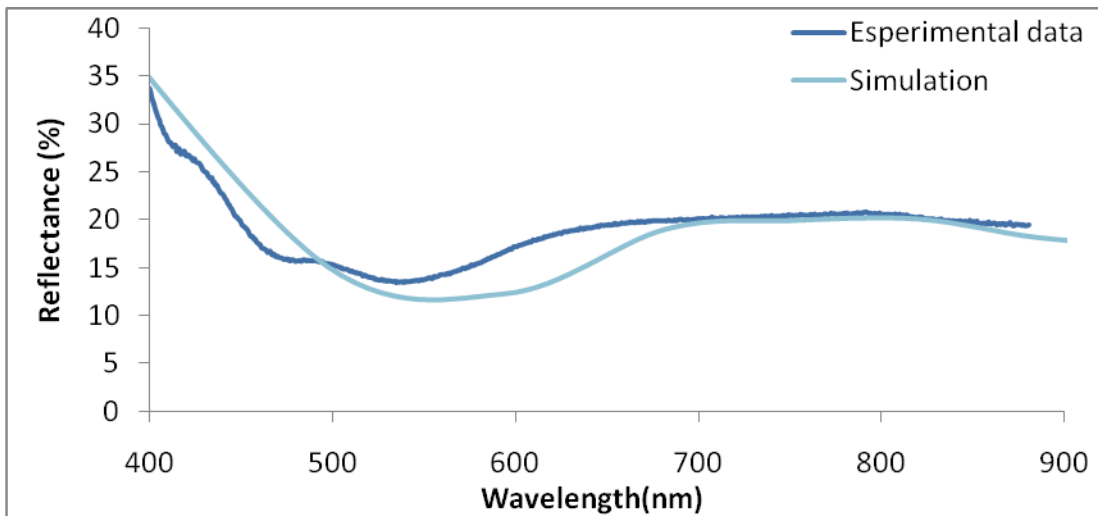


Fig.3. Comparison between simulation and experimental measurements for a rectangular PC.

Interplay between linear antenna modes and gap cavity modes within a single flat-gap nanoantenna

R. Esteban¹, A. Borissov² and J. Aizpurua¹

¹ Centro de Física de Materiales CSIC-UPV/EHU and Donostia International Physics Center
Paseo Manuel de Lardizabal 4 20018, Donostia-San Sebastián Spain

² Laboratoire des Collisions Atomiques et Moléculaires, CNRS-Université Paris-Sud
Bâtiment 351, 91405 Orsay FRANCE

ruben_esteban@ehu.es ; aizpurua@ehu.es

Linear wire antennas commonly used at radio frequencies¹ are very effective structures to scale antenna properties down to optical frequencies. A combination of metallic rods separated by a few nanometers, in so-called gap-antennas, produces strong near fields at the gap². Here we investigate the resonant behavior of such structures formed by flat interfaces at the gap and separation distances smaller than 1 nanometer. We perform electromagnetic simulations of the extinction and near-field properties of the flat-gap antennas using the boundary element method (BEM)³.

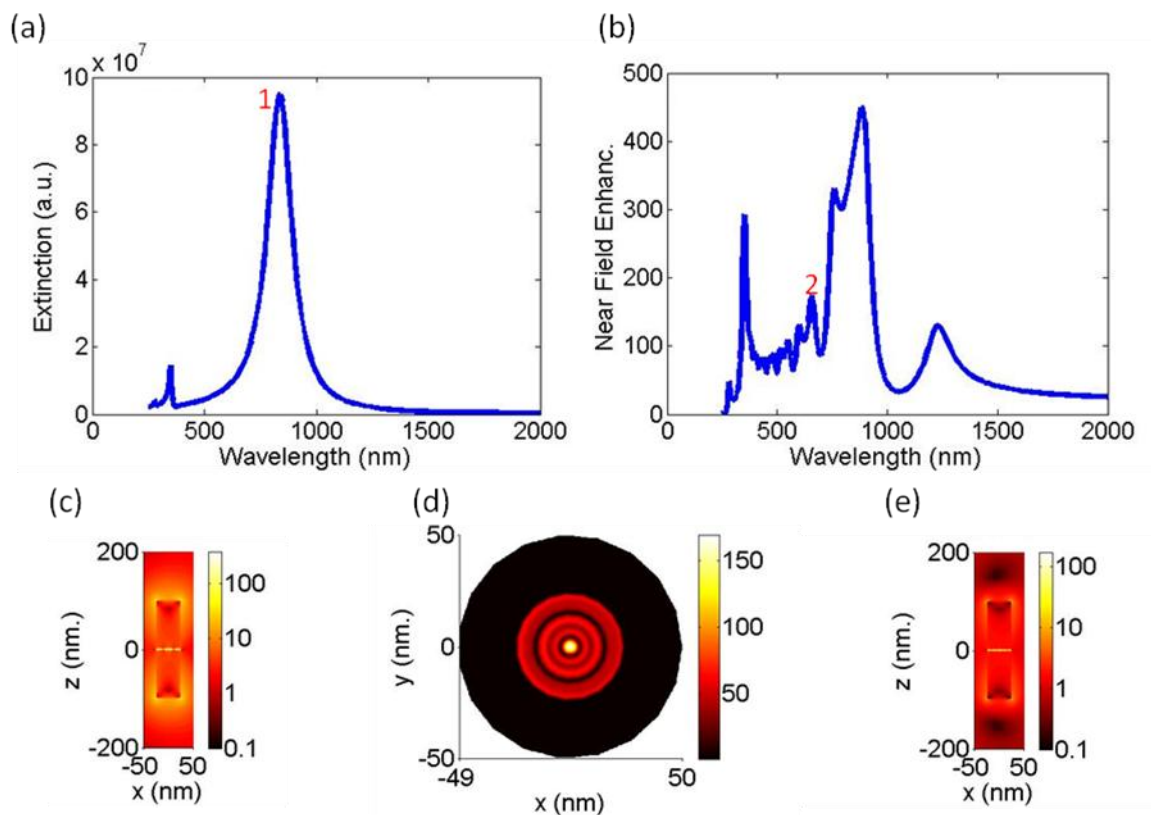
The extinction cross section is dominated by a clear maximum (Figure 1a) of dipolar nature, as revealed by the distribution of the near field (Figure 1c). Other weaker peaks appear at shorter wavelengths. As expected from previous work, decreasing the gap down to distances of a few nanometer results in a clear redshift of the dipolar peak. However, in contrast to previous work for metallic spheres⁴, we find a saturation of the redshift for distances smaller than approximately one nanometer. Similarly, the strength of the different extinction maxima also saturates. We connect this distinctive behavior with the dimensionality of the antenna flat-gap that allows the formation of a new set of very localized cavity modes.

The spectral behavior of the near fields at the gap center present a more complex structure, with numerous peaks as illustrated in Figure 1b. Both the position and strength of the maximum field enhancement show a non-trivial dependence with separation distance. We interpret our results in terms of the coexistence of two different sets of resonant plasmonic modes. The maxima in the extinction cross section correspond to charge oscillations along the antenna axis, in analogy to the behavior of classical wire antennas at radio frequencies. Nevertheless we notice that at optical frequencies one needs to consider the excitation of plasmons⁵ and how they are influenced by the gap. The spectral behavior of the near fields at the gap show considerably more peaks than the extinction, which we explain by the excitation of the second set of modes, associated to the gap. Such gaps can be seen as metal insulator metal structures supporting cavity modes⁶ in the horizontal direction, i.e. perpendicular to the antenna axis. These plasmonic modes have no equivalence in classical antenna theory. The interplay between the two different types of modes helps to explain not only the nature of the different peaks, but also their strength: stronger near fields are observed when modes along the rod axis and horizontal cavity modes in the gap coincide in their spectral positions.

Perspectives for future work include the use of experimental dielectric constants, instead of a Drude description as presented here, and the consideration of quantum effects for the smallest separation distances at the gap [7].

References

- [1] C. A. Balanis, Antenna theory and design, third edition (John Wiley & Sons, 2005).
- [2] P. Mülschlegel, H.-J. Eisler, O. J. F. Martin, B. Hecht and D. W. Pohl, Science, **308** (2005) 1607.
- [3] F. J. García de Abajo and A. Howie, Physical Review B, **65** (2002), 115418
- [4] I. Romero, J. Aizpurua, G. W. Bryant and F. J. García de Abajo, Optics Express , **14** (2006) 9988.
- [5] L. Novotny, Physical Review Letters **98** (2007) 266802.
- [6] R. Esteban, T. V. Teperik and J. J. Greffet, Physical Review Letters **104** (2010) 026802.
- [7] J. Zuloaga, E. Prodan and P. Nordlander, Nano Letters, **9** (2009) 887.



Figures 1: (a) Extinction spectra and (b) near field enhancement at the gap center, for a gap of 4 atomic units. (c) Near fields in a vertical plane for the resonance marked 1 in (a). (d,e) Near fields in a vertical (e) and an horizontal (d) plane for the resonance marked 2 in (b). Notice how the near-field spectrum in (b) peaks up at the position of the extinction maxima (a).

Transverse magneto-optical effects in Fe antidot arrays

J. F. Torrado¹, E. Th. Papaioannou², G. Ctistis³, P. Patoka⁴, M. Giersig⁴, G. Armelles¹ and A. Garcia-Martin¹

¹*Instituto de Microelectrónica de Madrid (IMM-CNM-CSIC),
Isaac Newton 8, Tres Cantos, 28770 Madrid, Spain*

²*Department of Physics and Astronomy, Uppsala University, 75121 Uppsala, Sweden*

³*Complex Photonic Systems (COPS), MESA+ Institute for Nanotechnology, University of Twente, The Netherlands*

⁴*Helmholtz-Zentrum Berlin für Materialien und Energie GmbH, 14109 Berlin, Germany
jforrado@imm.cnm.csic.es*

During the last decade, an increasing interest has been devoted to the analysis of the interplay between plasmon resonances and magneto-optical (MO) effects [1], since the plasmon resonances can be used to enhance the MO response [2-4] and the MO effect can be used to control the plasmon propagation [5].

A great number of the studies of the MO enhancement due to plasmon excitation have been carried out in the so-called Polar Kerr configuration for MO active nanostructures (either dots or antidots) [2] or when metal nanostructures have been put into contact with continuous films of MO active material [3]. However, in the Transverse Kerr configuration the studies focus on metallic nanostructures over continuous films [4].

Here we will cover that gap and study the Transverse Kerr Magneto-Optical Effect (TMOKE) of iron hexagonally perforated films (470nm pitch, 100nm thickness and radii of 248nm and 297nm respectively). We observe a large enhancement of the TMOKE signal with respect to that of the continuous film, and relate that frequencies to the possibility of surface plasmon excitations. We will also analyze their dependence on the hole radius and compare the results to a continuous iron film of same thickness.

Apart from the orientation of the magnetic field the TMOKE differs from the Polar configuration in the angle of incidence of the light beam: the Polar effect is studied at normal incidence, whereas the TMOKE needs to be off normal, since the signal is zero otherwise. This means that when the nanostructuring is realized in a periodic fashion (see Fig. 1) there is an additional parameter to take into account: the azimuth (in-plane) angle. We will thus also analyze the TMOKE enhancement as a function of the crystal orientation of the sample plane with respect to the incident light beam as shown in the experimental TMOKE spectra in Fig 1.

References:

- [1] G. Armelles, *et al.*, J. Opt. A: Pure Appl. Opt. **11** (2009) 114023.
- [2] J.B. González-Díaz, *et al.*, Adv. Mater. **19**, (2007) 2643; Small **4**, (2008) 202; G. Ctistis *et al.*, Nano Lett. **9**, (2009) 1; J.B. González-Díaz, *et al.*, Appl. Phys. Lett. **94**, (2009) 263101; E.Th. Papaioannou, *et al.*, Phys. Rev B *in press* (2010).
- [3] A.B. Khanikaev, *et al.*, Opt. Express **15**, (2007) 6612; V. I. Belotelov, *et al.*, Phys. Rev. Lett. **98**, (2007) 077401; G.A. Wurtz, *et al.*, New J. of Phys. **10** (2008) 105012; G.Armelles, *et al.*, Opt. Express **16**, (2008) 16104.
- [4] V.I. Belotelov, *et al.*, J. Opt. Soc. Am. B, **26** (2009) 1594; J.F. Torrado, *et al.*, submitted (2010).
- [5] J.B. González-Díaz, *et al.* Phys. Rev. B. **76**, (2007) 153402; E. Ferreiro-Vila, *et al.*, Phys. Rev. B **80**, (2009) 125132; V.V. Temnov, *et al.* Nature Photonics **4**, (2010) 107.

Figures:

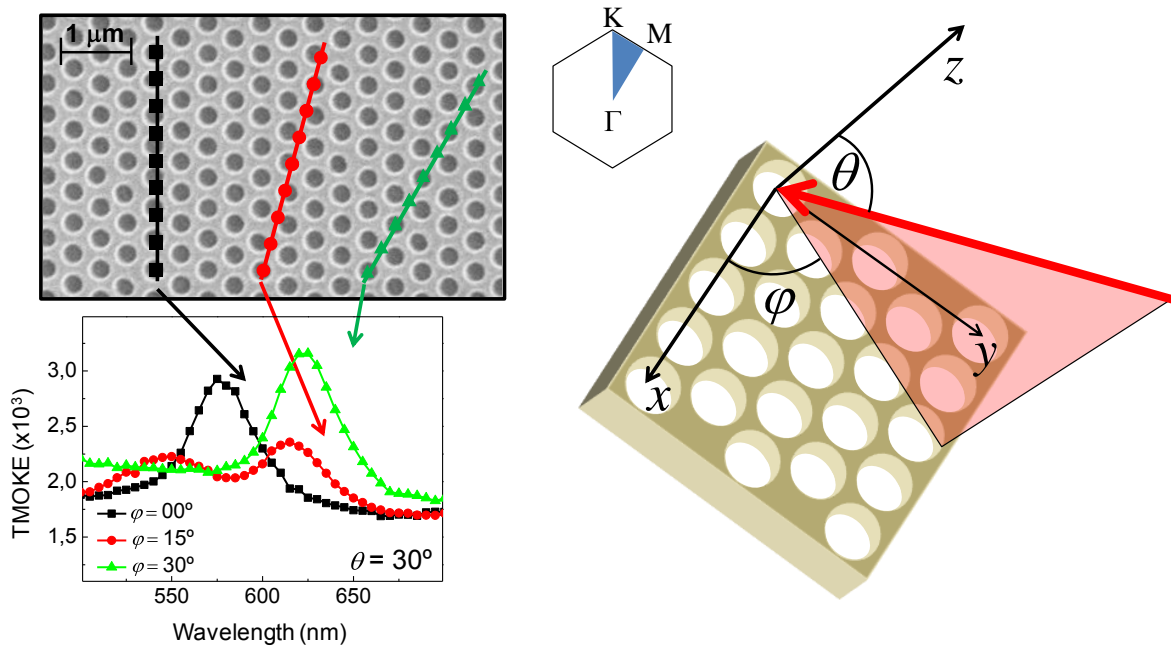


Fig. 1: Scanning Electron Micrograph of the Fe antidot array and a sketch showing the geometry and the first Brillouin zone of the in-plane lattice structure. Three characteristic TMOKE spectra obtained at different azimuth angles ($\theta=30$ deg) showing the dependence of the TMOKE signal on the relative orientation of the impinging beam and the 2-D crystallographic high symmetry axis.

FDTD study of quasi-random photonic structures obtained by electrochemical etching

Josep Ferré-Borrull¹, Mohammad Mahbubur Rahman¹, Ivan Maksymov², Lluís F. Marsal¹, and Josep Pallarès¹

(1) Departament d'Enginyeria Electrònica, Elèctrica i Automàtica

Universitat Rovira i Virgili Avda. Països Catalans 26, 43007 Tarragona, Spain

(2) Kharkov National University of Radio Electronics, 14 Lenina Ave., 61166, Kharkov, Ukraine

lluis.marsal@urv.cat

1. Introduction

Photonic crystals are structures with very relevant properties that come up from the periodic structuring at the wavelength scale[1, 2]. In this sense, they are not crystals in the sense of molecular crystals, but metacrystals with photonic properties beyond those of their constituent materials. On this basis, many new materials have been studied and applied in photonics, for instance metamaterials achieve negative refractive index with the proper periodic combination of the metallic and dielectric components[3]. There exist however, non-periodic structures with remarkable photonic properties based on their geometrical characteristics: quasicrystals may show complete photonic band gaps with lower refractive index contrast than their periodic counterparts because of their higher rotational symmetry[4], random photonic structures take advantage of Anderson localization to achieve random lasers[5].

In this communication we report on the investigation on a different kind of structures: random structures obtained by electrochemical etching. More concisely, we study macroporous silicon and nanoporous anodic alumina structures. Photonic crystals based on macroporous silicon are usually obtained by electrochemical etching after a previous lithography to define the periodic pattern. If this first step is omitted, the macropores grow randomly on Si but with a certain degree of order, giving rise to properties in-between those of the periodic and of the random structures. Nanoporous anodic alumina[6,7] is a material widely investigated and applied in nanotechnology[8]. It is obtained by the electrochemical etching of aluminium and, under the adequate conditions, the porous structure shows a self-ordered lattice with a two-dimensional triangular periodic arrangement[6,7]. The lattice constant can be tuned from some tens of nanometres up to some hundreds. Although this triangular arrangement can be achieved over a long range if a pre patterning on the aluminium surface is applied[9], in the absence of such preprocessing the regular triangular arrangement is broken into domains with a size of some tens of lattice sites and randomly oriented. Fig. 1 shows an example of each of the structures. Fig. 1a) corresponds to the surface of a random macroporous silicon sample, while Figs. 1b) and 1c) correspond to a nanoporous alumina structure.

A certain degree of order can be appreciated in the figures, for both structures. In this work we will study the photonic properties of such structures by means of FDTD calculations, and in particular, the existence of photonic pseudo-gaps and Anderson localization.

2. Results and discussion

As an example of the results obtained so far, Fig. 2 shows the result of the calculation of transmittance on a selected substructure of the nanoporous anodic alumina structure. The calculations have been performed by choosing a substructure of the structure in Fig. 1b) with a definite size and computing with the help of FDTD the transmission of a plane wave with a Gaussian frequency spectrum through the substructure. The chosen substructure is previously idealized by locating the positions of the pores by means of standard image processing techniques and by replacing such pores by ideal circular holes. The transmission spectrum through the structures is then normalized to the spectrum of the propagation in free-space of the same Gaussian beam. The spectra in Fig. 2 correspond to the average of 20 spectra corresponding to 20 substructures at different sites on the sample. The plots correspond to increasing sizes of the subset, as indicated in the caption. The graphs show also the standard deviation of the transmittance for the set of substructures.

These spectra show that, with increasing size of the sample subset, a minimum in the transmission, that can be denominated as a pseudo-gap, appears around the normalized frequency $\omega a/2\pi c=0.42$. Table 1 summarizes the pseudo-gap parameters for the different substructure sizes. This pseudo-gap appears in the frequency range corresponding to a characteristic distance of the same order of the average interpore distance in the sample. The widening of the low transmittance region indicates that, as the thickness of the structure increases, the photonic band gap effect becomes more intense.

3.- References

- [1] E. Yablonovitch, Phys.Rev.Lett. **58**, 2059 (1987).
- [2] S. John, Phys. Rev. Lett. **58**, 2486 (1987).
- [3] J. B. Pendry, D. Schurig, D. R. Smith, Science **312**, 1780 (2006).
- [4] M. E. Zoorob, M. D. B. Charlton, G. J. Parker, J. J. Baumberg, M. C. Netti, Nature **404**, 740 (2000).
- [5] H. Cao, Y. G. Zhao, S. T. Ho, E. W. Seelig, Q. H. Wang, R.P.H. Chang, Phys. Rev. Lett **82**, 2278 (1999).
- [6] A. Birner, U. Gruning, S. Ottow, A. Schneider, F. Muller, V.Lehmann, H. Foll, U. Gosele, Phys. Status Solidi A: Appl. Res. **165**, 111 (1998).
- [7] L.F. Marsal, L. Vojkuvka, P. Formentin, J. Pallares, J. Ferre-Borrull, Opt. Mat. **31**, 860 (2009).
- [8] D. J. Bergman, M. I. Stockman, Phys. Rev. Lett. **90**, 027402 (2003).
- [9] Choi, R. B. Wehrspohn RB, Gosele U, Electrochimica Acta **50**, 2591 (2005).

4. Acknowledgements

This work was supported by Spanish Ministry of Ciencia e Innovacion (MICINN) under grant number TEC2009-09551, HOPE CSD2007-00007 (Consolider-Ingenio 2010) and AECID-A/024560/09.

Figures and tables

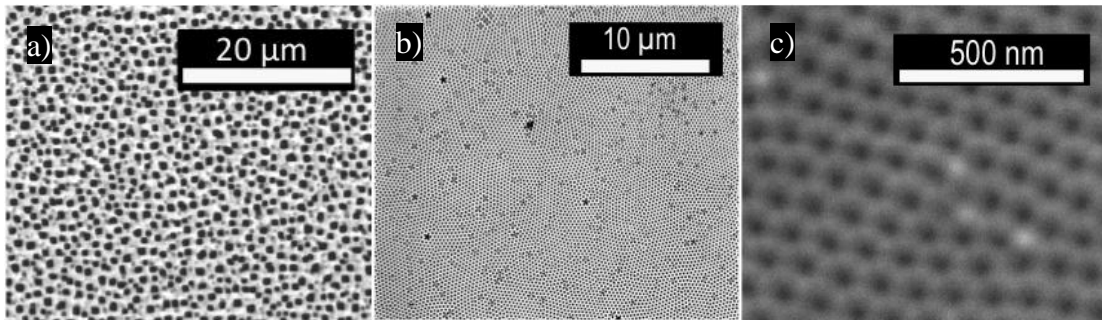


Figure 1. a) SEM micrograph of the surface of a random macroporous Si sample, b) SEM micrograph of a nanoporous anodic alumina sample where the local ordering and the breaking into domains can be appreciated, and c) magnified view of the nanoporous anodic alumina where the triangular arrangement of the pores and some dislocation points are illustrated.

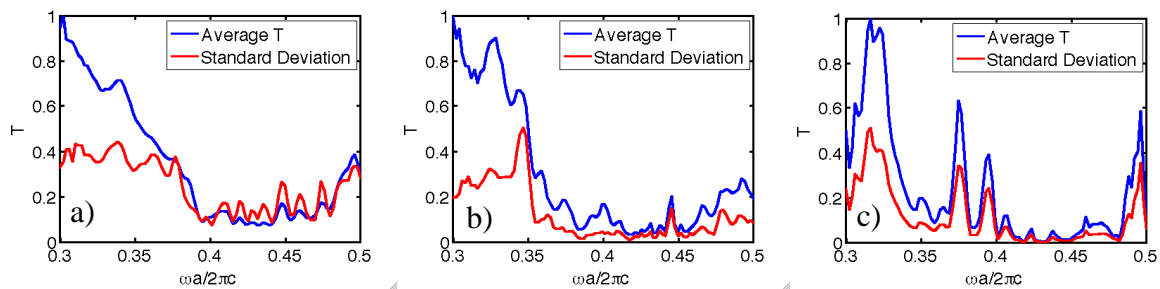


Figure 2. Average transmittance and standard deviation of the transmittance for the set of substructures considered for a defined substructure size. a) $5.1 \mu\text{m} \times 5.1 \mu\text{m}$, b) $6.3 \mu\text{m} \times 6.3 \mu\text{m}$ and c) $7.6 \mu\text{m} \times 7.6 \mu\text{m}$.

Substructure Size ($\mu\text{m} \times \mu\text{m}$)	Pseudo-gap lower limit ($\omega a/2\pi c$)	Pseudo-gap upper limit ($\omega a/2\pi c$)	Pseudo-gap width ($\omega a/2\pi c$)
5.1×5.1	0.41	0.44	0.03
6.3×6.3	0.40	0.44	0.04
7.6×7.6	0.41	0.46	0.05

Table 1. Pseudo-gap limits and pseudo-gap width for the different subset sizes for the TE polarization. The pseudo-gap is estimated by the largest continuous range with transmittance below 0.1.

Enhanced optical gain in photonic crystals

R. Sapienza¹, M. Leonetti^{2,3}, **L. S. Froufe-Pérez**², J. Galisteo-López², C. Conti⁴, and C. López².

¹ICFO - Institut de Ciències Fotòniques. Parc Mediterrani de la Tecnologia, Castelldefels 08860 Barcelona, Spain.

²Instituto de Ciencia de Materiales de Madrid (CSIC) and Unidad Asociada CSIC-UVigo, Cantoblanco, 28049 Madrid, Spain.

³Dipartimento di Fisica, Università di Roma La Sapienza, I-00185, Roma, Italy. ⁴Research Center INFM-CNR, c/o Università di Roma Sapienza, I-00185, Roma Italy.

luis.froufe@icmm.csic.es

We present the measurement of gain length in photonic crystals doped with laser dye. A gain enhancement is experimentally observed for light propagating along the Γ -K symmetry direction in reciprocal space, while a strong inhibition is measured for directions characterized by a lower degree of crystal symmetry. These results are theoretically explained by comparing the optical gain to the calculated density of states along the crystal directions.

We find a six-fold increase of the gain in opal photonic crystal, as compared to the homogeneous film, and a more than 20-fold variation between Γ -K and less symmetrical directions, in the same photonic crystal. This enhancement is due to a large increase of the density of the available modes around the Γ -K direction. Large variation of the gain in photonic crystal show the impact of the tailored density of states on light generation and amplification and open the way to enhancement of other phenomena like non-linear wave mixing and harmonic generation. Our result show how nanostructured media could be at the basis of the development of novel lasing sources with exceptional tunability, directionality and efficiency while being plastic photonics CMOS compatible, and candidates for in-board interconnections for future generation computers

Size Evolution of the Fröhlich Resonance for Magnetic Nanoparticles

Braulio García-Cámara, Francisco González and Fernando Moreno

Grupo de Óptica. Departamento de Física Aplicada. Universidad de Cantabria, Avda de los Castros s/n
39005, Santander (SPAIN)
garcia.cb@unican.es

Size effects on the dipolar plasmon resonance of small metallic particles were studied several years ago [1]. It is well known that for a spherical particle in the quasi-static limit (size $\rightarrow 0$), the electric plasmon resonance, also called “Fröhlich resonance”, appears at $\varepsilon = -2\varepsilon_m$, ε and ε_m being the electric permittivity of the particle and the surrounding medium, respectively. However, for finite size particles but still smaller than the incident wavelength, the plasmon mode is slightly shifted to the red part of the spectrum and follows the relation

$$\varepsilon = -\left(2 + \frac{12}{5}x^2\right)\varepsilon_m \quad (1)$$

where $x = kR = \left(\frac{2\pi}{\lambda}R\right)$ is the size parameter, R is the radius of the particle, k the wavenumber and λ the incident wavelength.

This theoretical result was obtained for particles that only have electric properties ($\mu=1$). However, the new engineered materials, known as *metamaterials* [2], are providing us with structures (from micro to nano scales) [3, 4] that respond to both the electric and the magnetic part of the incident field. Recent studies have extended this kind of materials from microwaves to the visible part of the spectrum, with the appearance of new phenomena like the negative refraction [5]. Also, metamaterials force us to generalize the well-known scattering theories by considering diffusers with electric and magnetic properties [6]. In particular, we have devoted this work to the analysis of the dipolar plasmon resonance, “the Fröhlich resonance”, for scatterers with unconventional optical properties.

Although metamaterials are internally structured or present complex geometries [7], when λ is long enough compared with their inner structures, we can model them as spherical particles with given size and effective optical properties [8]. In this sense, we have considered the diffuser system as a single spherical nanoparticle with ε and μ different from 1. In Fig. 1, we show the evolution of the electric permittivity for which the electric plasmon resonance is excited ($\varepsilon_{\text{resonant}}$) as a function of both the particle size and the magnetic permeability. It can be seen that if the particle size approaches zero, the resonant permittivity is located at $\varepsilon = -2$ (supposed $\varepsilon_m = 1$). If $\mu = 1$ (Fig. 1a), as R changes the section of the curve can be described with Eq. (1). However, for $\mu \neq 1$ the behavior becomes more complex. Also, if we consider negative values for the magnetic permeability (Fig. 1b), the size evolution of the resonance is even more complex than the positive case. In order to explain these new features, we have made a detailed analysis of the first Mie coefficient, a_1 (which produces the plasmon resonance), obtaining the equivalent relation to Eq.(1) but including the magnetic contribution. Finally, by means of the ε - μ symmetry that present the two first Mie coefficients [1], the results for the electric plasmon resonance, due to maximum values of a_1 , can be extended to the magnetic plasmon mode (maximum values of b_1).

References

- [1] C. F. Bohren and D. R. Huffman, *Absorption and Scattering of Light by Small Particles* (Wiley, New York, 1983).
- [2] A.K. Shalichev and V. M. Shalaev, *Electrodynamics of Metamaterials* (World Scientific, Singapore, 2007).
- [3] E. Ekmekci, K. Topalli, T. Akin and G. Turhan-Sayan, “A tunable multi-band metamaterial design using micro-split SRR structures”, *Opt. Express* **17**(18), 16046-16058 (2009)
- [4] J. K. Gansel, M. Thiel, M. S. Rill, M. Decker, K. Bade, V. Saile, G. von Freymann, S. Linden and M. Wegener, “Gold helix photonic metamaterials as broadband circular polarizer”, *Science* **325**, 1513-1515 (2009).
- [5] O. Hess, “Optics: Farewell to Flatland”, *Nature* **455**, 299-300 (2009).
- [6] B. García-Cámara, F. Moreno, F. González, J.M. Saiz and G. Videen, “Light scattering resonances in small particles with electric and magnetic properties”, *J. Opt. Soc. Am. A* **25**, 327-334 (2008).

[7] N. A. Mirin and N.J. Halas, "Light-bending nanoparticles", *Nano Lett.* **9**, 1255-1259 (2009).

[8] D.R. Smith, S. Schultz, P. Markos and C.M. Soukoulis, "Determination of effective permittivity and permeability of metamaterials from reflection and transmission coefficients" *Phys. Rev. B* **65**, 195104 (2002).

Figures

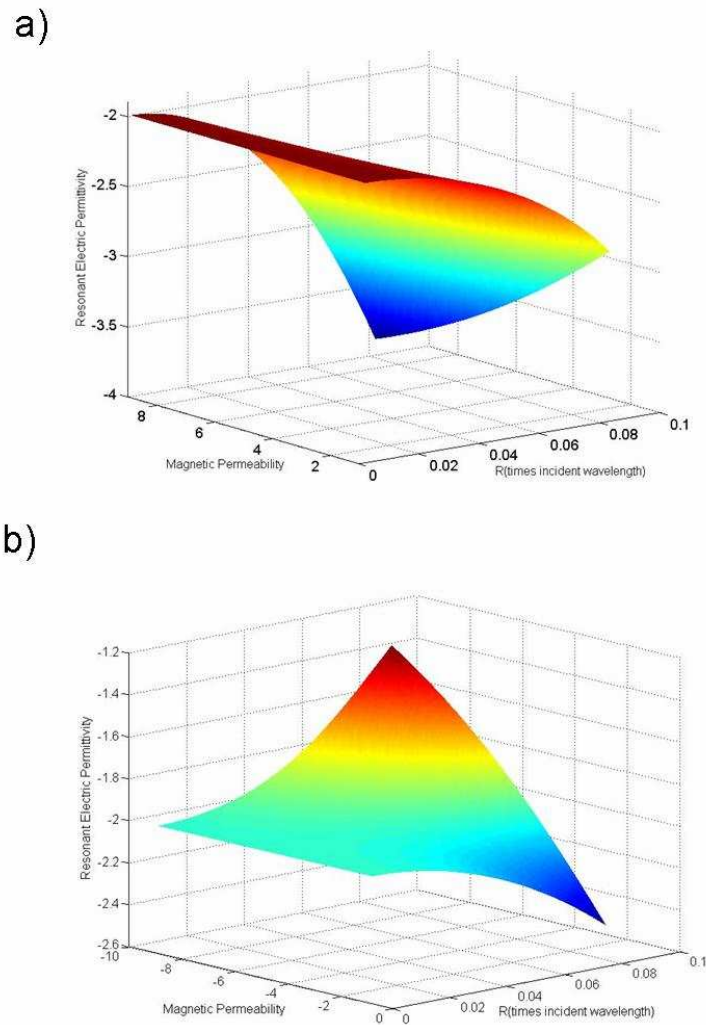


Fig. 1. 3D plot of the evolution of the resonant electric permittivity ($\epsilon_{\text{resonant}}$) for a spherical small particle as a function of the particle size (R) and the magnetic permeability (μ). μ has been considered either positive (a) or negative (b).

Acknowledgements

This research has been supported by the Ministry of Science and Innovation of Spain under the project FIS2007-60158. Braulio García-Cámara wants to thank to the University of Cantabria for his Ph.D. grant.

Dual Core Antiguide (DCA): A new platform for active - passive photonic integration.

Oscar Garcia-Lopez, Marko Galarza, Candido Aramburu, and Manuel Lopez-Amo

FideNa, Centro de I+D "Jerónimo de Ayanz", Campus de Arrosadía, C/Tajonar s/n, 31006 Pamplona, Spain

Departamento de Ingeniería Eléctrica y Electrónica, Universidad Pública de Navarra, 31006 Pamplona, Spain

oscar.garcia@fiden.es

In this poster we present a new platform for simple fabrication of monolithic photonic integration based on a vertically displaced waveguides for active and passive devices. Light is transferred between the waveguides via very low loss vertical resonant coupler to allow very compact and efficient active-passive power transference.

The most important feature of this platform is the upper core quasi guided mode that we call DCA mode. DCA mode presents a very atypical behavior in bends. The leakage loss has a resonant behavior when the radius of curvature is modified.

The use of DCA technology would make it possible to fabricate microring resonator devices without the requirements of wafer bonding or regrowth technology. This way, DCA technology would make it possible to produce microring laser anywhere in the chip.

References

[1] Fengnian Xia, Vinod M. Menon, Member, IEEE, and Stephen R. Forrest, Fellow, IEEE, "Photonic Integration Using Asymmetric Twin-Waveguide (ATG) Technology: Part I—Concepts and Theory", IEEE Journal Of Selected Topics In Quantum Electronics, Vol. 11, No. 1, January/February 2005

[2] Vinod M. Menon, Fengnian Xia, and Stephen R. Forrest, "Photonic Integration Using Asymmetric Twin-Waveguide (ATG) Technology: Part II—Devices", IEEE Journal Of Selected Topics In Quantum Electronics, Vol. 11, No. 1, January/February 2005

[3] Suematsu Y et al., "Integrated Twin-Guide AlGaAs Laser with Multiheterostructure", IEEE Journal of Quantum Electronics, 1975

Figures

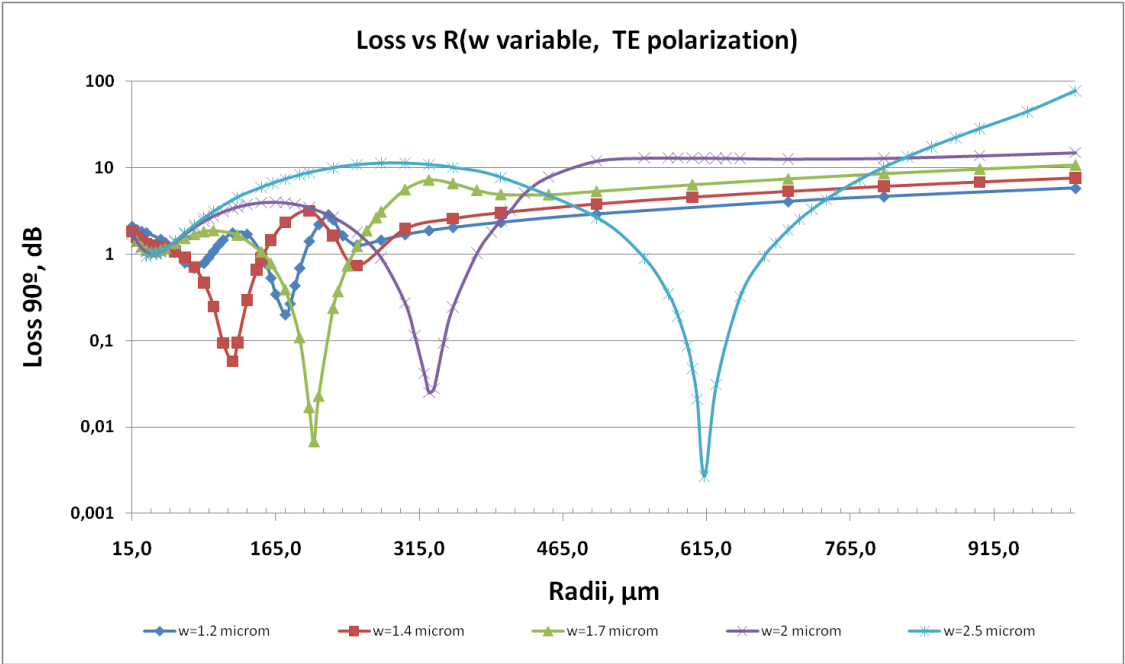


Figure 1 - DCA bend losses as a function of radius and for different waveguide widths. Antiresonant reflecting resonances are observed.

Radiative corrections to the polarizability tensor of an electrically small anisotropic dielectric particle

R. Gómez-Medina¹, S. Albaladejo², L. S. Froufe-Pérez¹, H. Marinchio³, R. Carminati³, J. F. Torrado⁴, G. Armelles⁴, A. García-Martín⁴ and J. J. Sáenz²

¹ Instituto de Ciencia de Materiales de Madrid, C.S.I.C.,
Campus de Cantoblanco, 28049 Madrid, Spain

² Departamento de Física de la Materia Condensada, Universidad Autónoma de Madrid,
Campus de Cantoblanco, 28049 Madrid, Spain

³ Institut Langevin, ESPCI ParisTech, CNRS UMR 7587, Lab. d'Optique Physique,
10 rue Vauquelin, 75231 Paris Cedex 05, France

⁴ Instituto de Microelectrónica de Madrid, C.S.I.C.,
Isaac Newton 8, Tres Cantos, 28760 Madrid, Spain
rgomezmedina@icmm.csic.es

Electromagnetic scattering from nanometer-scale objects has long been a topic of large interest and relevance to fields from astrophysics or meteorology to biophysics and material science [1]. During the last decade nano-optics has developed itself as a very active field within the nanotechnology community. Much of it has to do with plasmon (propagating) based subwavelength optics and applications [2]. Also, isolated metallic particles supporting localized plasmons have attracted a great deal of interest due to their ability to concentrate the electromagnetic field in subwavelength (some tens of nanometers) volumes. As a result, the studies in the field often involve the contributions of small elements or particles where the dipole approximation may be sufficient to describe the optical response. Examples of applications are on telecommunications [3], spontaneous emission rates and fluorescence [4], sensors [5], energy harvesting [6], optical forces and trapping [7] or medical therapy [8]. The capabilities and applicability of all these promising examples can be largely enhanced if some degree of tunability is added. These capacities can be endorsed by exploiting different x-optic effect (thermo-, electro-, magneto-, piezo-) where an external agent modifies some elements of the dielectric tensor, ϵ , in some extent [9] which, in general, will be non-diagonal. Most of the previous works on small anisotropic spherical particles, consider the dipolar approximation (DA) in the electrostatic limit [10]. By taking into account the fact that the polarization within the sphere is uniform, the polarizability is usually written as

$$\alpha_0 \equiv 3v(\epsilon - \epsilon_h \vec{I})(\epsilon + 2\epsilon_h \vec{I})^{-1} \quad (1)$$

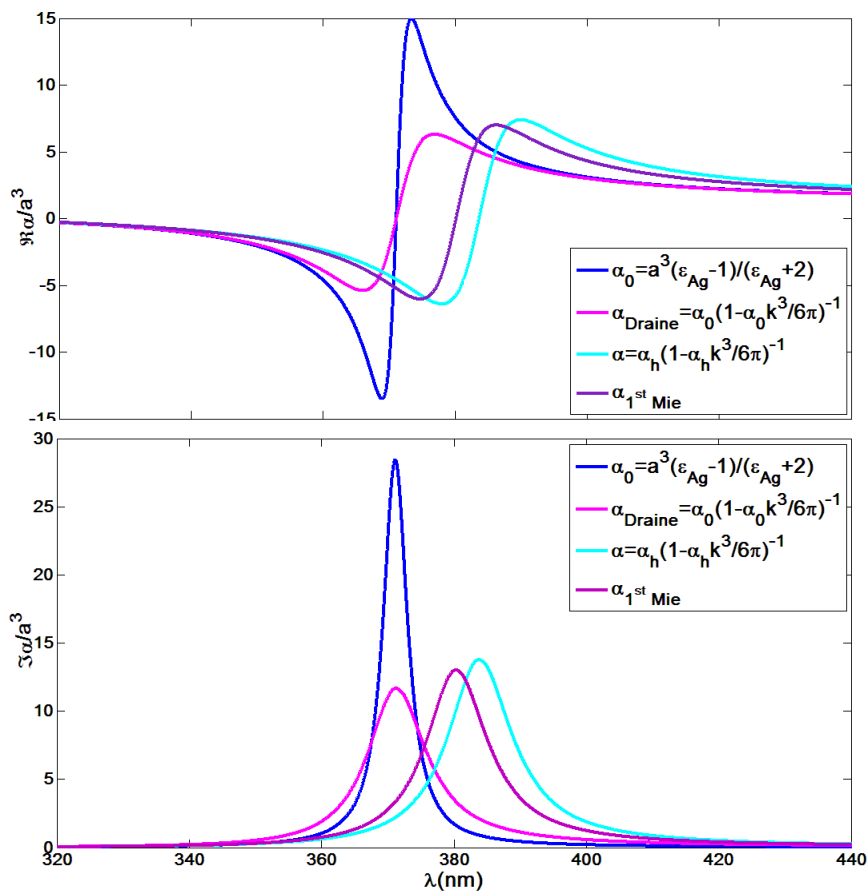
being $v=4\pi a^3/3$ the particle and ϵ_h the relative permittivity of the host medium at the point where the particle is placed. The host medium is assumed to be isotropic. Different extensions, including anisotropic and bianisotropic nonspherical particles, have been considered in the literature.

However, in most of the cases, the energy balance between absorption and scattering has not been considered. In particular, in absence of absorption, the polarizability tensor given by Eq. (1) does not fulfill the Optical Theorem. For isotropic particles (where the polarizability is a scalar quantity), radiative corrections to the electrostatic polarizability [1] solve the problem of energy conservation in absence of absorption. Even in the case of absorbing particles, extended radiative corrections have been shown to be relevant to determine the effective permittivity of metallic nanoparticle doped composites. However, these corrections have not been considered in the context of scattering from small anisotropic particles. In this work [11] we analyze the polarizability of small dielectrically anisotropic particles including radiative corrections. We describe the general properties of any polarizability tensor consistent with the Optical Theorem and we derive a generalized polarizability tensor equivalent to the extended polarizability tensor arising in the so-called "strong couple dipole method" (S-CDM). We show that, in absence of absorption, it is consistent with the optical theorem. These results are of general applicability. As an important application, we are going to restrict ourselves to the magneto-optical case, where the presence of a magnetic field alters some of the non-diagonal components of the dielectric tensor. Depending on the relative orientation of the sample, incidence plane and magnetic-field the affected elements will vary, conferring different effects. In the so-called "polar" configuration, where the magnetic field is applied perpendicular to the sample plane and parallel to the light incidence plane and the main effect is a rotation of the polarization state, it has been shown that the plasmon excitation largely modifies the rotation due to the strong enhancement and localization of the EM field. As we will show, the polarizability given by Eq. (1) wrongly predicts the absence of Kerr rotation for non-absorbing magneto-optical particles.

References

- [1] H. C. van de Hulst, *Light Scattering by small particles* (Dover, New York, 1981). C. F. Bohren and D. R. Huffman, *Absorption and Scattering of Light by Small Particles* (JohnWiley & Sons, New York, 1998). M. I. Mishchenko, L. D. Travis and A. A. Lacis, *Scattering, Absorption, and Emission of Light by Small Particles* (Cambridge Univ. Press, 2002). E. M. Purcell and C. R. Pennypacker, *Astrophys. J.* **186** (1973) 705. B. T. Draine, *Astrophys. J.* **333** (1988) 848. B. T. Draine and J. Goodman, *Astrophys. J.* **405** (1993) 685.
- [2] W. L. Barnes, A. Dereux, and T. W. Ebbesen, *Nature*, **424** (2003) 824.
- [3] J. Gómez Rivas, M. Kuttge, P. Haring Bolivar, H. Kurz, and J. A. Sánchez-Gil, *Phys. Rev. Lett.* **93** (2004) 256804. M. Sandtke and L. Kuipers, *Nature Photonics*, **1** (2007) 573. E. Moreno, S. G. Rodrigo, S. I. Bozhevolnyi, L. Martin-Moreno, and F. J. García-Vidal, *Phys. Rev. Lett.* **100** (2008) 023901.
- [4] R. Carminati, J. J. Greffet, C. Henkel and J. M. Vigoureux, *Opt. Commun.* **261** (2006) 368. L. S. Froufe-Pérez, R. Carminati and J. J. Sáenz, *Phys. Rev. A*, **76** (2007) 013835. M. Laroche, S. Albaladejo, R. Carminati and J. J. Sáenz, *Opt. Lett.* **32** (2007) 2762.
- [5] M. Spuch-Calvar, L. Rodríguez-Lorenzo, M. P. Morales, R. A. Álvarez-Puebla, L. M. Liz-Marzan, *J. Phys. Chem. C* **113** (2009) 3373.
- [6] V. E. Ferry, L. A. Sweatlock, D. Pacifici, and H. A. Atwater, *Nano Lett.* **8** (2008) 4391. D. M. Schaadt, B. Feng, and E. T. Yu, *Appl. Phys. Lett.* **86** (2005) 063106.
- [7] R. Gómez-Medina and J. J. Sáenz, *Phys. Rev. Lett.* **93** (2004) 243602. S. Albaladejo, M. I. Marques, M. Laroche, and J. J. Saenz, *Phys. Rev. Lett.* **102** (2009) 1136021. M. Righini, A. S. Zelenina, C. Girard, and R. Quidant, *Nature Phys.* **3** (2007) 477. M. Nieto-Vesperinas, J. J. Sáenz, R. Gómez-Medina and L. Chantada, *Opt. Express*, **18** (2010) 11428.
- [8] M.-R. Choi, K. J. Stanton-Maxey, J. K. Stanley, C. S. Levin, R. Bardhan, D. Akin, S. Badve, J. Sturgis, J. P. Robinson, R. Bashir, N. J. Halas, and S. E. Clare, *Nano Lett.* **7** (2007) 3759.
- [9] T. Nikolajsen, K. Leosson, and S. I. Bozhevolnyi, *Appl. Phys. Lett.* **85** (2004) 5833. J. B. Gonzalez-Diaz, A. García-Martin, G. Armelles, J. M. García-Martin, C. Clavero, A. Cebollada, R. A. Lukaszew, J. R. Skuza, D. P. Kumah, and R. Clarke, *Phys. Rev. B*, **76** (2007) 153402. M. J. Dicken, L. A. Sweatlock, D. Pacifici, H. J. Lezec, K. Bhattacharya, and H. A. Atwater, *Nano Lett.* **8** (2008) 4048.
- [10] D. Bedeaux and P. Mazur, *Physica*, **67** (1973) 23.
- [11] S. Albaladejo, R. Gómez-Medina, L. S. Froufe-Pérez, H. Marinchio, R. Carminati, J.F. Torrado, G. Armelles, A. García-Martin and J. J. Sáenz, *Opt. Express*, **18** (2010) 3556.

Figures



Normalized real and imaginary parts of electric polarizability in terms of the wavelength for a 25nm silver particle for different radiative corrections.

Transmission of light through arrays of holes in “optically” thin films

Sergio G. Rodrigo¹, A.Yu. Nikitin¹, F.J. García-Vidal² and L. Martín-Moreno¹

1 Instituto de Ciencia de Materiales de Aragón and Departamento de Física de la Materia Condensada, CSIC-Universidad de Zaragoza, E-50015 Zaragoza, Spain

2 Departamento de Física Teórica de la Materia Condensada, Universidad Autónoma de Madrid, E-28049 Madrid, Spain

sergut@unizar.es

Since the discovery of Extraordinary Optical Transmission (EOT) [1], through optically thick films drilled with arrays of square holes, numerous works have explored different parameter configurations of two-dimensional hole arrays (2DHAs) [2]. As regards to geometrical parameters, it has been found that the hole shape can strongly influence both the polarization properties and the intensity of the transmission. On the other hand, in the Ebbesen's configuration [1] the metal film is opaque. In this case, the EOT process involves surface modes at each side of the film which couple through the holes [3]. Note that continuous metal films (thin enough to be translucent), also present transmission resonances when periodically corrugated. In this configuration, resonant spectral features are related to the surface plasmon polaritons (SPPs) of the thin film, the so called Short Range SPPs (SRs) and Long Range SPPs (LRs) [4].

We present here a recent theoretical study on the optical transmission through square hole arrays drilled in optically thin films [5]. We study the effect of diminishing the film thickness, going from optically thick films to films as thin as approximately one “skin depth” (~20nm). The main finding is that EOT peaks are due to the excitation of SR resonances, therefore their spectral position depend strongly on both lattice parameter and metal thickness. On the contrary, LR do not appreciably contribute to transmission spectra. The figure below shows zero-order transmittance curves as a function of the film thickness, for a structure defined by the parameters given in the figure caption. As we can see in panel (b), both maxima and minima red-shift as the metal thickness decreases. We have also found transmission features appearing close to the SR plasmon polariton energies for small holes (not shown). Any relevant transmission feature seems to be related to the excitation of LR surface plasmons.

References

- [1] T. W. Ebbesen and H. L. Lezec and H. F. Ghaemi and T. Thio and P. A. Wolff, *Nature*, vol. 391, p. 667-669, 1998.
- [2] C. Genet and T. W. Ebbesen, *Nature*, vol. 445, p. 39-46, 2007.
- [3] L. Martín-Moreno and F. J. García-Vidal and H. J. Lezec and K. M. Pellerin and T. Thio and J. B. Pendry and T. W. Ebbesen, *Phys. Rev. Lett.*, vol. 86, p. 1114-1117, 2001.
- [4] E. N. Economou, *Phys. Rev.*, vol. 182, p. 539-554, 1969.
- [5] S. G. Rodrigo, L. Martín-Moreno, A. Y. Nikitin, A. V. Kats, I. S. Spevak, and F. J. García-Vidal, *Opt. Lett.* vol. 34, p. 4-6 2009.

Figures

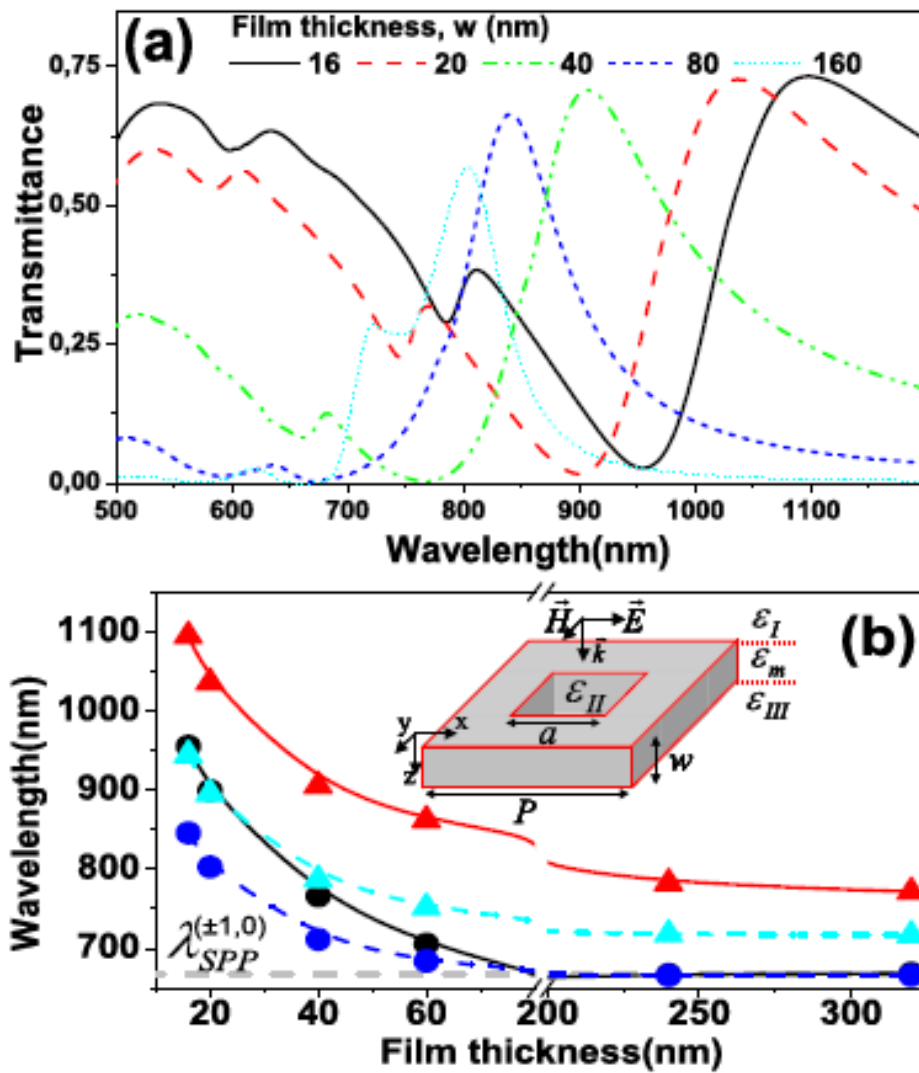


Figure: (a) Zero-order transmittance through 2DHAs in gold, as a function of the film thickness ($P=400\text{nm}$, $a=160\text{nm}$). The whole system is embedded in a dielectric medium ($\epsilon=2.25$). The spectral position as a function of w for both the EOT maximum (triangular symbols) and the EOT minimum (circular symbols) are shown in panel (b). Dashed lines summarize data obtained from panel (a), while solid lines are used for data taken from the asymmetric configuration where the hole array is placed on a substrate ($\epsilon=2.25$), air elsewhere. The horizontal dashed line renders the SPP energy at $k=2\pi/P$.

Size dependence of nonlinear optical response in Si-nanocrystals

S. Hernández,¹ A. Martínez,¹ O. Jambois,¹ P. Pellegrino,¹ P. Miska,² M. Grün,² H. Rinnert,² M. Vergnat² and B. Garrido¹

¹ MIND-IN2UB, Departament d'Electrònica, Universitat de Barcelona, Martí i Franquès 1, 08028 Barcelona, Spain.

² Institut Jean Lamour, UMR CNRS 7198 – Nancy Université – UPV Metz, France.

Contact e-mail: shernandez@el.ub.es

Silicon nanocrystals (Si-nc) embedded in oxide matrices have been proposed as active material for nonlinear photonic applications, as their nonlinear optical properties were found to be larger than the ones in silica or Si. A strong size dependence of their nonlinear optical properties has been observed by different authors, nevertheless they show a large scatter in their data [1, 2]. Therefore, an accurate knowledge of their nonlinear optical properties as a function of the Si-nc size is crucial for the conception and design of highly efficient new photonic structures and the control of their performance.

Here we present a z-scan study of SiO/SiO₂ multilayers exciting in the ns-regime with pulses of $\lambda = 1064$ nm. Films were deposited by evaporation and annealed up to 1000 °C in a conventional furnace for 10 minutes. As a consequence, Si-nc were precipitate with sizes from 2 nm up to 5 nm. In Fig. 1 we present an energy filtered TEM image of a typical sample with Si-nc of 3 nm. A high density of Si-nc can be observed homogeneously distributed along the films. Similar results were also obtained in the whole set of samples. Raman measurements have revealed a sharp feature around 518 cm⁻¹ indicating that the Si-precipitates have high crystal quality. A linear optical characterization of the layers has been performed by means of photoluminescence and optical absorption, finding that the energy emission and the band increase as the Si-nc size is reduced.

The nonlinear absorption and nonlinear refractive index have been measured by z-scan experiments using a ns-pulsed Nd:AG laser working at $\lambda = 1064$ nm. The z-scan traces have shown a position dependence transmittance in both the open and close aperture configurations, indicating that both absorptive and refractive nonlinearities arise in the Si-nc/SiO₂ system under these excitation conditions. The films have been analyzed in open and close aperture configurations, in order to determine both non-linear absorption and non-linear refractive index in the ns-regime. Using expression developed by Sheik-Bahae [3], we fitted the experimental from open and close aperture configurations and we extracted the nonlinear absorption coefficient and the nonlinear refractive index of the SiO/SiO₂ multilayer system.

In Fig. 2 we present the nonlinear absorption coefficient and nonlinear refractive index for SiO/SiO₂ multilayered samples with different Si-nc size. The nonlinear absorption coefficient and the nonlinear refractive increase from 1.0×10^{-6} to 1.8×10^{-5} cm/W and from -4.2×10^{-11} to -7.6×10^{-10} cm²/W, respectively, as the Si-nc increases from 2 to 5 nm. A similar increasing trend with the Si-nc size can be observed when the nonlinear response is normalized to the Si excess, as shown in the inset of Fig. 2, in contrast to previous studies performed in Si-nc where a reduction of the nonlinear optical response is observed for larger Si-ncs [1].

In order to determine the origin of the observed nonlinear behavior in the Si-nc/SiO₂ multilayered system, we have analyzed their nonlinear optical response using a nonlinear model which includes the changes in the free-carrier concentration and possible thermal contributions induced by the high excitation fluencies. In this time domain (ns), we found that the excitation of free carriers is the main mechanism contributing to the nonlinear optical response.

We acknowledge financial support from the Spanish Ministry of Science and Innovation (EUI2008-03806 and TEC2009-08359). One of the authors (A.M.) acknowledges support from *Departament d'Universitats i Recerca de la Generalitat de Catalunya and the European Social Fund*.

References

- [1] G. Vijaya Prakash, M. Cazzanelli, Z. Gaburro, L. Pavesi, F. Iacona, G. Franzò and F. Priolo, *J. Appl. Phys.* **91** (2002), 4607.
 [2] S. Vijayalakshmi, H. Grebel, G. Yaglioglu, R. Pino, R. Dorsinville and C. W. White, *J. Appl. Phys.* **88** (2000) 6418.
 [3] M. Sheik-Bahae, A. A. Said, T-H Wei, D. J. Hagan and E. W. Van Stryland, *J. Quant. Elect.* **26** (1990) 760.

Figures

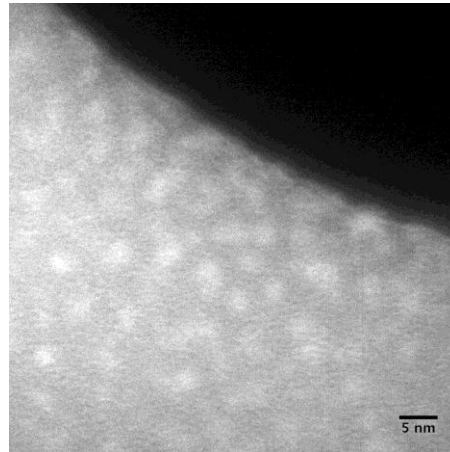


Figure1. EFTEM images of sample with Si-nc of 3 nm. The light contrast is referred to Si-nanoparticles.

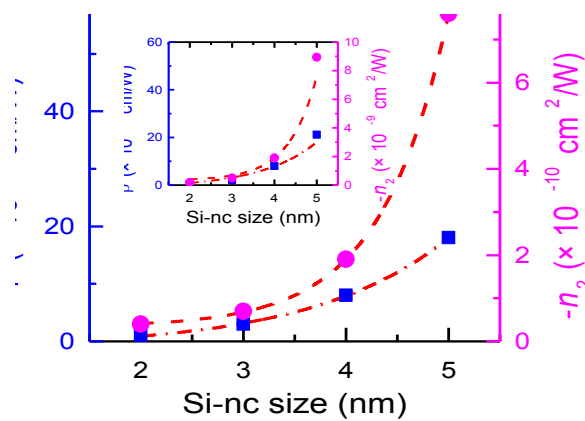


Figure 2. Nonlinear absorption coefficient (left axis, in blue) and nonlinear refractive index (right axis, in magenta) of the SiO/SiO₂ multilayered system as a function of the Si-nc size. In the inset, β and n_2 as a function of the Si-nc size, once normalized by the Si excess in the samples.

Controlling the optical properties of macroporous silicon structures

D. Hernández^a, T. Trifonov^b, M. Garín^c, and R. Alcubilla^b

a, Research Group in Micro and Nanotechnologies, Electronic Engineering Department, Universitat Politècnica de Catalunya, Jordi Girona 1-3, Mòdul C4, Campus Nord, 08034, Barcelona, Spain

b, Centre de Recerca en Nanoenginyeria, Universitat Politècnica de Catalunya, Pascual i Vilà 15, 08028, Barcelona, Spain

c, Centro de Tecnologías Físicas, Unidad Asociada ICMM- CSIC/UPV, Universidad Politècnica de Valencia, Av. De los Naranjos s/n. 46022 Valencia, Spain

hernandez@eel.upc.edu

Photonic crystals are artificial materials with a periodic variation in the index of refraction which leads to the formation of forbidden optical bands (the so-called photonic band gaps, PBG) [1]. Significant efforts have been undertaken in order to fabricate micro- and nano-structures that meet the requirements for 3D photonic crystals, such as periodicity in all three dimensions, high dielectric contrast and very good uniformity in large scales. Macroporous silicon [2], produced by electrochemical etching of silicon in HF solutions, has proved to meet these requirements and has become an excellent material for the development of 2D and 3D photonic crystals. An example of a macroporous silicon structure can be seen in Fig. 1.

A prominent feature of the electrochemical etching technique is its flexibility in 3D sculpturing of silicon. Since the distribution of the pores in the plane can be defined by a lithographic process and the periodicity along the pore axis can be controlled independently, a great variety of pore geometries and distributions can be designed to meet specific optical behaviors [3]. Consequently the dispersion relation may be modified by changing the shape of pore diameter modulation. The freedom in adjusting the pore diameter, makes it easier the incorporation of planar defects, whose dimensions and thus spectral positions, can be designed beforehand.

In this work we report on the fabrication and optical characterization of 3D macroporous silicon structures. FT-IR spectrometry measurements of the reflectivity and transmittivity along the pore axis reveal PBG, which are also confirmed by simulations of band dispersion, as seen in Fig. 2. We study the influence of pore modulation on the band gap properties (spectral width and position). In addition, thermal emission is inhibited in the band gap region which allows us to tailor the emission spectrum of the material.

We study the optical properties of three-dimensional structures obtained by post-etching treatments of the macroporous arrays. Adjacent pores can be widened [4] and become connected thus providing 3D structures with very high porosities and new photonic crystal geometries.

References

[1] J.D. Joannopoulos, R.D. Meade, J.N. Winn, *Princeton University Press*, Princeton (1995).

[2] V. Lehmann, and H. Föll, *J. Electrochem. Soc.* 137, 653-659 (1990).

[3] M. Garín, T. Trifonov, A. Rodríguez, R. Alcubilla, F. Marquier, C. Arnold, J.-J. Greffet, *Appl. Phys. Lett.* 93, 081913 (2007).

[4] M. Garín, T. Trifonov, A. Rodríguez, L.F. Marsal, R. Alcubilla, *Mater. Sci. Eng. B* 149, 275-280 (2008).

Figures

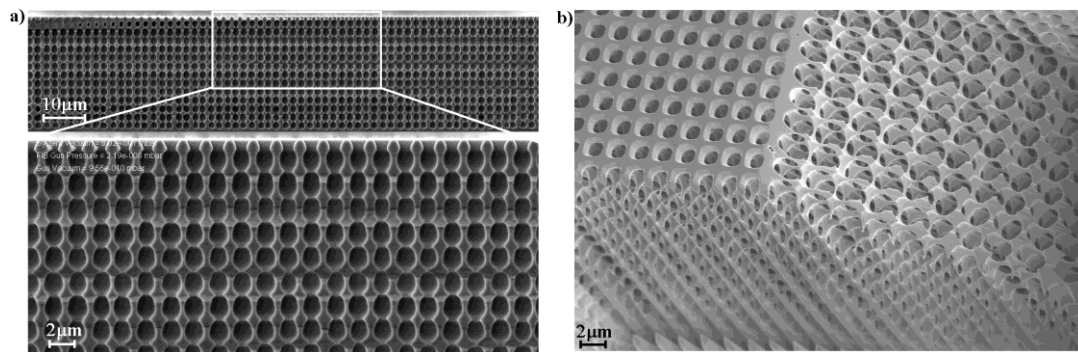


Fig. 1. SEM pictures of macroporous silicon samples with modulated pores. Periodicities are $2\mu\text{m}$ in all three dimensions. (a) Large-scale stable structures can be performed. (b) Post-processing allows the definition of new geometries and shapes.

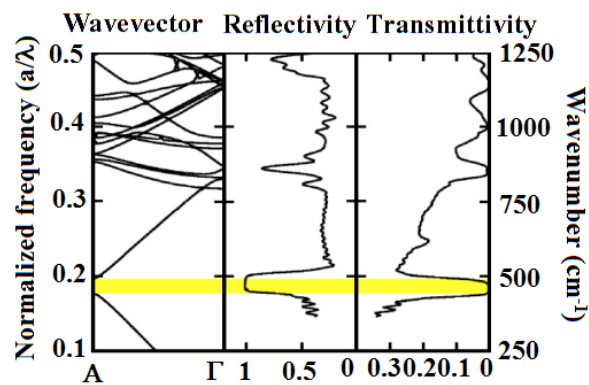


Fig. 2. Simulated dispersion relation of macroporous silicon sample in the pore direction. FT-IR measurements have been carried out with a $4\mu\text{m}$ -periodicity structure. PBG (shaded in yellow) reveals as a spectral region with 100% reflectivity and 0% transmittivity.

Transformation optics for plasmonics

P.A. Huidobro, M. L. Nesterov, L. Martín-Moreno, F. J. García-Vidal

Departamento de Física Teórica de Materia Condensada, Facultad de Ciencias, Universidad Autónoma de Madrid, Campus Cantoblanco, Ctra. Colmenar, Km.15., Madrid, Spain.
paloma.arroyo@uam.es

A new strategy to control the flow of surface plasmon polaritons (SPPs) at metallic surfaces is presented. It is based on the application of the concept of Transformation Optics (TO), a theoretical frame proposed [1,2] as a general technique to design complex electromagnetic (EM) media with unusual properties. TO provides us with expressions for the dielectric permittivity tensor, ϵ , and the magnetic permeability tensor, μ , that need to be implemented in order to obtain a medium with a designed functionality.

Practical realizations of the idea of TO include the construction of a two-dimensional cylindrical invisibility cloak for EM plane waves and the construction of broad-band ground-plane cloaks [3] in the microwave [4] and optical [5,6] regimes. These experiments made use of metamaterials, [7] artificially structured materials made up of subwavelength constituents and designed to implement a prescribed response to EM fields. Besides, a wide variety of applications other than cloaking has been recently presented, including beam shifters and beam dividers [8], or lenses with subwavelength resolution [9].

On the other hand, one of the main goals in Plasmonics is to control the flow of light at a metal surface by means of the SPPs that decorate a metal-dielectric interface. In our work [10], we present a new strategy to tackle this problem by showing that the TO framework can be applied to mold the propagation of SPPs at a metal surface. We develop a general methodology for the design of Transformation-Optical devices for SPPs, based on the use of TO to devise the optical parameters that need to be implemented in order to obtain the desired functionality. Then, we show that a simplified version of the TO recipe in which the optical parameters are implemented only in the dielectric on top of the metal surface leads to quasi-perfect functionalities. We analyze, for proof-of-principle purposes, three representative examples with different functionalities: a beam shifter (see Fig. 1), a cylindrical cloak (see Fig. 2) and a ground-plane cloak (see Fig. 3).

References

- [1] Pendry, J. B.; Schurig, D. and Smith, D. R., *Science* 312 (2006) 1780-1782.
- [2] Leonhardt, U., *Science* 312 (2006) 1777-1780.
- [3] Li, J. and Pendry, J. B., *Phys. Rev. Lett.* 101 (2008) 203901.
- [4] Liu, R.; Ji, C.; Mock, J. J.; Chin, J. Y.; Cui, T. J. and Smith, D. R., *Science* 323 (2009) 366-369.
- [5] Valentine, J.; Li, J.; Zentgraf, T.; Bartal, G. and Zhang, X., *Nat. Mater.* 8 (2009) 568-571.
- [6] Gabrielli, L. H.; Cardenas, J.; Pointras, C. B. and Lipson, M., *Nat. Photonics*, 43 (2009) 461-463.
- [7] Ziolkowski, R. W. and Engheta N., *Metamaterials: Physics and Engineering Explorations*, IEEE Press, John Wiley & Sons, Inc. (2006).
- [8] Rahm, M.; Cummer, S. A.; Schurig, D.; Pendry, J. B. and Smith, D. R., *Phys. Rev. Lett.* 100 (2008) 063903.
- [9] Schurig, D.; Pendry, J. B.; and Smith, D. R., *Opt. Express* 15 (2007) 14772-14782.
- [10] Huidobro, P. A.; Nesterov, M. L.; Martín-Moreno, L. and García-Vidal, F. J., submitted (2010).

Figures

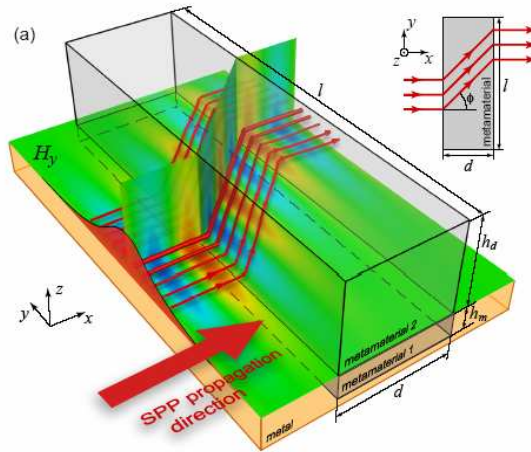


Figure 1: SPP at $1.5 \mu\text{m}$ travelling along a gold-vacuum interface and entering into a 3D beam shifter. The color map represents the normalized magnetic field pattern and the red lines are power flow streamlines. The beam shifter is constituted by two rectangular metamaterials with inplane dimensions $2.5 \mu\text{m} \times 10 \mu\text{m}$ and thicknesses $h_d = 6 \mu\text{m}$ in the dielectric side and $h_m = 50 \text{nm}$ in the metal side. The inset of the figure shows the basic geometry from a top view.

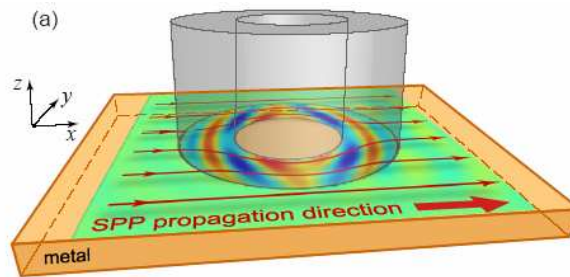


Figure 2: Schematic picture showing of a 3D cylindrical cloak for an SPP travelling through a gold-vacuum interface. The cylindrical region in the dielectric side comprised between the inner radius $a = 1.5 \mu\text{m}$ and the outer radius $b=2a$ and $6 \mu\text{m}$ high constitutes the metamaterial were the TO parameters are implemented. The color map at the metal surface is the normalized scattered magnetic field for a SPP at $1.5 \mu\text{m}$.

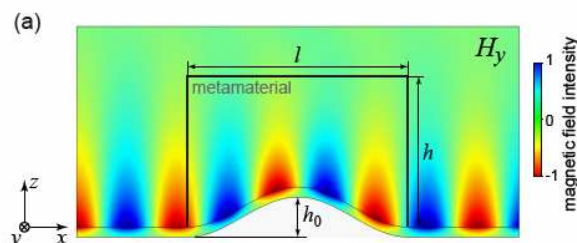


Figure 3: Two-dimensional ground-plane cloak for a SPP at 600nm that travels in the x-direction along a gold surface. The cloaked object is a \cos^2 -shaped gold bump, 1250nm long and with a height of $h_0 = 200 \text{nm}$. The metamaterial acting as the cloak is 750nm high. The color map shows the normalized magnetic field pattern.

Miniaturization Strategies for Soft/Hard and High Impedance Surfaces Design at Microwaves Frequencies

L. Inclán-Sánchez, J.J. Sáenz

Departamento de Física de la Materia Condensada
 Universidad Autónoma de Madrid. E-28049, Madrid. Spain. (luis.inclan@uam.es)

In this paper, novel soft/hard and high impedance surfaces based in new geometries are presented. We analyze the properties of surface wave propagation through these structures made of printed modified strips. The new shapes for the strips are the coupled lines topology and the spiral one, both are provided with metalised via holes in a lateral position. The size reductions for new shapes when compared with strip-loaded surface are 14% and 23% respectively. The presented structures are very suitable to improve efficiency and to reduce mutual coupling in antenna applications.

Periodic structures have received much attention in antenna applications during the last years. Very interesting case are the soft and hard surfaces. The basic implementations of these surfaces are corrugations in a metal plate or metal strips (Fig. 1) on a grounded dielectric slab [1]. Miniaturization of microwave components and antennas has become increasingly important in recent years [2][3][4]. In this paper miniaturized horizontal corrugations and miniaturized EBG elements, based on new topologies for the strips, are investigated. The work shows how a reduction in size can be achieved by taking advantage of the impedance transformation related with the new shape [3]. Different shapes are proposed including a coupled lines structure and a spiral shape. In the two cases the forbidden frequency band moves towards lower frequencies. These modified planar corrugations are composed of novel topologies for the strips and vias that connect the strip with the ground plane. These new structures achieve a size reduction compared to conventional horizontal corrugations and elements. A numerical characterization of the new topologies and its stop band behaviour is described in the paper.

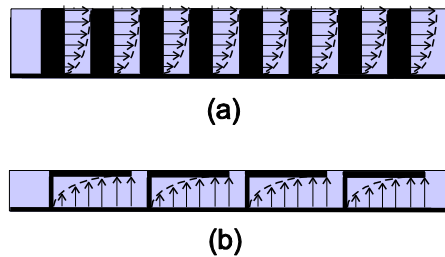


Fig. 1 Different realisations of soft surfaces. (a) Classical transverse corrugations. (b) Horizontal Corrugations

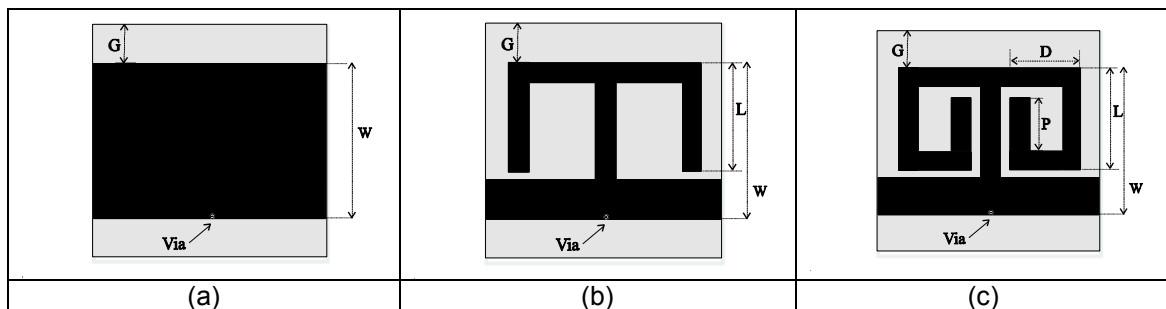


Fig. 2 Geometries of the studied surfaces. Strip-loaded with vias (a). Coupled lines shape (b). Spiral line shape (c)

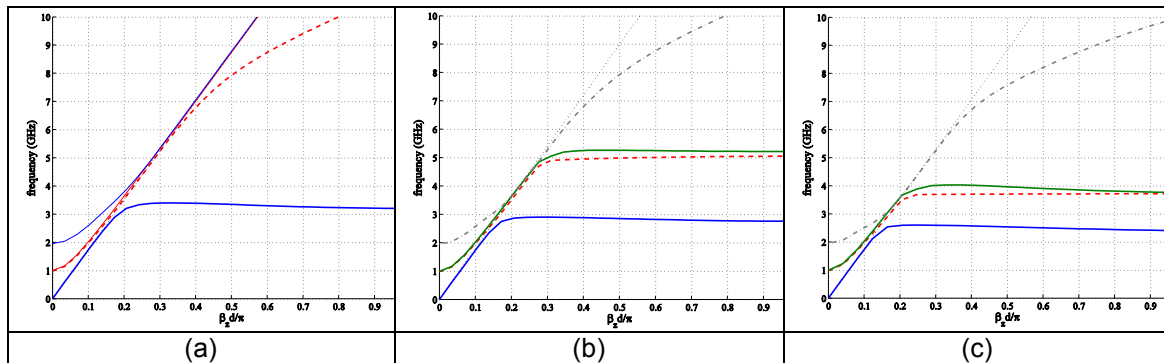


Fig. 3 Dispersion diagram for : (a) horizontal corrugations with vias. ($W=\lambda_e/4$, $G=0.1\lambda_e$, $\epsilon_r=4.4$). (b) Coupled line shape. ($W=\lambda_e/4$, $G=0.1\lambda_e$, $L=7W/10$, $\epsilon_r=4.4$). (c) Spiral shape. ($W=\lambda_e/4$, $G=0.1\lambda_e$, $L=7W/10$, $P\approx 4W/10$, $\epsilon_r=4.4$)

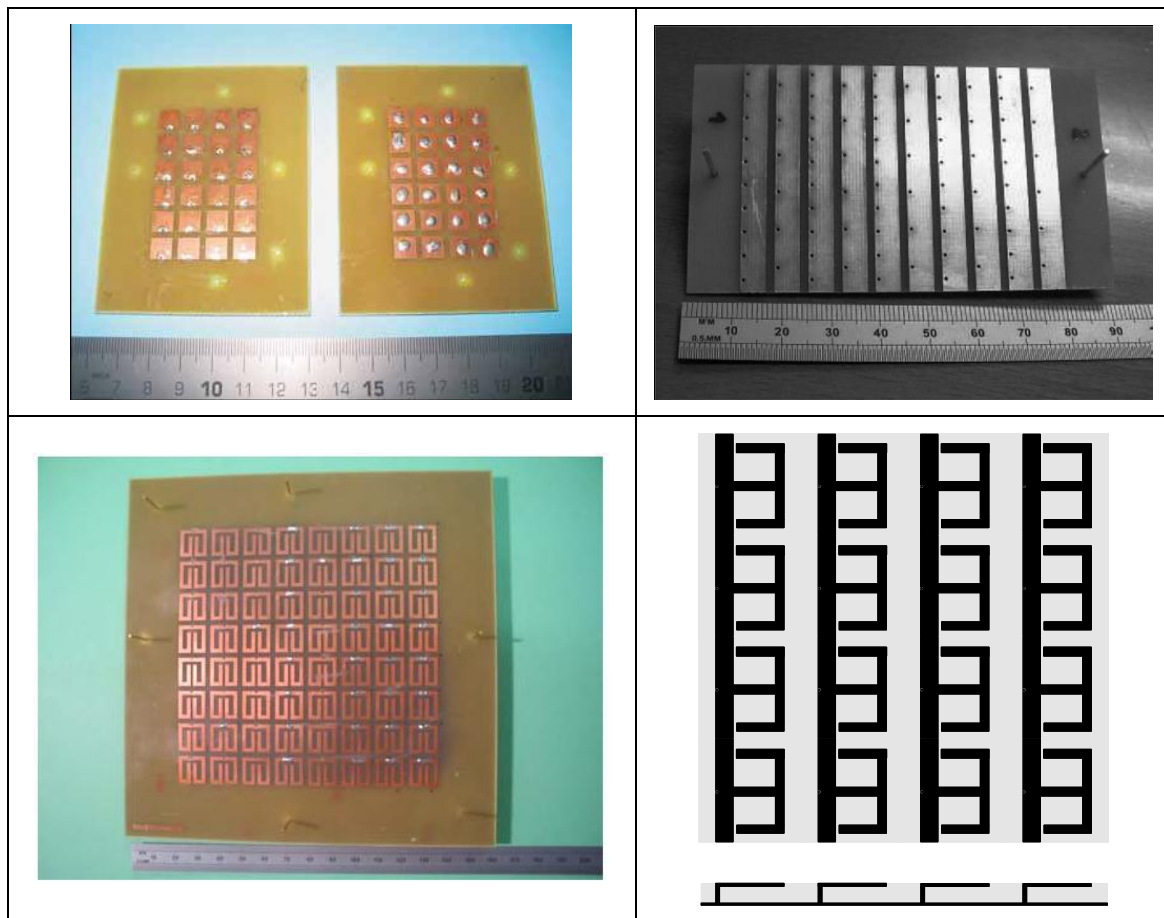


Fig. 4 Different realizations of Soft/Hard and High Impedance surfaces

This work was financed by the Regional Government of Madrid under MICROSERES project. One of the authors would like to acknowledge the financial support of the Universidad Autónoma de Madrid under Programa Alianza 4 Universidades.

- [1] E. Rajo-Iglesias, M. Caiazzo, L. Inclan-Sanchez and P. S. Kildal, "Comparison of bandgaps of mushroom-type EBG surface and corrugated and strip-type soft surfaces", IET Microwaves, Antennas and Propagation. Special Issue on Metamaterials EBG, vol. 1, pp. 184-189, Feb 2007.
- [2] E. Rajo-Iglesias, L. Inclan-Sanchez, J.L Vázquez-Roy and E. Garcia-Munoz, "Size reduction of mushroom-type EBG surfaces by using edge-located vias", IEEE Microwave and Wireless Components Letters, vol.17, no. 9, pp. 670-672, Sep 2007
- [3] L. Inclan-Sanchez, J.L Vázquez-Roy, E. Rajo-Iglesias and E. Garcia-Munoz, Compact EBG Surface based on Capacitively Loaded Loop Resonators with Grounded Vias, Proc. Antennas and Propagation, European Conference on 2007, vol. 1 pp. 226-228, Nov 2007
- [4] F. Caminita, S. Costanzo, G. D. Massa, G. Guarnieri, S. Maci, G. Mauriello and I. Venneri, "Reduction of patch antenna coupling by using a compact EBG formed by shorted strips with interlocked branch-stubs", IEEE Antennas and Wireless Propagation Letters, vol 8, pp. 811-814, 2009.

Plasmon-induced enhancement of light absorption in metallic nano-modified semiconductor

W. Jacak, J. Krasnyj, L. Jacak

Institute of Physics, Wrocław University of Technology, Wyb. Wyspińskiego 27, 50-370 Wrocław Poland
Theor. Phys. Group., International University of Odessa, Odessa Ukraine
witold.aleksander.jacak@pwr.wroc.pl

Experimental data on giant enhancement of photoluminescence and absorption of light by photo-diode system's semiconductor layer covered with metallic nanospheres [1-6] provides an evidence of a possibility to significantly increase efficiency of solar cells. Application of special metallic nanoparticle coverings of photo-active surfaces has been found to induce a light converting effect, collecting energy of incident photons in surface plasmon oscillations. This energy can be next transferred to semiconductor substrate in much more efficient manner in comparison to the direct photo-effect. Experimental observations suggest, that the near-field coupling between plasmons in nanospheres and electrons in the semiconductor substrate allows for significant growth of selective light energy transformation into a photo-current in a diode system. We argue that due to nanoscale of the metallic components the momentum is not conserved in this transition, which leads to allowance of all indirect optical interband transitions in semiconductor layer, resulting in enhancement of a photo-current in comparison to the ordinary photo-effect when only direct interband transitions were admitted. Though the effect is selectively ranged to a vicinity of the resonant plasmon frequency, the gain in the total efficiency would be enlarged by possible dispersing of dimension and shape (or by a dielectric coating) of metallic nanoparticles, widening the resonant spectrum. An explanation of a large plasmon-induced PV efficiency enhancement of metallic surface-modified photo-cell is presented by inclusion of all indirect inter-band electron transitions in semiconductor due to near-field coupling with plasmon radiation of a nano-scale metallic components. The model of nano-sphere plasmon is formulated within RPA-type approach in an analogy to Pines-Bohm bulk plasmon theory [7], adjusted to large clusters [8]. Damping of plasmons is analyzed including irradiation losses due to the Lorentz friction [9]. Probability of the interband transition in substrate semiconductor caused by the coupling with plasmons in near-field regime turns out to be 4-order larger than for coupling of electrons with planar-wave photons. Inclusion of proximity and interference effects allows for explanation of photo-current growth measured in experimental metallic modified photo-diode systems.

References

- [1] Pillai S, et al., Appl. Phys. Lett. **88** (2006) 161102
- [2] Westphalen M, et al., Sol. Energy Mater. Sol. Cells **61** (2000) 97
- [3] Gratzel M., J. Photochem. Photobiol. C: Photochem. Rev. **4** (2003) 145
- [4] Stuart H R and Hall D G, Appl. Phys. Lett. **73** (1998) 3815; Phys. Rev. Lett. **80** (1998) 5663
- [5] Schaadt D M, et al., Appl. Phys. Lett. **86** (2005) 063106
- [6] Okamoto K, et al., Nature Mat. **3** (2004) 601; Wen C, et al., Sol. Cells **61** (2000) 339
- [7] Pines D and Bohm D, Phys. Rev. **85** (1952) 338; Phys. Rev. **92** (1953) 609
- [8] Jacak J, et al., arXiv:0912.5026v1
- [9] Jacak W, et al., arXiv:0912.5024v1

Impact of a SNOM probe on photonic crystal optical modes

Gaëlle Le Gac¹, A. Rahmani⁴, Christian Seassal², Emmanuel Picard³, Emmanuel Hadji³, Ségolène Callard²

1 Instituto de Microelectrónica de Madrid (CNM, CSIC), Isaac Newton 8,
E-28760, Tres Cantos Madrid, Spain

2 Institut des Nanotechnologies de Lyon, UMR CNRS 5270, Ecole Centrale de Lyon, 36 avenue Guy de
Collongue 69134 Ecully Cedex, France

3 INAC /SP2M, Laboratoire SiNaPS, CEA Grenoble, 17 rue des martyrs, F-38054 Grenoble, France

4 Department of Mathematical Science, University of Technology, Sydney, NSW 2007 Australia

gaelle.legac@imm.cnm.csic.es segolene.callard@ec-lyon.fr

Two-dimensional photonic crystals (PC) structures possess very attractive features for integrated microphotonics. Their ability to modify, tailor and confine electromagnetic fields at the nanoscale has led to the design of compact laser sources and optical resonators. PC-based microcavity can present a large quality factor (Q) while preserving a small modal volume (V), thus enabling the high Q/V ratio required for studying cavity quantum electrodynamics at the single source level.

To analyze the coupling between the sources and the cavity, one must observe directly and locally the field distribution inside the cavity. Because of the small size of such a cavity, far-field techniques, which are usually diffraction-limited, fail to achieve the needed resolution. In previous study we showed that near-field scanning optical microscopy (NSOM) is an efficient tool to probe the local distribution of the electromagnetic field in the PC-based microcavity on a subwavelength level [1,2]. Indeed these information yield the real field distribution as far as the coupling between the NSOM probe and the photonic crystal mode remains weak.

In the present work, comparison between 3D-FDTD simulations and experimental results on active stick microcavities will be presented to emphasize the effect of the probe material on the emission wavelength and the relative induced losses [3], and the importance of the probe shape when observing directly and locally the field distribution with SNOM.

[1] N. Louvion, A. Rahmani, C. Seassal, S. Callard, D. Gérard, and F. de Fornel, "Near-field observation of subwavelength confinement of photoluminescence by a photonic crystal microcavity," *Opt. Lett.* **31**, 2160-2162 (2006).

[2] N. Louvion, D. Gérard, J. Mouette, F. De Fornel, C. Seassal, X. Letartre, A. Rahmani and S. Callard, "Local observation and spectroscopy of optical modes in an active photonic crystal microcavity", *Phys. Rev. Lett.*, **94**, 113907 (2005).

[3] G. Le Gac, A. Rahmani, C. Seassal, E. Picard, E. Hadji, and S. Callard, "Tuning of an active photonic crystal cavity by an hybrid silica/silicon near-field probe," *Opt. Express* **17**, 21672-21679 (2009)

Easy implementation tuning of self-assembled photonic-plasmonic crystals

M. López-García, J.F. Galisteo-López, A. Blanco, C. López

*Instituto de Ciencias de Materiales de Madrid (CSIC), c/ Sor Juana Inés de la Cruz 3, 28049,
Cantoblanco, (Madrid) Spain*
mlopez@icmm.csic.es

A. García-Martín

Instituto de Microelectrónica de Madrid (CSIC), c/ Isaac Newton 8, 28760, Tres Cantos, (Madrid) Spain

Tunability is challenging in photonics. The possibility to either passively or actively modify the optical properties of photonic devices opens new applications especially in sensing and light emitting devices. Among all the structures suitable to be implemented as tuning devices, photonic and plasmonic crystals have become two of the most powerful techniques. Recently, coupling between both kinds of structures has shown to provide exceptional properties especially concerning light emission control at visible and near infrared range [1]. From this point of view, more affordable implementations compared to usual lithographic techniques has been proposed making use of the high quality self-assembled photonic crystals fabrication methods. By growing a monolayer of polystyrene spheres (diameter size similar to working wavelength) on a gold substrate it is possible to obtain hybrid photonic-plasmonic resonances coupling [2]. Modal distribution of those hybrid modes is largely dependent on the lattice parameter as well as on the filling fraction of the monolayer of spheres. In addition, if an emitter is placed in the field confinement region for one given mode, emission can be enhanced as well as tuned to the required frequency by choosing the appropriate sphere diameter.

In this work we present an easy implementation method to tune the modal distribution of that system by homogeneously reduce sphere diameter while lattice parameter is kept constant. Applying oxygen plasma etching for a very accurate controlled time we have obtained control over filling fraction (ff) of the photonic crystal. Reductions were performed from the as-grown close packed ($ff = 0.52$) to largely reduced sphere size ($ff < 10$) while quality of the photonic lattice was shown to keep very high. Both experimental and theoretical study of the optical response was performed in normal incidence reflectance. Modes of the system (shown as large dips in reflectance) largely blueshift with sphere reduction, especially those with waveguided character. Sensibility of mode spectral position to filling fraction variations was investigated for 1 μm diameter polystyrene spheres by reflectance measurements in diameter reduction steps as low as 10 nm. Almost linear blueshift was observed for every mode. Numerical simulations for reflectance have shown good agreement with experimental results. Field profile into the structure was studied in order to evaluate how changes on sphere diameter affect mode shape. Larger changes were found for waveguided-like modes compared to plasmonic ones as would be expected from studies reported in bibliography for these structures (Figure 1).

As a step forward, changes on emission distribution with filling fraction was studied. To do that, red dye doped PS 520 nm diameter spheres (emission maxima at aprox. 590 nm) were grown on gold substrate. Several steps on sphere reduction were performed and changes for emission maxima were measured typically happening at the same spectral position were a dip in reflectance is shown. It was found that, as expected, emission spectrum was blueshift in the same amount that was is monitorize for reflectance (Figure 2). This provides a proof of principle of tuning of the emission peaks to the required spectral position while the structural modification is very accurately monitorize by normal reflectance measurements.

This results demonstrate that this fine tuning process could be used for passive or active devices leading to high performance but low cost structures as for example biosensors or OLED.

References

- [1] R.F Oulton, V.J. Sorger, T. Zentgraf, R. Ma, C. Gladden, L. Dai, G. Bartal, X. Zhang, *Nature* **2009**, 461, 629.
- [2] R. M. Cole, Y. Sugawara, J. J. Baumberg, S. Mahajan, M. E. Abdelsalam, P. Barlett, . *Phys. Rev. Lett.* **2006**, 97, 137401.

Figures

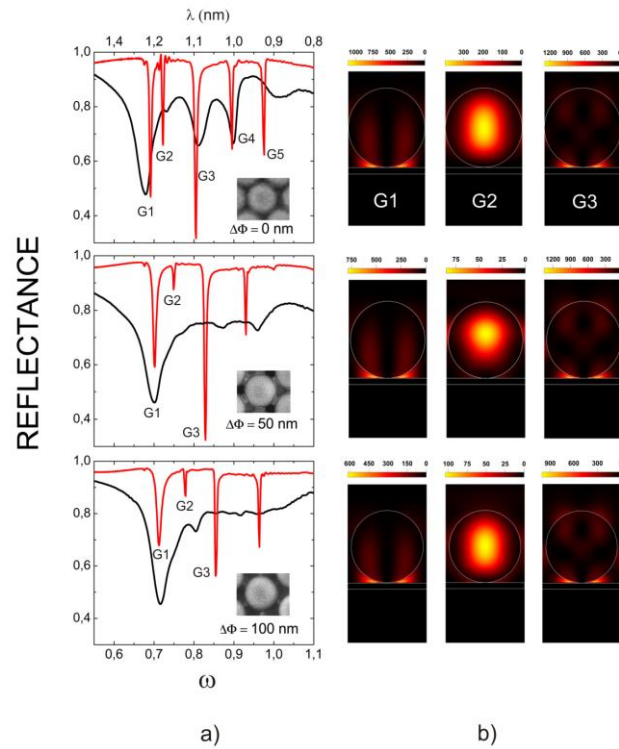


Figure 1. a) Normal incidence reflectance at three different etching steps. Top to bottom: $\Delta\Phi = 0, 50$ and 100 nm. Experimental (black) and theoretic spectra (red) are compared. b) Total field intensity distribution and its evolution with sphere resizing for the first three modes in the left panel.

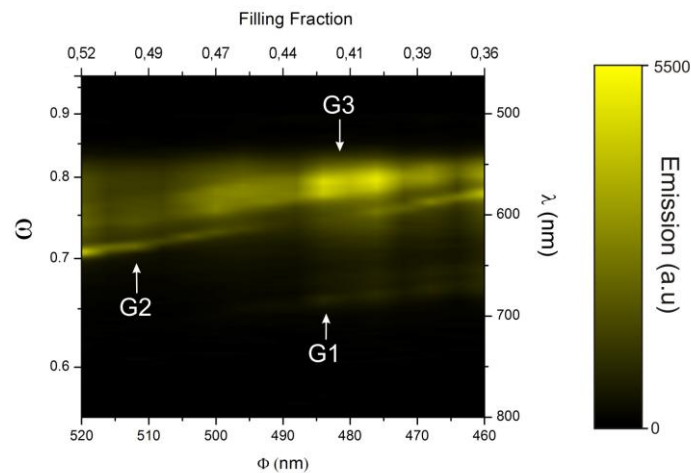


Figure 2. Emission (in arbitrary units) contour plot for a monolayer of 520 nm dye doped PS spheres in a continuous filling fraction reduction process. Oxygen plasma etching was carried out from the close packed scenario ($ff = 0.52$) to a final filling fraction of $ff = 0.36$.

In search of optimal performance for surface-plasmon Bragg mirrors

F. López-Tejeira¹, F. J. García-Vidal², L. Martín-Moreno¹

¹ICMA & Dpto. de Física de la Materia Condensada, CSIC-Universidad de Zaragoza, Zaragoza, Spain

²Dpto. de Física Teórica de la Materia Condensada, Universidad Autónoma de Madrid, Madrid, Spain
flt@unizar.es

From the theoretical side, the calculation of electromagnetic fields on a metal surface in the optical regime is a well-defined but difficult problem that requires a trade-off between ambition and numerical cost, as well as between quantitative and qualitative descriptions of the system under consideration. In the last five years, we have made use of the modal expansion technique in order to reach such a difficult balance when dealing with the scattering of surface plasmon-polaritons by one-dimensional nano-indentations [1-3]. Here, we continue our journey towards quantitative description of surface-plasmon Bragg mirrors by extending our study to the case in which surface impedance boundary conditions are applied to all metal/dielectric interfaces.

More precisely, we have carried out extensive numerical simulations with the aim of determining the set of geometrical parameters (depth, width and position of the indentations) that provide optimal performance under given fabrication and operation conditions. In addition to global figures of merit, we have also studied the relative influence of different parameters, which can be understood in terms of cavity mode excitation and in-phase reemission [4].

References

- [1] F. López-Tejeira et al., Phys. Rev. B, **72** (2005) 161405.
- [2] A.Yu. Nikitin et al., Phys. Rev. B, **75** (2007) 035129.
- [3] F. López-Tejeira et al., Appl. Phys. A, **89** (2007) 251.
- [4] F. J. García-Vidal et al., Phys. Rev. Lett., **90** (2003) 213901.

Subwavelength focusing at optical frequencies achieved by an inverse designed photonic silicon integrated device

José Marqués-Hueso¹, Lorenzo Sanchis¹, Benoit Cluzel², Frédérique de Fornel² and Juan Martínez-Pastor¹

¹UMDO, Institut of Material Science, Department of Applied Physics,
University of Valencia, P.O. Box 22085, 46071 Valencia, Spain

²Groupe d'Optique de Champ Proche, Laboratoire Interdisciplinaire Carnot de Bourgogne (ICB),
UMR CNRS 5209, Université de Bourgogne, 9, avenue A. Savary, BP 47870, 21078 Dijon, France
jose.marques@uv.es

Perfect lensing has been extensively studied since 2000, when Pendry [1] described how evanescent modes allow restoration of subwavelength detail at the image plane.

The structures for perfect lensing can be based on dielectric-based photonic crystals (PCs) [2] whose dispersion properties can be engineered so that at specific frequencies in the vicinity of the photonic band gap, negative refraction [3, 4] and subwavelength imaging [5] can be achieved. The first experimental evidence was obtained in the microwave regime and demonstrated single-beam negative refraction and superlensing in the valence band of a two-dimensional PC [6]. Subwavelength focusing experiments operating at optical frequencies have been done with photonic lenses made of air holes in a semiconductor slab. The measurements have been done by different techniques [7, 8], with the most accurate and detailed being the SNOM measurements [9, 10].

In this work, we have attempted an innovative approach in the field of subwavelength focusing through photonic crystals. We have designed a photonic crystal silicon integrated lens, able to focus an impinging front wave in a spot freely located by us, by an inverse design method based on a genetic algorithm and the bidimensional multiple scattering theory [11]. These techniques allow us to obtain unexpected structures with the desired functionality [12], in contrast to the inefficient direct design based in intuition and the “trial and error” scheme. The device consists of a matrix of holes of 300 nm diameter in a semiconductor slab where some voids have been selectively removed by the genetic algorithm (see Fig.1.a). As the calculation volume limits the design to a bidimensional space, the obtained 2D optimized PC structure has been simulated by a 3D finite difference time domain method to validate the design, with positive results (Fig.1.b-c).

The experimental demonstration has been achieved by the fabrication of the device in silicon and measurements of the field intensity distribution on the device surface by Scanning Near-field Optical Microscopy (SNOM).

The device has been fabricated by electron beam lithography and fluorinated ICP plasma etching in a 340 nm thick silicon layer on top of a silicon dioxide box-layer (Silicon-On-Insulator technology).

The experimental near-field measurements show the performance of the device (Fig.2.a-b), and the correlation with the theoretical results and simulations (compare Fig.1.c and Fig.2.b).

The device has shown subwavelength focusing in the vicinity of the silicon surface, with the measured full width at half maximum of the focus being $0.23\lambda_0$, which is in good agreement with the finite difference time domain method simulations (Fig.2.c), and which overcomes the diffraction limit in air, where the measurements are made.

Moreover, the lens has shown additional advantages over previous photonic devices. The design method allows us to position the focus in a location freely determined by us, which contrasts with the lenses based in the equifrequency curves, where the focus must be placed in the symmetry axis and near the photonic structure.

The inverse design also allows non-punctual sources to be dealt with, in our case with a plane wave front. Finally, the fabricated lens presents a performance over a broad bandwidth, experimentally demonstrated between 1500 and 1580 nm, while the previous PC lenses have a bandwidth of a few nanometers [10].

References

- [1] J. B. Pendry, Phys. Rev. Lett., **85** (2000) 3966.
- [2] J. D. Joannopoulos, R. D. Mead, and J. N. Winn, *Photonic Crystals* (Princeton University Press, Princeton, NJ, 1995).
- [3] C. Luo, S.G. Johnson, J.D. Joannopoulos, and J.B. Pendry, Phys. Rev. B, **65** (2002) 201104
- [4] M. Notomi, Phys. Rev. B, **62** (2000) 10696.
- [5] C. Luo, S. G. Johnson, J. D. Joannopoulos, and J. B. Pendry, Phys. Rev. B, **68** (2003) 045115.
- [6] E. Cubukcu, K. Aydin, E. Ozbay, S. Foteinopoulou, and C. M. Soukoulis, Phys. Rev. Lett., **91** (2003) 207401
- [7] A. Berrier, M. Mulot, M. Swillo, M. Qiu, L. Thylen, A. Talneau and S. Anand, Phys. Rev. Lett., **93** (2004) 073902
- [8] E. Schonbrun, T. Yamashita, W. Park and C.J. Summers, Physical Review B, **73** (2006) 195117
- [9] N. Fabre, L. Lalouat, B. Cluzel, X. Melique, D. Lippens, F. de Fornel, O. Vanbesien, Phys. Rev. Lett., **101** (2008) 073901
- [10] R. Chatterjee, N. C. Panoiu, K. Liu, Z. Dios, M. B. Yu, M. T. Doan, L. J. Kaufman, R. M. Osgood, and C. W. Wong, Phys. Rev. Lett., **100** (2008) 187401
- [11] L. Sanchis, A. Håkansson, D. López-Zanón, J. Bravo-Abad, and J. Sánchez-Dehesa. App. Phys. Lett., **84** (2004) 4460.
- [12] L. Sanchis, M. J. Cryan, J. Pozo, I. J. Craddock, and J. G. Rarity. Phys. Rev. B **76**, (2007) 045118.

Figures

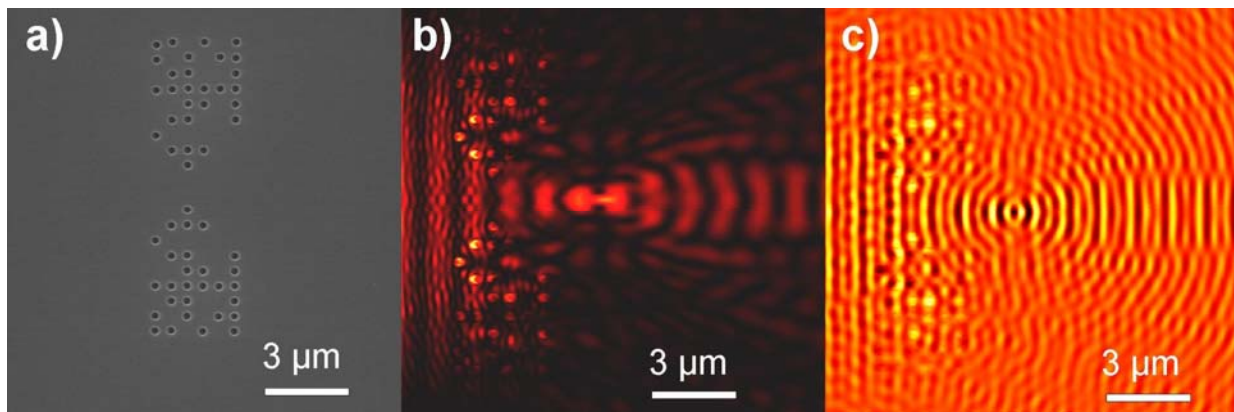


Figure 1. (a) SEM image of the fabricated photonic device. (b) Intensity of the electric field distribution calculated by FDTD on the surface of the designed device. (c) Intensity of the electric field distribution calculated by FDTD after the addition of a constant field.

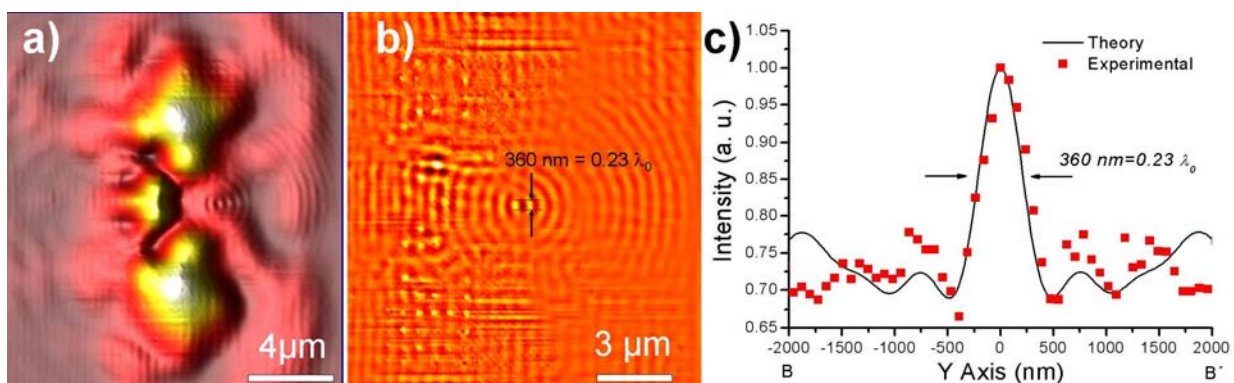


Figure 2. (a) Direct measurement of the electric field intensity by SNOM. (b) SNOM measurement after filtering the optical noise, showing agreement with the simulation of Fig.1.c, with transversal full width at half maximum of the focus of $0.23\lambda_0$. (c) Comparison of the transversal sections of the calculated and simulated electric field intensities.

Synthesis and characterization of polymer nanopillars for photonic and optoelectronic applications

R. Palacios, A. Santos, P. Formentín, E. Martínez-Ferrero[#], J. Pallarès, L. F. Marsal

Departament d'Enginyeria Electrònica, Eléctrica i Automàtica, Universitat Rovira i Virgili, Avda. Països Catalans 26, 43007 Tarragona, Spain

[#]Institute of Chemical Research of Catalonia (ICIQ), Avda. Països Catalans 16, 43007 Tarragona, Spain
lluis.marsal@urv.cat

Micro- and nanostructures fabricated from conjugated polymers have attracted interest due to their potential applications such as sensors, polymer light-emitting diodes, polymer solar cells, and other electronic and photonic devices [1]. Different synthesis methods have been proposed for fabrication of organic structures: nanoimprinting, nanolithography, electrospinning, template-assisted synthesis [2]. The last one has the advantage of being able to create large area and ordered arrays of structures with control over structural parameters. This method does not require specialized equipment and it is applicable to a wide range of materials such as polymers, metals and semiconductors [3]. Anodized aluminium oxide has become one of the most common nano-templates for the preparation of different nanometer-sized structures. Under appropriate anodization conditions, long-range-ordered anodic porous alumina with an ideally ordered nanopores arrangement can be obtained [4].

Herein, we report the fabrication of ordered nanostructures employing a template wetting method, which entails infiltration of a polymeric solution into self-ordered anodic aluminium oxide. Porous alumina template was prepared by two-step anodization process of aluminium metal in an acidic solution. This material is used as template because it is possible to fabricate nanoporous anodic alumina with quasi-hexagonal pore arrangement in an expensive way. The geometric features are controlled by adjusting of anodization voltage, temperature, kind of acid electrolyte and concentration. The resulting nanostructures present pore depths between 150 nm to 300 nm and pore diameters between 50 nm to 300 nm. Figure 1 shows the cross sectional and top view a ESEM images of the self ordered alumina template.

Polymer nanopillars were obtained via infiltration using different types of polymers such as poly(thiophenes) and polyfluorenes. Figure 2 shows ESEM images of poly(3-hexylthiophene-2,5-diyl) (P3HT) and poly(9,9-dioctylfluorene) (PFO) nanopillar structures after removing the alumina template by immersion in a sodium hydroxide (NaOH) solution.

The resulting polymeric nanostructures were characterized by optical (UV-Visible and photoluminescence) and electrical (current sensing atomic force microscopy) techniques. These polymer nanopillars were also analyzed by Raman spectroscopy and X-ray diffraction (μ -XRD) in order to study the orientation of the polymer chains inside the nanopillar.

The presented polymer ordered nanostructures can be used in different photonic and optoelectronic applications such as polymer light emitting diodes and nanostructured polymer solar cells. This fabrication process could be extended to other copolymers depend on later applications.

Acknowledgments

This work was supported by Spanish Ministry of Ciencia e Innovación (MICINN) under grant number TEC2009-09551, HOPE CSD2007-00007 (Consolider-Ingenio 2010) and AECID-A/024560/09.

References

- [1] a) M. Steinhart, J. H. Wendorff, A. Creiner, R. B. Wehrspohn, K. Nielsch, J. Schilling, J. Choi, U. Gösele, *Science*, **296** (2002) 1997. b) X. Chen, M. Steinhart, C. Hess, U. Gösele, *Advanced Materials* **18** (2006) 2153.
- [2] A. Santos, P. Formentín, J. Pallarès, J. Ferré-Borrull, L. F. Marsal, *Mater. Letters*, **64** (2010) 371.
- [3] L. F. Marsal, P. Formentín, R. Palacios, T. Trifonov, J. Ferré-Borrull, A. Rodriguez, J. Pallarès, R. Alcubilla, *Physica Status Solidi (a)*, **205** (2008) 2437.
- [4] H. Masuda, K. Fukuda, *Science*, **268** (1995) 1466.

Figures

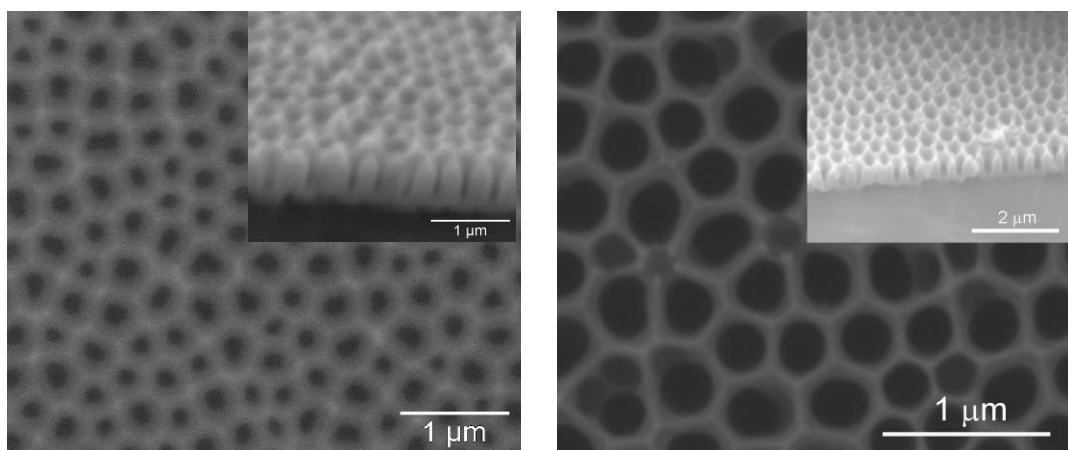


Figure 1. Cross-sectional and top view ESEM images of self-ordered alumina template with different pore depths and pore diameters.

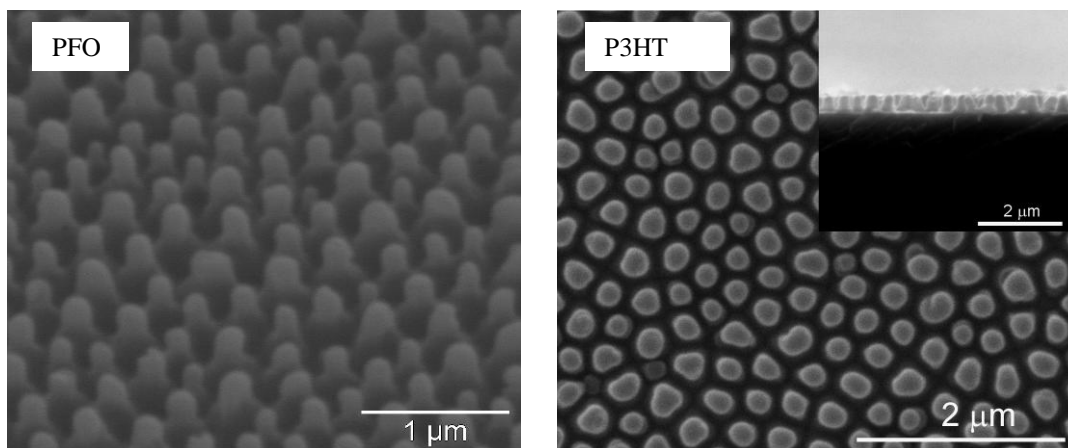


Figure 2. ESEM images of PFO and P3HT nanopillars after removing the alumina template.

Energy transfer between quantum emitters mediated by plasmonic waveguides

Diego Martín Cano¹, Esteban Moreno¹, F. J. García-Vidal¹, Sergio G. Rodrigo², Luis Martín Moreno²

¹ *Departamento de Física Teórica de la Materia Condensada, Universidad Autónoma de Madrid, Madrid, Spain*

² *Departamento de Física de la Materia Condensada-ICMA, Universidad de Zaragoza, Zaragoza, Spain*

The spontaneous emission properties of a quantum emitter can be affected by the presence of neighbour structures [1], due to the modification of the partial local density of states accessible from the emitter. Nearby metallic waveguides could enhance the decay rate into guided plasmonic modes compared with the rest of decay channels [2]. The above property enables strong and coherent coupling due to the small volume associated with the subwavelength confinement inherent in these modes [3], making them efficient energy carriers between emitters [4].

We present calculations studying the decay rates of an emitter in presence of neighbour metallic waveguides and the plasmonic energy transfer between two emitters coupled to them. These properties can be studied classically through the emitted power in the weak coupling regime replacing the quantum emitter by a classical dipole [5].

[1] "Principles of Nano-Optics", Lukas Novotny and Bert Hecht, University Press, Cambridge (2007).

[2] "Quantum Optics with Surface Plasmons", Phys. Rev. Lett., 97 (2006) 053002.

[3] "Generation of single optical plasmons in metallic nanowires coupled to quantum dots", Nature, 450 (2007) 402-406.

[4] "Molecular coupling of light with plasmonic waveguides", Optics Express, 15, 16 (2007). 9908-9917.

[5] "Quantum analysis and the classical analysis of spontaneous emission in a microcavity", Physical review A, 61 (2000) 033807.

Thermal imaging of liquids using luminescent NaYF₄:Yb³⁺,Er³⁺ nanoparticles.

Laura Martínez Maestro¹, F. Vetrone², R. Naccache², Emma Martín Rodríguez¹, Daniel Jaque¹, José García Solé¹ and J.A. Capobianco²

1: GIEL, Departamento de Física de Materiales, Universidad Autónoma de Madrid, Madrid, 28049, Spain

2: Department of Chemistry and Biochemistry, Concordia University, Montreal, Quebec, H4B 1R6, Canada.

lm.maestro@uam.es

In the present work, a temperature gradient induced in water under external optical excitation is measured by using luminescent nanoparticles and confocal fluorescent microscopy. A pump-and-probe experiment, in an aqueous solution containing NaYF₄:Yb³⁺,Er³⁺ nanoparticles, was designed for this purpose. Changes in a particular doublet emission of Er³⁺ ion are used to optically measure water temperature and temperature gradients. Temperature measurements in liquid solutions with sub-micrometer spatial resolution is a quite interesting and active research area.

For biomedical applications these thermal probes must be monodispersed in water. To date, many nano-temperature-sensitive compounds have been used as nano-thermometers. These compounds include metallic nanotubes, carbon nanotubes doped with gallium and a wide range of luminescent nanoparticles, such as ZnS:Mn²⁺ or CdTe.

It appears very interesting to use dielectric nanocrystals codoped with Er³⁺ and Yb³⁺ as nano-sensors. This is because this couple of luminescent ions has a relatively high infrared to visible up-conversion luminescence efficiency by means of an effective Yb³⁺→Er³⁺ energy transfer, and sharp emission lines due to acceptor Er³⁺ ion. In addition, the Yb³⁺ donor ion has absorption bands in the infrared, around 980nm, a wavelength that is in the so-called biological window.

To date, most of the studies in the field of temperature measurement with these nanocrystals have been limited to nanoparticles in powder form. However, NaYF₄ nanocrystals can be made monodispersed in liquids. Therefore they could be used as biocompatible nano probes.

Properly coated, these nanoparticles are soluble in polar solvents, as water. We used this solvent also because the idea was to take advantage of the heat load experienced by water under an infrared excitation beam at 980nm. Such excitation beam would produce a thermal gradient related to the absorbed power profile that can be imaged by means of the Er³⁺ luminescence of the nanoparticles.

For this purpose, hydrophilic NaYF₄: Yb, Er (PEI-capped) nanoparticles (2 mol % Er³⁺, 18 mol % Yb³⁺) with an average size of 18 nm were synthesized by a solvothermal process. Then they were solved in of water (1% in weight) and the solution was excited by 980nm, a radiation which is also absorbed by the Yb³⁺ ions that subsequently transfer its excitation to the Er³⁺ ions. To measure the temperature dependence of the Er³⁺ emitted light, the sample was mounted on the top of a resistor connected to a thermocouple, so that we could monitor the sample temperature and, at the same time, the luminescence of the nanoparticles. The emitted light was sent to a monochromator (SPEX Industries model 500 M) followed by a CCD mark Synapse. Data were processed through the program LabSpec 5. In Figure 1 the Er³⁺ spectrum in the wavelength range 510-580nm is shown for two different temperatures. A change in the relative intensities of the 520nm (⁴S_{3/2}→⁴I_{15/2}) and 540nm (²H_{11/2}→⁴I_{15/2}) Er³⁺ bands occurs when increasing temperature. This change is due to a thermal redistribution in the population of the ⁴S_{3/2} and ²H_{3/2} excited states of Er³⁺ ions.

Figure 2 shows a semi logarithmic plot of the $\frac{I_{520nm}}{I_{540nm}}$ intensity ratio versus the reciprocal temperature

$\left(\frac{1}{T}\right)$. From this graph we have a temperature calibration of our system by means of the Er³⁺

luminescence.

Once we have calibrated our nano-thermometer the next step is to estimate the possibility of "gradient temperature measurements". For this purpose a pump-probe experiment was designed. By one side, the sample was illuminated by a 1.7 W, 980nm tightly focused laser beam ("the pump") that produces a thermal gradient due to a gradient in the light absorbed by water at the focal area. The left side of Figure 3 shows this gradient measured by means of a fluorescence intensity image. The intensity is higher in the focal volume of the pump laser beam and becomes smaller as far as we get away from it. Now, by using another laser resonant to the Er³⁺ ions (488nm, "the probe") we were able

to determine a temperature map as can be seen on the right side of Figure 3. In this map we can clearly appreciate the temperature gradient from the focal point (29°) and the non illuminate area (22°). This result is quite promising for measuring intracellular temperature variations.

References:

- [1]. Boyer, J.C., et al., Journal of the American Chemical Society, **Synthesis of colloidal upconverting NaYF₄ nanocrystals doped with Er³⁺, Yb³⁺ and Tm³⁺, Yb³⁺ via thermal decomposition of lanthanide trifluoroacetate precursors**. 2006. **128**(23): p. 7444-7445.
- [2]. Fiore Vetrone et al. *ACS Nano (in press)*, **Temperature Sensing at the Nanoscale using Fluorescent Nanothermometers**.

Figures:

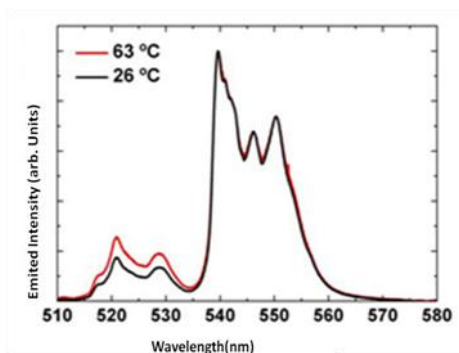


Figure 1. Upconversion emission spectra obtained at two different cuvette temperatures ($I_{exc}=920\text{nm}$)

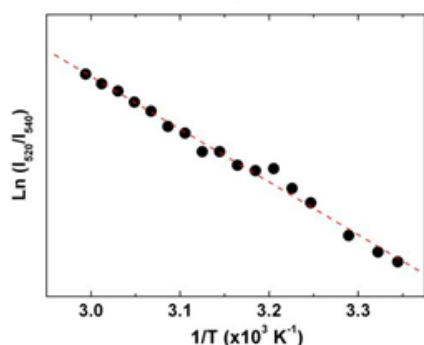


Figure 2. A plot of $\ln(I_{520\text{nm}}/I_{540\text{nm}})$ vs. $1/T$ to calibrate the thermometric scale for the water dispersible $\text{NaYF}_4:\text{Er}^{3+}, \text{Yb}^{3+}$ nanoparticles.

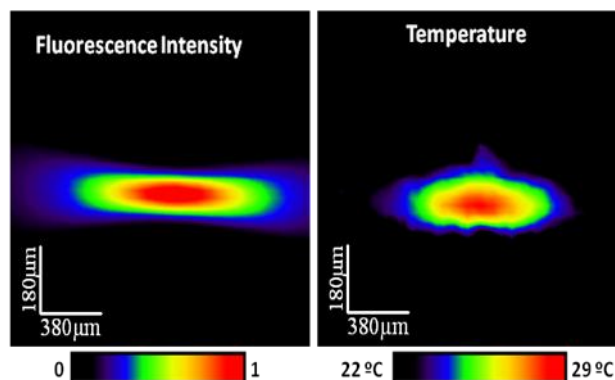


Figure 3. Right: Confocal image of the 980nm excited upconverted luminescence (pump absorbed profile). Right: Thermal image of the spot created by the 980nm pump profile

Plasmonic sensor based on gold nanodisk structures for toxic organic molecule detection

Mariluz Martínez-Marco, Francisco J. Rodríguez-Fortuño, Pedro Rodríguez-Cantó, Begoña Tomás-Navarro, Rubén Ortuño, Alejandro Martínez

Nanophotonics Technology Center, Universidad Politécnica de Valencia, Camino de vera s/n, 46022 Valencia, Spain.

pjrodrig@ntc.upv.es

Surface plasmons (SPs) are collective excitations of the free electrons at the interface between a metallic structure and a dielectric. This phenomenon can be optically observed in thin metals, in metal nanostructures and nanoparticles (NPs). Optical excitations remain localized in space in case of nanostructures [1–2]. Their unique properties enable a wide range of practical applications, having been in the past decade one of the most preferred sensing platforms for gas detection and biosensing [3] with high sensitivity and low cost. It is well-known that surface plasmon resonance (SPR) strongly depends on the refractive index of the surrounding medium (substrate, solvent, and adsorbates) of the surface/nanostructure [4]. Adsorption of molecules on the metal surface can lead to measurable spectral changes in both the wavelength and intensity of the SPR [2,5,6]. This high sensitivity allows SPR sensors to become a powerful analytical platform. In this work, we report experimental sensing results of a functionalized sensor based on plasmonic gold nanodisks, showing the capability to detect toxic organic molecules.

We designed plasmonic gold nanodisks arranged in a rectangular array on a silicon substrate [Fig. 1(a,b)] exhibiting a Mie resonance [Fig. 1(c)] around telecommunication wavelengths. Numerical CST Microwave Studio time domain simulations were performed. Simulated values are $d = 200$ nm, $h = 20$ nm and $a = 400$ nm. Silicon is modeled as $n_2 = 3.45$ and gold is modeled using Drude model with plasma frequency $\omega_p = 1.36 \times 10^{16}$ and collision frequency $\gamma = 1 \times 10^{14} \text{ s}^{-1}$. Simulations predict a sensitivity to variations in the surrounding index (n_1) of 40 nm/r.i.u. The gold nanostructure was fabricated on a silicon substrate by standard electron-beam lithography with a single PMMA (poly-methyl-methacrylate) layer followed by a lift-off process. Final thickness of the gold film is 20 nm and 5 nm layer of chromium is deposited before the gold to improve gold adhesion. Figure 1(d) shows an electron scanning microscope (SEM) image of the fabricated structure and the measured dimensions. The total sample area was $100 \times 100 \mu\text{m}$. Infrared (IR) transmission spectra for the fabricated structure were performed using a Bruker™ Fourier Transform IR spectrometer. The initial measurement after fabrication is shown in Figure 2. A resonance is observed around 1.1 μm , blueshifted with respect to simulations.

After the characterization of the plasmonic resonance spectrum and cleaning of the gold surface, we proceed chemical functionalization, performed by immersion of the gold surface in a 0,01M solution of 11-mercapto-undecanoic acid (MUA) in absolute ethanol for 3 hours. The deposition process is carried out at room temperature. In order to remove the excess reactants the sample is rinsed in absolute ethanol and deionized water and dried under a flow of dry air. The MUA monolayer is to be expected 1.7 nm thick with their thiol headgroup chemisorbed on the gold surface. The molecular axis is slightly tilted with respect to the gold surface normal [6].

For the sensing experiments we used first cadaverine (1,5-pentanediamine). The experiment was performed by immersion of the functionalized chip in 0,1 M aqueous solution of cadaverine for 10 seconds. Figure 2.A. shows the resulting transmission spectra after several binding events on the functionalized chip. The blue spectrum presents the resonance of the air-bare metal interface at 1.117 μm . The red spectrum, obtained after the metallic surface was modified with a monolayer of MUA, shows that the minimum in the transmission shifted to 1.133 μm . An additional shift to 1.186 μm , corresponding to green spectrum, was observed after the binding of cadaverine molecules to the MUA active sites. Removal of the self-assembled monolayer (SAM) from the Au surfaces is of key importance for the recycling of the sensor in order to re-obtain a clean surface. Therefore, the gold surface was cleaned with Piranha solution (1:3 mixture of 30% H_2O_2 -concentrated H_2SO_4) for 1 min, copious amount of deionized water and absolute ethanol [5]. The resonance frequency obtained from the clean surface returned nearly to the original position. Anyway, several cleaning treatments should lead to a decrease in sensing area caused by erosion of gold, which could change slightly the plasmon resonance peak of the gold nanostructure.

In order to demonstrate the gas detection capability of the optical sensor, we used another toxic organic molecule like methanediamine. In this case, the experiment was performed by exposing the functionalized chip to methanediamine vapour at 25°C for 10 s. Results from the spectral measurements are shown in Figure 2.B. Here, a relevant resonance signal shift is observed when gas molecules are adsorbed on the MUA layer. The blue spectrum corresponding to the bare gold structure presents a resonance at 1.179 μm . For the functionalized surface with MUA, the red spectrum shows a peak to 1.192 μm and, after exposing to methanediamine vapour, the resonance shifted to 1.212 μm .

We have demonstrated experimentally the use of plasmonic gold nanodisks for the detection of toxic organic molecules in both gas and in aqueous solution. It was found that the peak shift for the gas sensor is 0.011 μm and for the detection of diamine in water 0.053 μm . From these values, one can conclude that the gold nanodisk structure for sensing presents increased sensitivity with regard to other configurations like nanoholes, whose resonance shift is 0.009 μm [6]. **Acknowledgment.** Financial support by the Spanish MICINN under Contracts No. TEC2008-06871-C02-02 and CSD2008-00066 (Consolider EMET) is gratefully acknowledged.

References

- [1] S.A. Maier, M.L. Brongersma, P.G. Kik, S. Meltzer, et al, *Adv. Mater.*, 13 (2001), 1501.
- [2] R. Gradess, R. Abargues, A. Habbou, et al, *J. Mater. Chem.* 13 (2009), 10856.
- [3] R.W. Bogue, *Sensor Review*, 24 (2004), 253.
- [4] J.N. Anker, W.P. Hall, O. Lyandres, N.C. Shah, et. Al., *Nat. Mater.*, 7 (2008), 442.
- [5] K.A. Willets and R.P. Van Duyne, *Annu. Rev. Phys. Chem.*, 58 (2007), 267.
- [6] A.G. Brolo, R. Gordon, B. Leathem and K.L. Kavanagh, *Langmuir*, 20 (2004), 4813-4815.

Figures

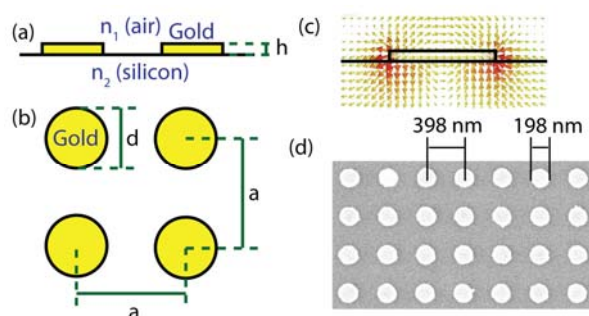


Figure 1: (a) Side view and (b) top view schematic of the designed gold nanodisks. (c) Electric field at Mie resonance. (d) Scanning electron microscope (SEM) photograph of the fabricated structure.

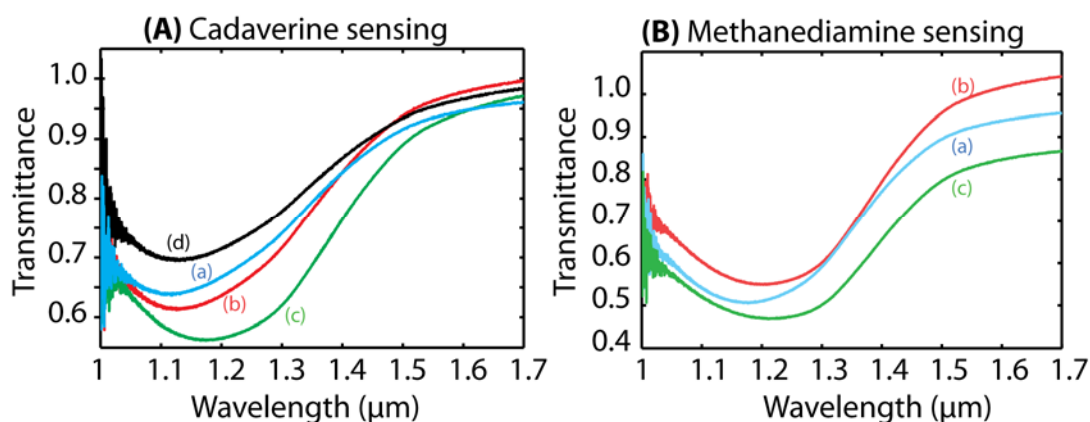


Fig. 2.A: Sensing of cadaverine in aqueous solution by chip immersion. (a) Measured transmittance spectra for the bare gold surface sample; (b) functionalized surface with MUA monolayer; (c) cadaverine detection (d) and regeneration of the resonance by cleaning of the gold surface. Fig. 2.B: Gas detection of Methanediamine. (a) Transmission spectra for the bare gold surface sample; (b) functionalized surface with MUA monolayer; (c) Resonance shift due to the adsorption of methanediamine molecules on the MUA layer.

Analysis of chromatic dispersion in symmetric and asymmetric silicon slot waveguides

Sara Mas, José Caraquitená, José V. Galán, Pablo Sanchis, and Javier Martí
Nanophotonics Technology Center, Universidad Politécnica de Valencia
Valencia 46022, Spain
smasq@ntc.upv.es

Abstract: We investigate the chromatic dispersion properties of silicon nanophotonic slot waveguides in a broad spectral region centered at $\sim 1.5\mu\text{m}$. The variation of the dispersion profile as a function of the slot fill factor, i.e., the ratio between the slot and waveguide widths, is analyzed. Symmetric as well as asymmetric geometries are considered. Two different dispersion regimes are identified.

1. Introduction

In general, any silicon-based photonic component is affected by chromatic dispersion. Then, the design and optimization of silicon photonics devices requires a very precise knowledge of the dispersion properties. In this context, the chromatic dispersion of a simple silicon waveguide with a cross-sectional area of a few μm^2 is primarily determined by the intrinsic silicon dispersion [1]. In contrast, when the cross-sectional area is reduced, the optical confinement is stronger and, then, the effective dispersion is the result of the interplay between the material and the waveguide or geometrical dispersion [2,3]. In fact, a careful control of the waveguide shape and size allows for the tailoring of the group velocity dispersion (GVD) so that normal, anomalous, or even zero GVD can be achieved in the spectral region centered at $\sim 1.5\mu\text{m}$ [2,3]. In this contribution, a detailed analysis of chromatic dispersion in silicon slot waveguides is performed. Our study shows that a careful control of the slot geometrical parameters, i. e., width and position, enables the tuning of the GVD characteristics.

2. Dispersion in silicon slot waveguides

The analysis is based on three different cross-sectional areas: $1\mu\text{m}^2$, $0.5\mu\text{m}^2$, and $0.1\mu\text{m}^2$. In addition, for simplicity, a fixed aspect ratio of 1-to-1.5 (height-to-width) will be assumed. We compute the effective index, $n_{\text{eff}}(\lambda)$, in a broad spectral range and by numerical differentiation the GVD parameter as a function of wavelength, $D_\lambda = -(\lambda/c_0)d^2n_{\text{eff}}/d\lambda^2$, is obtained. In Fig. 1(a), a typical geometry of a symmetric slot waveguide is shown. Note that the modal electric-field distribution has a strong discontinuity at the high-index-contrast interfaces and the optical field is significantly increased in the slot region. The resultant GVD curves are shown in Fig. 2(a-c), respectively. For each cross-sectional area, different slot fill factors have been considered, namely, 1:5, 1:10, 1:25, and 1:50. The fill factor is defined as the normalized ratio between the slot and the waveguide widths. The effect of the slot on the waveguide dispersion is different for each particular cross-sectional area. For a cross-sectional area equal to $1\mu\text{m}^2$, Fig. 2(a), a change in the slot fill factor translates into a relatively small variation in the GVD curve. In fact, all the dispersion profiles lie in the so-called material dispersion regime. Note that for larger fill factors, the dispersion profile exhibits a zero-GVD wavelength and, as a result, a spectral region with anomalous dispersion is found. For intermediate cross-sectional areas $\sim 0.5\mu\text{m}^2$, Fig. 2(b), we find that the slot width strongly determines the dispersion regime in which the waveguide operates. More particularly, for the fill factors 1:5 and 1:10 we have GVD profiles in a different region that we name geometrical dispersion regime while the fill factors 1:25 and 1:50 present

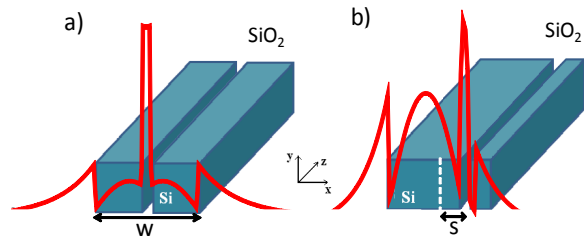


Fig. 1. (a) Symmetric slot and (b) asymmetric slot silicon-on-insulator channel waveguides with same cross sectional area. The electric field distribution of the quasi-TE mode in the x dimension corresponding to $\lambda=1.55\mu\text{m}$ is plotted.

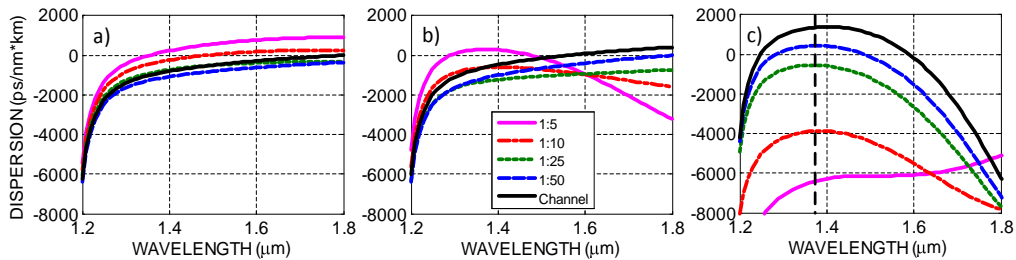


Fig. 2. Group velocity dispersion profiles of symmetric slot waveguides for different slot fill factors. Three different cross-sectional areas have been considered: (a) $1\mu\text{m}^2$, (b) $0.5\mu\text{m}^2$, and (c) $0.1\mu\text{m}^2$, with a fixed aspect ratio equal to 1:1.5. The dispersion curve of a conventional channel waveguide is also plotted.

GVD curves quite similar to the silicon material dispersion profile. For small cross-sectional areas, $0.1 \mu\text{m}^2$, Fig. 2(c), we find that the slot waveguide mostly works in the geometrical dispersion regime. Note that the dispersion curve is significantly up shifted when the slot fill factor is decreased while the wavelength with maximum-GVD is nearly constant at $1.4\mu\text{m}$. Interestingly, for 1:5 slot fill factor, a dispersion curve with a flat profile is obtained in the $\sim 1.4\mu\text{m} - 1.6\mu\text{m}$ spectral range.

In asymmetric silicon slot waveguides, the slot location is different than the geometrical center of the waveguide [4], as shown in Fig. 1(b). We define the asymmetry degree as $k=2s/w$, where s is the distance from the center of the waveguide to the center of the slot, in absolute value, and $w/2$ is half of the total width of the waveguide. We have analyzed the GVD for different asymmetry degrees, namely, $k = 0, 0.25, 0.5$, and 0.75 while keeping the same cross-sectional area. Figure 3, shows the results from numerical simulations for the three different above introduced cross-sectional areas with a fixed slot factor of 1:10. In general, we note in the figure that the GVD is more sensitive to asymmetry changes when smaller cross-sectional areas are considered. For large areas, $1 \mu\text{m}^2$, Fig. 3(a), the waveguide always operates in the material dispersion regime and a small change in the GVD is observed when the asymmetry degree is increased. For intermediate areas, $0.5 \mu\text{m}^2$, more significant changes are found in the GVD. In Fig. 3(b), by starting in the geometrical dispersion regime, a change in the asymmetry degree modifies the dispersion profile in such a way that the maximum-dispersion wavelength shifts to longer values. For larger asymmetry degrees, $k = 0.75$, the GVD is switched from the geometrical to the material dispersion regime. Finally, for small cross-sectional areas, $0.1 \mu\text{m}^2$, we find a significant larger GVD variation compared with previous examples. Note the different scales in the dispersion axis. In Fig. 3(c) the waveguide exclusively operates in the geometrical dispersion regime for all the asymmetry degrees but exhibits a variation in the maximum-dispersion wavelength.

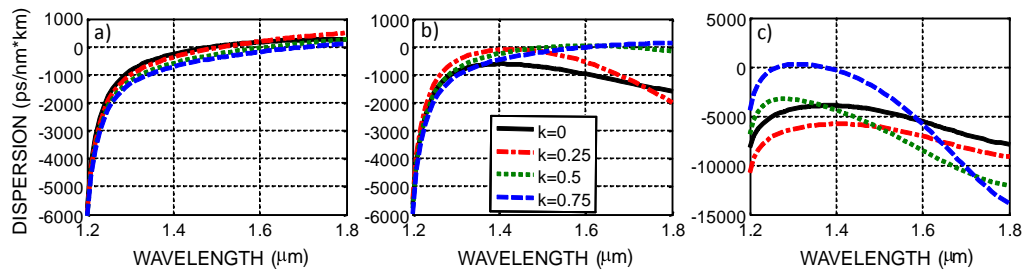


Fig. 3. Dispersion profiles for different asymmetry degrees. Three different cross-sectional areas are considered (a) $1 \mu\text{m}^2$, (b) $0.5 \mu\text{m}^2$, and (c) $0.1 \mu\text{m}^2$. The aspect ratio and the slot fill factor is 1:1.5 and 1:10, respectively.

- [1] H. K. Tsang, C. S. Wong, T. K. Liang, I. E. Day, S. W. Roberts, A. Harpin, J. Drake, and M. Asghari, *Appl. Phys. Lett.* **80** (2002) 416-418.
- [2] A. C. Turner, C. Manolatou, B. S. Schmidt, M. Lipson, M. A. Foster, J. E. Sharping, and A. L. Gaeta, *Opt. Express*, **14** (2006) 4357-4362.
- [3] L. Yin, Q. Lin, and G. P. Agrawal, *Opt. Lett.* **31** (2006) 1295-1297.
- [4] P. A. Anderson, B. S. Schmidt, and M. Lipson, *Opt. Express* **14** (2006) 9197-9202.

Aluminium nitride nano-particles and nanowires synthesised by using tube furnace

S.H. Mousavi, E. Abdoli, H. Haratizadeh

Department of Physics, Shahrood University of Technology, 3619995161, Shahrood, Iran
hadi_mousavi@yahoo.com

In recent years, researchers have been strongly focused on the synthesis of nano-crystalline AlN. In this study, the nonlinear optical properties of AlN nanostructures (nanoparticles and nanowires) in ethanol solution were studied by Z-scan technique using CW He-Ne laser at 632.8 nm. The results show a negative nonlinearity and large nonlinear refractive index. The magnitude and the sign of nonlinear refractive index, n_2 , were measured using single beam Z-scan technique. One of the principal aims of the investigation was to see how the size and morphology affects the nonlinear properties of the samples. [1-3]

In this work, we report a chemical technique for synthesis of AlN nano-particles in a horizontal three zone furnace with alumina tube. Aluminium nitride nanoparticles with different morphologies and sizes are grown on Alumina and Si substrates by thermal evaporation of a mixture of NH_4Cl and Al powders (different weight ratio) at 1000 °C for 3h under N_2 and Ar atmosphere. [4-6]

Also in this investigation, a Gaussian beam incident to a thin Kerr nonlinear sample was considered to obtain simple analytical formulas relating the z-scan curve obtained from the on axis intensity at the far field. Gaussian decomposition method has been used to analyze the characteristics of the z-scan curves for thin samples with small or large nonlinear phase shifts.

The laser beam shape and variation of the curvature radius of the wavefront have been simulated when the Gaussian laser beam passes through colloidal AlN nanowires and nanoparticles in ethanol. The effect of intensity is studied in the wave-front. The dependency of the curvature radius of the wave-front to the nonlinearity of the sample is reported. Also we have obtained the laser beam shape of AlN nanoparticle and nanowire samples as a nonlinear optical material and compared them with the experimental results. The other morphology synthesized using this method is the AlN nanowires that has been show in Fig. (2).

References

- [1] M. Miyamura, K. Tachibana and Y. Arakawa, Phys. Status Solidi a, **192** (2002) 33.
- [2] C.F. Lin, H.H. Yao, J.W. Lu, Y.L. Hsieh, H.C. Kuo and S.C. Wang, J. Cryst. Growth **261** (2004) 359.
- [3] Polyakov A Y, Smirnov N B, Govorkov A V, Frazier R M, Leifer J Y, Thaler G T, Abernathy C R, Pearton S J and Zavada J M Appl. Phys. Lett., **85** (2004) 4067.
- [4] J.H. He, R.S. Yang, Y.L. Chueh, L.J. Chou, L.J. Chen, and Z.L. Wang Adv. Mater., **18** (2006) 650-654.
- [5] Yu Qiu and Lian Gao, J. Euro. Ceram. Soc, **20** (2000) 783-787.
- [6] T. Xie, X.Y. Yuan, G.S. Wu, Y. Lin, X.X. Xu, G.W. Meng and L.D. Zhang, J. Phys.: Condens. Matter, **16** (2004) 1639–1644.

Figures

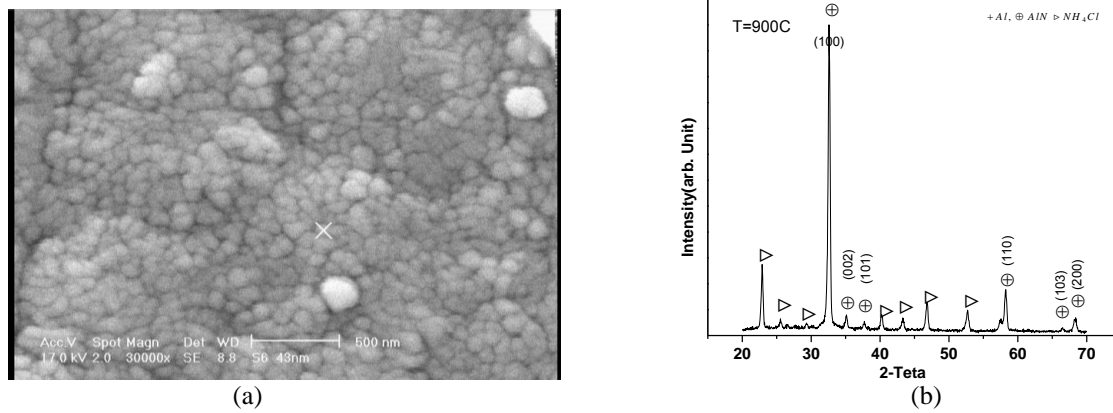


Fig. 1-(a) SEM image and (b) XRD graph of AlN nano-particles synthesized by chemical vapour deposition method.

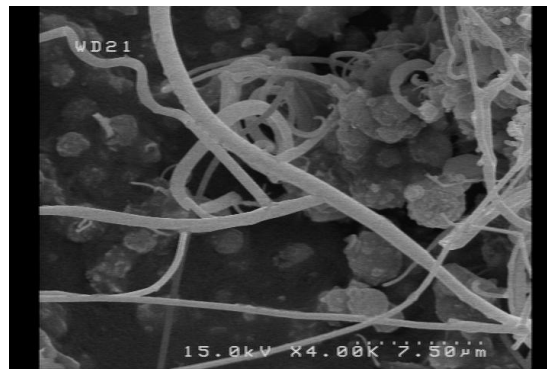


Fig (2) The FE-SEM image of synthesized nanowires

Si nanoclusters coupled to Er³⁺ ions in a SiO₂ matrix for optical amplification

D. Navarro-Urrios¹, A. Pitanti², F. Ferrarese-Lupi¹, O. Jambois¹, N. Daldosso², L. Pavesi² and B. Garrido¹

1 MIND-IN2UB, Dept. Electrònica, Universitat de Barcelona, C/ Martí i Franquès 1, 08028 Barcelona, Spain

2 Nanoscience Lab., Department of Physics, University of Trento, via Sommarive 14, Trento, Italy

dnavarro@el.ub.es

One of the scientific and technological challenges of silicon-based photonics consists in making silicon an efficient light emitter that can also provide amplification. This will allow combining both the functionality of silicon microelectronics with ultra-fast optical data generation, processing and transmission on a single silicon-based device.

Low dimensional silicon in the form of silicon nanoclusters (Si-nc) is a material with extremely interesting optoelectronic properties that differ strongly from those of bulk Si. In particular, the capacity of Si-nc to act as sensitizers of rare earth ions, specifically erbium ions (Er³⁺) [1], has opened the route towards an all-optical or electrically pumped Si based light amplifiers operating in the third telecommunication window. However, during the last years, several reports have shown what seems to be an intrinsic limit of the material itself, which is the low content of Er³⁺ taking advantage of an efficient indirect transfer mechanism [2-4].

We will focus our presentation on two studies that are crucial for the understanding and optimization of the performances of this material, in particular for samples produced by reactive magnetron co-sputtering:

i) An experimental characterization of the interaction mechanism process between excited Si-nc and Er³⁺ ions by means of fast time-resolved photoluminescence measurements. This study has revealed a Dexter type fast (less than 100ns) transfer mechanism. The energy released through a carrier intraband transition within the conduction band of the Si-nc excites the Er³⁺ ions nearby to the Si-nc surface mainly to the ⁴I_{11/2} level [5], as it can be understood from the scheme shown in figure 1.

ii) A study on the quantification of the different concentrations that determine the potentiality of the material for light amplification, which are: the total content of erbium present in the material; the concentration of ions that are optically active; the concentration of ions that are optically active and emit light; and the concentration of ions that are efficiently coupled to the Si-nc and emit light efficiently. We demonstrate the highest to date fraction of optically active Er ions coupled to Si-nc (» 52%), which produces an internal gain in waveguide samples of about 1dB/cm at 1.55μm.

References

- [1] A. J. Kenyon, P. F. Trwoga, M. Federighi, and C.W. Pitt, *J. Phys. Condens. Matter* **6**, (1994) L319
- [2] M. Wojdak, M. Klik, M. Forcales, O. B. Gusev, T. Gregorkiewicz, D. Pacifici, G. Franzò, F. Priolo, and F. Iacona, *Phys. Rev. B* **69** (2004) 233315.
- [3] G. Kik and A. Polman, *J. Appl. Phys.* **88**, (2000) 1992.
- [4] B. Garrido, C. Garcia, S. Y. Seo, P. Pellegrino, D. Navarro-Urrios, N. Dalosso, L. Pavesi, F. Gourbilleau, and R. Rizk, *Phys. Rev. B* **76**, (2007), 245308.
- [5] D. Navarro-Urrios, A. Pitanti, N. Dalosso, F. Gourbilleau, R. Rizk, B. Garrido, and L. Pavesi, *Phys. Rev. B*, **79**, (2009) 193312

Figures

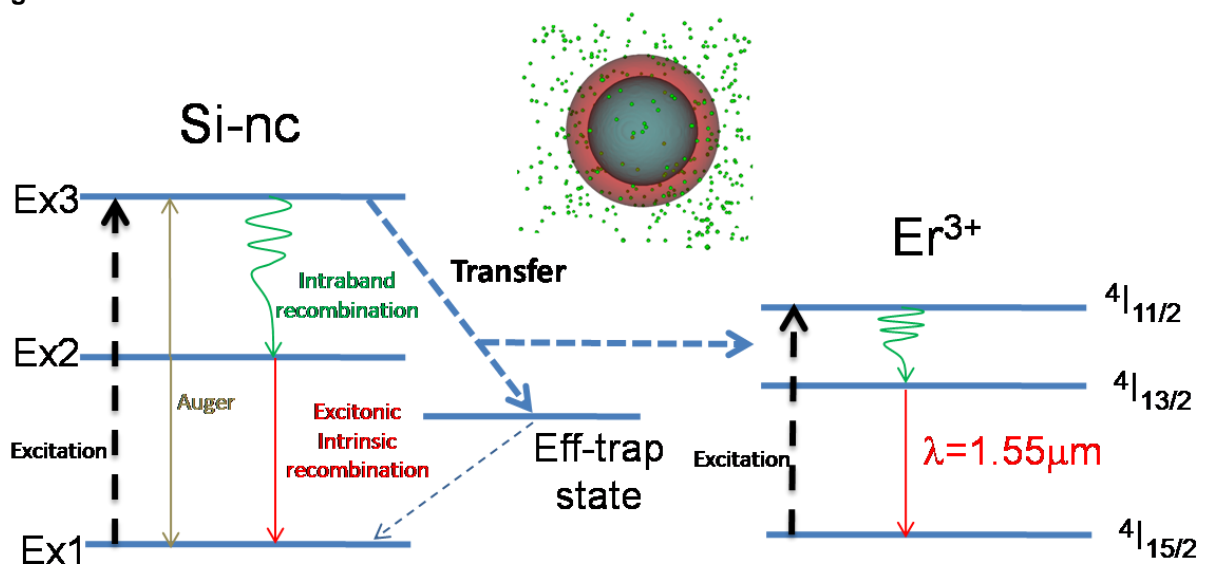


Figure 1. Scheme of the levels and transitions involved in the transfer mechanism

Geometrically induced plasmonics from the optical to the terahertz regime

M. L. Nesterov^{1,2}, D. Martin-Cano¹, A.I. Fernandez-Dominguez^{1,3}, E. Moreno¹, L. Martin-Moreno⁴,
F. J. Garcia-Vidal¹

¹Departamento de Física Teórica de la Materia Condensada, Universidad Autónoma de Madrid, España

²A. Ya. Usikov Institute for Radiophysics and Electronics, NAS of Ukraine,
12 Academician Proskura Street, 61085 Kharkov, Ukraine

³Physics Department, Blackett Laboratory, Imperial College London, Prince Consort Road,
London SW7 2BZ, United Kingdom

⁴Departamento de Física de la Materia Condensada-ICMA, Universidad de Zaragoza-CSIC,
Zaragoza, Spain

nesterovml@gmail.com

We demonstrate that the introduction of a subwavelength periodic modulation into a metallic structure strongly modifies the guiding characteristics of the surface plasmon polariton (SPP) modes supported by the system [1]. Moreover, it is also shown how a periodic corrugation could even create a new type of SPP-type mode, a domino plasmon polariton (DPP), Fig.1, in a structure that does not support surface plasmons in the non-corrugated configuration. We present a totally new design for surface plasmon polariton waveguides based on DPP for terahertz applications, which is easy to fabricate [2]. These waveguides are likely to enable interesting device applications stemming from their unique properties: a dispersion that is nearly insensitive to the waveguides' width, a nearly flat power distribution within the waveguide, an excellent field confinement factor, and reasonable loss figures.

References

[1] M. L. Nesterov, D. Martin-Cano, A. I. Fernandez-Dominguez, E. Moreno, L. Martin-Moreno, and F. J. Garcia-Vidal, *Optics Letters* **35**, (2010), 423.

[2] D. Martin-Cano, M. L. Nesterov, A. I. Fernandez-Dominguez, F. J. Garcia-Vidal, L. Martin-Moreno, and Esteban Moreno, *Optics Express* **18**, (2010), 754.

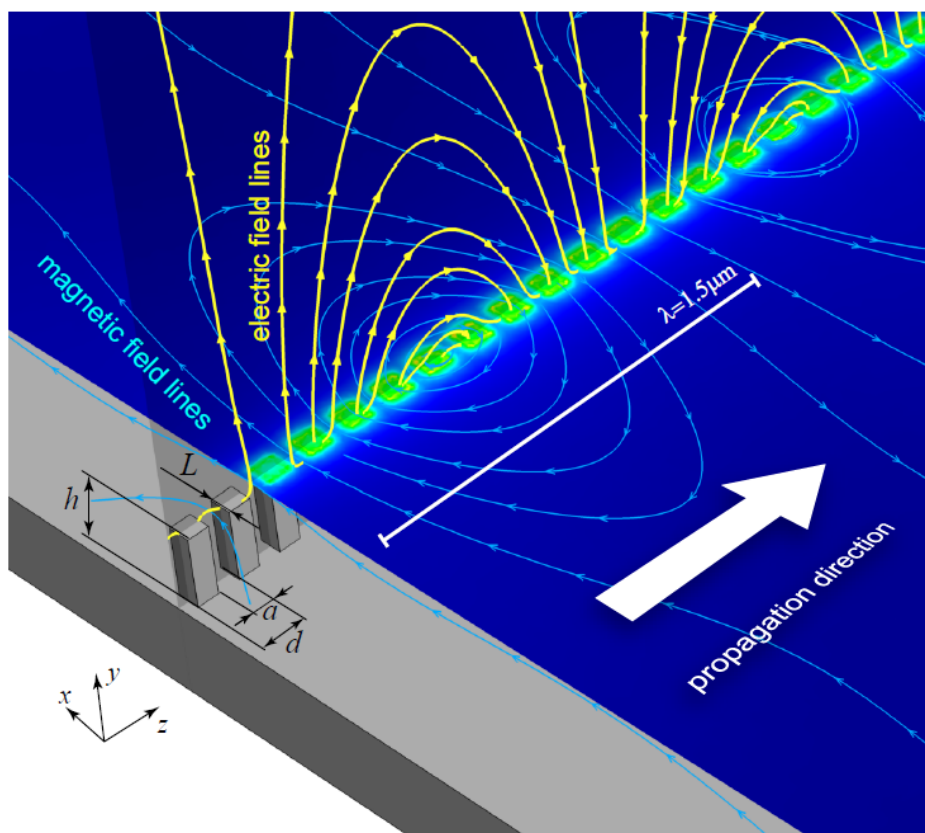


Fig. 1. Domino plasmon polariton field distribution.

Enhanced backscattering of light from randomly rough gratings on negative magnetic metamaterials

Ramón Paniagua-Domínguez, J.A.Sánchez-Gil

Instituto de Estructura de la Materia CSIC, Serrano 121 (28006), Madrid, Spain

Phone: +34 91 5616800, Fax: +34 91 5645557

P. Albella, J. M. Sáiz, F. González, F. Moreno

Grupo de Óptica, Departamento de Física Aplicada, Universidad de Cantabria,

Avd. de los Castros s/n (39005) Santander, Spain

ramon.paniagua@iem.cfmac.csic.es

We investigate the scattering formalism of the Green's theorem [1,2] including a discontinuity in the magnetic permeability μ (isotropic and homogeneous). For this purpose we make use of the continuity or saltus conditions for the EM field across the interface between media having different ε and μ . We consider the latter to be a 1D function $\zeta=\zeta(x)$ and linearly polarized light. We perform the analysis of both s-polarization and p-polarization. In this configuration we find that in p-polarization the discontinuity of the magnetic permeability has no effect on the discontinuity of the only non-zero component of the magnetic field, while in s-polarization it does affect to the discontinuity of the only non-zero component of the electric field. Having made such analysis, we find a symmetry in the intensity of the scattered fields between s- and p-polarizations when interchanging the values of ε and μ . In particular, this symmetry is also present for the intensity of the reflected fields. As a consequence, same backscattering patterns are found for s-polarization with given $\varepsilon>0$ and $\mu<0$ values and for p-polarization having ε and μ resulting of interchanging their values. Numerical analysis has been made with the aim of testing the reported symmetry for media having one of the constitutive parameters positive and the other negative. The rough surface is generated by the Montecarlo method and thus possesses a known Gaussian power spectrum characterized by the rms height δ and the correlation length of the random height a . Some studies have been performed in this direction [3] but, to the best of the authors' knowledge, the symmetry has never been pointed out.

Results

As an example, a numerical calculation of the incoherent intensities of the scattered light for p- and s-polarization is shown in Fig.1 for given values of permittivity and permeability, together with the same calculation for the symmetric situation. The enhanced backscattered peak in p-polarization for $\varepsilon=-5$ and $\mu=1$ stems from the multiple scattering of SPPs, in turn excited by sub-wavelength roughness. Conversely, s-polarized SPPs exist in the case of $\varepsilon=1$ and $\mu=-5$ [4]. Thus, enhanced backscattering peaks also occur in the angular patterns of s-polarized light (see Fig.1), identical to those of p-polarized light with interchanged ε and μ . Similarly, it will be shown that symmetric enhanced backscattering is also observed due to multiple scattering of light, when the surface roughness (correlation length a) is larger than the wavelength.

References

- [1] J. A. Sánchez-Gil, M. Nieto-Vesperinas, J. Opt. Soc. Am. A, Vol. 8, Issue 8, (1991) 1270-1286
- [2] J. A. Sánchez-Gil, J. V. García-Ramos, E. R. Méndez, Phys. Rev. B 62, (2000) 10515-10525
- [3] P. C. Ingreby, K. I. Hopcraft, E. Jakeman, Opt. Commun. 283, (2010) 1188-1191
- [4] R. Ruppin, Phys. Lett. A 227, (2000) 61-64

Figures

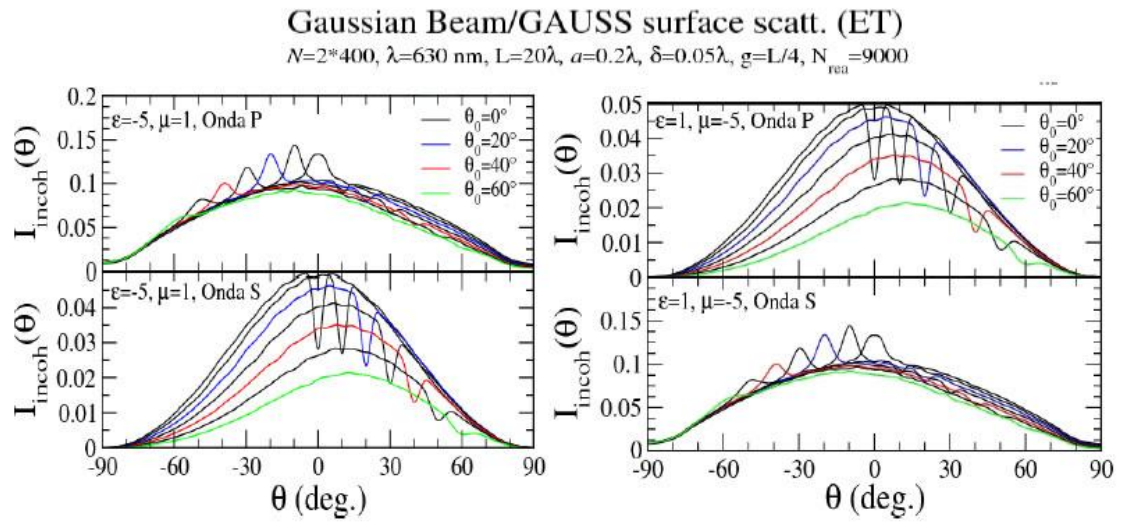


Fig.1. Angular distribution of intensities for the reflected fields. The incoherent intensities are plotted for each polarization. The reported symmetry can be readily observed.

TiO₂/Au plasmonic nanocomposite for anti-reflection coatings

Esteban Pedrueza*, J.L. Valdés, R. Abargues and J.P. Martinez-Pastor

Unidad de Materiales y Dispositivos Optoelectronicos (Unidad Asociada al IMM-CSIC), Instituto de Ciencias de los Materiales de la Universidad de Valencia, P.O. Box 22085, E-46071 Valencia, Spain

*E-mail: esteban.pedrueza@uv.es

Nanoplasmonics applied to photovoltaics is suggested as a promising strategy to increase short circuit photocurrent in solar cells, due to the enhancement of light absorption of the solar cell base material at resonant wavelengths with localized plasmons at noble metal nanoparticles (NPs) [1]. Applying a sol-gel method implemented with the spin-coating technique, one can synthesize Au NPs in solid Matrix Thin Films (MTF) of TiO₂ [2] and SiO₂ [3] on glass and Si(100) substrates, being this method easier, faster and lower cost than others.

The extinction coefficient spectrum shows a narrow band at around 2 eV (600 nm). If we increase the amount of gold present in the MTF the extinction coefficient intensity grows accordingly, as shown in Fig. 1. These spectra can be fitted (linewidth and position) by using the Mie scattering theory that takes into account the contributions of intra- and interband electrons [4,5]. With the parameters obtained from these fits and the Maxwell-Garnett effective-medium theory [6] we estimate the effective refraction index of the MTF deposited now on Si(100) and model the expected Reflectance under normal incidence of TiO₂ MTF as a function of the Au-NP filling factor (ration between the volume occupied by NPs and the total volume). By this way how the presence of Au NPs can affect the interferential behavior of the thin film Reflectance: a new minimum appears (and increase with the filling factor) on the short wavelength side of the NP Localized Surface Plasmon Resonance (LSPR), as observed in Fig. 2(a). This effect is also demonstrated experimentally, as shown in Fig. 2(b) for a MTF on silicon 90 nm thick (measured by SEM). This Reflectance minimum can be of interest in order to increase the light absorption in solar cells at the visible region, may be more useful in the case of crystalline and amorphous thin film solar cells.

References

- [1] K.R. Catchpole and A. Polman, *Optics Express*, **16** (2008) 21793.
- [2] D. Buso, J. Pacifico, A. Martucci and P. Mulvaney, *Adv. Funct. Mater.* **17** (2007), 347.
- [3] Y. Takeda, O. A. Plaksin and N. Kishimoto, *Optics Express*, **15** (2007) 6010.
- [4] H. Inouye, K. Tanaka K, I. Tanahashi, K. Hirao, *Phys. Rev. B*, **57** (1998), 11334.
- [5] L.B. Scaffardi, J. O Tocho, *Nanotechnology*, **17** (2006), 1309.
- [6] S. K. Ghosh, T. Pal, *Chem. Rev.*, **107** (2007), 4797.

Figures

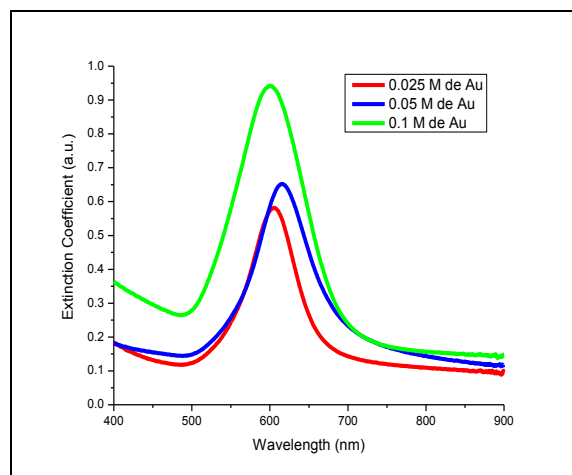


Fig. 1 Extinction coefficient spectra of TiO₂ MTF deposited on glass for different concentration of Au NPs.

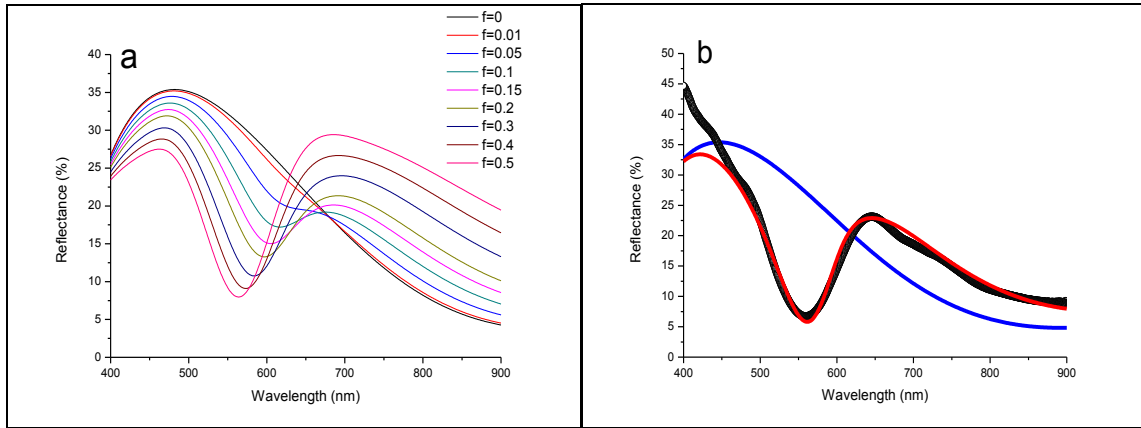


Fig. 2 (a) Reflectance of a 100nm thick TiO₂ MTF deposited on Si(100) as a function of the Au-NP filling factor, (b) Experimental reflectance for a 90 nm thick layer (black dots) with a best fitting curve using a filling factor of 0.2 (red line), in comparison to the calculated curve without nanoparticles (blue line).

Ultra low threshold room temperature lasing on photonic crystal microcavities with quantum wires

L.J. Martínez, I. Prieto, B. Alén, D. Fuster, Y. González, L. González, M.L. Dotor, L.E. Muñoz, M. Kaldirim and **P.A. Postigo**

Instituto de Microelectrónica de Madrid (IMM-CNM-CSIC)
Isaac Newton 8 –PTM- Tres Cantos 28760, Madrid, Spain
email: pabloaitor.postigo@imm.cnm.csic.es

Room temperature (RT) lasing in photonic crystal microcavities has been demonstrated around 1.3 μm using five stacked self-assembled InAs QD layers as active material [1-2]. Bordas *et al* recently reported a compact photonic crystal microlaser at RT with a single plane of InAs/InP quantum dots as gain medium [3]. Baba *et al* [4] showed RT lasing at 1.5 μm on quantum wells on InP with thresholds around 1.2 μW of effective pump power and $Q=20000$. Finally, a value of Q up to 28000 was reported by Frédérick *et al* [5] on InP- PC microcavities. In this work we show, for the first time, room temperature lasing at 1.5 μm in photonic crystal microcavities with a single layer of self-assembled quantum wires. Ultra low threshold values around 10 μW have been measured, along record quality factors exceeding $Q=55000$ using L7-type photonic crystal microcavities. Solid-source molecular beam epitaxy has been used for the synthesis of the InP/InAs epitaxial material comprising a single layer of InAs QWRs [6]. Fabrication procedure relies on electron-beam lithography and reactive ion beam etching techniques [7]. The main axis of the cavity is always parallel to the QWRs, which grow along the [1-10] direction. No lasing has been obtained for L7 cavities with axis parallel to the [110] (i.e., perpendicular to the direction of the QWRs). This shows the strong one-dimensional character of the QWRs inside the photonic cavity.

References

- [1] M. Nomura, S. Iwamoto, K. Watanabe, N. Kumagai, Y. Nakata, S. Ishida, and Y. Arakawa, *Opt. Express* 14, 6308-6315 (2006).
- [2] T. Yoshie, O.B. Shchekin, H. Chen, D.G. Deppe, and A. Scherer, *Electron. Lett.* 38, 967-968 (2002).
- [3] F. Bordas, Ch. Seassal, E. Dupuy, P. Regreny, M. Gendry, P. Viktorovich, M. J. Steel, and A. Rahmani, *Opt. Express* 17, No. 7, 5439-5445 (2009)
- [4] Kengo Nozaki, Shota Kita and Toshihiko Baba, *Opt. Express* 15, No. 12, 7506-7514 (2007)
- [5] Simon Frédérick, Dan Dalacu, Jean Lapointe, Philip J. Poole, Geof C. Aers, and Robin L. Williams, *Appl. Phys. Lett.* 89, 091115 (2006)
- [6] F. Suárez, D. Fuster, L. González, Y. González, J. M. García, and M. L. Dotor, *Appl. Phys. Lett.* 89, 091123 (2006)
- [7] L.J. Martínez *et al.* *Submitt. to J. Vac. Sci. Tech. B* (2009)

Different strategies towards the deterministic coupling of a Single QD to a Photonic Crystal Cavity Mode

I.Prieto¹, J.Herranz^{1*}, Y.González¹, P.A.Postigo¹, B.Alén¹, L.González¹, J.Martín-Sánchez¹, L.J.Martínez¹, M.Kaldirim¹, D. Fuster², J.Canet-Ferrer², G.Muñoz-Matutano², and J.Martínez-Pastor²

¹ IMM-Instituto de Microelectrónica de Madrid (CNM-CSIC), Isaac Newton 8, PTM, E-28760 Tres Cantos, Madrid, Spain

² UMDO (Unidad Asociada al CSIC-IMM), Instituto de Ciencia de Materiales, Universidad de Valencia, P.O. Box 22085, 4607 Valencia, Spain
*jesus@imm.cnm.csic.es

A single Quantum Dot (QD) coupled to a photonic cavity mode is the fundamental system for the study of Cavity Quantum Electrodynamics (CQED) phenomena in the solid state approximation[1]. These studies are essential for the development of devices such as single photon emitters and entangled photon pair sources, key elements for quantum information technologies. The successful fabrication of this kind of systems is very challenging due to the simultaneous requirements of spatial matching (the QD has to be placed at the maximum of the photonic cavity mode field) and spectral matching (both the wavelength of the QD emission and of the photonic cavity mode have to be the same) between the QD and the photonic cavity mode. Although coupling of single self-assembled QD to a photonic crystal (PC) cavity mode has already been demonstrated [2, 3], the technology is far from being mature. In this sense, the use of high spatial resolution lithographic techniques for site controlled QD formation[4, 5] is crucial in order to improve the yield of deterministic integration of a coupled QD – cavity mode[6,7].

In this work we present two strategies for coupling of InAs site-controlled QD with the mode of GaAs-based PC nanocavities. In both approaches InAs QD are formed at specific sites of the GaAs surface defined by the presence of nanoholes formed after desorption of the GaAs oxide points obtained by AFM local oxidation lithography. These site-controlled nanostructures show good optical emission properties and are efficient quantum emitters operating as single photon sources [5]. In both approaches the photonic crystal nanocavities are fabricated by e-beam lithography and dry etching (RIE) on GaAs epitaxial layers grown on 1 micron thick Al_{0.75}Ga_{0.25}As sacrificial layer by molecular beam epitaxy (MBE).

The first approach (Fig. 1) consists of the fabrication of photonic crystal nanocavities on a 105 nm thick GaAs slabs. We have fabricated L_n-type (L3 tuned, L7, L9) and H1 modified cavities. The slab thickness is smaller than the target (140 nm) for the final structure. On top of the microcavities, AFM local oxidation lithography is performed to define the nucleation site of a single QD at the the electric field maximum within the cavity. Then, a MBE re-growth process is developed for InAs QD formation and the increase (35 nm) of the thickness of the GaAs slab. This way, the final structure consists of a InAs single QD spatially located at the predefined position by AFM local oxidation lithography embedded in a photonic cavity slab with the appropriate thickness for optical coupling to the photonic cavity. Our results show that this process leads to a strong evolution of the round shape of the PC holes that degrades the quality factor (Q) of the cavity mode. Some attempts for minimizing the shape evolution of the round holes by changing the crystallographic direction along which the PC round holes are fabricated will be shown. Optical micro-PL emission carried out by confocal microscopy at 77K of the re-grown nanostructures will be shown.

In the second approach an etched ruler is fabricated by using e-beam lithography and dry etching (RIE) on a 65nm-thick GaAs epitaxial layer. Then, AFM local oxidation lithography is

performed to define the nucleation sites of InAs QDs and their position coordinates are recorded with respect to the fabricated ruler (Fig 2). The formation of InAs QD and the target thickness of the slab with the embedded site controlled InAs single QD is later completed by the developed MBE re-growth process. Micro-photoluminescence characterization of these site controlled QDs will be made in order to know their actual emission wavelengths. This way, we could access to know both the spatial coordinates and the emission wavelength of every QD. In this situation, a PC cavity can be designed for matching the emission wavelength of the embedded QD and later fabricate around the previously recorded position coordinates of the QD with respect to the ruler.

References

- [1] T. Yoshie et al., *Nature* **432** (2004) 200.
- [2] A. Badolato et al., *Science*, **308** (2005), 1158.
- [3] K. Hennesy et al., *Nature* **445** (2007), 896.
- [4] T. Sünner et al., *Opt. Lett* **33** (2008), 1759.
- [5] J. Martin-Sanchez et al., *ACS Nano* **3** (2009), 1513.
- [6] S. M. Thon et al., *App Phys Lett* **94** (2009) 111115.
- [7] D. Englund et al., *Proc. SPIE* **7611** (2010) 7611OP.

Figures

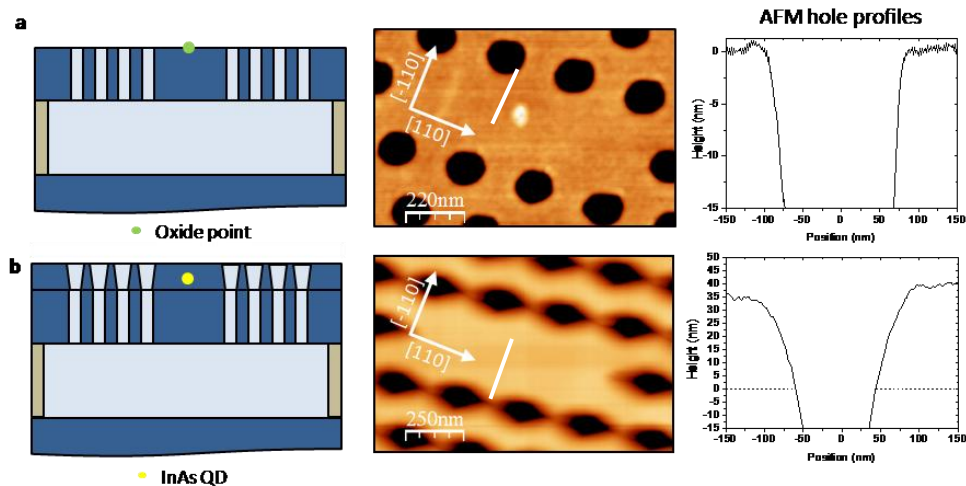


Figure 1. First approximation: Site controlled InAs QD fabrication at the maximum of the electric field of a pre-patterned photonic crystal cavity. Different process steps and the corresponding AFM images: (a) Fabrication of the photonic crystal structure (SEM-RIE) and GaAs oxide dot (AFM local oxidation) on a GaAs 105 nm thick slab; (b) The structure is completed by a MBE regrowth process up to 140nm thickness with an embedded site-controlled InAs QD placed 20nm below the surface. AFM profiles show the change on the hole shape due to the regrowth step.

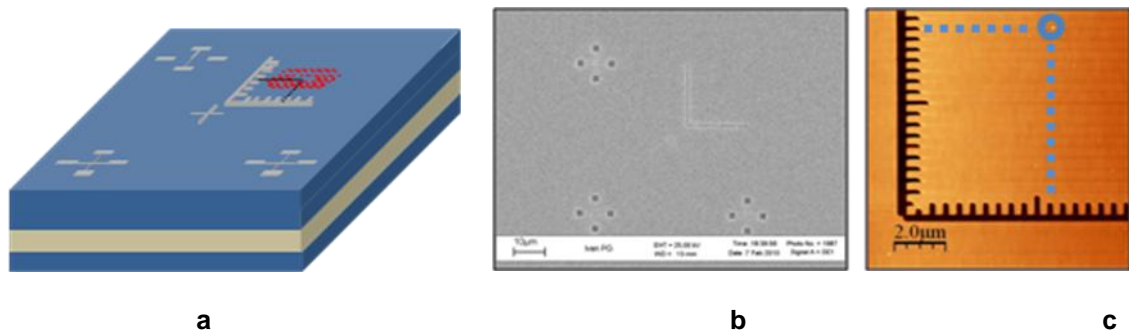


Figure 2. Second approximation: Deterministic cavity fabrication around site controlled InAs QD positioned respect to a pre-patterned etched ruler. (a) Sketch of the final structure with a photonic cavity fabricated at the position of a site-controlled InAs QD, with coordinates set by the etched ruler. (b) SEM image of the fabricated etched ruler with the alignment marks. (c) AFM image of an actual GaAs oxide dot obtained by AFM local oxidation with known coordinates respect to the ruler.

Thermal effects of quantum dots InAs/GaAs with In_xGa_{1-x}As confinement barriers

I. Suárez^a, D. Rivas^b, G. Muñoz-Matutano^b, L. Seravalli^c, G. Trevisi^c, P. Frigeri^c and J. Martínez Pástor^b

^a IMM Instituto de Microelectrónica de Madrid (CNM, CSIC), Isaac Newton, 28760 Tres Cantos, Madrid, Spain

^b Instituto de Ciencias de los Materiales, Universidad de Valencia, POBox 22085, 46071 Valencia, España

^c Instituto dei Materiali per l'Elettronica e il Magnetismo (CNR), Parco delle Scienze 37/a, I-431000 Parma, Italia

isaac.suarez@uv.es

Development of self assembled InAs/GaAs quantum dot (QDs) has led an important advance in the optoelectronic technology. One of its main interests comes from the emission of entangled photons [1], and the possibility to integrate such quantum optical active medium with the GaAs technology [2]. However these nanostructures have usually disadvantages, as for example strong decrease of the emission intensity with the temperature or difficulties to obtaining QDs with emission wavelengths over 1 μm [3]. This work studies the effect of growing InAs QDs under In_xGa_{1-x}As confinement layers (CLs) [4] [5], in order to reduce the QD-CL band discontinuities and to achieve a redshift in the emission wavelength. For this purpose self assembled QDs have been grown on a GaAs substrate under 10 nm of an In_xGa_{1-x}As layer. Four samples with different In compositions ($x = 0, 0.1, 0.2, 0.3$) have been prepared. The final structures were capped by 20 nm GaAs layer. Samples have been characterized by photoluminescence (PL) and time resolved luminescence (TRPL) in function of the temperature.

PL experiments show emission between 1 and 1.4 μm . The exact emission wavelength depends on the barrier composition; being the emission wavelength proportional to the amount of indium in the barrier. All samples have a bimodal size distribution. Temperature dependence of the PLs shows a constant intensity for temperatures lower than 120 K and a double decay time evolution when the temperature is raised. First of all, there is a slow decay for temperatures between 120 and 220 K, and then a fast decay appears when the temperature is higher than 220K. The behaviour can be modelled by Arrhenius dependence with two activation energies, involving two different mechanisms of escape. The second activation energy (fast decay) is always close to the difference between the wetting layer (WL) and QD energy. Thus, this second mechanism has been attributed to escape from the QD to the WL. The exact activation energy depends on the indium content, implying an important role of this barrier into the QD's dynamics.

TRPL's measurements have been realized in function of the temperature at the corresponding emission energies of the two families. As well, the sample with highest indium content ($x = 0.3$) has been thoroughly studied, covering the whole emission range. TRPL behaviour strongly depends on the emission energy and the barrier composition, but in all cases recombination times increase with temperature before a strong decay when the temperature reaches 220 K. This behaviour is attributed to the appearance of dark states as has been proposed elsewhere [6, 7].

Red-shift and room temperature behaviour obtained in the nanostructures proposed in this work could be helpful in the implementation of new optoelectronic devices, because nowadays there is a great interest of developing quantum optical devices at long wavelengths (in particular the telecommunication windows 1.3 and 1.55 μm).

References

- [1] R.J. Warburton, *Contemporary Physics*, **43**, 3 (2002) 51
- [2] A. J. Shields, *Nature Photonics*, **1** (2007) 215
- [3] L. Seravalli, M. Minelli, P. Frigeri, S. Franchi, G. Guizzetti, M. Patrini, T. Ciabattini, and M. Geddo, *Journal of Applied Physics*, **101** (2007) 024313
- [4] T.V. Torchynska, J.L. Casas Espinola, L.V. Borkovska, S. Ostapenko, M. Dybiec, O. Polupan, N. O. Korkunska, A. Stintz, P.G. Eliseev and K.J. Malloy, *Journal of Applied Physics*, **101** (2007) 024323
- [5] G. Trevisi, L. Seravalli, P. Frigeri, and S. Franchi, *Nanotechnology* **20** (2009) 415607.
- [6] J. Gomis, J. Martínez-Pástor, B. alén, D. Granados, J.M. García and P. Roussignol, *The European Physics Journal B*, **54** (2006) 471
- [7] C.H. Lin, H.S. Lin, C.C. Huang, S.K. Su, S.D. Lin, K.W. Sun, C.P. Lee, Y.K. Liu, M.D. Yang and J.L. Shen, *Applied Physics Letters*, **94** (2009) 183101

Surface integral formulation for light scattering from 3D objects: surface plasmon resonances in metallic nanoantennas

Rogelio Rodríguez-Oliveros, J.A.Sánchez-Gil

Instituto de Estructura de la Materia CSIC, Serrano 121 (28006), Madrid, Spain

Phone: +34 91 5616800, Fax: +34 91 5645557

Rogelio@iem.cfmac.csic.es

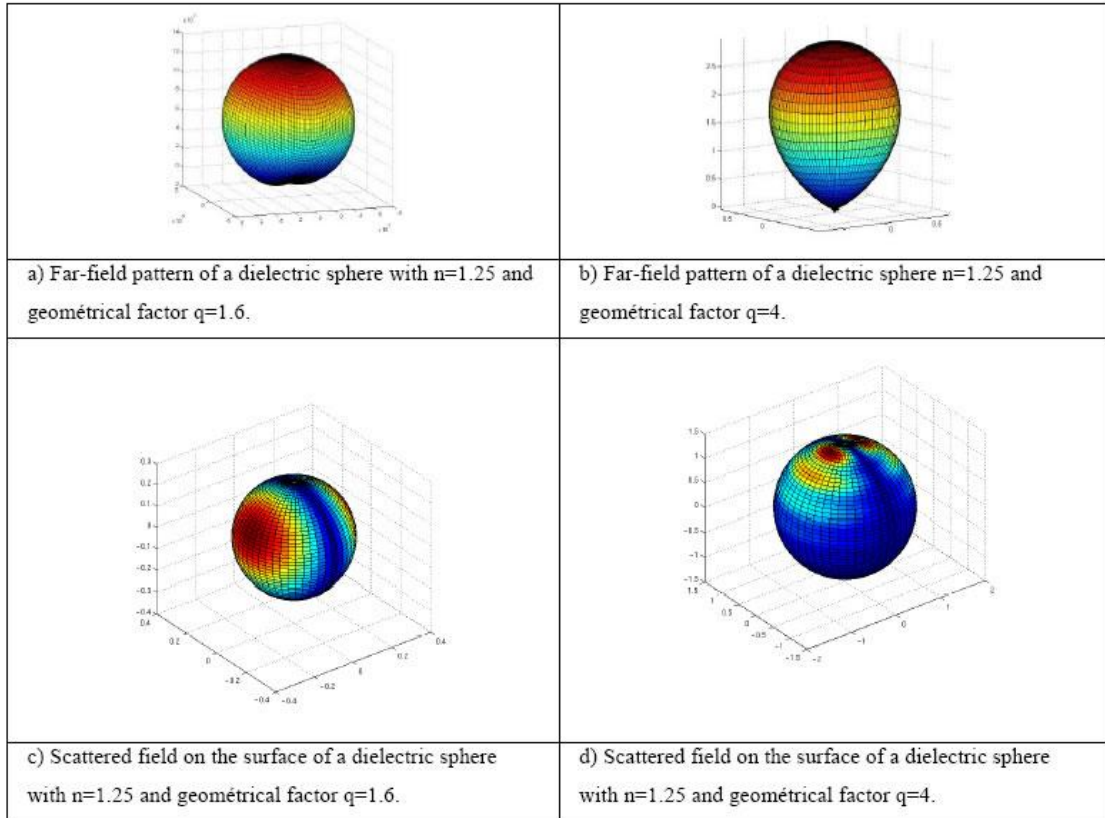
We develop theoretically and numerically a rigorous method to investigate the EM wave scattering from 3D objects with arbitrary surfaces and dielectric function. The formulation is based on the surface integral equations for the electric and magnetic fields given by the Stratton-Chu formulas [1,2,3]. The integral equations are generalized for a 3D object with its surface in parametric coordinates (recently derived for 2D objects in Ref. [4]). The electric and magnetic fields are expressed in terms of two tangential components to the surface and a normal one, in order to get physical insight into the induced EM fields in the surface of the scatterer. In fact, it is shown that the surface integral equations are remarkably simplified if the parametric coordinates are chosen so that an orthonormal basis can be defined on the surface, and if the chosen basis is an intrinsic basis of the surface, defined in terms of two tangent vectors and the normal one. This simplification is in turn crucial in the numerical implementation of the surface integral scattering equations, converted into matrix equations for the surface EM field components by discretizing the surface through a quadrature scheme.

Finally, it should be emphasized that this formalism straightforwardly allows one to deal with an arbitrary number of scatterers and shapes, with the advantage that it scales with the scatterer surface (rather than its volume). In particular, this method will be exploited to investigate surface plasmon resonances in complex 3D metallic nanoparticles, obtaining far-field patterns Fig(1)(a,b), scattering cross sections, near-field maps and surface charge distributions Fig(1)(c,d) as done for 2D nanoparticles (nanowires) in Ref. [4]. If a point dipole source is considered instead of a plane wave, single molecule fluorescence (and/or quantum dot emission) close to metallic nanoantennas can be thoroughly explored by calculating radiative and nonradiative decay rates (and quantum yields), addressing crucial issues as the modification and enhancement (or quenching) of spontaneous emission in (bio)molecular and optoelectronic systems due to the strong impact on the local EM density of states of surface plasmon resonances in dimer nanoantennas [5].

References

- [1]P. Tran and A. A. Maradudin, *Opt. Commun.* 110 , 269-273 (1994).
- [2]Andreas M. Kern and Olivier J. F. Martin, *J. Opt. Soc. Am. A* 26 (4), 732-740 (2009)
- [3]Manuel Nieto-Vesperinas, *Scattering and diffraction in physical optics.* (Wiley-Interscience, New York 1991)
- [4]V.Giannini and J.A.Sánchez-Gil, *J.Opt.Soc.Am.* 24 , 2822-2830 (2007) .
- [5]O.L.Muskens, V.Giannini, J.A.Sánchez-Gil, and J.Gómez Rivas. 7 , 2871-2875 (2007).

Figures



All-nanoparticles based Optical Resonators for detection of gases and liquids

Olalla Sánchez-Sobrado, Mauricio.E.Calvo, Nuria Núñez, Manuel Ocaña, Gabriel Lozano and Hernán Míguez*

Instituto de Ciencia de Materiales de Sevilla (CSIC-US), Sevilla (Spain)

herman@icmse.csic.es

In last years, nanoparticles based one dimension photonic crystals (NP-1DPC) have developed high optical and structural qualities. They have already become a very important component of photonic devices like dye solar cells. They also present an important potential as optical resonators, due to their capacity to house many different types of light emitters, with many different irregular shapes, like rare earths based nanophosphors. Herein we show that the photoemission spectrum of nanophosphors can be precisely controlled by integrating them in a rationally design photonic environment. In this work, we present a versatile method to embed these kind of nanophosphors of arbitrary shape in optical resonators built up within NP-1DPC [1]. By precise control of the spectral features of such cavity modes, luminescence is amplified or suppressed in selected and tuneable wavelength ranges. We also demonstrate that the porous character of the building blocks of these photonic crystals provides a responsive multifunctional matrix, totally different emission spectra being attained from the same nanophosphors by environmentally induced changes of the cavity modes. This fact makes these structures perfect for the detection of liquids and gases.

References

[1] O.Sánchez-Sobrado, M.E.Calvo, N.Núñez, M.Ocaña, G.Lozano, H.Míguez, *Nanoscale*, 10.103a/b9nr00338

Figures

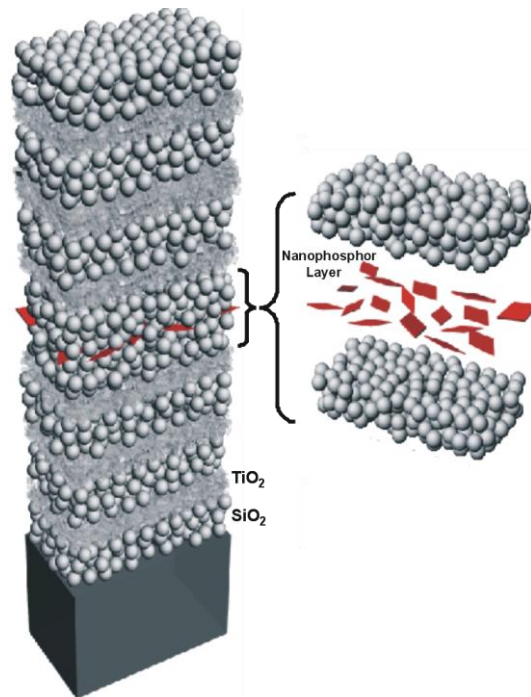


Figure 1. Model of the proposed all-nanoparticle based optical resonator. Spherical beads represent SiO_2 nanocolloids, smaller ones of irregular shape are TiO_2 nanocrystals and (red) rhombic particles are the embedded nanophosphors. On the left, the different components of the optical cavity are amplified and separated for the sake of clarity.

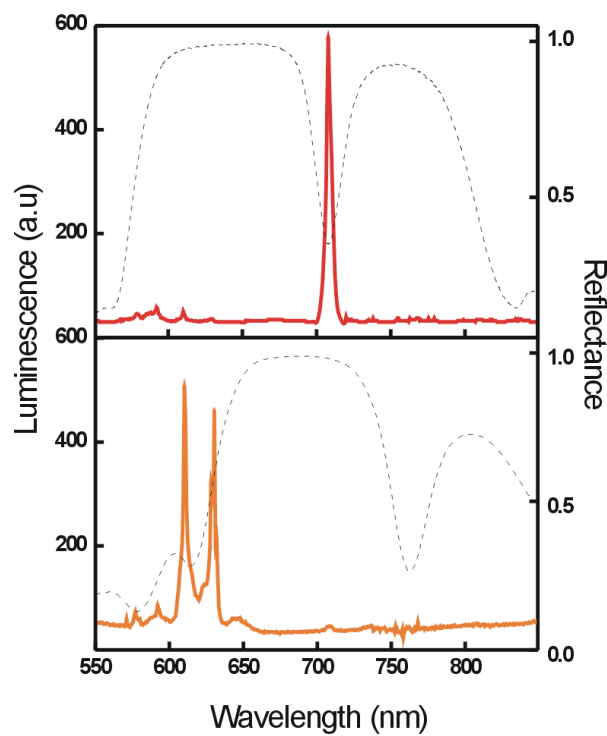


Figure 2. Luminescence (thick lines) and reflectance (thin lines) spectra obtained from a nanophosphor containing optical resonator built using two Bragg mirrors made of 5 unit cells (a) before and (b) after being infiltrated with ethanol.

Photonic Hall-effect for a single nanoparticle

Irene Suárez-Lacalle and Juan José Sáenz

Departamento de Física de la Materia Condensada, Universidad Autónoma de Madrid,
Campus de Cantoblanco, 28049 Madrid, Spain.

Quantum Hall effect arises when electrons are subject to a large magnetic field due to the fact that electrons experience a Lorentz force as they are charged. Despite the absence of photonic charge, it has been observed that a similar effect, a photonic Hall-effect, appears when light is subject as well to a magnetic field, although the origin of the effect is very different.

This photonic Hall-effect, or magneto-transverse anisotropy, in light scattering, is of actual interest and is the basis of interesting phenomena [1,2]. The Hall effect of a single scatterer is important by itself. In particular, Hall effect for a Mie sphere has been addressed long before [3]. In these studies it was argued that in the small particle regime (the so called Rayleigh scattering regime) there were no net magneto-transverse scattering effects [3].

Radiative corrections have shown to be important to analyze magneto-optic properties of small nanoparticles [4]. As we will show, Optical Hall-effect in small dipolar particles does exist, arising as a consequence of the radiative corrections to the polarizability.

References

- [1] Z. Wang, Y. Chong, J.D. Joannopoulos & M. Soljacic, *Nature* **461**, 772 (2009)
- [2] F.D. Haldane, S. Raghu, *Phys. Rev. Lett.*, **100**, 013904 (2008)
- [3] D. Lacoste, B.A. van Tiggelen, G.L.K.A. Rikken, A. Sparanberg, *J. Opt. Soc. Am.*, **15**, 1636 (1998)
- [4] S. Albaladejo et al., *Opt. Express* **18**, 3556 (2010).

Zero bandwidth mode on a split ring resonator loaded waveguide at cutoff

B. Tomás-Navarro, F. J. Rodríguez-Fortuño, R. Ortuño, C. García-Meca and A. Martínez.
Nanophotonics Technology Center, Universitat Politècnica de Valencia, 46022 Valencia, Spain
betomna@ntc.upv.es

Abstract. We analyze the electromagnetic field propagation through a rectangular metallic waveguide loaded with an array of SRRs. If the split ring resonator frequency matches the cutoff frequency f_c of the hollow metallic waveguide, a flat mode is attained. To perform our study we calculate the dispersion relation using a simple transfer matrix model and confirm the results with electromagnetic simulations.

It is well known that left-handed propagation can be obtained in a structure conformed by SSRs (that can achieve negative permeability) inserted in a medium with a negative permittivity in the same region [1][2]. A square waveguide can model a one-dimensional plasma [3] with negative effective permittivity below cutoff, and therefore by introducing an array of SRRs, effective negative permeability and permittivity lead to a left-handed behavior. In this presentation we further study such configuration and obtain further interesting results in the case in which the SRR resonant frequency f_0 approaches the cutoff frequency f_c of the waveguide. We evade the effective medium explanation, due to the fact that we do not restrict ourselves to a subwavelength periodicity, and instead develop a model based on transfer matrix theory.

The structure that we analyze is shown in Fig. 1(a). The proposed circuit model for the unit cell can be seen in Fig. 1(b). Note that the model does not include electric excitation of the SRR resonance since it is small and will hardly affect the obtained response. The transmission matrix of the unit cell model is given by:

$$\mathbf{T} = \mathbf{SRR}(\omega, R, L, C, M) \cdot \mathbf{TL}(\omega, \beta, Z_c, a_z) \quad (1)$$

where $\mathbf{TL}(\omega, \beta, Z_c, a_z)$ represents the transmission matrix of a transmission line with propagation constant $\beta = \sqrt{\omega^2 \mu \epsilon_{\text{eff}} - (\pi/a)^2}$, characteristic impedance $Z_c = \omega \mu / \beta$ and length a_z , and $\mathbf{SRR}(\omega, R, L, C, M)$ represents the transmission matrix of the SRR [4][5]. Equating $2 \cos(ka_z)$ with the sum of the diagonal elements of \mathbf{T} yields the dispersion relation of the periodic structure [6], given by:

$$2 \cos(ka_z) = f(\omega) = 2 \cos(\beta a_z) + \frac{\omega \cdot M^2}{L} \left(\frac{1}{1 - \omega_0^2 / \omega^2 - jR/L\omega} \right) \cdot \frac{\sin(\beta a_z)}{Z_c} \quad (2)$$

where k is the Bloch wavevector and a_z is the periodicity. Note that a propagating mode exists at a given frequency ω only if $-2 < f(\omega) < 2$. The first term of $f(\omega)$ is the term corresponding to the waveguide without rings and the second one is due to the presence of the rings. The second term is asymptotic at f_0 and responsible for the passband that appears near f_0 . The width of this passband can be controlled by $\omega \cdot M^2 / L$ and $\sin(\beta a_z)$ so that their value at f_0 determines the bandwidth of the mode. Interestingly, the bandwidth tends to zero when the resonance of the rings f_0 takes place at a frequency at which $\sin(\beta a_z) \rightarrow 0$. This condition can be stated as:

$$\beta \Big|_{f=f_0} a_z = m\pi \quad (3)$$

In particular, if f_0 coincides with the cutoff frequency of the waveguide ($\beta = 0$), the condition (3) is achieved and a zero bandwidth mode is obtained. In order to check this result, we study a similar configuration to that presented in [3] where Marques *et. al.* demonstrate that a left-handed passband arises when the resonance frequency of the SRRs occurs below the cutoff frequency of the hollow metallic waveguide. We adjust the shape and dimensions of the SRRs to vary their resonance frequency. In particular we study in depth what occurs when the operation frequency of the SRRs is either below, above or coincident with the cutoff frequency of the waveguide. To do so we perform eigenmode electromagnetic simulations using the commercial software CST Microwave StudioTM in order to compare the numerical results with the predictions of the model. In Fig. 1(c-e) the dispersion relation described by the model and that obtained with the simulations are shown. We vary the resonance frequency of the rings around the cutoff frequency f_c of the waveguide (we call f_c to the cutoff frequency of the waveguide *without* SRRs, but considering the substrate placed inside). In the first case, when the resonance frequency of the rings (f_0) is lower than f_c a left-handed passband is observed, in

agreement with [3]. When $f_0 > f_c$ the slope of the band flips its sign. At the threshold between both cases, when $f_0 \approx f_c$, a zero-bandwidth band arises. Note that in that case the original cutoff frequency of the TE₁₀ mode is slightly upshifted in frequency away from the flat passband. These phenomena are predicted by the model and confirmed by the simulations. In Fig. 1(f) a plot of the group velocity at the inflection point of the passband (the point of maximum group velocity) as a function of f_0 is shown. The flip in the sign of the slope is clearly seen, as well as the point of zero group velocity. Note that, at cutoff, the waveguide shows no phase advance ($\beta = 0$), so each successive SRR “feels” the effect of the other SRRs with no phase retardation, which can be key to understanding the existence of the zero-bandwidth passband. A similar argument stands for the general condition given by Eq. (3) [although for odd values of m , the phase advance of the fields propagating in the waveguide between successive SRRs is π].

In conclusion, we have modeled a rectangular metallic waveguide loaded with an array of SRRs with a simple transfer matrix model. The calculated dispersion relation shows very close agreement with the simulations. A forward, backward or zero-bandwidth mode can be easily achieved by choosing f_0 adequately. A condition for achieving a zero-bandwidth passband is presented.

Financial support by the Spanish MICINN under contract CONSOLIDER EMET (CSD2008-00066) is gratefully acknowledged. F.J. Rodríguez-Fortuño, C. García-Meca and R. Ortuño acknowledge financial support from grants FPI of Generalitat Valenciana, FPU of MICINN and FPI of Universidad Politécnica de Valencia, respectively.

References

- [1] J. B. Pendry, A. J. Holden, D. J. Robbins and W. J. Stewart, IEEE Trans. on Mic. Th. And Techniques. **47** (1999) 2075-2084
- [2] R. A. Shelby, D. R. Smith, and S. Schultz, *Science*, **292** (2001) 77-79
- [3] R. Marqués, J. Martel, F. Mesa and F. Medina, Phys. Rev. Lett. **89** (2002) 183901
- [4] R. R. A. Syms, E. Shamonina and V. Kalinin, J. Appl. Phys. **97** (2005) 064909
- [5] L. Solymar and E. Shamonina, “Waves in metamaterials” (Oxford University Press US, 2009)
- [6] L. Brillouin, “Wave propagation in periodic structures” (McGraw-Hill, London, 1946)

Figures

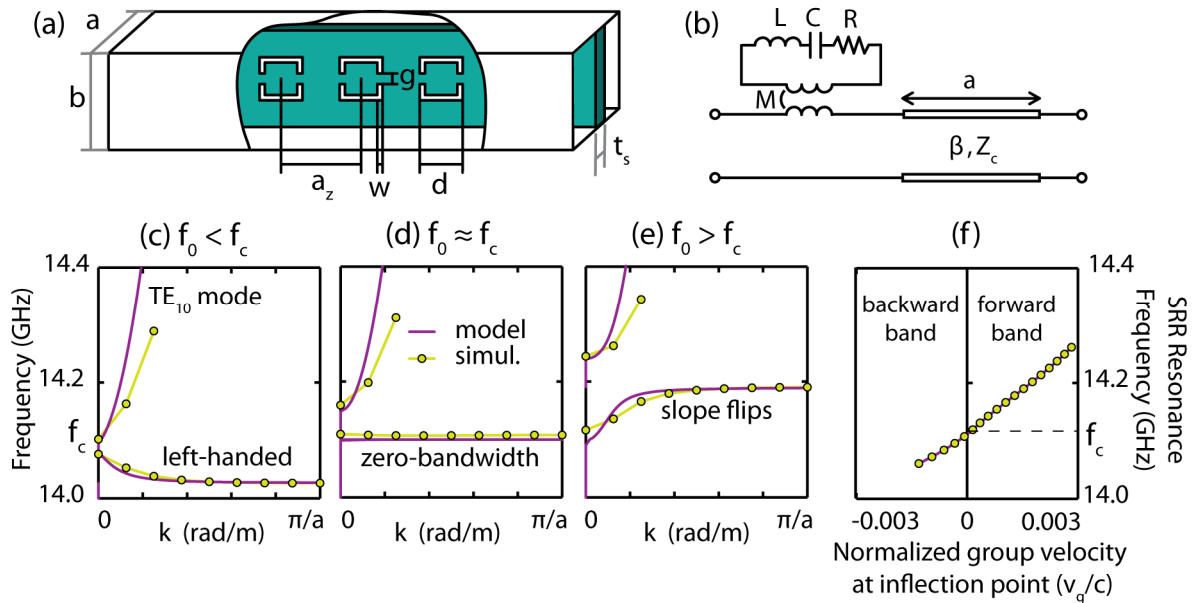


Figure 1. (a) Simulated SRR loaded waveguide. (b) Proposed circuit model for the SRR-loaded waveguide unit cell. (c-e) Modeled and simulated dispersion relations for (c) $\omega_0 < \omega_c$, (d) $\omega_0 \approx \omega_c$, and (e) $\omega_0 > \omega_c$. The parameters in the simulation (all dimensions are in mm) are: $a = b = a_z = 6$, $d = 5.2s$, $w = 0.5s$, $g = 1s$, $a_z = 10$, $t_s = 0.49$, $\epsilon_{\text{substrate}} = 3.45^2$ and thickness of the metal $t_m = 0.017$, where s is a reference feature size (c) $s = 0.48$, (d) $s = 0.4765$, (e) $s = 0.473$. The parameters used in the model are $\mu = \mu_0$, $\epsilon_{\text{eff}} = 3.14\epsilon_0$, $M^2/L = 4.7/\omega_0$, and (c) $f_0 = 14.026$ GHz, (d) $f_0 = 14.1$ GHz, (e) $f_0 = 14.19$ GHz. The parameters in the model such as M or ϵ_{eff} where chosen to fit simulations. (f) Simulated normalized group velocity at the passband inflection point plotted against the resonance frequency of the SRRs.

Spectral Behaviour of Thick Metal Films Perforated with Nanoholes

Ahmad Reza Hajiaboli¹, Mojtaba Kahrizi¹, **Vo-Van Truong**²

¹Department of Electrical and Computer Engineering, Concordia University

²Department of Physics, Concordia University 1455 de Maisonneuve Blvd. West, Montreal, QC, Canada

Email: truong.vo-van@concordia.ca

In the absence of a universally accepted model that describes the physics of the anomalous transmission spectrum of an array of nanoholes on optically thick metallic films, an extensive numerical calculation is presented in this paper to relate the scattering modes observed to transmittance spectral behavior. Surface plasmon polariton Bloch Waves (SPP BW), Wood's Anomalies (WA) and Localized Surface Plasmon Resonances (LSPR) at the rim of the nanoholes are investigated based on scattering modes that form the features of the transmission spectrum, i.e. maxima and minima. The impact of each of these optical phenomenon on the transmission process is discussed. The Finite Difference Time Domain (FDTD) method is applied to calculate the transmission intensity from films of gold and silver subjected to variations in geometrical parameters such as film thickness, hole spatial period (i.e. center to center distance of the holes) and hole diameter. Analysis of transmission spectra showed that the cut-off frequency of the array of subwavelength holes is mostly defined by the thickness of the film and the diameter of the holes rather than the periodicity of the structures.

Optical Near-Field Characterization of Plasmonic and Magnetoplasmonic Nanostructures

A. Vitrey, E. Ferreiro-Vila, A. García-Martín, M. U. González, J.M. García-Martín

Instituto de Microelectrónica de Madrid, IMM-CNM-CSIC, Calle Isaac Newton, 8
28760 Tres Cantos, Spain
alan.vitrey@imm.cnm.csic.es

Most plasmonic devices are passive devices since their electromagnetic properties depend mainly on fixed properties such as the shape of the structures, their constitutive materials, and the dielectric media. A way to turn plasmonic devices into active ones is to use ferromagnetic metals, since due to their magneto-optical (MO) activity the optical response when applying an external low magnetic field can be modified. Unfortunately, plasmon resonances are critically broadened in ferromagnetic materials due to their important electromagnetic losses. An alternative is to combine ferromagnetic materials with noble metals. Recently, we have demonstrated that Au/Co/Au nanodisks exhibit enhanced magnetoplasmonic properties such as a significant increase of the MO activity when the localized surface plasmon (LSP) resonance is excited^[1,2].

Understanding the interplay between the LSP excitation and the MO activity is relevant from both fundamental and technological viewpoints. A path to this comprehension is to correlate the behavior of the LSP induced electromagnetic field and the MO activity. It has been clearly shown that the increase of MO activity is related to the enhancement of electromagnetic field penetrating into the Co layer^[2]. In that way, the goal of this work is to characterize the distribution of the near field at the surface of the nanostructures as a function of their morphologies but also as a function of the position and the size of the ferromagnetic layer. This study is achieved by combining Scanning Near-field Optical Microscopy (SNOM) with far-field optical and MO characterization as well as with FDTD simulations (see Figure). The lasers used to perform near field experiments and the LSP resonance of structures must have their wavelength close enough to couple efficiently the light with the LSP. Our studies concerning Au and Au/Co/Au nanostructures will be presented and compared to recent results^[3-5].

References

- [1] J. B. González-Díaz *et al.*, *Small* **4**, (2008) 202
- [2] G. Armelles *et al.*, *J. Opt. A: Pure Appl. Opt.* **11**, (2009) 114023
- [3] G. Laurent *et al.*, *Phys. Rev. B* **71**, (2005) 045430
- [4] G.W. Bryant *et al.*, *Nano Lett.* **8**, (2008) 631
- [5] H. Okamoto and K. Imura, *Progress in Surface Science* **84**, (2009) 199

Figures

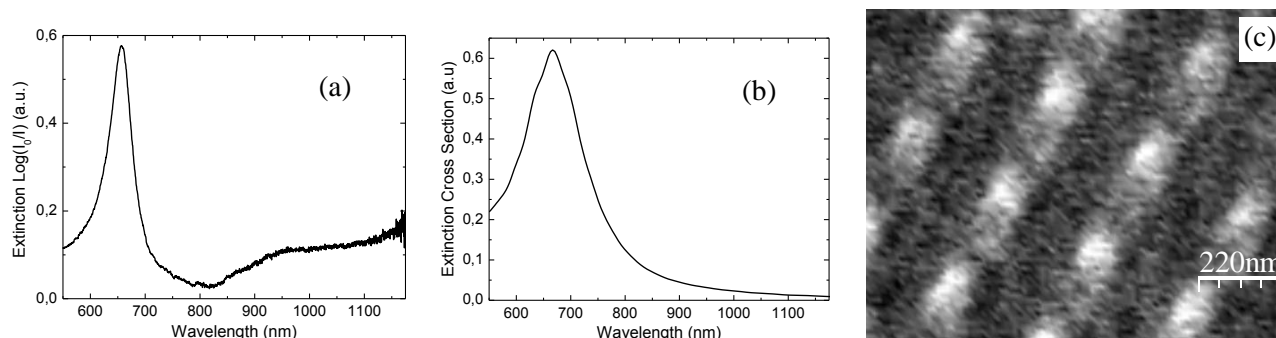


Fig.: (a) Extinction spectra and (b) simulated cross section for Au nanodisks ($h=60\text{nm}$, $d=120\text{ nm}$); (c) SNOM image in illumination mode of an array of Au nanostructures.

Wave intensity fluctuations in small disordered systems

Miztli Yépez, Silvia Albaladejo and Juan José Sáenz

Departamento de Física de la Materia Condensada, Universidad Autónoma de Madrid,
Campus de Cantoblanco, 28049 Madrid, Spain.

The statistical properties of wave transport through diffusive media have long been a topic of large interest and relevance to fields from astrophysics or “white paints” to electronic transport in mesoscopic media. Most of the work has been focused on the diffusive and localization regimes where the system size is much larger than the mean free path. The most useful theoretical approach that takes into account both multiple scattering effects as well as the system size is the (Dorokov-Mello-Pereyra-Kumar) DMPK equation. The statistical properties of a thin slab (“building block”) of length dL has been recently derive [1] from a potential model and used to find the evolution with length of the expectation value of different physical quantities. It was found that the corresponding statistical properties of the full system depend only on the mean free paths and on no other property of the slice distribution. The universality that arises demonstrates the existence of a generalized central-limit theorem. However, these results were restricted to quasi-one-dimensional (Q1D) geometries.

Here we present a detailed analysis of the statistics of wave (light or electrons) intensity fluctuations and correlations in the limit when the system thickness is much smaller than the mean free path. The results of extensive numerical calculations are in good agreement with analytical results based on perturbative expansions. The extension of this perturbative approach to study wave transport through disordered thin films without the Q1D constrain will be discussed.

[1] L.S. Froufe-Pérez, M. Yépez, P.A. Mello and J.J. Sáenz,
Phys. Rev. E **75**, 031113 (2007).

SEM image of P3HT/PCBM coated SU-8 composite

P. Chamorro-Posada, J. Martín-Gil, L. M. Navas-Gracia S. K. Kassegne, P. Martín-Ramos, M. Majzoub, G. Ozturk

Applied Optoelectronics Group for Agricultural Engineering, Universidad de Valladolid, Spain
pedcha@tel.uva.es

SEM image of a sample anode after PEDOT:PSS was applied

P. Chamorro-Posada, J. Martín-Gil, L. M. Navas-Gracia S. K. Kassegne, P. Martín-Ramos, M. Majzoub, G. Ozturk

Applied Optoelectronics Group for Agricultural Engineering, Universidad de Valladolid, Spain
pedcha@tel.uva.es

Controlling the optical properties of macroporous silicon structures

D. Hernández, T. Trifonov, M. Garín, and R. Alcobilla

Research Group in Micro and Nanotechnologies, Electronic Engineering Department, Universitat Politècnica de Catalunya, Jordi Girona 1-3, Mòdul C4, Campus Nord, 08034, Barcelona, Spain
hernandez@eel.upc.edu

L7-type microcavity fabricated on an InP substrate with quantum wires in the active region

I. Prieto, L.J. Martínez, B. Alén, M. Kaldirim, L. E. Muñoz, D. Fuster, L. González, Y. Gonzalez, M. L. Dotor and P.A. Postigo

Instituto de Microelectrónica de Madrid (CNM, CSIC), Isaac Newton 8, E-28760, Tres Cantos Madrid, Spain
pabloaitor.postigo@imm.cnm.csic.es

SEM image of high aspect ratio SU-8 posts

P. Chamorro-Posada, J. Martín-Gil, L. M. Navas-Gracia S. K. Kassegne, P. Martín-Ramos, M. Majzoub, G. Ozturk

Applied Optoelectronics Group for Agricultural Engineering, Universidad de Valladolid, Spain
pedcha@tel.uva.es

SEM micrographs of nanoimprinted photonic crystals in PMMA-based copolymer doped with (CdSe)ZnS nanocrystals (Inset) SEM micrographs of tilted view of a silicon stamp containing two-dimensional array of pillars

V. Reboud, G. Leveque, T. Kehoe, D. Dudek, N. Kehagias, M. Striccoli, T. Placido, A. Panniello, M. L. Curri, J. A. Alducin, D. Mecerreyes and C. M. Sotomayor Torres

Catalan Institute of Nanotechnology, Campus de Bellaterra, Edifici CM7, ES 08193 – Barcelona, Spain
vincent.reboud@cin2.es

